2D MODELLING OF TURBULENT TRANSPORT OF COHESIVE SEDIMENTS IN SHALLOW RESERVOIRS

JWL DE VILLIERS

A THESIS SUBMITTED IN PARTIAL FULFILMENT OF THE REQUIREMENTS FOR THE DEGREE OF MASTER OF SCIENCE IN ENGINEERING

DEPARTMENT OF CIVIL ENGINEERING
UNIVERSITY OF STELLENBOSCH
DECEMBER 2006

DECLARATION

I declare that this thesis is my own work and that it has not been submitted for a degree at another university.

JWL de Villiers, 08 / 03 / 2006

ABSTRACT

Modelling of the transport of fine cohesive sediments, as found in most South African reservoirs, has not been well developed. This is because the transport processes that are involved are complex and the theories not as implicit as the traditional equilibrium transport theories for coarse non-cohesive sediment. Advection and dispersion are found to be the processes that best describe the transport of fine sediments in turbulent flow conditions.

A two-dimensional modelling tool, MIKE 21C, which simulates reservoir hydrodynamics and cohesive sediment transport processes with an advection-dispersion model, was evaluated in this thesis. The creation of such a numerical model involves the setting up of a suitable curvilinear grid and requires data on the bathymetry, recorded inflows as well as water levels. It also requires sediment characteristic parameters and transport parameters. These parameters have to be specified by the user based on previous studies and field measurement data.

MIKE 21C was applied to laboratory flume tests and reservoir case studies in the field in order to determine the effects that these parameters have on the sediment transport in a series of sensitivity studies. Ranges were determined within which these parameter values should fall. A procedure was also developed through which reservoir sedimentation models can be calibrated.

OPSOMMING

Die modellering van die vervoer van fyn, kohesiewe sedimente, soos aangetref in Suid Afrikaanse reservoirs, is nie goed ontwikkel nie. Dit is as gevolg van die komplekse sedimentvervoerprosesse en teorieë wat nie so implisiet is soos die tradisionele vervoerteorieë vir growwe, nie-kohesiewe sediment nie. Adveksie en dispersie is die prosesse wat die vervoer van fyn sediment in turbulente vloei die beste beskryf.

'n Twee-dimensionele modelleringsagtewarepakket, MIKE 21C, wat reservoirhidro-dinamika en kohesiewe sedimentvervoerprosesse deur middel van 'n adveksie-dispersiemodel simuleer, is in hierdie tesis geëvalueer. Om so 'n numeriese model op te stel word 'n geskikte kurwe-lineêre rooster, opmeetdata van die topografie en gemete data van die invloeie asook watervlakke benodig. Dit verg ook parameters van die sedimenteienskappe asook sedimentvervoerparameters. Hierdie parameters moet deur die gebruiker gespesifiseer word, gebaseer op vorige navorsing en gemete velddata.

Die MIKE 21C sagteware is gebruik om laboratoriumkanaaltoetse en reservoirgevalle-studies te simuleer en sodoende die invloed wat die parameters op die gesimuleerde sedimentvervoer het te bepaal in 'n reeks sensitiwiteitstudies. Sodoende is grense vasgestel waarbinne die parameterwaardes moet val. 'n Prosedure is ook ontwikkel waarmee hierdie reservoirsedimentasiemodelle gekalibreer kan word.

ACKNOWLEDGEMENTS

I gratefully acknowledge my study leader, Professor GR Basson of the Department of Civil Engineering at the University of Stellenbosch, who provided me with assistance and guidance during the execution of this thesis. I would also like to thank my parents, John and Elmari, for their tremendous support.

TABLE OF CONTENTS

DECLARATION ii
ABSTRACT iii
OPSOMMING iv
ACKNOWLEDGEMENTS v

1. INTRODUCTION 1

1.1 Background 1
1.2 Domain of this Research 2
1.3 Objectives of this Research 3
1.4 Research Methodology 3
1.5 Limitations of this Research 5

2. RESERVOIR SEDIMENTATION 7

2.1 Background 7
2.2 Sedimentation Measurement Techniques 8
2.2.1 Stream Sampling 10
2.2.2 Reservoir Surveys 11

2.3 Implications of Reservoir Sedimentation 12
2.4 Measures to Deal with Reservoir Sedimentation 14

3. SEDIMENT TRANSPORT AND MATHEMATICAL MODELLING 16

3.1 Background 16
3.2 Turbulent Sediment Transport 17
3.2.1 Incipient Motion 17
3.2.2 The Applied Unit Stream Power Theory 19
3.2.3 Incipient Motion Criteria with the Stream Power Theory 21
3.2.4 Suspended Load and Bed Load 24

3.3 Traditional Equilibrium Sediment Transport Theories 25
3.4 Non-equilibrium Sediment Transport 31
3.4.1 Cohesive Sediment 31
3.4.2 Non-equilibrium Sediment Transport Background 32
3.4.3 Non-equilibrium Sediment Transport Theories for Steady Flow 33

3.5 Advection and Dispersion 38

3.6 Integrated Mathematical Modelling of Unsteady Flow Suspended Sediment Transport and Morphological Change 40
3.6.1 Background 40
3.6.2 Mathematical Model Assumptions 43
3.6.3 One-dimensional Mathematical Modelling 43
3.6.4 The Non-equilibrium Adaptation Length 45
3.6.5 One-dimensional RESSASS Model: Tarbela Reservoir, Pakistan 46
3.6.6 Two-dimensional Mathematical Modelling 48
3.6.7 The Quasi-2D Stream Tube Concept 49
3.6.8 Quasi-2D GSTARS Model: Tarbela Reservoir, Pakistan 52
3.6.9 Three-dimensional Mathematical Modelling 59
3.6.10 Three-dimensional Model: Three Gorges Reservoir Project, China 61

3.7 Density Currents 67

4. THE MIKE 21C MATHEMATICAL SEDIMENTATION MODEL 69

4.1 Background 69

4.2 Basic Setup Parameters 70
4.2.1 Generation of the Curvilinear Grid 70
4.2.2 Bathymetry Development 71
4.2.3 Simulation Period 72
4.2.4 Boundary Specifications 72
4.2.5 Source and Sink 73
4.2.6 Flood and Dry Conditions 73

4.3 Hydrodynamic Parameters 74
4.3.1 Initial Surface Elevation 74
4.3.2 Eddy Viscosity 74
4.3.3 Resistance 75
4.3.4 Helical Flow 75

4.4 Hydrodynamic Integration 77
4.4.1 The Fully Hydrodynamic Module 79
4.4.2 The Quasi-Steady Hydrodynamic Module 81

4.5 Traditional Equilibrium Transport Equations for Non-cohesive Sediments 83
4.5.1 Implementing the Equilibrium Transport Theories 87
4.5.2 The Bed Load Model 88
4.5.3 The Suspended Load Model 88

4.6 The Cohesive Sediment Transport Model 90
4.6.1 The Advection-Dispersion Equation 90
4.6.2 Limitations of the Cohesive Sediment Model 92

4.7 Morphological Change Models 93
4.7.1 Planform Model 93
4.7.2 Alluvial Resistance Model 94
4.7.3 Large-scale Morphological Model 94
4.8 The Selection of Hydrodynamic Module and Models to be Implemented 95
4.8.1 Calibration 95

5. MIKE 21C MODEL VARIABLES 96

5.1 Sensitivity Study Numerical Model Setup 96
5.2 Sediment Particle Size 97
5.3 Sediment Relative Density 97
5.4 Sediment Porosity 98
5.5 Bed Roughness 98
5.6 Settling Velocity 98
5.7 The Stream Wise Advection Constant 100
5.8 Critical Shear Stress for Deposition 101
5.9 Critical Shear Stress for Erosion 103
5.10 Erosion Constant 104
5.11 Exponent of Erosion 106
5.12 Dispersion 107

6. LABORATORY TESTS 108

6.1 Objectives 108
6.2 Design and Methodology 108
6.3 Test Setup 110
6.4 Test Procedure 112
6.5 Calibration 113
6.6 Determining the Sediment Particle Size 115
6.7 Sampling Procedure 116
6.8 Determining the Roughness of the Channel 117
6.9 The Vertical Velocity Profiles for the Test Conditions 118
6.10 Results from the Laboratory Tests 121

7. MIKE 21C SIMULATIONS OF LABORATORY TESTS 122

7.1 Numerical Model Setup 122
7.2 Laboratory Test Model Calibrations 123
7.3 Findings 128

8. LONG TERM NUMERICAL STUDIES OF SEDIMENTATION 130

8.1 Background 130
8.2 Welbedacht Reservoir Model 130
8.2.1 Calibration: 1973 – 1976 132
8.2.2 Validation: 2000 – 2002 141
8.2.3 Long Term Sedimentation Simulations 145

8.3 Vaal Reservoir Model 147
8.3.1 Calibration: 1988 – 2003 148
8.3.2 Validation 161

8.4 Winam Gulf Model, Lake Victoria, Kenya 163
8.4.1 Calibration: 1950 – 2004 165
8.4.2 Validation: the Sediment Core Dating Study 167

9. CONCLUSIONS AND RECOMMENDATIONS 173

9.1 Modelling with MIKE 21C 173
9.1.1 Small Scale Flume Modelling 173
9.1.2 Large Scale Reservoir Modelling 174

9.2 Recommended Parameter Calibration Procedure 177
9.2.1 Sediment Size 177
9.2.2 Settling Velocity 177
9.2.3 Critical Shear Stress for Deposition 177
9.2.4 Critical Shear Stress for Erosion 178
9.2.5 Stream Wise Advection Constant 179
9.2.6 Calibration Data 179
9.3 Research Recommendations 180

10. REFERENCES 181

APPENDICES 189

Appendix A: Laboratory Test Calculations 190
Appendix B: ASTM Method for Determining Particle Size Distribution 194
Appendix C: Laboratory Results 197
Appendix D: Determining the Roughness of the Laboratory Channel 200
Appendix E: Laboratory Test Velocity Distribution Calculations 202
Appendix F: Welbedacht Reservoir Sediment Data 206
Appendix G: Welbedacht Sediment Load Calculations 208
Appendix H: Vaal Reservoir Sediment Data 210

Appendix I: Vaal Reservoir Suspended Sediment Data 215
Appendix J: Nyando River Suspended Sediment Data 218
Appendix K: Nyando Inflow Time-series and Sediment Concentrations 219

LIST OF TABLES xi
LIST OF FIGURES xii
LIST OF SYMBOLS xv

LIST OF TABLES

Table 3-1:	Comparison between the calculated and measured deposits for different reaches	64
Table 5-1:	Sensitivity study model parameters	96
Table 6-1:	The laboratory test flow parameters	109
Table 6-2:	Test flow and sediment parameters	112
Table 6-3:	Time measurements of the drawdown intervals	114
Table 7-1:	The simulation model constants	122
Table 7-2:	The simulation model variables and input concentrations	122
Table 7-3:	Attempted calibration parameters for Test 1	123
Table 7-4:	Attempted calibration parameters for Test 2	124
Table 7-5:	Attempted calibration parameters for Test 3	126
Table 7-6:	Attempted calibration parameters for Test 4	127
Table 8.2-1:	Calibration model variables	135
Table 8.2-2:	Validation model variables	142
Table 8.3-1:	Model calibration variables	153
Table 8.4-1:	Calibration model variables	166
Table 8.4-2:	Measured Cs-137 in the cores analysed	170
Table 9-1:	The laboratory test and simulation parameters	173
Table 9-2:	The reservoir model parameters	176

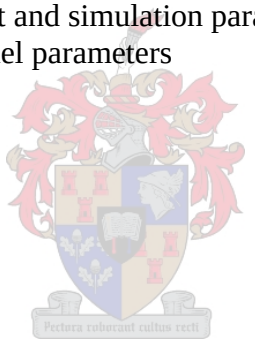

LIST OF FIGURES

Figure 2-1:	Historical growth in storage capacity and sediment deposition worldwide	7
Figure 2-2:	Sedimentation of reservoirs in South Africa	9
Figure 3-1:	Shields' diagram	18
Figure 3-2:	Variation in power input and applied power	19
Figure 3-3:	Critical conditions for cohesionless particles	23
Figure 3-4:	Simulated and surveyed longitudinal profile of Tarbela Reservoir	48
Figure 3-5:	Tarbela Dam and Reservoir	55
Figure 3-6:	Hydrology and dam operation for Tarbela Reservoir	55
Figure 3-7:	Two reservoir cross-sections showing uniform sedimentation	56
Figure 3-8:	Results of the simulation of the Tarbela delta advancement over a period of 22 years	57
Figure 3-9:	Comparison of measurements and GSTARS3 computation for two cross sections in the upstream region of Tarbela Reservoir	58
Figure 3-10:	Comparison of measurements and GSTARS3 computation for two cross-sections in the reservoir region of the study reach	58
Figure 3-11:	Relative error of the thalweg elevation predictions	59
Figure 3-12:	River Configuration in the Dam Area of Three Gorges Project	63
Figure 3-13:	Development of the deposition of the entire and near dam reaches	66
Figure 3-14:	The plunge line with floating debris where the Nzoia River flows into Lake Victoria, Kenya.	68
Figure 4-1:	A curvilinear grid created for a river and reservoir system	71
Figure 4-2:	The grid with complete interpolated bathymetry	72
Figure 4-3:	Typical time-series of measured reservoir water levels and inflow	73
Figure 4-4:	Helical flow in river bends	75
Figure 4-5:	The vertical distributions of primary flow and helical flow	76
Figure 4-6:	The curvilinear flow parameters	79
Figure 5-1:	Sediment concentrations for different settling velocities	99
Figure 5-2:	Deposited layer thickness for different settling velocities	99
Figure 5-3:	Sediment concentrations for different stream wise constants	100
Figure 5-4:	Deposited layer thickness for different stream wise constants	100
Figure 5-5:	Sediment concentrations for different shear stresses for deposition	101
Figure 5-6:	Deposited layer thickness for different shear stresses for deposition	102
Figure 5-7:	Sediment concentrations for different shear stresses for erosion	103
Figure 5-8:	Deposited layer thickness for different shear stresses for erosion	103
Figure 5-9:	Sediment concentrations for different erosion constants	105
Figure 5-10:	Deposited layer thickness for different erosion constants	105
Figure 5-11:	Sediment concentrations for different erosion exponents	106
Figure 5-12:	Deposited layer thickness for different erosion exponents	106

Figure 6-1:	The dry laboratory channel	108
Figure 6-2:	A schematic drawing of the laboratory setup	110
Figure 6-3:	The sediment dispersing pipe	111
Figure 6-4:	The laboratory test setup	111
Figure 6-5:	The magnetic flow meter voltage versus pipe discharge	113
Figure 6-6:	The particle size distribution of laboratory sediment	115
Figure 6-7:	The suspended sediment samplers at their three different measuring depths	116
Figure 6-8:	Sampling in progress	117
Figure 6-9:	The velocity profile for tests 1 and 2, with an average velocity of 0.1 m/s	120
Figure 6-10:	The velocity profile for tests 3 and 4, with an average velocity of 0.05 m/s	120
Figure 6-11:	The results from the laboratory tests	121
Figure 7-1:	Concentration results of the calibration runs for Test 1	124
Figure 7-2:	Concentration results of the calibration runs for Test 2	125
Figure 7-3:	Concentration results of the calibration runs for Test 3	126
Figure 7-4:	Concentration results of the calibration runs for Test 4	127
Figure 7-5:	The vertical velocity profiles of turbulent flow and a density current	128
Figure 8.2-1:	The observed loss in storage capacity of Welbedacht Reservoir	131
Figure 8.2-2:	The longitudinal profiles of Welbedacht Reservoir	131
Figure 8.2-3:	An aerial photo of Welbedacht Reservoir	132
Figure 8.2-4:	The curvilinear grid (in plan) used in the Welbedacht model	132
Figure 8.2-5:	The 1973 bathymetry (in plan) used in the Welbedacht model	133
Figure 8.2-6:	Median particle sizes of bed grab samples taken along Welbedacht reservoir	134
Figure 8.2-7:	The 1973 to 1976 time-series for the model's inflow and downstream water level based on observed data	135
Figure 8.2-8:	Deposited sediment layers at section 41 for different settling velocities	136
Figure 8.2-9:	Deposited sediment layers at section 26 for different settling velocities	137
Figure 8.2-10:	Deposited sediment layers at section 9 for different settling velocities	137
Figure 8.2-11:	Deposited sediment layers at section 41 for different shear stresses for deposition	138
Figure 8.2-12:	Deposited sediment layers at section 26 for different shear stresses for deposition	139
Figure 8.2-13:	Deposited sediment layers at section 9 for different shear stresses for deposition	139
Figure 8.2-14:	Deposited sediment layers at section 41 for different stream wise constants	140
Figure 8.2-15:	Deposited sediment layers at section 26 for different stream wise constants	140
Figure 8.2-16:	Deposited sediment layers at section 9 for different stream wise constants	141
Figure 8.2-17:	The 2000 survey bathymetry used for the validation	142
Figure 8.2-18:	The 2000 to 2002 time-series for the model's inflow and downstream water level	143
Figure 8.2-19:	Deposited sediment layers at section 41 for the validation simulation	143

Figure 8.2-20: Deposited sediment layers at section 26 for the validation simulation 144
Figure 8.2-21: Deposited sediment layers at section 9 for the validation simulation 144
Figure 8.2-22: Historic longitudinal bed profiles with future sedimentation levels 145
Figure 8.2-23: The simulated 2029 bathymetry in plan 146
Figure 8.2-24: Section 41 profile and flood levels 147
Figure 8.3-1: An aerial photo of Vaal Reservoir 148
Figure 8.3-2: The curvilinear grid used for the Vaal Reservoir model 149
Figure 8.3-3: The original 1988 surveyed bathymetry 149
Figure 8.3-4: The grab sediment sampler with a typical load of cohesive sediment from Vaal Reservoir 150
Figure 8.3-5: The bed sediment particle size distribution 150
Figure 8.3-6: 1993-1995 Measured suspended sediment yield/discharge data and the trendline 151
Figure 8.3-7: The 1988 to 2003 time-series for the model's inflow and water level based on observed data 153
Figure 8.3-8: The upstream input sediment concentration time series 154
Figure 8.3-9: Deposited sediment layers at section 51 for different settling velocities 155
Figure 8.3-10: Deposited sediment layers at section 30 for different settling velocities 155
Figure 8.3-11: Deposited sediment layers at section 2 for different settling velocities 155
Figure 8.3-12: Deposited sediment layers at section 51 for different shear stresses for deposition 156
Figure 8.3-13: Deposited sediment layers at section 30 for different shear stresses for deposition 157
Figure 8.3-14: Deposited sediment layers at section 2 for different shear stresses for deposition 157
Figure 8.3-15: Deposited sediment layers at section 51 for different stream wise constants 158
Figure 8.3-16: Deposited sediment layers at section 30 for different stream wise constants 159
Figure 8.3-17: Deposited sediment layers at section 2 for different stream wise constants 159
Figure 8.3-18: Deposited sediment layers at section 51 for the parameter variations 160
Figure 8.3-19: Deposited sediment layers at section 30 for the parameter variations 160
Figure 8.3-20: Deposited sediment layers at section 2 for the parameter variations 160
Figure 8.3-21: Simulated and measured concentrations versus discharge upstream of Vaal Marina 161
Figure 8.3-22: Vaal Reservoir Inflow Time-series 161
Figure 8.4-1: A satellite image of the Winam Gulf study area 163
Figure 8.4-2: The curvilinear grid of the Winam Gulf study area 164
Figure 8.4-3: The 2005 surveyed bathymetry superimposed on the grid 164
Figure 8.4-4: Nyando river measured concentrations versus discharge 165
Figure 8.4-5: The 1950 to 2004 time-series for the Nyando River inflow and the Rusinga Channel water level based on observed data 166
Figure 8.4-6: The original locations of the core samples 168
Figure 8.4-7: Historical Cs-137 fallout 169
Figure 8.4-8: The simulated 54 year accumulated sediment layer thickness 172
Figure 8.4-9: A satellite image showing the movement of sediment laden water through the gulf 172

LIST OF SYMBOLS

A	flow cross-section
A	Ackers and White equation coefficient
α	coefficient by Yang (1984)
α	adjustment coefficient (Falconer and Owens, 1990)
α	non-equilibrium adaptation or recovery coefficient
α	helical flow calibration constant
a	calibration parameter that can be interpreted as mean settling depth
a	reference level at which the bed concentration is determined
α_1	coefficient by Rooseboom (1975)
α_2	coefficient by Rooseboom (1975)
α_{01}	stream wise advection constant
α_{02}	secondary flow advection constant
a_1 - a_8	bed load coefficients by Meyer-Peter and Muller (1947)
α_3 α_4	coefficients by Yang (1973)
α_5 α_6	coefficients by Yang (1973)
α_{bx} , α_{by}	direction cosines of the bed shear stresses
a , b	alluvial resistance model calibration coefficients
β	parameter by Rozovskii
β	constant by Yang (1984)
β_i	percentage of a sediment fraction in the bed composition by de Silvio (1995)
C	Chezy friction factor
C_b	bed load concentration
C_{eq}	constant equilibrium concentration
C_{eq}^*	ratio of relative equilibrium concentration
C_a	reference concentration
C_d	drag coefficient
C_o	maximum bed concentration (van Rijn, 1984)
C_o	initial value of sediment concentration (Mehta and Partheniades, 1973)
C	total load sediment concentration
C_{ci}^*	the transporting capacity of a sediment fraction
C_{tk}	section averaged sediment concentration
C_{*tk}	the suspended load transport capacity
C_{tk}	depth-averaged sediment concentration
C^*	equilibrium sediment transport
C_k	depth-averaged suspended load concentration
C_{*k}	suspended load transport capacity
C_k^*	potential transport capacity of size class k of suspended load

CT^{*j}	average concentration of sediment transporting capacity
c	concentration
c_a	bed layer concentration (Falconer and Owens, 1990)
c'	Ackers and White equation coefficient
c_b	the reference concentration near the bed
c_e	equilibrium concentration
c_k	local concentration of the *k*-th size class of suspended sediment load
c_{b*k}	equilibrium concentration at the reference level *z*.
$\overline{c}_{bk}$	average concentration of bed load at the bed load zone
D	depth of flow
D_L	grain size of a sediment group
D_*	dimensionless particle diameter
D_{Txx}	turbulence coefficients in x direction
D_{Tyy}	turbulence coefficients in y direction
D_{Txy}	turbulence coefficients in the transverse direction
D_{xx}	dispersion in the x-direction (includes advection and turbulent diffusion)
D_{yy}	dispersion in the y-direction (includes advection and turbulent diffusion)
D_{xx}, D_{xy},	dispersion terms due to the effect of secondary flow
D_{yx}, D_{yy}	dispersion terms due to the effect of secondary flow
D_{bk}	deposition rate
d_{50}	median particle diameter
d_{gr}	Ackers and White dimensionless sediment particle size
d_j	Soares sediment particle diameter
d	particle diameter
Δ	step height for the vertical velocity profile
δ_b	saltation height
δ_s	deviation in stream direction due to helical flow
δ	bed load layer thickness
δ_{j3}	Kronecker delta
E	eddy viscosity
E_{bk}	entrainment rate
E	erosion rate
E_0	erosion constant
$\in$	coefficient of turbulent exchange
ξ_1	sediment transport under non-equilibrium conditions for deposition
ξ_2	sediment transport under non-equilibrium conditions for erosion
ε_s	Turbulence diffusivity coefficient of sediment
F	van Rijn coefficient
Fr	Froude number
F_i	external forces including gravity per unit volume
F_s	entrainment function
F_{gr}	Ackers and White a mobility number
f_c	Coriolis coefficient

G_{gr}	Ackers and White sediment transport function
g	gravitational acceleration
γ_s	specific weight of sediment
γ	specific weight of water
H	water level
h	water depth
I	bed slope or slope of water surface
i_s	helical flow intensity
K_3	empirical coefficient by Zhang (1959)
K_4	empirical coefficient by Zhang (1959)
K_5	empirical coefficient by Zhang (1959)
k	representative sediment size class
κ	Von Karman constant
k_s	absolute bed roughness
L_i^*	adaptation length for a sediment fraction
l	mixing length
λ_b	linear sediment concentration
M	Manning's roughness M
m	coefficient of erosion
m	Ackers and White equation coefficient
m	parameter related to sediment concentration by Zhang (1959)
μ	dynamic viscosity of water
μ_d	dynamic friction coefficient (Engelund and Fredsoe, 1976)
N	total number of size classes
n	Ackers and White equation coefficient
n	sediment porosity
n	secondary orthogonal coordinate axis
n	Manning's roughness n
η	non-dimensional vertical coordinate of the velocity profile
η_o	no slip level
P	wetted perimeter
P_L	percentage by weight of the sediment group
p	pressure
p	probability of a moving sediment particle
p'	bed material porosity
p_{bk}	availability factor of sediment
p_{bk}	bed material gradation at the mixing layer
p, q	flux field of curvilinear n and s axis
p', q'	modified curvilinear flux field
ψ	suspension parameter correction coefficient
ϕ	coefficient used in Engelund Hansen equation (1976)
ϕ	depth integrated transport capacity
Q	discharge
Q_s	sediment flux

Q_{tk}	actual sediment transport rate
Q_{t*k}	sediment transport capacity or the so-called equilibrium transport rate
q_{lk}	side inflow or outflow sediment discharge from bank or tributary streams per unit channel length
q_s	suspended sediment unit flux
q_b	bed load sediment unit flux
q	unit flux
q_s	sediment discharge per unit width at the exit
q_{st}	sediment carrying capacity
q_{s0}	sediment discharge per unit width at the entrance
q_{bk}^*	potential transport capacity of size class *k* of bed load
q_d^j, q_e^j	fluxes of deposition and erosion of sediment
q_{tkx}, q_{tky}	components of the total load sediment transport in the *x*- and *y*- directions
Φ	section averaged transport capacity
Φ_{bl}	non-dimensional bed load transport rate
Φ_{sl}	suspended sediment load
R_s, R_n	radius of curvature of s- and n-line, respectively
R	hydraulic radius
Re	Reynold's number
R_0	radius of eddies formed against bed
ρ	density of water
ρ_s	particle density
S_{bl}	bed load transport rate
S_{sl}	suspended load transport rate
S_{tl}	total sediment transport load
S_x, S_y	dispersion terms to account for the effect of the non-uniform distributions of flow velocity and sediment concentrations
s	slope
s	primary orthogonal coordinate axis
ss	source/sink term for advection-dispersion equation
T	width of flow (Soares, 1982)
T_{xx}, T_{xy},	depth-averaged turbulent stresses
T_{yx}, T_{yy}	depth-averaged turbulent stresses
T	transport stage parameter
t	time
τ	bed shear stress
τ_{cd}	critical shear stress for deposition
τ_{ij}	turbulent stresses determined by a turbulence model
τ_{ce}	critical shear stress for erosion
τ_{cme}	critical shear stress for mass erosion
$\tau_{b\min}$	threshold value of bed shear stress

τ_{bx}, τ_{by}	bed shear stresses in the *x*- and *y*- directions
τ_{sx}, τ_{sy}	shear stresses on the water surface caused by wind
θ	Shield's parameter
θ	coefficient used in Engelund Hansen equation (1976)
θ'	non dimensional skin shear stress
$\tan\alpha$	ratio of tangential shear to normal force
$\tan\delta_s$	limiting angle between average and helical flow shear stress directions
τv	stream power
U	depth-averaged flow velocity
U'_f	friction velocity related to skin friction
u_g	bed shear velocity
u	mean flow velocity
u_{i-}	velocity components (i = 1, 2, 3)
u_*	friction velocity
u'_f	friction velocity related to skin friction
u_{bs}	particle velocity
$u_{f,cr}$	Shield's critical bed shear velocity
V	volume
V	section-averaged flow velocity
V_v	volume of voids in a material
Vss	settling velocity
v	velocity
$\overline{v}$	average velocity
vs_{cr}	the critical input stream power for incipient motion
υ	kinematic viscosity of water
w	settling velocity
x	cartesian coordinate
y	cartesian coordinate
y	vertical distance from the bed
y_0	distance from bed where velocity mathematically equals zero
y_1	rotational point distance from the bed
Z	Rouse suspension parameter
Z'	modified suspension number
z	Cartesian coordinate
z_1	suspension theory coefficient as derived by Rooseboom (1975)
z'	suspension theory coefficient
z_s	water surface elevation

1. INTRODUCTION

1.1 Background

Sediment is any particulate matter that can be transported by fluid flow and which is eventually deposited as a layer of solid particles on the bed of a body of water. Sedimentation is the deposition by settling of suspended material. Sedimentation occupies an important position in the field of civil engineering because it determines the life span and affects the function of many hydraulic projects. Studying reservoir sedimentation is important to determine capacity loss, the useful life of the reservoir, and the impact that dam operations have on the reservoir's deposition pattern.

Sediments in reservoirs are heterogeneous mixtures of soil particles and rock fragments, detached from the earth's crust, transported and deposited in the reservoir basin. Mineral sediments are predominant as either cohesive or non-cohesive solid materials, coming into the reservoir from the river-catchment system, as a result of the erosive action of water, air, ice and human activities on the Earth's surface.

Damming created by the construction of a dam causes reduced sediment transport capacity in the waters upstream of the dam and the result is therefore sediment deposition. This causes a gradual loss of live storage capacity as well as a reduced firm abstraction yield from the reservoir.

The cohesive sediments are relatively homogeneous conglomerates of very fine clay and silt particles, which are bound by electro-chemical forces (cohesion). The non-cohesive sediments are non-homogeneous mixtures of sand, gravel, and fractions of rock. The ratio between cohesive and non-cohesive sediments in a reservoir depends mainly on the climatic conditions, geological structure, vegetation growth and human activities in the region.

The percentage fine material found in the bed sediments can have a profound effect on the sediment transport characteristics of the bed sediments. It has been found that as little as 7% clay and silt in sediment means that the sediment will effectively have

the properties of cohesive sediments (Beck and Basson, 2003). This means that the sediments are much more resistant to erosion, especially after they have been allowed to consolidate.

Although many models have been developed for suspended sediment transport, modelling of the transport of cohesive sediment as found in most South African reservoirs, is still not well developed.

1.2 Domain of this Research

Turbulent suspended sediment and density current sediment transport have been identified as the main sediment transport processes for fine sediment through most South African reservoirs. The occurrence of density currents are very seldom and only exists under very specific circumstances while turbulence is the mechanism for 96% of all sediment transport (Rooseboom, 1992).

Numerous theories and equations have been developed for the calculation of equilibrium sediment transport in turbulent flow. These were developed and calibrated for the transport of coarse sediments only. Various theories for non-equilibrium transport have also been established for steady flow conditions. Because of the highly dynamic nature of sedimentation processes within reservoirs, this research investigates the calibration of an unsteady two-dimensional (2D) advection-dispersion equation as implemented by the MIKE 21C software. MIKE 21C is a 2D curvilinear modelling tool for the simulation of the hydrodynamics and morphological changes in rivers and reservoirs, developed by the Danish Hydraulic Institute (DHI).

MIKE 21C simultaneously solves the fully dynamic 2D St.Venants equations of continuity and momentum and the 2D advection-dispersion equation for sediment transport. The advection-dispersion equation is solved continuously with the dynamic output of two-dimensional flux, water level and bed level from the hydrodynamic module. The MIKE 21C modelling tool requires that various transport calibration parameters are specified. It also requires that detailed sediment characteristics are specified by the user.

This study is therefore directed at the calibration of non-equilibrium dynamic modelling of turbulent sediment transport of cohesive sediment in reservoirs.

Basson (1996) calibrated the one-dimensional (1D) unsteady advection-dispersion equation for various sediment types using measured flume data and the 1D MIKE 11 simulation model. This study aims to calibrate a 2D advection-dispersion equation as implemented in the MIKE 21C software for flume and large scale reservoir applications. Calibration of a numerical model comprises the adjustment for a particular situation by making use of some measured data. The parameters of flow, sediment characteristics and sediment transport will be investigated and calibrated for varying laboratory and reservoir case studies.

1.3 Objectives of this Research

This research investigates the 2D modelling of cohesive sediment transport using the MIKE 21C software.

The calibration process for the MIKE 21C hydrodynamic and morphologic model involves the tuning of a number of calibration factors for each simulation. All the calibration factors have physical meanings and should not be arbitrarily given values outside their realistic ranges to obtain agreement with observed data.

These parameters include the sediment characteristics, the flow parameters as well as the parameters of sediment transport, as required by the advection-dispersion model. It is the aim of this research to produce insight into the modelling of cohesive sediment transport in reservoirs so that accurate predictions of sedimentation can be made which can be used in the design and operation of reservoirs.

1.4 Research Methodology

A study into the traditional equilibrium theories for coarse, non-cohesive sediment transport was carried out. This is considered as necessary background as it gives insight into the hydraulic processes that causes sediment deposition and entrainment.

The non-equilibrium sediment transport theories for cohesive sediments are then investigated in detail. Recent developments in this field can be simplified to the following three modelling methods:

- One-dimensional modelling of turbulent transport with advection and dispersion as implemented in MIKE 11
- Two-dimensional modelling of turbulent transport with advection and dispersion as implemented in MIKE 21C
- Three dimensional modelling of turbulent transport with advection and dispersion.

Examples of numerical models for each of these methods are discussed. MIKE 21C is then applied on a small scale to model flow in a laboratory flume before it is applied to model the sedimentation in large bodies of water.

Firstly a straight rectangular glass flume with steady uniform turbulent flow conditions was modelled. A constant sediment concentration was added at the upstream boundary. A sensitivity study was then conducted to investigate the working of the transport parameters and also to establish likely ranges of their values.

Four laboratory tests were then carried out in a rectangular glass flume for varying conditions of turbulent flow and different initial upstream sediment concentrations. The concentrations were measured at regular intervals along the flume to monitor the decreasing suspended sediment concentration. Numerical models were then created in MIKE 21C to simulate these laboratory conditions. The model's sediment and transport parameters were then calibrated so that the numerical models produced similar results to the laboratory tests.

The field where the MIKE 21C software is most likely to be used is reservoir sedimentation. Numerical models were created for two South African reservoirs, Welbedacht Reservoir and Vaal Reservoir. These two are considered very different regarding size, hydraulics, sediment load and transport characteristics. The purpose was to calibrate both of these models and thereby determine the suitability of the software for the modelling of South African reservoirs.

Another model was created for Winam Gulf of Lake Victoria in Kenya. The sediment processes within the gulf are considered to be the same as in a shallow reservoir, and can therefore be modelled in the same way. All three bodies of water are experiencing sedimentation of fine cohesive particles.

As part of this research, field work was conducted during 2004 and 2005 at these three locations to gain information on sediment characteristics. Bed grab samples and suspended sediment samples were taken throughout these bodies of water to calibrate their numerical models' sediment characteristics. Measured flow and water level data were obtained from different water authorities.

1.5 Limitations of this Research

- The version of MIKE 21C that was available for this research was specifically designed by DHI for the modelling of cohesive sediment in reservoirs using the advection-dispersion equation. It allows the user to model the transport of one sediment size fraction only during a simulation. This particle size has to be representative of the real sediment size distribution. In the latest MIKE 21C package as well as the one-dimensional MIKE 11, a number of representative size fractions of clay and silt can be modelled simultaneously.

- This MIKE 21C version incorporates a number of shortcuts. Only some of the sediment transport parameters can be defined by the user. The others, such as the horizontal dispersion coefficients are calculated by the model itself based on the flow profiles. This creates a limitation to this methodology in that these parameters cannot be calibrated. It also greatly simplifies the research.

- The computational time for some simulations exceeded a week, while others needed only a few minutes. The average run time for the reservoir models was around 15 hours. This limited the number of calibration runs that could be completed in the allowed research time.

- The MIKE 21C package does require of the user to build up experience in the usage of the software before attempting large scale applications such as reservoirs. Creating a suitable curvilinear grid, for instance, can take a considerable amount of time and experience.

2. RESERVOIR SEDIMENTATION

2.1 Background

Reservoir sedimentation is a worldwide problem with the annual loss in storage capacity due to sedimentation estimated at 1% of the original storage capacity, or 50km^3 per annum (Batuca and Jordaan, 2000). This equates to a replacement cost estimated by the World Bank at USD 13 billion per year needed to maintain the current total storage capacity (Palmieri, 2003). Worldwide the average age of reservoirs is now about 35 years. Most of the existing reservoirs will be completely silted up in 200 years time, assuming no intervention. Figure 2-1 shows the historical growth in the storage capacity and sediment deposition worldwide.

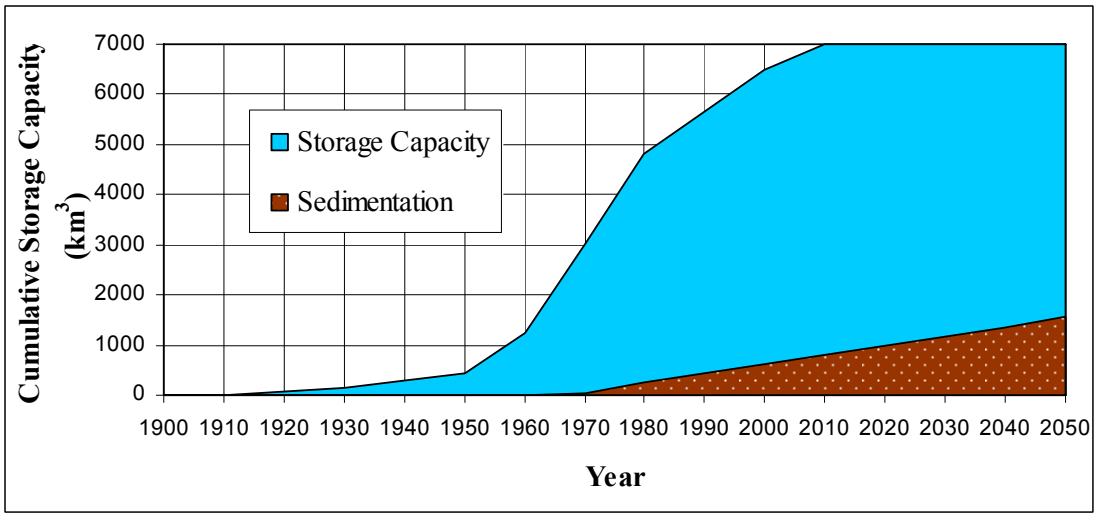

Figure 2-1: Historical growth in storage capacity and sediment deposition worldwide (Basson and Olesen, 2004)

In South African reservoirs, Jordaan (1989) found the average sedimentation rate to be 0.5%, equivalent to the loss of 150 million m^3 of storage capacity each year. Beck and Basson (2002) calculated this rate to be 0.34%, based on more recent data.

Engineering designs are still focused on dealing with clean water rather than sediment laden water, which is more difficult to predict and control. Reasons for reservoir sedimentation underestimates can be related to a number of misconceptions at the

time of reservoir design, and can be grouped into sediment yield misjudgements and engineering problems (Basson and Rooseboom, 1997):

The sediment yield misjudgements are due to:

- Small or short data bases of river sediment transport data or reservoir surveys
- Limited information on regional sediment yields linked to soil types, topography and climatic variables
- Land-use changes and increased erosion and sediment yields.

Engineering problems have occurred due to incorrect prediction of reservoir sediment trap efficiency resulting from:

- Overestimation of sediment transporting capacity through reservoirs
- Overestimation of the efficiency of outlet structures to sluice/flush sediment from the reservoirs
- Changed operation during the life of reservoirs
- Overestimation of the effectiveness of soil conservation schemes in the catchment.

Worldwide there are many cases where extreme sedimentation has reduced a reservoir's lifespan to only a few years. A well known example of where these problems have occurred in South Africa is Welbedacht Reservoir on the Caledon River in the Free State Province. This dam was constructed in 1973 with the purpose of supplying water to the city of Bloemfontein via the 115 km long Caledon-Bloemfontein pipeline. By 1988, 15 years after construction, it had already lost 73.2 % of the original storage capacity at an average annual sedimentation rate of 4.5 % (Clarke, 1990).

Flushing operations were carried out but with limited success. The reduction in storage created problems in meeting the city of Bloemfontein's demand at an acceptable level of reliability and as a result, the 50m high off-channel Knellpoort Dam had to be constructed in 1988. By 2002 Welbedacht Reservoir had lost 89.9% of it's original storage capacity (DWAF, 2006). It can be seen in Figure 2-2 that

Welbedacht Reservoir is the worst of the selected reservoirs, but not the only reservoir experiencing heavy sedimentation in South Africa.

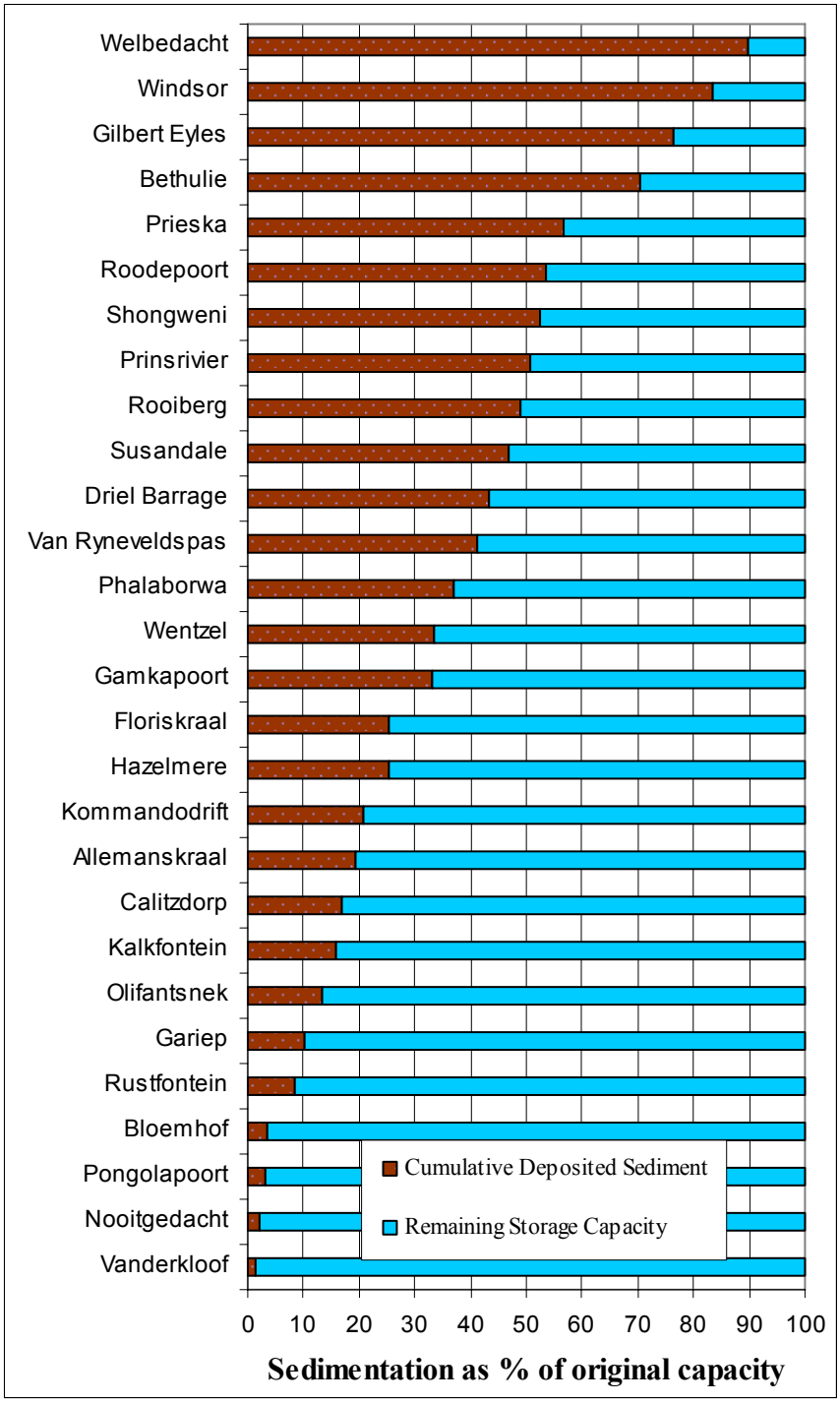

Figure 2-2: Sedimentation of reservoirs in South Africa

2.2 Sedimentation Measurement Techniques

There are basically two techniques to measure sedimentation rates. These are stream sampling and reservoir surveys.

2.2.1 Stream Sampling

In South Africa, river sediment sampling was initiated in 1919 and daily sampling programmes were initiated up until the 1970's. The sampling was mostly done by filling bottles just below the surface of the stream. The question arises whether these daily samples can be representative of the daily sediment load of a deep and wide river.

Studies by Rooseboom (1975) showed that concentrations varied little with depth and only slightly across a stream. He also found that a correction factor of 1.25 provides for the tendency of bottled samples to under-represent actual concentrations and it also brings into account the bed load sediment and changes in concentrations with depth and width. In the 1950's depth integrated and bed load sediment samplers were developed with which the total load can be determined with greater accuracy.

Available data of sediment concentrations upstream of a reservoir can be compared to the measured discharge into the reservoir at the time that the sample was taken and a relationship can be established between the two in the form of a simple dependency equation. Using this equation, sediment concentrations can then be found for any discharge. The sediment flux, Q_s, is found by multiplying the concentrations with the measured discharges. The total sediment volume that flowed into the reservoir over a certain period can then be derived by integrating a time-series graph of the sediment flux.

Even with very low flow velocities within South African reservoirs, concentrations are rarely lower than 0.001% by mass. During flood conditions this value vary between 0.1% and 3%, with the high values of 6.5% recorded at Jammersdrift, just upstream of Welbedacht Reservoir (Rooseboom, 1992), and 9.6% recorded on the Olifants River (Limpopo Province) in 1996 (Basson, 1996).

2.2.2 Reservoir Surveys

Since the 1970's the emphasis in monitoring of sediment loads has shifted from daily stream sampling to regular resurveying of existing reservoirs to record sediment accumulation rates.

Historically, hydrographic surveys of rivers and reservoirs were often completed using line-of-sight techniques to survey a section of river or reservoir. Reservoir surveys have been carried out using conventional equipment e.g. theodolite, plane table, range finders, sounding rods, echo-sounders and slow moving boats. The surveys conducted by this method are time consuming and sometimes it takes up to three years to complete a survey of a major reservoir such as Vaal Reservoir. During such a long time of surveying, the bed levels can also change.

Updating of sediment measurement techniques and introducing the latest technology available in the field substantially reduced the difficulties faced with conventional methods, especially in major reservoirs. It drastically reduced the time required for surveys and also increased the quality of data. Automatic data collection systems comprising of computers, global positioning systems and echo-sounders are now being used for conducting hydrographic surveys. The development of the global positioning system has revolutionised the way hydrographic surveys are carried out.

By using GPS it is feasible to collect enough coordinate data to effectively map the entire reservoir bed. This data can then be used to develop a digital terrain model as required for 2D numerical modelling tools such as MIKE 21C. With such a terrain model, changes in reservoir sedimentation levels from one survey to the next are easily and accurately calculated and mapped.

Reservoir re-surveys are necessary to obtain reliable data regarding the rate of sedimentation as well as for studying the impact of annual losses of storage over a period of time on the reduction of intended benefits in the form of irrigation, hydropower, flood absorption capacity and water supply for domestic and industrial uses. The results are also used in the estimation of loss of storage capacity in planned

reservoirs, as well as evaluating the effectiveness of soil conservation measures carried out in a catchment area.

Proper monitoring can determine:

- storage losses caused by sediment deposition
- annual sediment yield rates
- current location of sediment deposition
- sediment densities
- lateral and longitudinal distribution of deposited sediment
- reservoir trap efficiencies

It is important that reservoir surveys also include the areas above the full supply level of the reservoir, since up to 20% of the total sediment deposit can occur above this level (Rooseboom, 1992). After each survey has been completed, the remaining storage volume is calculated. The total volume of sediments deposited in the reservoir between successive surveys is the difference between the remaining storage volumes of the successive surveys. As the average densities of deposits vary with time, this needs to be taken into consideration when deposit volumes are converted into sediment deposit masses.

2.3 Implications of Reservoir Sedimentation

Hydropower now accounts for 21% of the world's electricity output, while storage reservoirs augment the cultivation of 17% of the world's irrigated crop land (Le Moine, 1990; Postel, 1989).

Sediment deposition in reservoirs causes not only loss of water storage capacity, but also impairment of navigation, loss of flood control benefits, increased flooding upstream, sediment entrainment in hydropower equipment, blockage of control gates etc. It also causes serious economic, environmental and social problems. These impacts were defined by Basson and Rooseboom (1997).

The economic impacts include:

- increased maintenance costs of irrigation schemes and power stations
- water losses due to reduced storage capacity
- additional chemical treatment due to higher turbidity levels
- costs of repairing agricultural land after degradation, deposition of infertile material and impairment of natural drainage
- impacts on infrastructure such as roads, bridges and water distribution systems
- higher energy costs due to the use of alternative sources of power
- remedial measures such as reconstruction of outlets.

Environmental impacts include:

- detrimental impacts on fish, bird and animal habitats due to degradation of the original river bed both upstream and downstream of a dam
- reduced nutrient loads related to reduced sediment loads downstream of the dam can impact seriously on the local fishing industry
- toxic chemicals can build up in reservoirs and with events such as flushing, high concentrations of toxic material might be flushed downstream.
- increased phosphorus and nitrogen accumulation can affect the water quality and eventually lead to algal growth and eutrophic conditions
- the downstream discharge regime modification causes erosion of the downstream channel, undercutting of the banks and eventual widening of the river channel.

Social impacts include:

- land expropriation and relocation of people due to increased flooding levels upstream of the dam
- impacts on the water rights of riparian farmers.

The construction of dams and irrigation schemes also lead to rapid economic development. Industries and communities become dependant on a reservoir for power supply, which could eventually become less reliable as a result of sedimentation.

2.4 Measures to Deal with Reservoir Sedimentation

In the planning and design of a reservoir, engineers must make provision for sedimentation problems and include in their design measures to regulate sediment accumulation within the reservoir, such as adequately sized deep bottom sluice gates for sediment flushing. Sedimentation control techniques are necessary to minimize the impacts of reservoir sedimentation, thereby ensuring a longer lifespan for a reservoir. There are various options for reservoir sediment control (Basson and Rooseboom, 1997):

a) Minimize sediment loads entering the reservoir through:

- soil and water conservation programmes
- upstream trapping of sediment
- bypassing of heavy sediment loads

b) Minimize deposition of sediment within a reservoir through:

- sluicing: passing of floods with high sediment loads through the reservoir by means of water level drawdown
- density current venting
- controlling the location of sediment deposits for later dry excavation

c) Remove accumulated sediment deposits through:

- flushing by means of water level drawdown during the rainy season when excess water is available
- excavation by dredging

d) Compensate for reservoir sedimentation by:

- maintaining storage capacity by raising the dam
- decommissioning the reservoir and constructing a new reservoir or water scheme

Sluicing, flood flushing and venting of density currents are costly in terms of water releases and the effectiveness of such measures needs to be predicted and monitored. For these types of operations, water to be released is the major constraint. In practice,

the most efficient passing through of sediment is obtained when the reservoir capacity is less than 5% of the mean annual runoff.

3. SEDIMENT TRANSPORT AND MATHEMATICAL MODELLING

3.1 Background

It is evident from the previous chapter that reservoir sedimentation problems can only be analyzed with knowledge of the sedimentation and hydraulic processes involved. It is not possible to understand the transportation of sediment without a proper understanding of the hydraulic flow processes within rivers and reservoirs.

In South African rivers, the sediment transport rate is often not limited by the hydraulic conditions, but rather by the sediment availability from the catchment. Within reservoirs though, this changes, and it is possible to quantify sediment transport capacity in terms of hydraulic conditions.

While coarser sediment is generally deposited in the upstream part of a storage reservoir, fine sediments (silt and clay fractions, $d < 0.065$mm) are transported much further into the reservoir. The three main mechanisms of transportation of sediments in reservoirs can be identified, namely turbulent suspended sediment transport, density currents and colloidal suspension (Rooseboom, 1992):

- **Turbulent suspension sediment transport** is the dominant mechanism of sediment transport through most reservoirs and accounts for roughly 96% of the sediment being transported. This mechanism will be discussed thoroughly in this chapter.

- **Density currents** occur primarily on the steep slopes of the deposits within the delta areas of very large reservoirs. They develop where a layer of fluid moves in beneath a layer of lower density (or lower sediment concentration). This mostly occurs during flood events when inflow volumes and sediment concentrations into a reservoir are high and are likely to penetrate deep into the reservoir.

- **Colloidal suspensions** are due to electrostatic forces on very small clay particles, and their transport is therefore not related to the effect of gravity. They fall within the size range of 10^{-3} to 1 micron, between particles that are dissolved and particles that are in turbulent suspension. Colloidal suspension makes a small contribution to total sediment transport through a reservoir (maximum 3%) and is not dealt with in this research.

3.2 Turbulent Sediment Transport

3.2.1 Incipient Motion

The particles on an erosive bed are not perfectly round and they lie on a surface which may be rough and may not be horizontal. The force of the flowing water will only cause motion if the force is sufficient to overcome the natural resistance to motion of the particle. At the interface, the moving water will apply a shear force on the exposed surface of a particle. If this force is gradually increased, a point will be reached where particle movements can be observed. The 'threshold of motion' occurs when widespread sediment motion occurs. The particles will begin to roll along the bed. This type of sediment transport is referred to as bed load. With further increments in the shear force, another point is reached at which the finer particles are swept up from the bed. This defines the inception of a suspended load (Rooseboom, 1992).

Several theories exist for the relationship between the major parameters of the transport processes namely Froude number, sediment properties, fluid properties, shear stress, bed roughness or bed form size and rate of sediment transport.

Shields (1936) showed that particle entrainment was related to a form of Reynolds' number, based on the friction velocity u_*, as shown below. The friction velocity u_* is a reference value that is a function of the fluctuating horizontal components of velocity in turbulent flow, according to Prandtl's model of turbulence.

$$\mathrm{Re}_* = \frac{\rho u_* d}{\mu} \qquad (3\text{-}1)$$

where ρ is the density of the water, d is the particle diameter, and μ is the viscosity of the water. Shields plotted this value against an entrainment function F_s, which is the ratio of shear force to gravitational force:

$$F_s = \frac{\tau}{(\rho_s - \rho)gd} \tag{3-2}$$

where τ is the shear stress applied to the particle by the flowing water, ρ_s is the density of the particle, ρ the density of the water and g the gravitational acceleration. Figure 3-1 indicates that there is a well defined band of results indicating the threshold of motion.

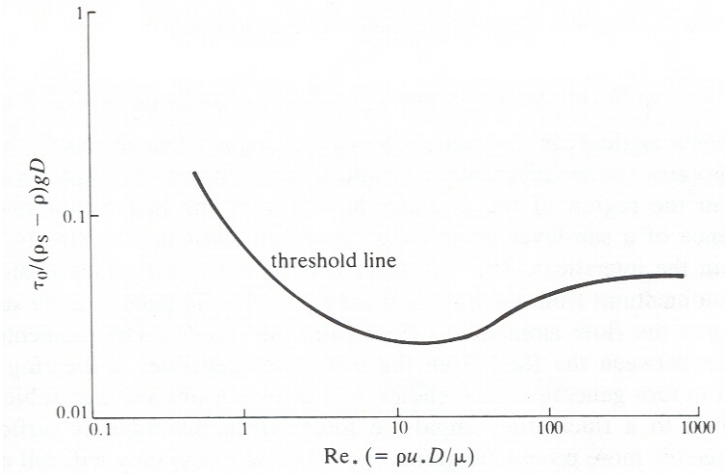

Figure 3-1: Shields' diagram (Chadwick and Morfett, 1998)

This relationship may be used to estimate the minimum stable particle size for a given channel and flow, or the critical shear stress for a given particle size.

The main shortcoming of this method is that transportability is not truly represented by particle size. The settling velocity of particles is a more significant measure in the case of non-cohesive sediments, while cohesive forces play a determining role in the entrainment of cohesive sediments.

3.2.2 The Applied Unit Stream Power Theory (Rooseboom 1975)

Consider a uniform one-dimensional stream with depth of flow D and slope s as in Figure 3-2 below:

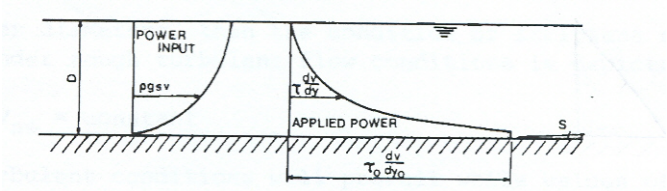

Figure 3-2: Variation in power input and applied power (Rooseboom, 1975)

According to the principle of conservation of power the total amount of applied power equals the total power input and the enclosed areas are thus equal for both laminar and turbulent flow. The term $\tau(dv/dy)$ represents the power applied per unit volume to maintain motion of an element of water whereas the term ρgsv represents the amount of power made available by the element, where v is the velocity at the depth of interest. The value of the applied unit stream power $\tau(dv/dy)$ reaches a maximum value close to the bed.

In the case of **laminar flow**, the shear stress τ can be related to the velocity gradient through the Newtonian equation:

$$\tau = \mu \frac{dv}{dy} \tag{3-3}$$

and the velocity distribution can be found from:

$$v = \frac{\rho gs}{2\mu}\left(2Dy - y^2\right) \tag{3-4}$$

where y is the vertical distance from the bed.

In the case of **turbulent flow**, the shear stress is given by:

$$\tau = \rho l^2 \left(\frac{dv}{dy} \right)^2 \tag{3-5}$$

where l is the mixing length expressed as $l = \kappa y$ where κ is the Von Karman dimensionless constant (equal to 0.4). The velocity at a vertical distance y from the bed for turbulent flow is given by the log-deficiency equation:

$$v = \sqrt{2\pi g D s}.\ln\left(\frac{y}{y_0} \right) \tag{3-6}$$

where y_0 is the distance from the bed at which the velocity is mathematically zero, found by:

$$y_0 \approx \frac{R_0}{14.8} \approx \frac{k_s}{29.6} \tag{3-7}$$

R_0 is the radius of the eddies formed against the bed and k_s is the absolute roughness of the bed.

In turbulent flow it is not possible for turbulent fluid layers to slide over one another as in the case of laminar flow. A thin sectional element over the depth of the fluid therefore has to move as a unit. Since the velocity near the bed equals zero, the only means of movement is through rotation of the element around a point near the bed. Fluid movement in a canal is translational and such movement is only possible if there is a rotation centre point that also translates.

According to the concept of least applied power, flow near a boundary will be either turbulent or laminar, depending upon which type of flow requires the smallest amount of power per unit volume, $\tau(dv/dy)$ to maintain it. This means that where the two alternative modes of flow exist, there will be a laminar sublayer next to a smooth boundary below the turbulent flow zone.

By setting the applied stream power of laminar and turbulent flows equal for a given value of τ, the distance y_1 of this rotational point from the bed, is found by:

$$y_1 = \frac{\sqrt{2\pi}.v}{\sqrt{gDs}} \tag{3-8}$$

This is also the depth of the transition between laminar and turbulent flow. At this level the velocity of laminar flow would be:

$$v = \sqrt{2\pi gDs} \tag{3-9}$$

which is the required translatory velocity of the centre of rotation for turbulent flow.

3.2.3 Incipient Motion Criteria with the Stream Power Theory (Rooseboom, 1992)

For non-cohesive sediments, incipient motion is determined according to the sediment transport model used. The power approach provides us with the ability to define both the transporting capacity of a stream and the effort required to transport material in directly comparable terms.

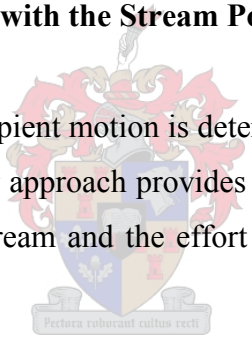

Critical Conditions for Cohesionless Sediment

The applied power required per unit volume to suspend a particle with density ρ_s and settling velocity, w, in a fluid with density ρ equals:

$$\tau\left(\frac{dv}{dy}\right) = (\rho_s - \rho)gw \tag{3-10}$$

where $w \propto \left[\frac{(\rho_s - \rho)gd}{\rho C_d}\right]^{\frac{1}{2}}$ (3-11)

For rough turbulent conditions, the value of the applied unit stream power to maintain motion along the bed is:

$$\tau\left(\frac{dv}{dy}\right) = \frac{\rho g s D\sqrt{gDs}}{d} \tag{3-12}$$

Setting these two equations equal, and assuming that the value of the drag coefficient C_d for determining w is a constant (which is true for large diameters), then the condition of incipient motion under rough turbulent flow conditions is given by:

$$\frac{\sqrt{gDs}}{w} = \text{constant} = 0.12 \tag{3-13}$$

For smaller particles where the value of $\frac{\sqrt{gDs}.d}{v} < 13$ the relationship for incipient motion is found to be:

$$\frac{\sqrt{gDs}}{w} = \frac{1.6}{\frac{\sqrt{gDs}.d}{v}} \tag{3-14}$$

Figure 3-3 shows the critical conditions for cohesionless sediment particles according to the applied stream power principle. Note that V_{ss} in Figure 3-3 equals w, the settling velocity.

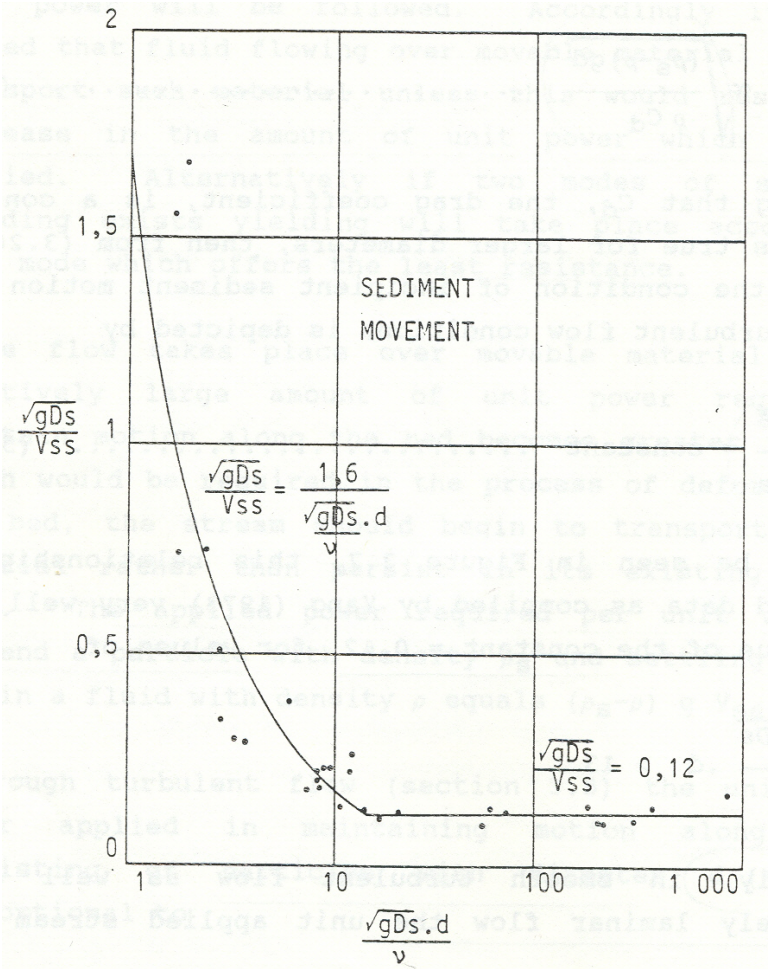

Figure 3-3: Critical conditions for cohesionless particles (Rooseboom, 1992)

Critical Conditions for Cohesive Sediment

In the case of cohesive soils neither particle size nor settling velocity represents erodibility (Rooseboom, 1992). Direct comparison becomes possible if both fluid and sediment movement are considered in similar terms. Incipient movement of cohesive sediment is therefore treated as flow of a medium with high viscosity. With this approximation, Rooseboom and Mulke (1982) developed a system through which initiation of severe erosion along a steep slope can be forecast. Incipient motion conditions for cohesive sediment are usually described by shear stress at the bed.

In the MIKE 21C software that will be used to model the transport of fine sediment in this research, a critical shear stress for erosion is specified. Erosion will commence at a rate of erosion, E, as soon as the bed shear stress exceeds this value, according to the erosion function:

$$E = E_0 \left(\frac{\tau}{\tau_{ce}} - 1 \right)^m, \quad \tau > \tau_{ce} \tag{3-15}$$

where E_0 and m are the dimensionless coefficient and exponent and τ_{ce} is the user specified critical shear stress for erosion. Very little information is available on estimating a value for this parameter. The higher the percentage of fine material on the bed, the higher stresses will be required to erode the bed because of the cohesiveness. Throughout this research, a critical shear stress value of 1.04 N/m^2 is used for a cohesive bed.

3.2.4 Suspended Load and Bed Load

If water is flowing, it can carry suspended particles. The settling velocity of a suspended particle, *w*, is given by Stoke's Law (Chadwick and Morfett, 1998):

$$w = \frac{(\rho_s - \rho) g d^2}{18 \mu} \tag{3-16}$$

As there will always be a range of different particle sizes in the flow, some will have sufficiently large diameters that they settle on the river or stream bed, but still move downstream. This is known as bed load and the particles are transported via mechanisms such as saltation, rolling and sliding.

3.3 Traditional Equilibrium Sediment Transport Theories

Equilibrium in this case refers to actual sediment transport being equal to the transport capacity at a section. This is a realistic approach only when coarse sediments are transported without any constraints of sediment availability.

These sediment transport equations have thus been tested and calibrated for sand transport only and not for fine sediment. These equations basically consists of two groups: the equations that predict bed load and suspended load separately and those that predict a total sediment load. Traditionally, the equations of hydraulics and sediment transport are based on the conservation of mass, energy and momentum. Most of these are for river applications and not for reservoir applications. Four existing theories are presented in the following paragraphs as described by Basson and Rooseboom (1997):

a) Engelund and Hansen (1967)

Engelund and Hansen related input power per unit area of channel boundary to sediment discharge using dimensional analysis and proposed the following relationship:

$$\frac{2gDs}{v^2}\phi = 0.1 \cdot \theta^{5/2} \tag{3-17}$$

The Engelund and Hansen coefficients, ϕ and θ, are described by:

$$\phi = \frac{Q_s}{\sqrt{\left(\frac{\gamma_s - \gamma}{\gamma}\right) g d^3}} \quad \text{and} \quad \theta = \frac{\rho g D s}{(\gamma_s - \gamma) d}$$

The total sediment discharge in then given by:

$$Q_s = \frac{v^2}{20gDs}\sqrt{\left(\frac{\gamma_s - \gamma}{\gamma}\right) g d^3} \cdot \left(\frac{\rho g D s}{(\gamma_s - \gamma) d}\right)^{5/2} \tag{3-18}$$

where:

D = Flow depth
g = Gravitational acceleration
v = Flow velocity
s = Slope
Q_s = Total sediment discharge
γ = Specific weight of water
γ_s = Specific weight of sediment
d = sediment diameter

b) Ackers and White (1973)

Also by using dimensional analysis, Ackers and White derived an equation representing total sediment discharge in terms of three dimensionless numbers; a sediment transport function G_{gr}, a mobility number F_{gr} and a dimensionless sediment particle size d_{gr}:

$$G_{gr} = c'\left(\frac{F_{gr}}{A} - 1\right)^m = \frac{c'D}{\gamma_s d/\gamma}\left(\frac{\sqrt{gDs}}{v}\right)^n \tag{3-19}$$

$$F_{gr} = \frac{\left(\sqrt{gDs}\right)^n}{\sqrt{gd\left(\gamma_s/\gamma - 1\right)}}\left(\frac{v}{\sqrt{32}\log(10D/d)}\right)^{1-n} \tag{3-20}$$

$$d_{gr} = \left(\frac{g\left(\gamma_s/\gamma - 1\right)}{\upsilon^2}\right)^{1/3} \tag{3-21}$$

where υ = kinematic viscosity, equal to 10^{-6} m^2/s. The coefficients c', A, m and n are functions of sediment particle size and have the following values for coarse sediment where $d_{gr} > 60$: $n=0$, $A=0.170$, $m=1.50$ and $c'=0.025$. For values of $d_{gr} < 60$, their values are given by these equations:

$$n = 1 - 0.56\cdot\log(d_{gr}),\ A = \frac{0.23}{\sqrt{d_{gr}}} + 0.14,\ m = \frac{9.66}{d_{gr}} + 1.34 \text{ and}$$

$$\log c' = 2.86\cdot\log(d_{gr}) - \log^2(d_{gr}) - 3.53$$

c) Van Rijn (1984)

In this transport model the sediment load is divided between bed load and suspended load according to the relative magnitudes of the bed shear velocity, and the particle falling velocity. When the bed shear velocity exceeds the falling velocity, sediment is transported as both suspended and bed load.

Van Rijn Bed Load

Bed load is considered to be transported by rolling and saltation and the rate is described as a function of saltation height. The reference concentration is determined from the bed load transport. Bed load is computed from the product of particle velocity, u_{bs}, saltation height, δ_b, and the bed load concentration, C_b:

$$q_b = u_{bs}\delta_b C_b \tag{3-22}$$

Expressions for the particle velocity and saltation height were obtained by numerical solving of the equations of motion applied to a solitary particle. These expressions are given in terms of two dimensionless parameters which are considered to adequately describe bed load transport; a dimensionless particle diameter, D_*, and a transport stage parameter, T, as defined below:

$$D_* = d_{50}\left[\frac{(s-1)}{v^2}g\right]^{1/3} \tag{3-23}$$

$$T = \frac{\left(u_g\right)^2 - \left(u_{f,cr}\right)^2}{\left(u_{f,cr}\right)^2} \tag{3.24}$$

where u_g is the bed shear velocity, related to grains, u is the mean flow velocity, $u_{f,cr}$ is the Shields critical bed shear velocity and d_{50} is the median particle diameter. u_g is the effective bed shear and is so defined in order to eliminate the influence of bed forms since form drag was not considered to contribute to bed load transport.

Extensive analysis of flume measurements of bed load transport yielded the following expression for the bed load concentration:

$$C_b = 0.18\frac{T}{D_*}C_0 \tag{3.25}$$

where C_0 is the maximum bed concentration.

Combining equations for particle mobility and saltation height with equation 3.25 gives the following expression for bed load transport, q_b, valid for particles in the range of 0.2mm to 2.0mm.

$$q_b = \frac{0.053 \cdot T^{2.1}}{D_*^{0.3}}\sqrt{(s-1)gd_{50}^3} \tag{3.26}$$

Van Rijn Suspended Load

The suspended load is determined from the depth-integration of the product of the local concentration and flow velocity. The suspended load method is based on the computation of a reference concentration determined from the bed load transport, thus the reference concentration, C_a, is described as a function of D_* and T.

$$C_a = 0.015\frac{d_{50}T^{1.5}}{aD_*^{0.3}} \tag{3.27}$$

where the reference level, *a*, at which the bed concentration is determined is given by:

$$a = \max\begin{pmatrix} 0.01h \\ 2d_{50} \end{pmatrix}$$

where *h* is the water depth.

Van Rijn (1984) derived the following expression for the suspended load:

$$q_s = FuDC_a \tag{3.28}$$

in which $F = \dfrac{\left[\dfrac{a}{D}\right]^{z'} - \left[\dfrac{a}{D}\right]^{1.2}}{\left[1-\dfrac{a}{D}\right]^{Z'}\left[1.2 - Z'\right]}$ (3.29)

where the modified Rouse suspension number is given by $Z' = z + \psi$, and the correction factor, ψ, is given by: $\psi = 2.5\left[\dfrac{w}{u_g}\right]^{0.8}\left[\dfrac{C_a}{C_0}\right]^{0.4}$ for values of ψ between 0.1 and 1.0 with z the Rouse suspension parameter and u_g the bed shear velocity.

The Van Rijn equations are based on several empirical relationships and draws the distinction between bed load and suspended transport which cannot be justified from fundamental theory. The equations do however provide for changes in bed roughness and energy dissipation for different flow regimes and sediment transport modes.

d) Unit (input) stream power (Yang, 1973, Rooseboom, 1975)

The basic principles of this approach were proven in South Africa in 1974 and has since been used in the planning and design of various reservoir sedimentation studies.

Rooseboom (1975) found that the suspension theory (Rouse, 1937) can be used to describe both bed and suspended load and the incipient motion criteria, and is therefore well suited to analysis of total carrying capacity.

Sediment transport capacity per unit width in terms of flow parameters can be calculated if it is assumed that sediment particles are transported at the same velocity as the fluid:

$$q_s = \int_{y_0}^{D} Cv \cdot dy \qquad (3\text{-}30)$$

where:

$C \propto \left(\tau \dfrac{dv}{dy}\right)^z$ and $\tau \dfrac{dv}{dy}$ the applied power,:

C = Sediment concentration
τ = Bed shear stress
w = Settling velocity
κ = Von Karman coefficient

$z = \frac{w}{\kappa\sqrt{gDs}}$ is the suspension theory coefficient and y_0 the distance from the bed where $v = 0$ mathematically, which after integration leads to an equation of the form (Rooseboom, 1975):

$$\log\frac{q_s}{q} = \alpha_1 \log\bar{vs} + \log\left(\frac{\alpha_1\alpha_2 C_0}{\frac{\left(sD\sqrt{2\pi gDs}\right)^{z_1}}{y_0}}\right) \tag{3-31}$$

where:

α_1, α_2 = Coefficients
z_1 = The suspension theory coefficient as derived by Rooseboom (1975)
C_0 = Sediment concentration at the bed where $v = 0$ at $y = y_0$
$\bar{v}$ = Average flow velocity

Yang (1972) found that equation 3-31 described sediment transporting capacity particularly well. Yang used a slightly different approach by including a critical stream power value for incipient motion in equation 3-32 below. The equation by Yang was, however, only calibrated with laboratory data.

$$\log\left(\frac{q_s}{q}\right) = \alpha_3 + \alpha_4 \cdot \log(\bar{vs} - vs_{cr}) \tag{3-32}$$

with α_3, α_4 a constant and coefficient, vs_{cr} the critical input stream power for incipient motion. Yang (1973) then also defined sediment transport capacity in terms of the settling velocity, w:

$$\log\left(\frac{q_s}{q}\right) = \alpha_5 + \alpha_6 \cdot \log\left(\frac{\bar{vs} - vs_{cr}}{w}\right) \tag{3-33}$$

with α_5 and α_6 the constant and coefficient respectively and w the settling velocity. The last term in equation 3-31 was found not to vary considerably and can be equated to the α_5 coefficient of Yang.

In 1984, Yang proposed a gravel transport equation with an incipient motion term. The maximum sediment transport capacity of a stream can therefore be determined by an equation of the type:

$$\log \frac{q_s}{q} = \alpha \cdot \log \bar{v}s + \beta \qquad (3\text{-}34)$$

where $\bar{v}s$ represents the average input unit stream power at a cross-section in a reservoir or river, and α = coefficient and β = constant.

3.4 Non-equilibrium Sediment Transport

3.4.1 Cohesive Sediment

Cohesive sediments are very fine (d < 0.065mm) negatively charged clay minerals which have a certain capacity to absorb cations. Small particles (d < 0.002mm) can remain in colloidal suspension for a long time because of the repulsive magnetic forces between them. Cohesive sediments are normally transported as suspended load.

Deposits of cohesive sediment are held together by the bonding force of positive and negative ionic charges of the clay minerals. Cohesive sediments are characterized by two main properties: plasticity and cohesion, due to surface physico-chemical forces on the sediment particles smaller than 2 microns. Under the influence of these and fluvial conditions, colliding fine particles stick to each other forming agglomerations known as flocks, with sizes and settling velocities exceeding by orders of magnitude those of the individual particles.

The boundary between cohesive and cohesionless sediment is not clearly defined and generally varies with the type of sediment. Dominance of interparticle cohesion over

gravitational force increases with decreasing particle size. Thus the effect of cohesion on the behaviour of clays (< 0.004mm) is much more pronounced than on silts (0.004-0.065mm). Beck and Basson (2003) found that with as little as 7% clay and silt in sediment mixtures the sediments will effectively have the properties of cohesive sediments. For reservoir conditions, it is of utmost importance to forecast the transport of fine sediments (silt and clay), since in most South African impoundments they form the main sediment body. In practice, the prediction of the transport of fine sediments within reservoirs is based on different approaches:

- Use of the diffusion equation by Zhang (1980) as discussed in section 3.4.3
- Use of the equilibrium sediment transport equations which were recalibration with fine sediment transport data
- Combinations of sediment transport equations for sand fractions and diffusion equations for fine sediments
- Use of computational models such as DHI's 2-dimensional MIKE 21C with an advection-dispersion model for the transport of fine sediment.

3.4.2 Non-equilibrium Sediment Transport Background

With the equilibrium transport equations, a state of sediment equilibrium is reached within each time step of the calculation. Equilibrium refers to actual sediment transport being equal to the transport capacity at a section. It is assumed that the sediment load at the next section is equal to the capacity at that section for the same time-step and that the difference in sediment between the two sections will either deposit or erode during that time-step. This assumption is called instantaneous adaptation and is only valid for the transport of coarse sediment.

With fine sediments, however, the adjustment to the saturated sediment transport capacity is not instantaneous and time and distance lags are associated with the change in sediment transport, until equilibrium is reached. This lag, often called "adaptation length", is due to the extremely small settling velocities of the fine sediments (Basson and Rooseboom, 1997).

Two types of non-equilibrium sediment transport modes can be identified (Batuca and Jordaan, 2000):

- **Undersaturated transport** occurs when the availability of the sediment from surface erosion is limited and the actual sediment concentration is less than the transport capacity.

- **Oversaturated transport** occurs as the sediment concentration exceeds the transport capacity. Adaptation lengths can even be longer than the reservoir itself in the case of very fine sediments in deep reservoirs.

3.4.3 Non-equilibrium Sediment Transport Theories for Steady Flow (Rooseboom and Basson, 1997)

a) Mehta and Partheniades (1973) showed that suspended sediment concentration in reservoirs diminishes rapidly from an initial value, C_o, to a constant equilibrium concentration value, C_{eq}. The value of C_{eq} decreases with decreasing bed shear stress, τ, becoming zero at a threshold value of $\tau_{b\min}$. It was shown that the ratio of relative equilibrium concentration, $C_{eq}^{*} = C_{eq} / C_o$, remained constant, independent of the initial concentration, C_o, but dependant on the bed shear stress, τ.

This adjustment to a single equilibrium concentration is attributed to the adjustment of the stream power to minimize energy dissipation. This equilibrium is not the maximum equilibrium sediment transport, but rather an undersaturated transport due to limited sediment availability.

b) Han and He (1990) calibrated non-equilibrium equations with field data and established criteria for non-equilibrium sediment transport calibration coefficients for rivers and reservoirs. Most of these equations have the format of a steady advection-dispersion equation.

Sediment transport estimations were until recently done by using an equilibrium transport equation, although sediment transport is often in non-equilibrium. Equilibrium formulae based on uniform flow experiments in hydraulic laboratories are no longer considered as a satisfactory component of a mobile-bed modelling system. Time and space lags between actual and equilibrium transported sediment load should therefore be considered (Cunge, 1989).

c) Zhang (1980) found the basic equation of 2D diffusion to be of the form:

$$v\frac{\partial C}{\partial x} = \in \frac{\partial^2 C}{\partial z^2} + w\frac{\partial C}{\partial z} \tag{3-35}$$

with:

C = Sediment concentration
$\in$ = Coefficient of turbulent exchange
w = Settling velocity of sediment particles
v = Flow velocity

Zhang determined the analytical solution for **deposition** as:

$$\frac{dC_{cp}(x)}{dx} = \propto w\left[C_{Kp} - C_{Cp}(x)\right]/q \tag{3-36}$$

with the following boundary conditions:

- at the water surface: $z = D,\ \in\frac{\partial C}{\partial z} + wC = 0$
- on the reservoir bed: $z = 0,\ \frac{\partial C}{\partial z} = -\frac{w}{\in}C_{K,0} = \text{constant}$
- at the entrance to the reservoir: $x = 0,\ \mathrm{C} = \mathrm{C}_0 \cdot f(z)$

By substituting initial conditions, $x = 0,\ C_{cp}(x) = C_0$, the final expression of the rate of change in sediment concentration along the reservoir is:

$$q_s = q_{st} + e^{(-\propto wx/q)}(q_{s0} - q_{st}) \tag{3-37}$$

with:

q_s = Sediment discharge per unit width at the exit
q_{st} = Sediment carrying capacity
q_{s0} = Sediment discharge per unit width at the entrance

In the case of **erosion**, the same equation can be derived:

$$q_s = q_{st} + e^{(-\propto wx/q)}(q_{s0} - q_{st}) \tag{3-38}$$

If $\xi = e^{(-\propto wx/q)}$ denotes sediment transport under non-equilibrium conditions, the final expression for ξ, with the inclusion of the empirical coefficients (K_3, K_4 and K_5) reads:

For deposition: $\xi_1 = \exp\ (-K_3\ C^{K_4}(0.41 - 0.77/gC)\cdot(x/q))$ (3-39)

For erosion: $\xi_2 = \exp\ (-K_5\ Q^{0.3}\ s^{0.5}\cdot(x/q))$ (3-40)

d) Soares (1982) derived equations for non-equilibrium suspended sediment transport, similar to those of Zhang (1980). The mass balance of sediment of a given size d_j is:

$$Q\left(\frac{\partial C^j}{\partial x}\right)\Delta x = (-q_d^j + q_e^j)T\Delta x \tag{3-41}$$

q_d^j, q_e^j = Fluxes of deposition and erosion of sediment
Q = Flow rate
T = Width
($\frac{\partial C}{\partial t}$ is neglected in this equation)

Let $CT^{*j}=$ average concentration of sediment transporting capacity, then if $CT_i^j > CT_{i+1}^{j*}$ (deposition), the rate of deposition:

$q_d^j = -w_j(C^j - CT^{j*})$ and equation 3-41 becomes:

$$\frac{\partial C^j}{\partial x} = -w_j(C^j - CT^{j*})T/Q \qquad (3\text{-}42)$$

Integrating between two sections:

$$C_{i+1}^j = (C_i^j - CT_{i+1}^*)\ \exp\ (-w_j \Delta x T/Q) \qquad (3\text{-}43)$$

if $C_i^j \le CT_{i+1}^*$ (erosion will occur depending on the availability of sediment of the given size, d_j, on the stream bed.

The rate of erosion: $q_e^j = \lambda(C_b^j - C^j)$ (3-44)

Erosion is proportional to the difference between the availability on the bed and the concentration carried by the flow. Although erosion is dominant, deposition will still occur at rate $w_j C^j$ and equation 3-41 becomes:

$$\frac{\partial C^j}{\partial x} = -(C^j - \frac{\lambda_j}{\lambda_j + w_j} C_b^j)\frac{T}{Q}(\lambda_j + w_j) \qquad (3\text{-}45)$$

Integration of equation 3-45 between sections i and $i+1$ yields:

$$C_{i+1}^j = \left(C_i^j - \frac{\lambda_j}{\lambda_j + w_j} C_b^j\right)\ \exp\ \left[-\left(\lambda_j + w_j\right)\frac{T\Delta x}{Q}\right] + \frac{\lambda_j}{\lambda_j + w_j} C_b^j \qquad (3\text{-}46)$$

When Δx is large, flow in section $(i+1)$ will approach it's transport capacity CT_{i+1}^{j*}:

$$CT_{i+1}^{j*} = \frac{\lambda_j}{\lambda_j + w_j} C_b^j \tag{3-47}$$

and the final equation is:

$$C_{i+1}^{j} = CT_{i+1}^{j*} + (C_i^j - CT_{i+1}^{j*}) \exp\left[-\frac{T \Delta x}{Q} (\lambda_j + w_j) \right] \tag{3-48}$$

which is similar to the equations presented by Karanshev (1963) and Zhang (1980).

e) Di Silvio (1995) proposed the use of the following non-equilibrium transport equation:

$$\frac{\partial C_i}{\partial x} = \frac{1}{L_i^*} (\beta_i C_{ci}^* - C_i) \tag{3-49}$$

where:

C_i = the actual sediment transport per fraction
β_i = the percentage of i-th fraction in the bed composition
L_i^* = the adaptation length for each fraction
C_{ci}^* = the transport capacity of the i-th fraction

For fine particles, $L_i^* \to vD / w_i$, which means that the adaptation length of silt and clay may be even larger than the length of the reservoir.

All the non-equilibrium sediment transport theories and equations that have been discussed in the preceding paragraphs were derived for steady flow conditions. Reservoir sedimentation processes are highly dynamic and it has therefore been decided to describe them by using an unsteady advection-dispersion equation.

3.5 Advection and Dispersion

Terminology on the subject of advection and dispersion frequently differs from engineering to chemical and geological literature. For the remainder of this research, the processes of advection and dispersion will be defined as follows:

When a fluid of higher sediment concentration is injected at a point into a turbulent flow it will be subjected to two distinct processes: (a) it will be swept along (advected) with a velocity comparable to that of the flow and (b) it will be mixed (diffused) due to turbulence and molecular diffusion. Diffusion due to turbulence is normally two or more orders of magnitude larger than molecular diffusion, so the latter will be omitted from further consideration. Dispersion is then the combination of advection and diffusion (Chadwick and Morfett, 1998).

The 1D unsteady advection-dispersion equation has the following form (Basson and Rooseboom, 1997):

$$\frac{\delta C}{\delta t} + u\frac{\delta C}{\delta x} - D\frac{\delta^2 C}{\delta x^2} = ss \qquad (3\text{-}50)$$

where:

D = The one-dimensional dispersion coefficient
u = Flow velocity
t = Time
x = Distance in the direction of flow

The source/sink (ss) term represents the increase in suspended sediment concentration as a result of erosion and also the decrease in the concentration due to deposition of the suspended sediment.

In the case of **non-cohesive** sediments the source/sink term is represented by:

$$ss = \frac{(C^* - C)}{aT} \qquad (3\text{-}51)$$

where:

C^* = The equilibrium sediment transport calculated with a sediment transport formula
T = The time scale defined as settling time (water depth divided by settling velocity)
a = A calibration parameter and can be interpreted as a mean settling depth

Basson and Rooseboom (1997) used suspended sediment concentration data from a series of channel tests to calibrate the parameter a for non-equilibrium transport of sediments using the MIKE 11 software for one-dimensional modelling. Thereby certain value ranges for a were established for the finer fractions of various sediment types.

For **cohesive** sediment fractions the source/sink term should be represented by:

$$ss = 0 \;;\; \tau < \tau_{ce} \qquad \text{(No erosion)}$$

$$ss = E\left(\frac{\tau}{\tau_{ce}} - 1\right)^m \;;\; \tau_{ce} < \tau < \tau_{cme} \qquad \text{(Surface erosion)}$$

$$ss = \frac{\left(C^* - C\right)}{\Delta t} \;;\; \tau > \tau_{cme} \qquad \text{(Mass erosion, no lag)}$$

where:

τ = Bed shear stress
τ_{ce} = Critical shear stress for erosion
τ_{cme} = Critical shear stress for mass erosion
E = Erosion rate

The source/sink term usually includes a deposition function that is implemented once the bed shear stress has exceeded the critical shear stress for deposition, τ_{de} (DHI, 2003):

$$D = w_s c\left(1 - \frac{\tau}{\tau_{cd}}\right) \ , \ \tau < \tau_{cd} \qquad (3\text{-}52)$$

where:

w_s = Settling velocity
τ_{cd} = Critical shear stress for deposition
c = Concentration

3.6 Integrated Mathematical Modelling of Unsteady Flow, Suspended Sediment Transport and Morphological Change

3.6.1 Background

Reservoir sedimentation and morphological processes are amongst the most complex and least understood phenomena in nature. In early times, the sedimentation research methodologies were primarily based on field observation and physical modelling. This chapter is focused on the methodologies of mathematical modelling, more precisely numerical-empirical modelling which is sometimes referred to as computational modelling. Although sedimentation, as a science, only has a sixty-year history and some of the fundamental problems are still unclear, it is nevertheless possible to predict sediment transport through mathematical modelling (Wang and Wu, 2004).

The initial attempts in application of mathematical models in conjunction with empirical functions obtained from laboratory experiments to the investigation of river sedimentation and morphological processes can be found in the 1950's.

The basic equation for non-equilibrium sediment transport was first obtained by Dou (1963) using a heuristic approach in his study of tidal flows. It was later elaborated and derived mathematically by Han (1980), Lin and Shen (1984) and Lin et al. (1983) for both 1D and 2D cases.

The three-dimensional transport of suspended sediment is governed by the equation (Zhou et al. 2004):

$$\frac{\partial c}{\partial t}+\frac{\partial}{\partial x_i}u_i c-\frac{\partial}{\partial x_i}v_s\frac{\partial c}{\partial x_i}=w\frac{\partial c}{\partial x_3}\qquad (i=1,2,3) \tag{3-53}$$

where c is the sediment concentration, x_i the spatial coordinates, u_i the flow velocities, v_s the coefficients of diffusion, w the settling velocity of sediment particles and t the time duration. The transport equation for one- and two-dimensional problems may be obtained by integrating equation 3.53 over a cross-section (1D) or a depth (2D) with suitable conditions imposed at the loose bed. Thus the following depth- and section-integrated equations are obtained for 2D and 1D cases, respectively (Zhou and Lin, 1998):

2D) $$\frac{\partial C}{\partial t}+\frac{\partial U_i C}{\partial x_i}=-\alpha\frac{w}{h(C-\phi)}\qquad (i=1,2) \tag{3-54}$$

1D) $$\beta^s\frac{\partial S}{\partial t}+V\frac{\partial S}{\partial x_1}=-\alpha^s\frac{w}{D}(S-\Phi) \tag{3-55}$$

where C and U are respectively the depth-averaged sediment concentration and flow-velocity, S the section-averaged sediment concentration, V the section-averaged flow velocity and, h the depth of flow for the 2D case. D the section-averaged depth of water for the 1D case, and ϕ and Φ the depth–integrated and section averaged transport capacities, respectively. Falconer and Owens (1990) defined the adjustment coefficient as the ratio of the bed layer concentration to the depth-averaged concentration; $\alpha = c_a / C$.

Equation 3.53 is free from any empirical parameters. The equations for 2D and 1D cases however contain parameters α, ϕ and Φ that must be determined before these equations may be solved. For 3D computations, properly imposed boundary conditions over the bed must be given. There are several possible ways to accomplish this. For example, one may adopt the concentration at a reference level (Dirichlet

condition), or a gradient bed layer concentration (Neumann condition), or a combination of the two (mixed condition) (Zhou et al., 2004)

This branch of research was intensified and broadened in the 1970's. Since then a number of 1D models (eg. Cunge *et al*.,1980; Thomas, 1982; Rahuel and Holly, 1989; Wu and Vieira, 2002) were applied to sedimentation studies in rivers and reservoirs. More recently, numerous 2D and 3D numerical-empirical (eg. Sheng, 1983; Wang and Adeff, 1986; Spasojevic and Holly, 1993; Jia and Wang, 1999; Wu *et al*., 2000) have been developed to simulate sediment transport processes and morphological changes in channels with mobile bed and banks, both in the laboratory and in nature.

In the early development stage, the sediment transport model only considered either bed load or suspended load with a single representative size. Realistically, sediments in rivers are often heterogeneous (non-uniform) in size, not to mention that they have variable shape and density. Furthermore, the transport mode changes from bed load to suspended load and vice versa with flow conditions.

Traditionally, the transport of sediment, especially bed load, was simulated based on the assumption of local instantaneous equilibrium. Due to the observed spatial and temporal lags between the sediment motion and water flow, it was found that the traditional equilibrium transport models need to be improved to take into account the non-equilibrium features of sediment transport, especially under unsteady flow conditions (Wang and Wu, 2004).

To meet the needs in engineering practice, the capability of river and reservoir sedimentation modelling have been further advanced remarkably in recent years. Many established models are capable of simulating non-cohesive and cohesive sediment transport, local scouring, channel widening and meandering.

3.6.2 Mathematical Model Assumptions

The phenomena of flow and sediment transport in rivers are characterised by turbulence, free-surface variation, bed change, phase interaction, etc. A model capable of including all of these effects accurately has yet to be developed. At the present, most sediment transport models have adopted the following assumptions (Wang and Wu, 2004):

- Sediment concentration is so low that the interaction between flow and sediment movement can be neglected. Therefore, the clear-water flow and the sediment transport equations can be solved separately.

- Bed change is much slower than flow movement. Therefore, at each time-step the flow can be calculated assuming a "fixed" bed.

- The hiding and exposure mechanism in bed material is considered through the introduction of correction factors in the non-uniform sediment transport capacity formulas. The interactions among different size classes of moving sediment are ignored. Thus the transport of each size class of sediment can be handled individually.

Based upon the above assumptions, 1D, 2D and 3D governing equations of flow, sediment transport and morphological changes have been developed. These equations will be discussed in detail in the following sections.

3.6.3 One-dimensional Mathematical Modelling

One-dimensional models are mostly used in river and reservoir applications around the world, although computationally "heavy" two-dimensional and even 3D models have been developed. With 1D modelling, conditions are averaged over the width and depth, so that variations are limited to the x direction i.e. the direction of the mean velocity of flow. It must be emphasized that the concentration is assumed to be fully mixed over the cross section.

With laterally integrated 1D models, the shallow water flow is governed by the well-known St.Venant equations. The sediment transport can be separated as bed load and suspended load according to sediment transport models. The governing equation for the non-equilibrium transport of non-uniform sediments is (Wang and Wu, 2004):

$$\frac{\partial(AC_{tk})}{\partial t}+\frac{\partial Q_{tk}}{\partial x}+\frac{1}{L_s}\left(Q_{tk}-Q_{t*k}\right)=q_{lk}\quad(k=1,2,...,N) \tag{3-56}$$

where:

t = Time
A= Flow cross-section
x = Longitudinal coordinate
C_{tk} = Section averaged sediment concentration
Q_{tk} = Actual sediment transport rate
Q_{t*k} = Sediment transport capacity or the so-called equilibrium transport rate
L_s = Non-equilibrium adaptation length
q_{lk} = Side inflow or outflow sediment discharge from bank or tributary streams per unit channel length
k = Representative sediment size class
N= Total number of size classes

This equation can be applied to bed load or suspended load depending on how the sediment transport rate and the adaptation length are defined. For example, defining $L_s=Uh/(\alpha w_{sk})$, $Q_{tk}=QC_{tk}$ and $Q_{*tk}=QC_{*tk}$, one can rewrite equation 3-56 as the commonly used suspended load transport equation with the exchange term $\alpha w_{sk}(C_{tk}-C_{*tk})$. Here, U is the section averaged velocity, h is the flow depth, w_{sk} is the settling velocity of sediment particles, α is the non-equilibrium adaptation or recovery coefficient, and C_{*tk} is the suspended load transport capacity. When equation 3-56 is applied to the bed load, the transport rate Q_{tk} is the sum of bed load and suspended load transport rates. The bed deformation due to size class k is determined by means of:

$$(1-p')\left(\frac{\partial A_b}{\partial t}\right)_k=\frac{1}{L_s}(Q_{tk}-Q_{*tk})\quad(k=1,2,...,N) \tag{3-57}$$

where p' is the bed material porosity and $(\partial A_b / \partial t)$ is the bed deformation rate caused by size class *k*. Combining equations 3-56 and 3-57 leads to the sediment continuity equation, which could also be used to calculate the bed deformation.

It should be noted that as the sediment size increases, the adaptation length L_s reduces. As a result, the exchange term becomes dominant in equation 3-56. In such a case, equation 3-56 reduces to $Q_{tk} = Q_{*tk}$, which is the traditional assumption of local equilibrium. Therefore, the equilibrium sediment transport model is a special case of the non-equilibrium transport model.

The sediment transport capacity can be written in a general form as:

$$Q_{*tk} = p_{bk} Q_{tk}^{*} \tag{3-58}$$

where p_{bk} is the availability factor of sediment, which is defined here as the bed material gradation in the mixing layer and Q_{tk}^{*} is the potential sediment transport capacity for size class *k*, which can be determined with the help of empirical relationships.

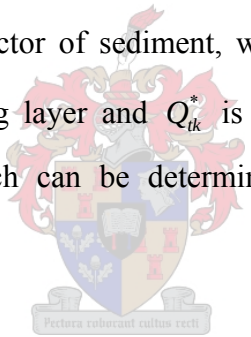

3.6.4 The Non-equilibrium Adaptation Length

The non-equilibrium adaptation length L_s, which characterises the distance required for sediment to adjust from a non-equilibrium state to an equilibrium state, is a very important parameter in the non-equilibrium transport model. Traditionally, the non-equilibrium adaptation length of suspended load is given with $L_s = Uh/(\alpha w_{sk})$. The coefficient α can be calculated with the method of Armanini and Di Silvio (1988) or other semi-empirical methods. Values of α calculated from these methods are usually larger than 1. However, in practice, α has been given different values by many researchers, most of them being less than 1. It has been suggested that α=1 for the case of strong erosion, α = 0.25 for strong deposition and α = 0.5 for weak deposition and erosion (Wang and Wu, 2004).

3.6.5 One-dimensional RESSASS Model: Tarbela Reservoir, Pakistan (HR Wallingford, 1998)

a) Background

Tarbela Dam was built between 1970 and 1975 and is located on the Indus River. The dam is vital to Pakistan's economy as it provides 40% of the country's water storage, crucially important for irrigation during the dry season, and 35% of the country's energy requirements from hydroelectric generation. About 25% of the original live storage had been lost and the sediment delta was approaching the dam by 1997.

b) Description of the Model

The mathematical model RESSASS of HR Wallingford was used to simulate reservoir sedimentation in Tarbela Reservoir. The model is one-dimensional in the sense that all hydraulic variables are considered constant at any cross-section at any particular time. The model is based on the equations that describe flow and sediment movement. Within the model, sediment transport calculations are carried out for a range of different sediment sizes. The model is a time-stepping one, that is, initial conditions are input to equations which predict water levels and bed levels a short time later, typically one day. These predictions then provide the input conditions for the next time step. The process is repeated many times to make predictions over the required time period. Cross-sections are used to specify the geometry of the reservoir. The model then predicts revised bed levels and the location and composition of sediment deposits.

The model runs on a 60 year sequence of sediment and water inflows. The sequence consists of the 1967 to 1996 inflows to Tarbela repeated once to give the required 60 year sequence. The inflows are based on the flow records at Besham Qila, located upstream of the reservoir. The sediment inflows were calculated using the sediment rating equation on these inflows together with the Ackers and White equation. For the model verification runs, the model water levels were matched to the observed levels since the first impoundment of the reservoir.

The model operates with the following boundary conditions:

- Variations of incoming flow with time
- Corresponding variations of incoming sediments with time
- Variations of water level at the dam as defined by the operating policy

This means that, at any particular time, the model computes the outflow through the dam (the model does not take into account where that outflow occurs or whether the infrastructure at Tarbela is capable of delivering that discharge). It also computes the outflow of sediments at any particular time based on flow conditions immediately upstream of the dam.

c) Verification of the Model Performance

The model was verified by simulating the observed sediment deposition from the date of impoundment to 1996. The observed flow sequence at Besham Qila from 1975 was used together with the appropriate sediment rating curve. Observed historic reservoir water levels were used for the downstream boundary conditions. Based on field observations, the model was set up with two sand sizes, 0.155mm and 0,200mm, and five silt sizes giving a range of settling velocities between 0.000002m/s and 0.0036m/s. With these realistic parameters the model gave good agreement between observed and predicted bed levels and volumes of deposition. Figure 3-4 shows the predicted and observed stage-storage curves for 1996, respectively.

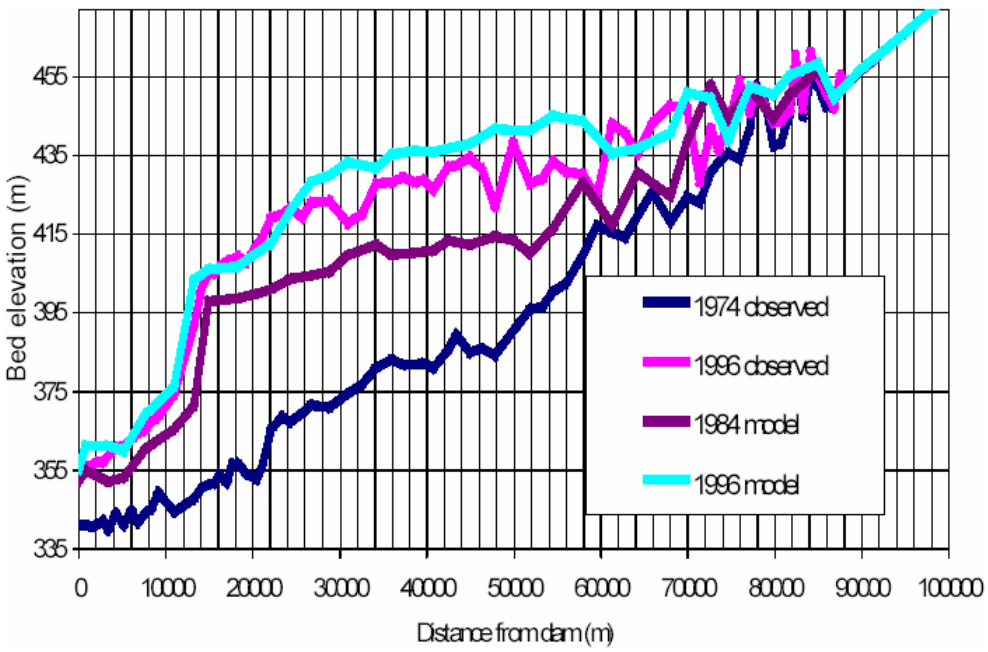

Figure 3-4: Simulated and surveyed longitudinal profile of Tarbela Reservoir (HR Wallingford, 1998)

It can be seen that agreement between the model and the observed values is good. The agreement between the observations and predictions is particularly good close to the dam. One can state that the model is representing the processes of sediment deposition within Tarbela Reservoir accurately.

3.6.6 Two-dimensional Mathematical Modelling

Two-dimensional modelling is of specific benefit when considering (Basson and Rooseboom, 1997):

- deposition outside the main channel across the wide-open reservoir basins often encountered in South Africa.
- sediment build-up at a specific position in a reservoir, such as at a tunnel intake; and
- modelling of flushing when sediment transport conditions vary across the main channel.

3.6.7 The Quasi-2D Stream Tube Concept

A simple approach to two-dimensional modelling may be used for reservoirs. In this the reservoir is assumed to be sub-divided into a series of stream-tubes (Batuca and Jordaan, 2000).

Lopez (1978) most probably developed the first quasi two-dimensional models for reservoir sedimentation, based on the stream tube concept of Holly and Cunge (1975). The river-reservoir system was divided for modeling purposes into three distinct zones: a) the river zone, upstream of the reservoir, where one-dimensional unsteady flow and sediment transport were assumed, b) the transition zone from the river to the reservoir, where the flow was simulated by means of jet theory, and c) the reservoir zone, where the flow and sediment transport were simulated by means of the stream-tube concept in order to obtain the longitudinal and transverse distribution of sediment within the reservoir.

The discharge through each stream-tube is assumed to be constant. The initial conditions are established for the starting (upstream) section. The cross-sectional areas are not constant, but vary in such a way as to maintain constant discharge in each stream-tube. The dispersion process is broken down into:

a) the streamwise advection in each tube:

$$A\frac{\partial C}{\partial t}+\frac{\partial}{\partial x}\left[AuC\right]=0 \tag{3-59}$$

b) the streamwise diffusion in each tube:

$$A\frac{\partial C}{\partial t}=\frac{\partial}{\partial x}\left[AD_{xx}\frac{\partial C}{\partial x}\right] \tag{3-60}$$

c) and the transverse diffusion between neighbouring stream-tubes:

$$A\frac{\partial C}{\partial t}=\left[y\cdot D_{Txy}\frac{\partial C}{\partial y}\right]_{avg}-\left[y\cdot D_{Txy}\frac{\partial C}{\partial y}\right]_{avg} \tag{3-61}$$

where y is the depth of the flow and D_{Txy} is the coefficient of turbulence in the transverse direction. The terms within brackets in the above equation represent the mean conditions within a stream-tube.

It is assumed that the transverse velocities are small compared to the streamwise velocities. Holly and Cunge (1975) used the following equations for the turbulence coefficients: $D_{Txx} = 5.93 \cdot u \cdot y$ and $D_{Tyy} = 0.23 \cdot u \cdot y$. These approximations are sufficient for river and reservoir applications, but for coastal and estuarial problems the turbulent flow field is often more complex than this.

Generally 2D modelling is either depth-integrated or width-integrated. The depth-integrated model is more often used in river and reservoir engineering analysis. This model applies to simulating shallow water flow and is governed by the depth-integrated continuity and Navier-Stokes equations (Wang and Wu, 2004):

$$\frac{\partial h}{\partial t} + \frac{\partial (hU)}{\partial x} + \frac{\partial (hV)}{\partial y} = 0 \tag{3-62}$$

$$\frac{\partial (hU)}{\partial t} + \frac{\partial (hUU)}{\partial x} + \frac{\partial (hVU)}{\partial y} = -gh\frac{\partial z_s}{\partial x} + \frac{1}{\rho}\frac{\partial (hT_{xx})}{\partial x} + \frac{1}{\rho}\frac{\partial (hT_{xy})}{\partial y} + \frac{\partial D_{xx}}{\partial x} + \frac{\partial D_{xy}}{\partial y} + \frac{1}{\rho}(\tau_{sx} - \tau_{bx}) + f_c hV \tag{3-63}$$

$$\frac{\partial (hV)}{\partial t} + \frac{\partial (hUV)}{\partial x} + \frac{\partial (hVV)}{\partial y} = -gh\frac{\partial z_s}{\partial y} + \frac{1}{\rho}\frac{\partial (hT_{yx})}{\partial x} + \frac{1}{\rho}\frac{\partial (hT_{yy})}{\partial y} + \frac{\partial D_{yx}}{\partial x} + \frac{\partial D_{yy}}{\partial y} + \frac{1}{\rho}(\tau_{sy} - \tau_{by}) + f_c hU \tag{3-64}$$

where:

$x, y =$	Horizontal Cartesian coordinates
$h =$	Flow depth
$U,V =$	Depth averaged flow velocities in the x- and y- directions
$z_s =$	Water surface elevation
$g =$	Gravitational acceleration
$\rho =$	Density of fluid

f_c = Coriolis coefficient

τ_{bx}, τ_{by} = Bed shear stresses in the *x*- and *y*- directions

τ_{sx}, τ_{sy} = Shear stresses on the water surface caused by wind

$T_{xx}, T_{xy}, T_{yx}, T_{yy}$ = Depth-averaged turbulent stresses

$D_{xx}, D_{xy}, D_{yx}, D_{yy}$ = Dispersion terms due to the effect of secondary flow

The depth-averaged 2D transport equation for suspended sediment is (Wang and Wu, 2004):

$$\frac{\partial(hC_k)}{\partial t}+\frac{\partial(UhC_k)}{\partial x}+\frac{\partial(VhC_k)}{\partial y}=\frac{\partial}{\partial x}\left(\varepsilon_s h\frac{\partial C_k}{\partial \partial x}\right)+\frac{\partial}{\partial y}\left(\varepsilon_s h\frac{\partial C_k}{\partial y}\right)+\frac{\partial S_x}{\partial x}+\frac{\partial S_y}{\partial y}$$

$$+\alpha w_{sk}(C_{*k}-C_k) \quad (k=1,2,...,N) \tag{3-65}$$

where:

C_k = Depth-averaged suspended load concentration

C_{*k} = Suspended load transport capacity

ε_s = Turbulence diffusivity coefficient of sediment determined by $\varepsilon_s = \nu_t / \sigma_c$ in which σ_c is the turbulent Prandtl-Schmidt number, usually in the order of 0.5 to 1.0.

α = Non-equilibrium adaptation coefficient

S_x, S_y = Dispersion terms to account for the effect of the non-uniform distributions of flow velocity and sediment concentrations

The bed deformation can be calculated using the overall sediment balance equation or the following equation:

$$(1-p_m')\left(\frac{\partial z_b}{\partial t}\right)_k=\alpha w_{sk}(C_k-C_{*k})+(q_{bk}-q_{b*k})/L_s \quad (k=1,2,...,N) \tag{3-66}$$

The formulas for the suspended load and bed load can be written as:

$$C_{*k}=p_{bk}C_k^* \qquad q_{b*k}=p_{bk}q_{bk}^* \quad (k=1,2,...,N) \tag{3-67}$$

where p_{bk} is the bed material gradation at the mixing layer; C_k^* is the potential transport capacity of size class *k* of suspended load; and q_{bk}^* is the potential transport capacity of size class *k* of bed load.

3.6.8 Quasi-2D GSTARS Model: Tarbela Reservoir, Pakistan (Yang and Simoes, 2003)

The Tarbela Reservoir is again modelled here, using a 2D model. The Tarbela Dam, located in Northern Pakistan along the Indus River, is the largest earth-fill dam in the world. The reservoir, with a gross storage capacity of 14 340 million m^3, is a 38km long run of river type reservoir with two major tributaries, the Siran and the Brandu. The reservoir's storage capacity has been continuously depleted since the dam has been constructed in 1974 with an annual inflow rate of 265 million tons of sediment, most of which is in the silt and clay range.

a) Mathematical Model Description

GSTARS3 (Generalised Sediment Transport Model for Alluvial River Simulation version 3.2) is the most recent version of a series of numerical models for simulating the flow of water and sediment transport in alluvial rivers developed at the Sedimentation and River Hydraulics Group of the Technical Service Center, U.S. Bureau of Reclamation, Denver.

GSTARS version 3.2 is based on version 2.1 (Yang and Simoes, 2000) and consists of four major parts. The first part uses both the energy and the momentum equations for backwater computations. This feature allows the program to compute the water surface profiles through combinations of subcritical and supercritical flows. In these computations, GSTARS3 can handle irregular cross sections regardless of whether single channel or multiple channels are separated by small islands or sand bars.

The second part is the use of the stream tube concept, which is used in the sediment routing computations. Hydraulic parameters and sediment routing are computed for each stream tube, thereby providing a transverse variation in the cross-section in a

semi two-dimensional manner. Although no flow should be transported across the boundary of a stream tube, transverse bed slopes and secondary flows are phenomena accounted for in GSTARS3 that contribute to the exchange of sediments between stream tubes. The position and width of each stream tube may change after each step of computation. The scour or deposition computed in each stream tube gives the variation of channel geometry in the vertical (or lateral) direction. The water surface profiles are computed first. The channel is then divided into a selected number of stream tubes with the following characteristics: (1) the total discharge carried by the channel is distributed equally among the stream tubes; (2) stream tubes are bounded by channel boundaries and by imaginary walls; (3) the discharge along each stream tube is constant (i.e., there is no exchange of water through stream tube boundaries).

The third part is the use of the theory of minimum energy dissipation rate (Yang, 1976; Yang and Song, 1986) in it's simplified version of minimum total stream power to compute channel width and depth adjustments. The use of this theory allows the channel to be treated as an unknown variable, which is one of the most important capabilities of GSTARS3. Whether a channel width or depth is adjusted at a given time step depends on which condition results in less total stream power.

The fourth part is the inclusion of a channel bank side stability criteria based on the angle of repose of bank materials and sediment continuity. GSTARS is a general mathematical model developed for a personal computer to simulate and predict river and reservoir morphological changes caused by natural and engineering events. Although GSTARS3 is intended to be used as a general engineering tool for solving fluvial hydraulic problems, it does have the following limitations from a theoretical point of view (Yang and Simoes, 2003):

a) GSTARS3 is a quasi-steady flow model. Water discharge hydrographs are approximated by bursts of constant discharges. Consequently , GSTARS3 should not be applied to rapid, varied, unsteady flow conditions.

b) GSTARS3 is a semi-two-dimensional model for flow simulation and a semi-three-dimensional model for simulation of channel geometry change. It should not be

applied to situations where a truly two-dimensional or truly three-dimensional model is needed for detailed simulation of local conditions.

c) GSTARS3 is based on the stream tube concept. Secondary currents are empirically accounted for. The phenomena of diffusion and super elevation are ignored.
d) Many of the methods and concepts used in GSTARS3 are simplified approximations of real phenomena. Those approximations and their limits of validity are therefore embedded in the model.

b) Model Setup

In this example, GSTARS3 is used to simulate 22 years of reservoir sedimentation (from 1974 through 1996) for a reach that spans nearly 95 kilometres upstream from the Tarbela Dam (see Figure 3-5). The hydrology of the system is depicted in Figure 3-6, together with dam operation information. The tributaries make a relatively small contribution when compared to the main stem discharge, therefore they are not included in Figure 3-6 (they are however included in the computations).

There is a percentage of silt and clay in the sediments being transported, but there is no data to simulate them using the Krone/Ariathurai methods. Secondly, analysis of the 1996 cross-sectional data suggests that deposition occurs in the form of a horizontal fill as can be observed in Figure 3-7.

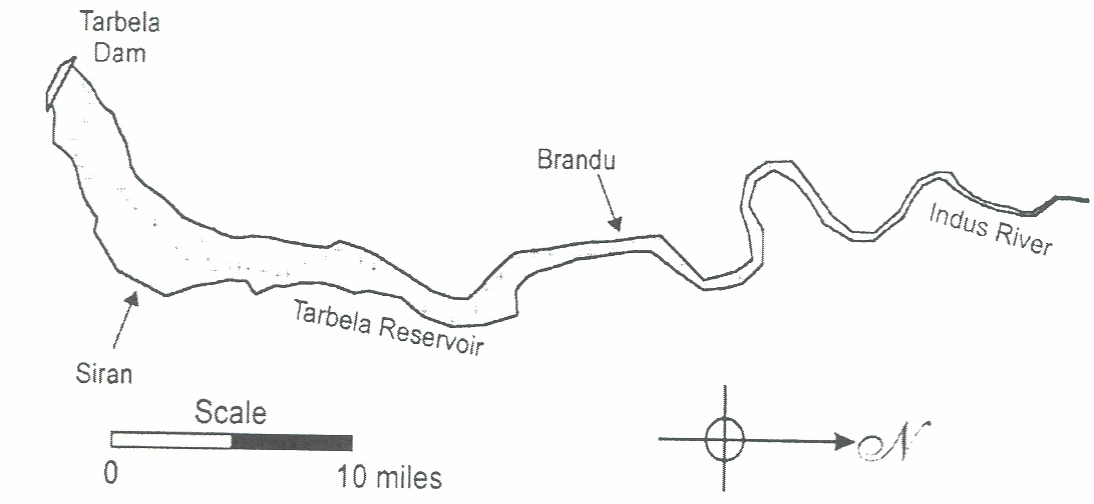

Figure 3-5: Tarbela Dam and Reservoir (Yang and Simoes, 2003)

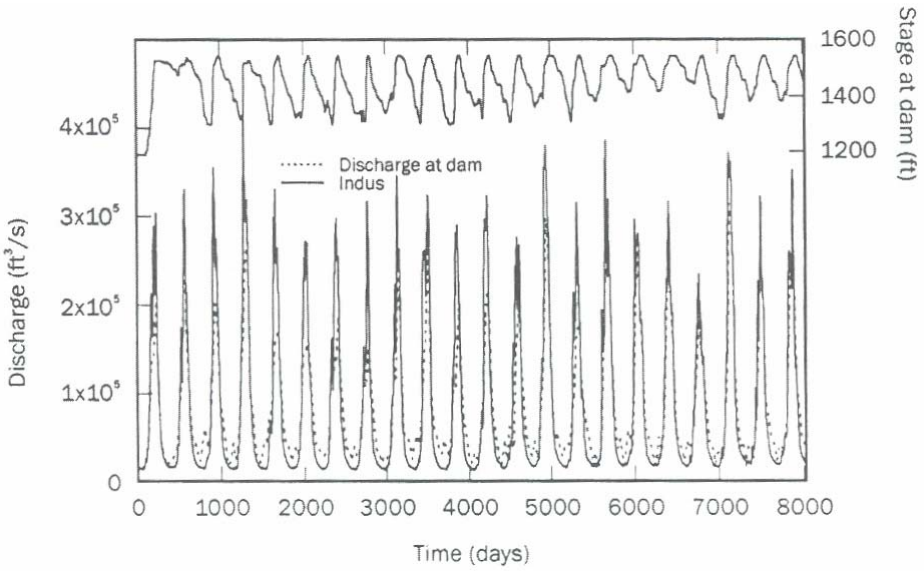

Figure 3-6: Hydrology and dam operation for Tarbela Reservoir (1974 to 1996) (Yang and Simoes, 2003)

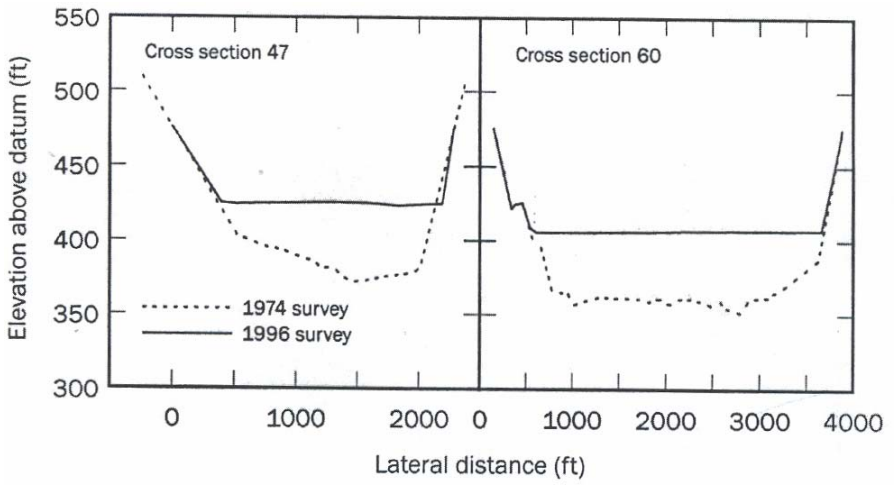

Figure 3-7: Two reservoir cross-sections showing uniform sedimentation (Yang and Simoes, 2003)

The Tarbela Reservoir's bathymetry was discretised using existing surveyed cross sections along the length of the reservoir. The horizontal sediment deposition observed in Figure 3-7 indicates that there is not much transverse variation in the sedimentation processes, therefore GSTARS3 simulations were carried out using only one stream tube.

Yang's equation was used for this study. Because there is no information concerning the deposition characteristics of the silt and clay fractions, it is difficult to use the Krone/Ariathurai methods effectively. Instead, the equation by Yang (1973) was extrapolated for these size ranges (The particle size distributions are in the range of 0.002 to 2.0mm). This approach can sometimes yield good results, especially in mainly depositional processes such as those occurring in large reservoirs. However, the results of the simulations should always be confirmed by careful validation using field data.

Twenty-four hour time steps for the hydraulic computations and 4.8 hours for sediment routing computations (8 040 time steps for hydraulics, 40 200 time steps for sediment) were used.

c) Simulation Results

The results of a 1996 survey carried out in Tarbela Reservoir at the end of the period of simulation, are used here. Note that this example does not constitute an exhaustive and definitive study of the sedimentation processes in Tarbela Reservoir for the 1974 to 1996 period.

The simulation results for the thalweg are shown in Figure 3-8. They are in good agreement with measurements, especially as far as the location of the frontset of the delta and it's slope are concerned. The cross-sectional geometries were better predicted in the downstream reservoir region than in the upstream region. That is because the upstream part is more riverine in character, and assuming horizontal deposition in not the most appropriate technique for this circumstance. However, this region is limited to the first 21 cross sections, which represent less than one fourth of the entire simulated distance. Even then, deposition volumes are generally well predicted, even though the thalweg elevations are not very accurate. Two representative cross-sections in this region are shown in Figure 3-9 for comparison purposes.

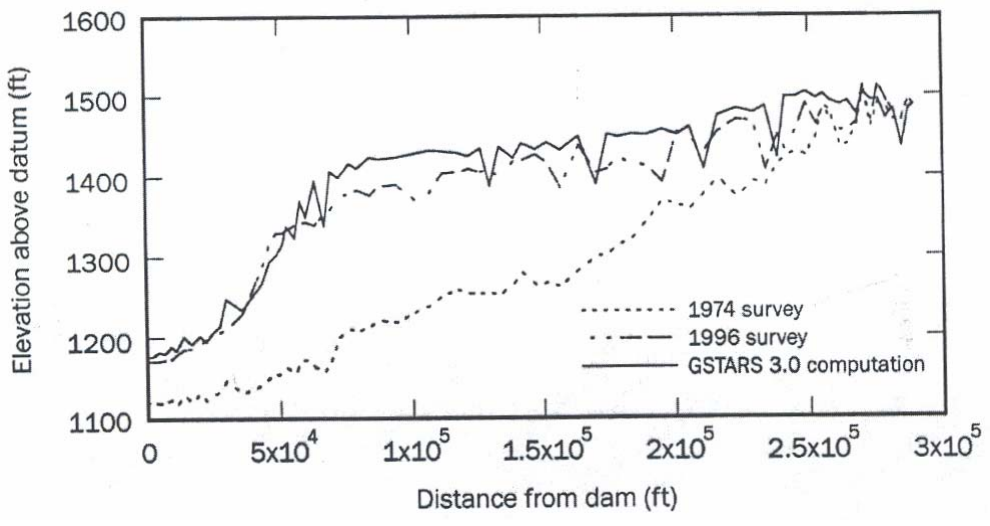

Figure 3-8: Results of the simulation of the Tarbela delta advancement over a period of 22 years (Yang and Simoes, 2003)

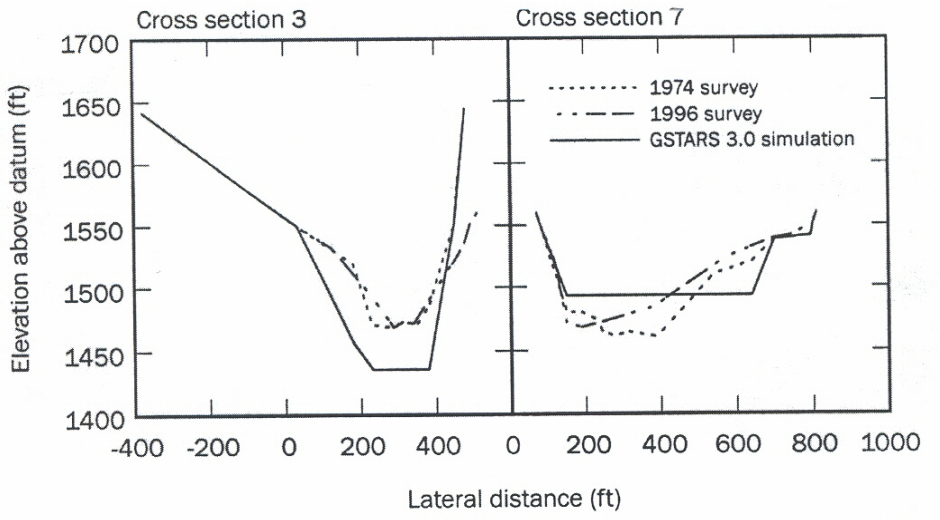

Figure 3-9: Comparison of measurements and GSTARS3 computation for two cross sections in the upstream region of Tarbela Reservoir (Yang and Simoes, 2003)

In the reservoir region, which constitutes the focus area of the study, deposition volumes are well predicted, in spite of a weak tendency to overpredict the thalweg elevations. Two representative cross sections are shown in Figure 3-10. These cross-sections were taken from the downstream reservoir region.

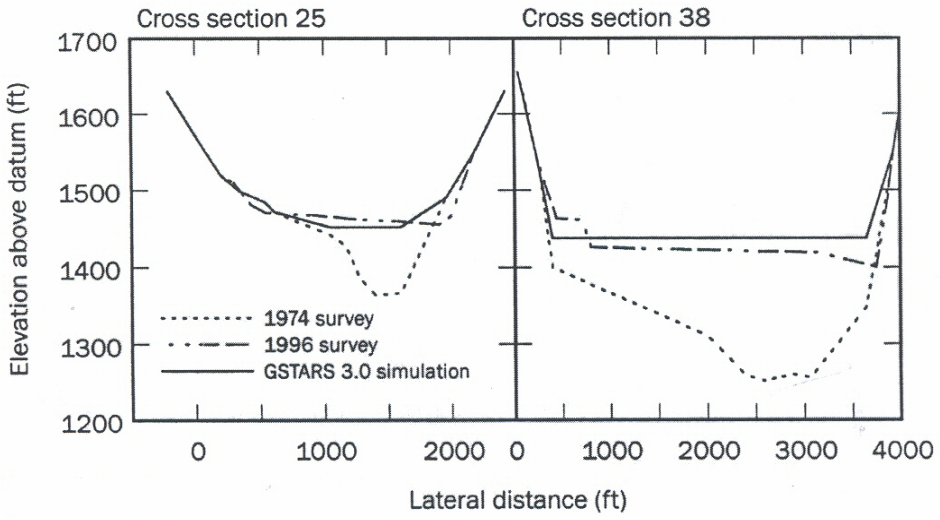

Figure 3-10: Comparison of measurements and GSTARS3 computation for two cross-sections in the reservoir region of the study reach (Yang and Simoes, 2003)

The error associated with the predicted thalweg is shown in Figure 3-11. Most data are inside the 20% error band, which is a very good result for this type of simulation

(22 years of sedimentation spanning a 36km reach). However, the results could easily be improved by using some additional data. Such data would comprise more accurate bed-sediment size distributions, as well as more information about the inflowing sediment sizes being carried by the Indus River. Further improvements could be attained from a study of the cohesive sediment fraction properties within the reach (Yang and Simoes, 2003).

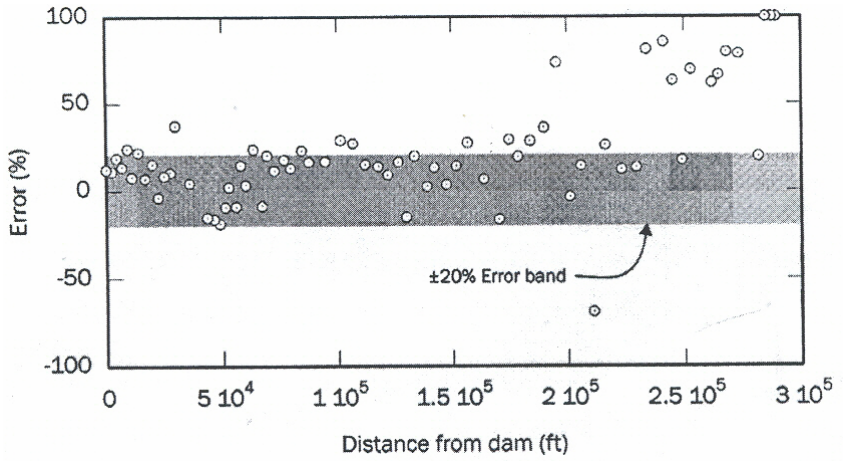

Figure 3-11: Relative error of the thalweg elevation predictions (Yang and Simoes, 2003)

3.6.9 Three-dimensional Mathematical Modelling

Generally, the 3D flow field is determined by the following Reynolds-averaged continuity and Navier-Stokes equations (Wang and Wu, 2004):

$$\frac{\partial u_i}{\partial x_i} = 0 \tag{3-68}$$

$$\frac{\partial u_i}{\partial t} + \frac{\partial (u_i u_j)}{\partial x_j} = F_i - \frac{1}{\rho}\frac{\partial p_i}{\partial x_i} + \frac{1}{\rho}\frac{\partial \tau_{ij}}{\partial x_j} \tag{3-69}$$

where:

u_{i}= Velocity components (i = 1, 2, 3)
F_i= External forces including gravity per unit volume
p = Pressure
τ_{ij} = Turbulent stresses determined by a turbulence model

For shallow water flow, the pressure variation can be assumed to be hydrostatic and all the vertical components of fluid acceleration can be ignored, thus yielding the quasi-3D governing equation (Wang and Wu, 2004):

$$\frac{\partial u}{\partial x}+\frac{\partial v}{\partial y}+\frac{\partial w}{\partial z}=0 \tag{3-70}$$

$$\frac{\partial u}{\partial t}+\frac{\partial (uu)}{\partial x}+\frac{\partial (vu)}{\partial y}+\frac{\partial (wu)}{\partial z}=-g\frac{\partial z_s}{\partial x}+\frac{1}{\rho}\frac{\partial \tau_{xx}}{\partial x}+\frac{1}{\rho}\frac{\partial \tau_{xy}}{\partial y}+\frac{1}{\rho}\frac{\partial \tau_{xz}}{\partial z}+fv \tag{3-71}$$

$$\frac{\partial v}{\partial t}+\frac{\partial (uv)}{\partial x}+\frac{\partial (vv)}{\partial y}+\frac{\partial (wv)}{\partial z}=-g\frac{\partial z_s}{\partial y}+\frac{1}{\rho}\frac{\partial \tau_{yx}}{\partial x}+\frac{1}{\rho}\frac{\partial \tau_{yy}}{\partial y}+\frac{1}{\rho}\frac{\partial \tau_{yz}}{\partial z}-fu \tag{3-72}$$

where f is the Coriolis coefficient.

The hydrostatic pressure variation assumption brings significant simplification to the full 3D equations 3-68 and 3-69. However, this simplification is valid only for gradually varying open-channel flows. A full 3D model without this simplification should be used in regions of rapidly varying flows.

Sediment transport is sub-divided into a suspended load and a bed load and hence the flow domain is divided into a bed-load layer with thickness δ and the suspended load layer above it with thickness $h-\delta$. The exchange of sediment between the two layers is through deposition (downward sediment flux) at a rate of D_{bk} and the entrainment from the bed load layer (upward flux) at a rate of E_{bk}. The distribution of the sediment concentration in the upper layer is governed by the following advection-dispersion equation:

$$\frac{\partial c_k}{\partial t}+\frac{\partial [(u_j-w_{sk}\delta_{j3})c_k]}{\partial x_j}=\frac{\partial}{\partial x_j}\left(\frac{\nu_t}{\sigma_c}\frac{\partial c_k}{\partial x_j}\right) \tag{3-73}$$

where c_k is the local concentration of the k-th size class of suspended sediment load; δ_{j3} is the Kronecker delta with j=3 indicating the vertical direction. At the free surface, the vertical sediment flux is zero and hence the condition applied is:

$$\frac{\nu_t}{\sigma_c}\frac{\partial c_k}{\partial z} + w_{sk} c_k = 0 \tag{3-74}$$

At the lower boundary of the suspended sediment layer, the deposition rate is $D_{bk} = w_{sk} c_{bk}$, while the entrainment rate, E_{bk} equals:

$$E_{bk} = -\frac{\nu_t}{\sigma_c}\frac{\partial c_k}{\partial z} = w_{sk} c_{b*k} \tag{3-75}$$

where c_{b*k} is the equilibrium concentration at the reference level $z = z_b + \delta$, which needs to be determined by using an empirical relation. In the 3D model, the bed load transport is simulated by using the equation:

$$\frac{\partial(\delta_b \bar{c}_{bk})}{\partial t} + \frac{\partial(\alpha_{bx} q_{bk})}{\partial x} + \frac{\partial(\alpha_{by} q_{bk})}{\partial y} + \frac{1}{L}(q_{bk} - q_{b*k}) = 0 \quad (k = 1, 2, ..., N) \tag{3-76}$$

where $\bar{c}_{bk}$ is the average concentration of bed load in the bed load zone, q_{bk} is the bed load transport rate of the *k*-th size class and q_{b*k} is the corresponding bed load transport capacity. α_{bx} and α_{by} are the direction cosines of the bed shear stresses, known from the flow calculation.

The bed change can be determined by either the exchange equation:

$$(1 - p'_m)\left(\frac{\partial z_b}{\partial t}\right)_k = D_{bk} - E_{bk} + \frac{1}{L_s}(q_{bk} - q_{b*k}) \tag{3-77}$$

or the overall sediment mass-balance equation integrated over the water depth *h*:

$$(1 - p'_m)\left(\frac{\partial z_b}{\partial t}\right)_k = \frac{\partial(hC_{tk})}{\partial t} + \frac{\partial q_{tkx}}{\partial x} + \frac{\partial q_{tky}}{\partial y} = 0 \tag{3-78}$$

where C_{tk} is the depth-averaged sediment concentration and q_{tkx} and q_{tky} are the components of the total load sediment transport in the *x*- and *y*- directions:

$$q_{tkx} = \alpha_{bx} q_{bk} + \int_{\delta}^{h} \left(u c_k - \frac{\nu_t}{\sigma_c} \frac{\partial c_k}{\partial x} \right) \partial z; \qquad q_{tky} = \alpha_{by} q_{bk} + \int_{\delta}^{h} \left(v c_k - \frac{\nu_t}{\sigma_c} \frac{\partial c_k}{\partial x} \right) \partial z \tag{3-79}$$

3.6.10 Three-dimensional Model: Three Gorges Reservoir Project, China (Dou et al., 2004)

This study applies a 3D mathematical model for suspended load motion in turbulent flows and is based on the following new components:

- A new stress model based on the stochastic theory of turbulent flows by Dou (1980)
- Refined wall function for treatment of solid walls
- Introduction of traditional equations of suspended load motion and sorting of bed material into a 3D model
- Orthogonal curvilinear grid system, with horizontal layers employed over the water depth

The equation system is solved by using the SIMPLE–C algorithmic. The above model is first validated using hydrological data collected before and after the construction of the existing Gezhouba Dam. The model is then applied to the sedimentation problem of the much larger Three Gorges Project (located upstream of the Gezhouba Dam) and predictions are made of the sediment deposition pattern, the size distribution of the deposits and the flow fields.

a) Background

The dam area of the Three Gorges Project is located within Xiling Gorge on the Yangtze River. A 16km long river reach was simulated between Miaohe and the dam axis at Sandouping, a deep valley of heavily weathered anticline diorite and granite, with low mountains and hills on both sides. The width of the river in this section is usually 600m to 700m during a flooding period. The maximum width of 1 400m is found near Sandouping. The river reach under investigation contains slight bends. The

inlet is at Miaohe with a width of only about 500m. Figure 3-12 shows the river regime in the dam area. The river bed consists of gravel and cobble. The slope is steep with rapid flows. The water surface gradient during dry and flooding periods varies between 0.375% and 0.506%. This reach is among the worst in terms of navigation conditions in Sichuan province. Since the impoundment of Gezhouba Reservoir, the reach falls within the perennial backwater area; during dry periods the water level rises 15m to 20m, during flooding periods it rises 2m to 4m, and the gradient becomes 0.016% to 0.297%.

The Yangtze River has a high runoff volume, and the sediment discharge is also large. The average annual runoff is $4.39 \times 10^{12} m^3$, and the average annual suspended load discharge is 526 million tons.

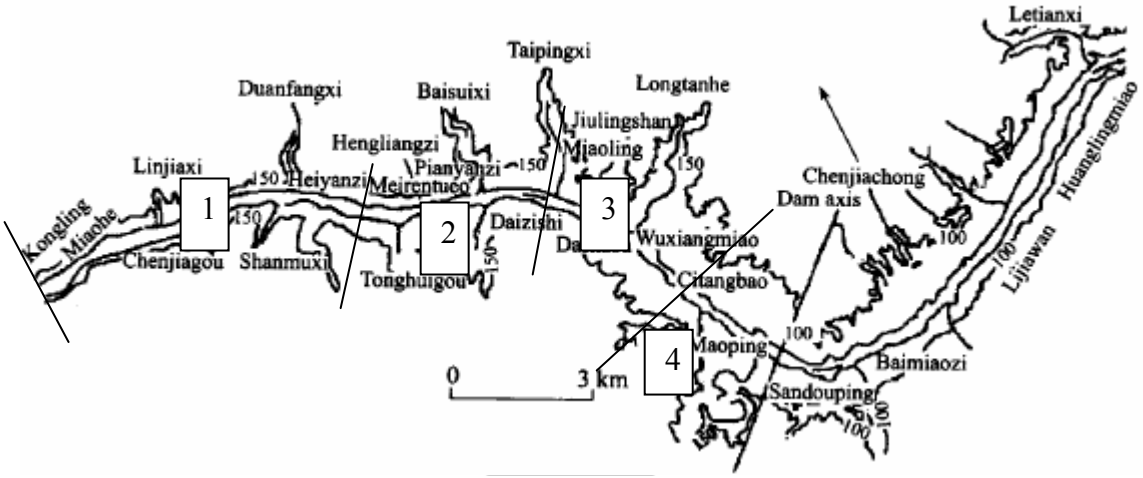

Figure 3-12: River Configuration in the Dam Area of Three Gorges Project (Dou et al., 2004)

b) Generation of Computational Grids

A total of 163 layers of mesh have been arranged along the longitudinal direction, and 81 layers across the river width. At the maximum water depth there are 15 layers in the vertical direction. Orthogonal curve grids are generated numerically and the total number of grid points is 163 x 81 x 15.

c) Verification of Deposition in the Three Gorges Dam Site Area Due to Gezhouba Reservoir

A period of three years was selected for the reservoir sedimentation verification (from June 1981, after the impoundment of the existing Gezhouba Reservoir to December 1984) Calculation time steps were 3 to 4 days on average. Calculation of sediment concentration of suspended load was performed for 7 grain size groups, and the average values during the period 1981 to 1984 were used for the percentage of each grain size.

Table 3-1 provides a comparison between calculated and measured amounts of deposition for the reaches numbered 1 to 4 on Figure 3-12. It can be seen from Table 3 that the predictions were quite close to the measured values.

Table 3-1: Comparison between the calculated and measured deposits for different reaches (10^4 m^3) (Dou et al., 2004)

Reach	1	2	3	4	Total
Calculated	271.2	231.9	300.4	432.6	1236.1
Measured	310.5	224.6	240.4	418	1193.5
Error (%)	-12.7	3.2	25	3.5	3.6

d) Calculation Conditions for Predictions of the Three Gorges Project

The incoming hydrographs of runoff and graded suspended load entering Three Gorges Project dam area have been provided by the Yangtze River Scientific Research Institute based on a 1D model.

During initial operation of the reservoir both the amount of suspended load and the grain sizes will be small. After 90 year of operation, most suspended load will reach the dam area and the median diameter will be increased to 0.027mm, close to the average annual median diameter of natural suspended load, i.e. 0.031mm, For large discharges, the median diameter could be larger than 0.031mm.

Though the grain size distribution of suspended sediment entering the dam area may vary with time and discharge, it is assumed that the size distribution is related to D_{50}.

In this model study, the following equation by Zhou (1997) was used. It is based on statistical analysis of data from the Yangtze River Scientific Research Institute:

$$P_L = 1 - e^{-0.639\left(\frac{D_L}{d_{50}}\right)} \qquad (3\text{-}80)$$

where D_L is the representative grain size (mm), P_L the percentage by weight of the sediment interval in question. The above equation is used for determining the size distribution of suspended load. A total of 7 intervals for suspended load were used in the calculation.

e) Hydrological Series in the Simulation

The hydrological series adopted for the calculation is a 10-year series, based on observed data during the period 1961 to 1970. The average incoming water and sediment loads during the 10 years is close to the annual averaged amounts, and are considered to be representative. In order to take into consideration the impact of extra-large flood and sediment years during long-term simulation, it has been suggested that after 30 years of operation of the reservoir an extra high- flood-high-sediment year, 1954, be inserted into the hydrological series. In total, a period of 76 years was simulated.

f) Sediment Deposition at the Upper Reach of the Dam Area

Figure 3-13 depicts deposition development of the entire 16km reach compared to that of the 6.8km near dam reach.

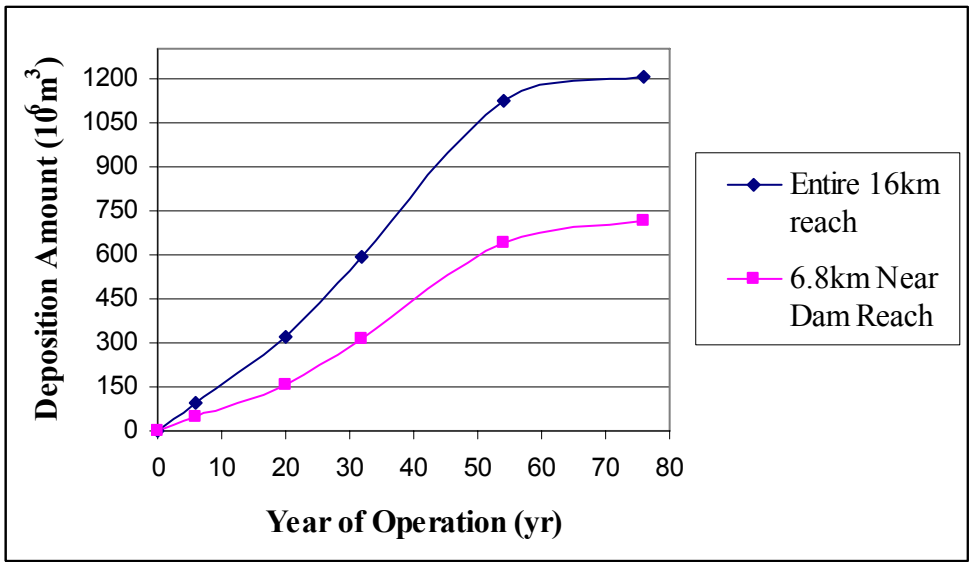

Figure 3-13: Development of the deposition of the entire and near dam reaches (Dou et al., 2004)

The simulated results indicate that during the initial 32 year period, the regime is mainly characterised by large cross-sectional areas and small flow velocities. Though sediment concentration is small and the grain size is fine at the inlet reach of the dam area, it still maintains a saturated state. The entire river reach appears to undergo uniform and unidirectional deposition. The accumulated deposition in the entire river reach and near-dam reach will be 589 million m^3 and 312 million m^3 respectively. The average thickness in the upper reach will be 33.3m and that of the near-dam reach 24.3m.

After 60 to 70 years of operation, the upper reach of the dam area will reach a state of equilibrium, i.e. both erosion and deposition will occur in the dam area without unidirectional deposition. After 76 years , the accumulated amount of deposition in the entire reach will be a steady 1.208 million m^3 and that of the near dam reach will be 714 million m^3, with the average thickness in the upper reach 56.3 m and that in the near-dam reach 56.0m, values which are very close to one another.

The results of the Three Gorges model demonstrate that within 30 years of reservoir operation, the cumulative sediment deposition will have no serious impact on the project's normal operation both in the dam area and in the fluctuating backwater region. But several decades later, sediment deposition in the fluctuating backwater region might

affect the navigation and harbour operation during extremely dry years when the reservoir's water surface drops down to it's lowest level.

g) Sediment Concentration Field

The largest difference between 3D and 2D models is that 2D models can only simulate depth-averaged flow fields and sediment concentration fields, while 3D models can predict flow fields and sediment concentration fields at different water depths or elevations. The 3D simulated results however show that the distribution of sediment concentrations over the depth is relatively uniform. Sediment concentration at the riverbed is slightly larger than that in the middle and near the surface.

h) Bed Material Constituents

The simulated results show that the average bed grain size after 76 years of operation is between 0.057mm and 0.062mm.

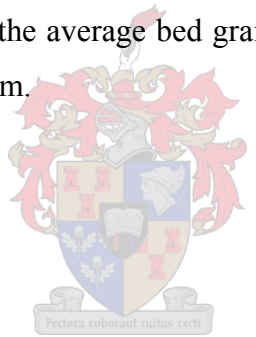

3.7 Density Currents

Apart from turbulent suspended sediment transport, which is the dominant mechanism by which sediment is transported through most reservoirs, density currents in certain reservoirs provide an additional mechanism to transport sediment.

Density differences often exist between discharges in tributaries and receiving reservoirs. These inflows tend to plunge when their densities are greater than those of the surface layer in the receiving system, entering as density currents or turbidity currents. If the density of the inflow is less than that of the surface layer, the inflow will tend to travel along the surface, thus entering as an overflow. If local mixing is inadequate in the region of the inflow to eliminate density differences, the density or turbidity current will plunge and travel along the sloping bottom as an underflow. These processes are accompanied by entrainment of ambient water. If a depth is encountered where the density of the underflow equals that of the water column, the

buoyant density current separates from the bottom and enters into that layer as an interflow (Basson and Rooseboom, 1997).

Density currents can form in reservoirs when heavy rains wash mud into rivers. Density currents commonly flow until they reach the flat bottom of a basin, where they slow down, which causes the sediment particles to fall to the bottom. If a density current flows all the way through a basin, it is reflected, or turned back, by the wall at the end of the basin. Visual evidence of a density current is the presence of a "plunge line" where the inflowing river converts into a density current. At this point, stable floating debris can be observed as in Figure 3-14, held in position by the zero velocity of the overlying water mass.

The next chapter describes the 2D MIKE 21C model which was extensively tested and validated during this research.

Figure 3-14: The plunge line with floating debris where the Nzoia River flows into Lake Victoria, Kenya (IWE, 2005)

4. THE MIKE 21C MATHEMATICAL SEDIMENTATION MODEL

4.1 Background

MIKE 21C is a 2D curvilinear modelling tool for the simulation of morphological changes in rivers and reservoirs. It incorporates a varying size mesh design with state-of-the-art hydrodynamic and morphological technology.

The model components can run simultaneously, thus incorporating dynamic feedback from changing hydraulic resistance, bed topography and bank lines affecting the hydro-dynamic behaviour of the river or reservoir (DHI, 2003).

Creating a hydrodynamic river or reservoir model using MIKE 21C involves the following four steps:

- The extent of the modeling area is selected and the computational grid is designed for the river or reservoir area.
- The bathymetry is entered onto the computational grid, i.e. bed levels are specified in each computational grid point. This is done by creating a data input file of coordinates and their heights above sea level. The processes used to determine this data typically involves conversions, interpolation and extrapolation of coordinates and their heights from survey data.
- Specification of the boundary conditions for instance a time series of discharge at the inflow boundary, and a time series of water level at the downstream model boundary.
- Either of the two simulation modules is chosen. The first option is 'Hydrodynamics only' which only gives the output of water depth, surface elevation, unit discharges and velocities throughout the model. The other option is 'Hydrodynamics and river morphology' which in addition gives as output the changes in the bed levels due to sediment transport, deposition and erosion.

The complete modelling procedure is described in the following section, including grid generation, bathymetry development, choice of hydrodynamic and sediment transport models. The order of the topics is as it is found on the MIKE 21C Curvilinear Flow Model setup interface.

4.2 Basic Setup Parameters

4.2.1 Generation of the Curvilinear Grid

MIKE 21C is designed to function on an orthogonal curvilinear grid. The numerical grid is created by means of the Grid Generator utility program. To do this an accurate description of the bank lines is required within which the grid is drawn. The coordinates of bank lines can be derived from orthophotos or survey data. The amount of grid cells in the flow direction and also across the flow is then chosen after which the grid is automatically generated with an anisotropic conformal mapping method by the Grid Generator. Often the shape of the generated gridlines and cells does not accurately describe the topography or expected flow pattern and the cells must then be reshaped by hand.

Generation of an orthogonal curvilinear grid is an iterative process in which gridlines are smoothened until the computational grid is acceptable and without unacceptably large gradients in grid cell spacing and curvature of grid lines. This is the most time consuming part of setting up any model and also the most important since it forms the basis of a reliable simulation model. It is important to keep in mind that the size of the grid determines the run time of the simulation since the calculations of hydrodynamics and sediment transport are done at every single grid point at every time-step. Therefore with more cells the output will be more detailed, but the computational time will increase.

Initial hydrodynamic simulations may still reveal the need for further refinements and adjustments of the grid. It is preferable to use cells that are elongated in the flow direction for these types of models. To keep the simulation from becoming unstable, the water should not be allowed to flow through the length of one grid cell within one

time-step. The minimum cell length can thus be determined from the expected flow velocities.

Areas of special interest can be focused on by using a higher density of grid lines at these locations. Figure 4-1 shows an example of a curvilinear grid.

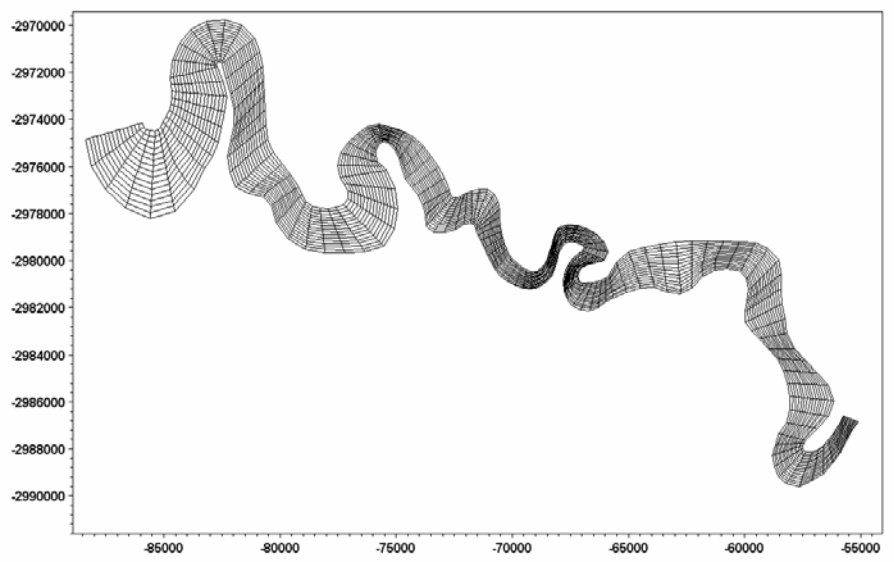

Figure 4-1: A curvilinear grid created for a river and reservoir system

4.2.2 Bathymetry Development

The sectional bathymetry data, as seen below, is obtained from reservoir hydrographic surveys. The survey data exits of points with known heights above sea level along transverse sections at regular intervals along the reservoir. A data file is created in which only the coordinates and their heights above sea level appear. This data file is then imported onto the grid. The rest of the bathymetry is established by interpolation between the sections along the gridlines. The complete bathymetry is depicted below in Figure 4-2.

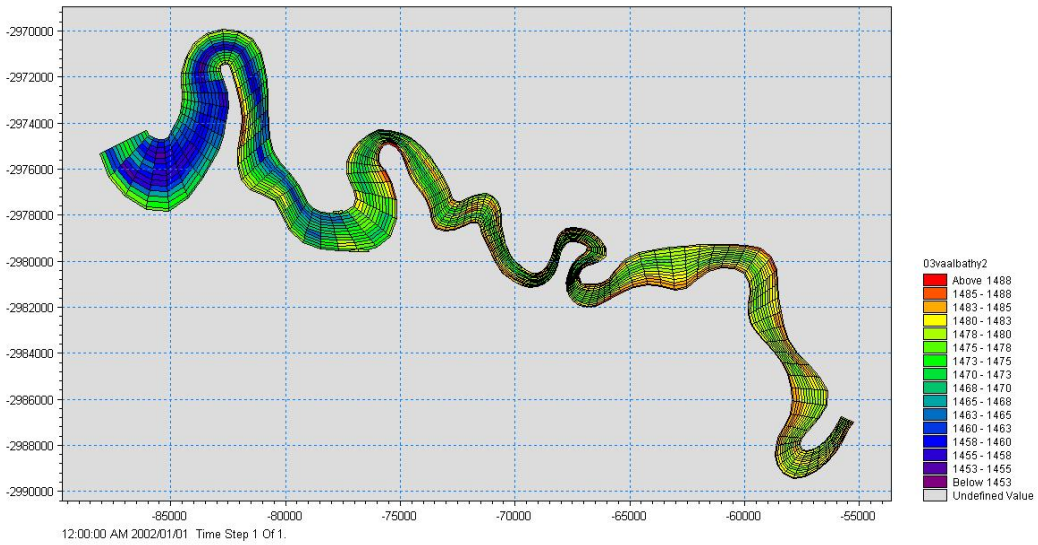

Figure 4-2: The grid with complete interpolated bathymetry

The process of creating the grid and bathymetry with the Grid Generator program is thus complete. The following headings and interfaces are found on the MIKE 21C program.

4.2.3 Simulation Period

On the simulation period interface the duration of the simulation is chosen and a fixed starting and finishing date and time is specified. Also the hydrodynamic time step intervals are defined at which the flow and sediment transport calculations will be carried out.

4.2.4 Boundary Specifications

The model boundaries can be defined by the user or detected by the program itself.
For the modelling of reservoirs, there are usually only two boundaries; the upstream discharge into the model from the river and the downstream water level at the dam or other hydraulic structure. The data is obtained from historic records and equidistant time-series of these values for both boundaries are created using the MIKE 21C Toolbox utility program. The time-series of water level brings the effect of the reservoir's operation into consideration. Typical time-series of water level and inflow can be seen in Figure 4-3.

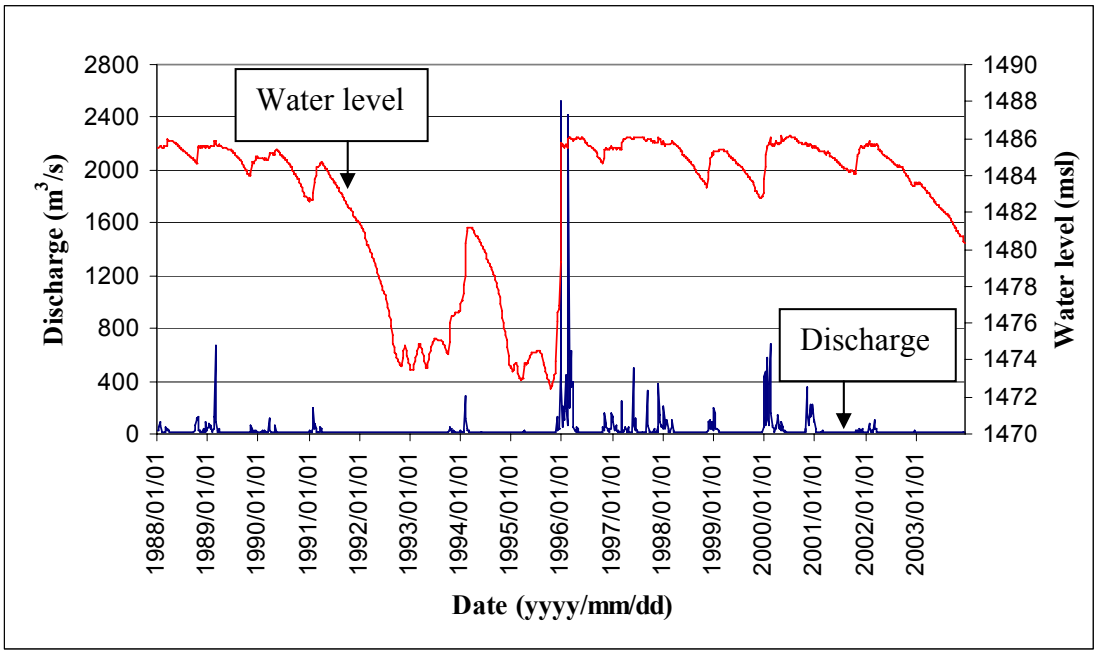

Figure 4-3: Typical time-series of measured reservoir water levels and inflow

4.2.5 Source and Sink

This interface is only used if the model has another source, such as an inflowing tributary, or an abstraction (such as irrigation pumps), other than the upstream and downstream boundaries. For the domain of this research, there will be only two boundaries and this feature will therefore not be used.

4.2.6 Flood and Dry Conditions

In rivers and reservoirs, water levels rise and fall continuously. This often creates dry banks around which the water is diverted. This can seriously complicate hydrodynamic model calculations and it might even cause the process to become unstable. For this reason, two safety factors, the dry depth and the flood depth, are defined to function as a warning for the simulation process of when an island is about to form or dry land is about to be flooded. The dry depth is the local water depth below which a grid point is defined as land. The flood depth is the local water depth above which a grid point is considered to be submerged. These values are specified to ensure the stability of the hydrodynamic model. The default values are 0.2m for the dry depth and 0.3m for the wet depth. In between these levels there is a height

difference to avoid alternative swapping, which can lead to instability of the hydrodynamic calculations (DHI, 2003).

For the reservoir models described in this research, the entire model domain will remain wet. These models are not expected to experience wetting and drying, but because of changing bed levels due to sedimentation, it can occur. The default values are used throughout this research.

4.3 Hydrodynamic Parameters

4.3.1 Initial Surface Elevation

This is the initial surface level at the start of the simulation. This can either be a constant horizontal level throughout the whole model domain or it can have an initial hydraulic gradient as defined by an input data file. All the reservoirs that were modelled in this research had an initial hydraulic gradient merely to initiate flow in the right direction. Some model simulations, mostly those with low discharges and water levels, even became unstable when this technique was not implemented.

4.3.2 Eddy Viscosity

The eddy viscosity is taken as constant throughout the model. If the model is applied to a reservoir system, this value can be taken as $0.01 m^2/s$. For small scale models such as flumes with small grid spacing relative to the depth, the eddy viscosity may be neglected. Eddy viscosity becomes important when the horizontal grid spacing of a model is much larger than the water depth, as in the case of reservoir models (DHI, 2003).

4.3.3 Resistance

Manning's M value ($m^{0.33}/s$) describes the roughness of the river or reservoir bed. The M value is the inverse of the original Manning's n value. A constant value is defined here for the whole model for the whole duration of the simulation. The MIKE 21C Alluvial Resistance model can be used if changing bed resistance is required.

4.3.4 Helical Flow

Helical flows occur in curved flows, especially in river bends. They arise from the imbalance between the pressure gradient and the centripetal acceleration working on a water particle moving along a curved path. Near the river bed the helical flow is directed towards the center of flow curvature. The secondary flow is directed towards the centre of curvature near the bottom and outwards in the upper part of the cross-section as illustrated in Figure 4-4 and Figure 4-5. The *s* and *n* axes form the curvilinear axis system which is based on the shape of the grid. The *s*-axis represents the main direction of flow while the *n*-axis represents the transverse or secondary direction of flow. The helical flow velocity rarely exceeds 5-10% of the main flow velocity in natural rivers (DHI, 2003).

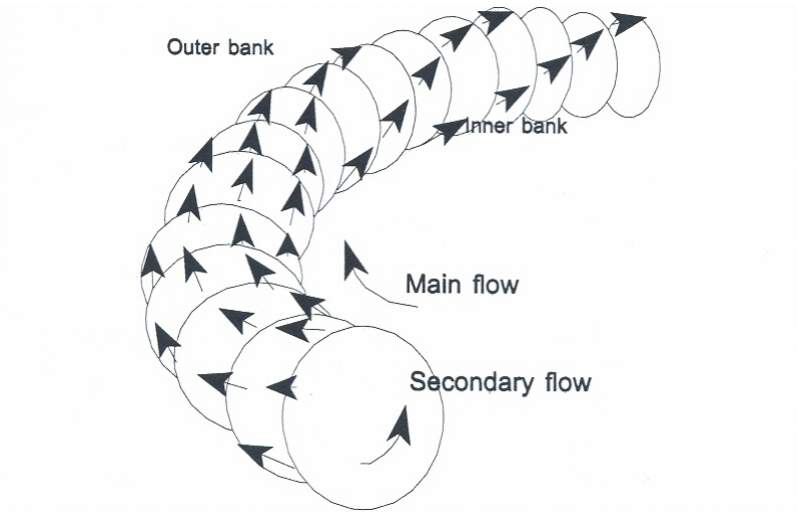

Figure 4-4: Helical flow in river bends (DHI, 2003)

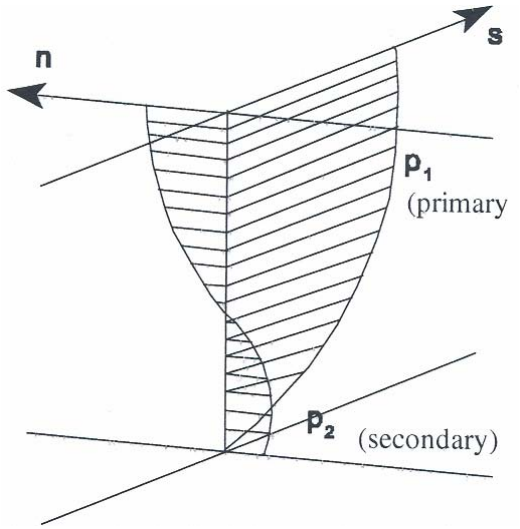

Figure 4-5: The vertical distributions of primary flow and helical flow (DHI, 2003)

The magnitude of the secondary flow can be shown to be proportional to the main flow velocity, the depth of flow and the curvature of the main flow stream lines. The intensity of the helical flow is the magnitude of the transverse velocity component (n-axis) and is defined by de Vriend (1981) as:

$$i_s = u\frac{h}{R_s} \tag{4-1}$$

where:

u = Main flow velocity
R_s = Radius of curvature of streamlines
i_s = Helical flow intensity
h = Water depth

The strength of the helical flow is used when determining the direction of both bed and suspended load sediment transport. Secondary flow due to curving streamlines causes a small deviation δ_s in the flow direction near the bed, away from the main stream direction. This also causes a deviation in the bed shear stress direction. The angle between bed shear stress and depth averaged shear stress (in the main flow direction) is given by the logarithmic model by Rozovskii (1957):

$$\tan \delta_s = -\beta \frac{h}{R_s} \tag{4-2}$$

The parameter β is defined as:

$$\beta = \alpha \frac{2}{\kappa^2}\left(1 - \frac{\sqrt{g}}{\kappa C}\right) \tag{4-3}$$

where:

κ = Von Karman's constant (0.4)
g = Acceleration due to gravity (9.81 m/s^2)
C = Chezy friction factor
α = Calibration constant

Helical flow is a principal secondary flow phenomenon in rivers and has a significant influence on the sediment transport direction and hence the morphological changes in the river channel. Helical flow is therefore analyzed in sediment transport simulations when larger scale morphology is modeled. More detail about the sediment transport and morphology models will be given in subsequent paragraphs.

Helical flow is included via the calibration constant α. This is entered either as a constant value throughout the model domain, or as a spatially varying value from a data file. The default value is 1.0. A limiting angle ($\tan \delta_s$), between the depth averaged flow shear stress direction and the helical flow shear stress direction must also be specified (DHI, 2003).

4.4 Hydrodynamic Integration

The hydrodynamic module simulates the water level and flow variation throughout the model. On this menu the type of hydrodynamic integration module is chosen. It can be either one of the following:

- Fully Dynamic
- Scaled Dynamic

- Quasi-Steady
- Steady

The hydrodynamics of rivers and reservoirs are characterised by complex three dimensional flow patterns. This has to be taken into account when these systems are modelled. However to apply a fully three dimensional model for long term simulations of river morphology requires excessive computational efforts. By introducing simplifications to the Navier-Stokes equations, the governing hydrodynamic equations can be reduced to two-dimensional equations representing conservation of momentum and mass in the two horizontal directions of a curvilinear coordinate system (DHI, 2003).

The curvilinear coordinate system is based on the shape of the grid with the s-axis in the main direction of flow while the n-axis represents the transverse direction of flow. Three dimensional effects are maintained in the depth-averaged model by introducing a separate model of the helical flow (secondary flow) component and by assuming similarity of the vertical distribution of the main flow velocities at all computational points. Three main approximations are adopted (DHI, 2003):

- Shallow water approximation where lateral exchange of momentum due to friction in the fluid is neglected.

- In the hydrostatic pressure distribution the component of vertical velocity is neglected

- The Rigid lid approximation implies that the water surface is considered as being a rigid impermeable and shear stress free plate.

To summarise, the flow model is valid for shallow, gently varying topography and mild curved and wide channels with small Froude numbers. The following effects are included in the equations when used for river and reservoir applications (DHI, 2003):

- flow acceleration around bends and through narrow sections
- advection and cross-momentum flow
- pressure gradients (water surface slopes)
- bed shear stresses
- Coriolis forces (only for large estuary and ocean models)
- wind forces (not included in this research)
- flow curvature and secondary helical flow

There are basically two main modules with which hydraulic calculations can be done. The first is the fully hydrodynamic module and the second is the quasi-steady module.

4.4.1 The Fully Hydrodynamic Module

The key characteristic of the module is that it solves the fully dynamic and vertically integrated St. Venant equations of continuity and conservation of momentum in the two horizontal directions thereby producing a parameterised description of the vertical distribution of primary flow. The two horizontal directions are the *s* (main flow direction) and *n* (transverse flow direction) axes. These directions are dependent on the shape of the grid as shown in Figure 4-6.

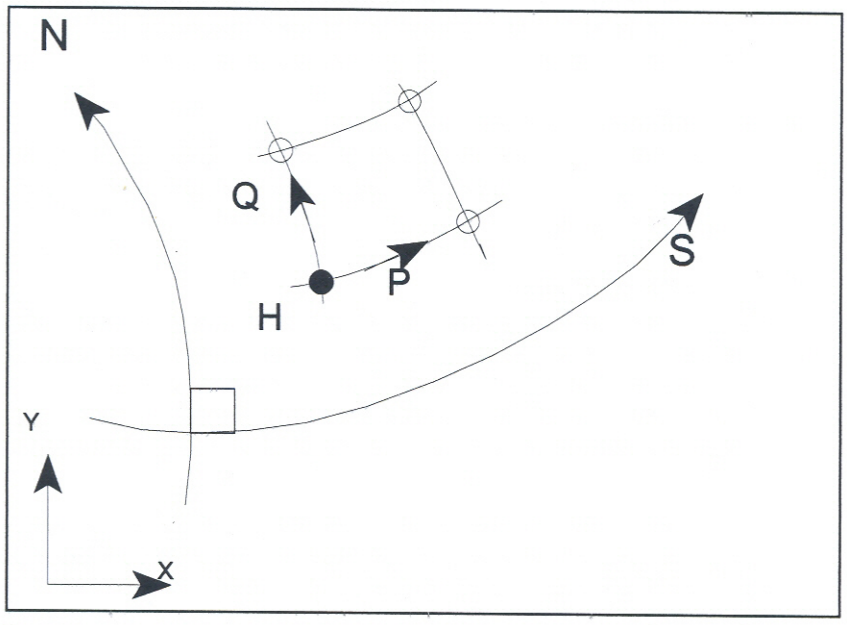

Figure 4-6: The curvilinear flow parameters (DHI, 2003)

The two horizontal axes (*s* and *n*) are described in a curvilinear orthogonal coordinate system, where one axis follows the bank lines of the river or reservoir. This makes the mathematical and numerical description substantially simpler. *Q* and *P* are the mass fluxes in the *s* and *n* directions respectively, while *H* is the flow depth at the specific grid point under consideration.

The curvature of the grid lines gives rise to additional terms in the partial differential equations for the flow. The dynamic equations solved are (DHI, 2003):

$$\frac{\partial p}{\partial t}+\frac{\partial}{\partial s}\left(\frac{p^2}{h}\right)+\frac{\partial}{\partial n}\left(\frac{pq}{h}\right)-2\frac{pq}{hR_n}+\frac{p^2-q^2}{hR_s}+gh\frac{\partial H}{\partial s}+\frac{g}{C^2}\frac{p\sqrt{p^2+q^2}}{h^2}=RHS \qquad (4\text{-}4)$$

$$\frac{\partial q}{\partial t}+\frac{\partial}{\partial s}\left(\frac{pq}{h}\right)+\frac{\partial}{\partial n}\left(\frac{q^2}{h}\right)-2\frac{pq}{hR_s}+\frac{q^2-p^2}{hR_n}+gh\frac{\partial H}{\partial n}+\frac{g}{C^2}\frac{q\sqrt{p^2+q^2}}{h^2}=RHS \qquad (4\text{-}5)$$

with: $$\frac{\partial H}{\partial t}+\frac{\partial p}{\partial s}+\frac{\partial q}{\partial n}-\frac{q}{R_s}+\frac{p}{R_n}=0 \qquad (4\text{-}6)$$

where:

s, n = Coordinates in the curvilinear coordinate system
p, q = Mass fluxes in the s- and n-directions respectively
H = Water level
h = Water depth
g = Gravitational acceleration
C = Chezy roughness coefficient
R_s, R_n = Radius of curvature of s- and n-line, respectively
RHS = The right hand side describing a.o. Reynold stresses, Coriolis force, wind friction and atmospheric pressure

These equations can also be written in terms of the cartesian rectangular co-ordinate system (DHI, 2003):

$$\frac{\partial p}{\partial t}+\frac{\partial\left(p^2/h\right)}{\partial x}+\frac{\partial\left(pq/h\right)}{\partial y}+\frac{gp\sqrt{p^2+q^2}}{C^2h^2}+gh\frac{\partial s}{\partial x}=h\frac{\partial}{\partial x}\left(E\frac{\partial(p/h)}{\partial x}\right)+h\frac{\partial}{\partial y}\left(E\frac{\partial(p/h)}{\partial y}\right) \qquad (4\text{-}7)$$

$$\frac{\partial q}{\partial t}+\frac{\partial\left(pq/h\right)}{\partial x}+\frac{\partial\left(q^2/h\right)}{\partial y}+\frac{gp\sqrt{p^2+q^2}}{C^2h^2}+gh\frac{\partial s}{\partial y}=h\frac{\partial}{\partial x}\left(E\frac{\partial(q/h)}{\partial x}\right)+h\frac{\partial}{\partial y}\left(E\frac{\partial(q/h)}{\partial y}\right) \quad (4\text{-}8)$$

where: $\frac{\partial h}{\partial t}+\frac{\partial p}{\partial x}+\frac{\partial q}{\partial y}=0$ (4-9)

and E is the eddy viscosity.

4.4.2 The Quasi-steady Hydrodynamic Module

This solver is a predictor-corrector algorithm that originates from methods for incompressible fluid flow. It is mostly used for reservoir applications.

Quasi-steady flow is suitable for slowly varying flow conditions. An example of this is a long term flood that occurs over weeks or even months, where gradual changes in flow occurs. A dynamic solver has restrictions limiting the length of the time step, which can make long term simulations computationally unfeasible. The quasi-steady solver is designed to perform simulations using a much longer time step than a dynamic solver, thus reducing computational effort. The solver uses a semi-implicit method for the continuity equation. Increasing the time step also means that the computational speed is substantially increased.

The reason why this solver can function in the way that it does, is the dynamic term in the continuity equation. With the fully hydrodynamic solver for unchanged flow conditions, the term is zero, but the dynamic term is still taken into account because it is the only link between the pressure and the continuity equation. In incompressible flows, the dynamic term is removed from the continuity equation. If the term is removed, it becomes difficult to use the continuity equation for obtaining the pressure.

It demands the use of a completely different solution strategy, namely one that allows the pressure to be determined from the continuity equation. For incompressible flow, advanced solution methods such as SIMPLE or PISO are used to determine the pressure. The pressure is thus not determined by the equations of continuity. The result is that the calculations at every time-step are much simpler and more stable and the quasi-steady solver can therefore run at an increased time-step, which effectively reduces the simulation time.

The governing equations of the quasi-steady module in terms of a Cartesian, rectangular coordinate system are (DHI, 2003):

$$\frac{\partial p}{\partial t} + gh\frac{\partial s}{\partial x} + \frac{gp\sqrt{p^2+q^2}}{C^2h^2} = h\frac{\partial}{\partial x}\left(E\frac{\partial(p/h)}{\partial x}\right) + h\frac{\partial}{\partial y}\left(E\frac{\partial(p/h)}{\partial y}\right) \text{ and} \tag{4-10}$$

$$\frac{\partial q}{\partial t} + gh\frac{\partial s}{\partial y} + \frac{gp\sqrt{p^2+q^2}}{C^2h^2} = h\frac{\partial}{\partial x}\left(E\frac{\partial(q/h)}{\partial x}\right) + h\frac{\partial}{\partial y}\left(E\frac{\partial(q/h)}{\partial y}\right) \tag{4-11}$$

$$\text{with: } \frac{\partial h}{\partial t} + \frac{\partial p}{\partial x} + \frac{\partial q}{\partial y} = 0 \tag{4-12}$$

The total time derivative is given by:

$$\frac{d}{dt} = \frac{\partial}{\partial t} + \frac{\partial}{\partial x}\frac{p}{h} + \frac{\partial}{\partial y}\frac{q}{h} \tag{4-13}$$

where x and y are the coordinates in the Cartesian rectangular co-ordinate system.

The only difference between the quasi-steady governing equations and the fully hydrodynamic equations is that the dynamic terms are left out. These terms are important in the fully hydrodynamic equations of continuity since they are used to determine the pressure.

The dynamic terms that are left out are:

$\frac{\partial\left(p^2/h\right)}{\partial x}+\frac{\partial\left(pq/h\right)}{\partial y}$ on the left hand side of equation 4-7, and

$\frac{\partial\left(pq/h\right)}{\partial x}+\frac{\partial\left(q^2/h\right)}{\partial y}$ on the left hand side of equation 4-8.

The output from both these basic hydrodynamic modules are the water flux and flow velocities in two directions, water depth and water surface elevation at all computational points at all time steps.

For both of these hydrodynamic modules any combination of the models listed below can be implemented simultaneously.

4.5 Traditional Equilibrium Transport Equations for Non-cohesive Sediments

Four equilibrium sediment transport theories are presently available in MIKE 21C. These were specifically formulated for the transport of coarse or non-cohesive sediments. They are:

- Engelund and Hansen (1967)
- Van Rijn (1984)
- Engelund and Fredsoe (1976)
- Meyer-Peter and Muller (1947)

The sediment transport models developed by Engelund & Fredsoe, 1976, and van Rijn, 1984, which distinguish between bed and suspended load, form the basis for the sediment transport description in MIKE 21C. It is also possible to use the formulas of Engelund-Hansen and Meyer-Peter and Muller (DHI, 2003).

In 2D mathematical modeling of sediment transport and morphology in rivers with large suspended load transports, it is necessary to distinguish between bed and suspended load in order to:

- simulate the dynamic development of bed dimensions and deposited layer thicknesses
- account for the effect of helical flow as well as the bed slope on the sediment transport direction

The theories of Engelund and Hansen (1967) and van Rijn (1984) have been discussed previously. The remaining two theories of Engelund and Fredsoe(1976) and Meyer-Peter and Muller (1947) will now be discussed.

a) Engelund and Fredsoe (1976)

The bed load transport rate is estimated from:

$$S_{bl} = 5p\left(\sqrt{\theta'} - 0.7\sqrt{\theta_c}\right)\sqrt{(s-1)gd_{50}^3} \tag{4-14}$$

where p, the probability of a sediment grain moving, can be determined by the expression:

$$p = \left[1 + \left(\frac{\frac{\pi}{6}\mu_d}{\theta' - \theta_c}\right)^4\right]^{-\frac{1}{4}}, \quad \theta' > \theta_c \tag{4-15}$$

with the dynamic friction coefficient μ_d equal to 0.51. The non dimensional skin shear stress is defined by:

$$\theta' = \frac{u_f^{'2}}{(s-1)gd_{50}} \tag{4-16}$$

and the friction velocity related to skin friction is calculated from the assumption of a logarithmic velocity profile as follows:

$$u_f^{'} = \frac{u}{6 + 2.5 \ln\left(\frac{h}{2.5 d_{50}}\right)} \tag{4-17}$$

The suspended load transport rate is obtained from:

$$S_{sl} = c_b u h \int_0^1 u(\eta) \cdot c(\eta) d\zeta \tag{4-18}$$

where c_b, the reference concentration near the bed, is calculated from:

$$c_b = \frac{0.65}{\left[1 + \frac{1}{\lambda_b}\right]^3} \tag{4-19}$$

with the linear sediment concentration λ_b, calculated from:

$$\lambda_b = \sqrt{\frac{\theta' - \theta_c - \frac{\pi}{6}\beta p}{0.020 s \theta'}} \tag{4-20}$$

The velocity profile is assumed to be:

$$u(\eta) = \frac{\sqrt{g}}{0.4C} \ln\left(\frac{\eta}{\eta_0}\right) \tag{4-21}$$

where the non-dimensional vertical coordinate η, is determined from:

$$\eta_j = \eta_{j-1} + \Delta \tag{4-22}$$

with the step height Δ determined from:

$$\Delta = \frac{1}{\left(\frac{1 - 1.05^{99}}{1 - 1.05}\right) - 1} \tag{4-23}$$

The no slip level η_o, is obtained from:

$$\eta_o = \exp\left(\eta_o - 1 - \frac{0.4C}{\sqrt{g}}\right) \tag{4-24}$$

The normalized vertical profile is specified in the following way:

$$c(\eta) = \left(\frac{1-\eta}{\eta} \cdot \frac{a}{1-a}\right)^z \tag{4-25}$$

The reference level a is defined by:

$$a = \frac{2d_{50}}{h} \tag{4-26}$$

The equilibrium mass concentration c_e is determined from:

$$c_e = \frac{S_{sl}}{uh} s \cdot 10^6 \tag{4-27}$$

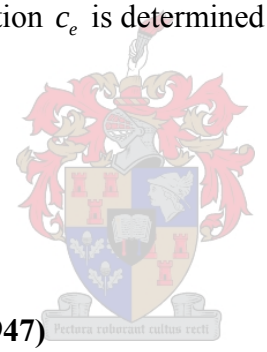

b) Meyer-Peter and Muller (1947)

A number of different sediment transport formulas can be encompassed by a common formula with flexible coefficients. The empirical expression for the sediment transport of bed load and suspended load is formulated to be generally acceptable. It can be defined using eight flexible coefficients. The general empirical bed load formula yields:

$$\Phi_{bl} = a_1 \cdot \left[\left(\frac{d_{90}}{d_{30}}\right)^{a2} I^{a3} C^{a4} \theta^{a5} \cdot \left[a_6 \theta^{a7} - \theta_c\right]^{a8}\right] \tag{4-28}$$

where:

Φ_{bl} = Non-dimensional bed load transport rate
I = Bed slope or slope of water surface
θ = Shields parameter for either total or skin friction

The Meyer-Peter & Muller formula is specified with the following set of coefficients for bed load calculations: $a_1 = 8.0,\ a_2 = 0.0, a_3 = 0.0,\ a_4 = 0.0,\ a_5 = 0.0,\ a_6 = 1.0,\ a_7 = 1.0, a_8 = 1.5$.

The same formula can be used to determine the suspended sediment load by only using other coefficients.

$$\Phi_{sl} = a_1 \cdot \left[\left(\frac{d_{90}}{d_{30}} \right)^{a2} I^{a3} C^{a4} \theta^{a5} \cdot \left[a_6 \theta^{a7} - \theta_c \right]^{a8} \right] \tag{4-29}$$

The equilibrium concentration is then given by:

$$c_e = \frac{S_{sl}}{uh} s \cdot 10^6 \tag{4-30}$$

4.5.1 Implementing the Equilibrium Transport Theories (DHI, 2003)

A feature of MIKE 21C is that the transport of different sediment fractions can be modeled, each with its own grain size, porosity, critical Shields parameter and initial concentration. Each of these fractions can then be defined as either sediment transported as bed load or suspended load or a combination of both by allocating load factors. With this model it is possible to simulate the sorting in space and time of graded sediment.

The total load sediment transport formulas, such as that of Engelund & Hansen (1967) can therefore not be used for river applications with consideration of helical flow and bed slope without a separate specification of how the sediment is distributed between bed load and suspended load. It is possible though to run simulations with MIKE 21C with a total transport formula only by disregarding the effect of helical flow and bed slope.

If the suspended sediment transport is negligible compared to the bed load transport, the suspended sediment model can be switched off, so only a bed load model (or a

total load model) is employed. Either one or both of the transport mechanisms can be implemented in a model.

4.5.2 The Bed Load Model

For bed load, a bed load factor can be applied to the selected transport formula for the specific fraction. The default value is 1.0, and values can vary between 0.5 and 2.0.

In MIKE 21C, the bed load transport is calculated explicitly from one of the selected formulas, eg. Engelund & Fredsoe, Van Rijn, or Meyer-Peter & Muller. These formulas relate the transport rate to the bed shear stress and the grain diameter.

On a horizontal bed, the transport direction will coincide with the direction of the bed shear stress. The direction of the bed shear stress may, however, deviate from the direction of the depth-averaged main flow due to the helical flow as described previously. On sloping beds, the gravity will have influence on the transport direction. This is brought into account by the bed slope calculations.

The output from the bed load model is the bed load transport rate and direction at every computational grid point.

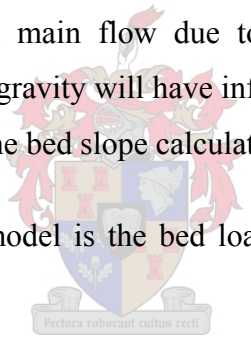

4.5.3 The Suspended Load Model

For suspended load a suspended load factor can be applied to the selected transport formula for a specific fraction. As for bed load the default value is 1, and values can vary between 0.5 and 2.0. The maximum concentration or suspended sediment transport capacity must be specified by the user.

These standard methods for calculations of suspended load are not applicable in the case of detailed modeling (including cohesive sediment) of rivers and reservoirs. It is necessary to include the time and space lag in the sediment transport response to changes in local hydraulic conditions. This is because the suspended load is not only a

function of changing hydraulic conditions, it is also a function of what takes place upstream and earlier in time.

A relevant time scale for the time lag is the settling time for a sediment grain in the water column. Correspondingly, a length scale for the space lag is the horizontal distance traveled by the grain during settlement.

The space lag effect is modeled here by means of a depth-averaged advection-dispersion model which represents the transport and the vertical distribution of suspended solids and flow. This model is an extension of the two dimensional model by Wang (1989). The model by Wang, however, did not include the effect of helical flow. This effect is essential in the case of river and reservoir applications because the suspended load direction will be different from the main flow direction due to helical flow.

The secondary flow profile is computed in MIKE 21C and used together with the primary flow profile and the concentration profile when the suspended load is integrated over the depth. As the concentration is highest near the river bed, the suspended load transport will be deflected towards the center of flow curvature.

In contrast to bed load, the transverse river bed slope does not influence the direction of suspended load transport.

The depth-averaged advection-dispersion model requires an expression for the equilibrium concentration. The models by Engelund & Fredsoe (1982) or Van Rijn (1984) can be used for that purpose. The empirical formulas implemented in MIKE 21C can also be used assuming that the equilibrium concentration equals the suspended load divided by the water flux.

The output from the suspended load model is the concentration of suspended sediment as well as the suspended load transport direction at every computational grid point.

4.6 The Cohesive Sediment Transport Model

MIKE 21C was originally designed only to model non-cohesive sediment transport in two dimensions. Recently though, DHI also developed a special version for cohesive sediment transport with the advection-dispersion model. Cohesive Sediment transport can now also be modeled using the fully hydrodynamic or the Quasi-steady hydrodynamic modules. This feature does not appear on the main MIKE 21C program interface and needs to be implemented in the programming code itself. Throughout this research, simulations will be carried out using this added feature.

This module describes the erosion, transport and deposition of cohesive sediments (mud, silt and clay). The transport of mud is entirely based on the advection dispersion module for very fine sediments as described in the preceding paragraphs.

The advection-dispersion model brings into account the effects of time and space lag in the transport processes of the fine sediment. This model also takes into account the consolidation of the river bed.

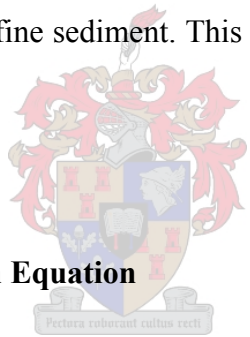

4.6.1 The Advection-Dispersion Equation

Mass transport is controlled by two mechanisms: advection and dispersion. As previously stated, advection accounts for the movement of the solute, linked to the fluid, with the average water velocity. Diffusion accounts for mixing caused by turbulence or by the random particle movement from a higher concentration to a lower concentration. The combination of advection and diffusion is termed dispersion.

The advection-dispersion model is used to describe the transport, dispersion, erosion and deposition of suspended fine sediments. The transport of the suspended sediments is described by an advection-dispersion (AD) equation:

$$\frac{\partial hc}{\partial t}+\frac{\partial p'c}{\partial x}+\frac{\partial q'c}{\partial y}=\frac{\partial}{\partial x}\left(hD_{xx}\frac{\partial c}{\partial x}\right)+\frac{\partial}{\partial y}\left(hD_{yy}\frac{\partial c}{\partial y}\right)+E-D \qquad (4\text{-}31)$$

where:

p', q' = Modified flux field (m^2/s) according to equation 4-32 below
c = Concentration (mg/ℓ)
D_{xx} = Dispersion in the x-direction (includes advection and turbulent diffusion)
D_{yy} = Dispersion in the y-direction (includes advection and turbulent diffusion)
E = Erosion function
D = Deposition function

The dispersion in the equation originates from the flow profile functions. The dispersion coefficients are therefore determined by the model itself. Additional molecular diffusion can be added although no molecular diffusion function is activated in the simulations in this research.

The modified flux field that describes the transport of the suspended sediments is derived from the depth integrated flux field in the manner (DHI, 2003):

$$\begin{pmatrix} p' \\ q' \end{pmatrix} = \alpha_{01} \begin{pmatrix} p \\ q \end{pmatrix} + \alpha_{02} \frac{h}{R} \begin{pmatrix} -q \\ p \end{pmatrix} \tag{4-32}$$

Where α_{01} and α_{02} are functions of the distribution of momentum and sediment over the water column. The term h/R is the water depth divided by the streamline radius of curvature; the latter derived from the flow field. The modified flux field calculations arise from the three-dimensional character of the flow.

α_{01} modifies the steam wise advection, and represents the fact that the sediment concentration rises towards the bed, while the velocity rises towards the surface. The stream wise advection of the sediment is hence not as effective, as α_{01} =1 would imply. A value of α_{01} =1 is found for uniformly distributed sediment i.e. very fine material. Though we are dealing with fine sediments, it should nonetheless be remembered that the velocities in the reservoir are small, so the sediment will be located close to the bed. The value of α_{01} can be calculated from the logarithmic velocity profile and the distribution of sediment.

α_{02} represents the impact of secondary flow, and reflects advection across the streamlines. α_{02} is calculated from the helical flow taken from standard theory and the distribution of sediment.

The α_{01} and α_{02} parameters are calculated from local values of the flow velocity, flow resistance and settling velocity. The calculation is done for each morphological time-step in describing the change in sediment concentration and sedimentation in time.

An implicit scheme is applied for the AD equation in which the local availability of sediment is accounted for by limiting erosion to the available sediment volume in the cell. The implicit solution of the AD equation furthermore allows for implicit updating of the local sediment layer thickness, which is done through the source/sink terms of the equation (sediment entering the water column comes from the bed, and vice versa). The implicit AD scheme is unconditionally stable for any choice of time step.

As previously stated in chapter 2, a standard cohesive model gives the erosion and deposition rates via the following functions (DHI, 2003):

$$E = E_o\left(\frac{\tau}{\tau_{ce}} - 1\right)^m \quad , \ \tau > \tau_{ce} \quad \text{and} \tag{4-33}$$

$$D = w_s c\left(1 - \frac{\tau}{\tau_{cd}}\right) \quad , \ \tau < \tau_{cd} \tag{4-34}$$

4.6.2 Limitations of the Cohesive Sediment Model

One of the limiting factors of the specific MIKE 21C version that was available for this research is that the user is unable to specify the magnitude of the helical flow and therefore α_{02} . The effects of secondary helical flow is however still included in the computations, only without lag-effects, i.e. it is assumed that the secondary flow adapts instantaneously to flow curvature of the mean flow.

Full advection and turbulent diffusion is implemented by the AD equation. The dispersion coefficients in the two horizontal directions are determined by the model itself according to the flow profiles and are also not specified by the user. Additional molecular diffusion can be added if it is required, but it has very little effect on the overall dispersion of the sediments.

The model does require that a value of between 0 and 1 for $\alpha_{01,}$ the stream wise constant for advection, is specified by the user. Another limitation is that the transport of only one size particle at a time can be simulated with this model. This is done by specifying the representative settling velocity w.

Other parameters of the sediment and transport that need to be specified are:

- critical shear stress for erosion
- critical shear stress for deposition
- erosion constant
- erosion exponent
- sediment porosity
- sediment density

4.7 Morphological Change Models

The models below are available in the MIKE 21C program, but will not be implemented further in this research:

4.7.1 Planform Model

Bank erosion is a very important morphological process and it's appropriate description is vital to get the full picture of the overall morphological change of the area. In MIKE 21C, the bank erosion is simply simulated simultaneously with the sediment transport and hydrodynamic simulations. This is done by a simple equation that calculates the bank erosion rate in meter per second. The extra sediment which is removed from the bank is included in the sediment continuity equation.

On the program interface the number of eroding banks is specified, usually 2 for a river or reservoir model. The erosion characteristics of each bank are specified. The maximum bank erosion rate is also specified by the user as a limiting factor.

4.7.2 Alluvial Resistance Model

It is extremely difficult to determine the hydraulic resistance in alluvial rivers because it largely depends on the form of the bed. The bed forms are determined by the sediment transport and flow and therefore continuously change with time. There are basically two components; form friction (caused by the drag on the bed form) and skin friction (caused by shear forces on the bed). The models of Engelund-Hansen and Ackers and White are semi-empirical and link the alluvial resistance to the instantaneous hydraulic conditions. There can however be a significant time lag between bed form development and the hydraulic conditions.

For most applications though, the differences in bed resistance due to rapidly changing bed levels may be more important than the differences in bed resistance due to the increase or decrease in the flow rate.

Thus a simpler alluvial bed resistance model as in equation 4-48 was found to be used in most cases:

$$C = ah^b \tag{4-35}$$

where C is the Chezy friction factor, h is the local depth and a and b are calibration constants.

The two calibration constants are defined by the user when implementing the model. The default values of the coefficient and the exponent are 30 and 0 respectively. The upper and lower limits of computed bed resistance are also specified.

4.7.3 Large-scale Morphological Model

This model incorporates bed level changes and plan form changes due to bank erosion. The change of bed level is quite easily determined by integrating the net inflow and outflow within a control volume and thus a much larger time step than the hydrodynamic time step can be applied without the model becoming unsteady.

Three kinds of boundary conditions can be specified for the morphological model at the upstream boundary: total sediment transport, bed level changes, or concentration of suspended sediment.

For this model the number of deposited sediment layers below the existing bed level has to be specified. If this value is set to zero, it means that the bed is an infinitely deep layer of sediment. This model has as output bed level and bed level changes.

The output from the large-scale morphological model is sediment transport (bed load as well as suspended load), the bed level and bed level changes at every grid point and at every time step. Also accumulated bank erosion and new grid co-ordinates are output from the model if the bank erosion and grid update modules are activated (DHI, 2003).

4.8 The Selection of Hydrodynamic Module and Models to be Implemented

When modelling the transport of cohesive sediments in large reservoirs the changes in water level and discharge into the model vary relatively slowly and therefore longer time steps can be used between hydrodynamic calculations. Longer periods can thus be simulated for the same computational effort. Long sedimentation simulation periods are necessary before significant changes in the bed level of a reservoir can be observed. The quasi-steady hydrodynamic solver is perfectly suited for this type of model. The velocities are also smaller in reservoirs than in rivers and thus non-cohesive sediments could be deposited at the upstream boundary already. The cohesive sediment on the other hand tends to be carried further into the reservoir. The available special version of MIKE 21C with the advection-dispersion model for cohesive sediment transport is used to simulate the transport processes of these fine particles.

4.8.1 Calibration

The calibration process for the MIKE 21C hydrodynamic and morphologic model involves tuning of a few calibration parameters. All the calibration factors have a physical meaning and should be given values inside realistic ranges to obtain agreement with observed data.

5. MIKE 21C MODEL VARIABLES

5.1 Sensitivity Study Numerical Model Setup

In this chapter each of the sedimentation parameters specified in the MIKE 21C interface were investigated. Some of these variables had definite pre-determined values, for instance the physical parameters of sediment size, density and porosity. All the other transport parameters, such as settling velocity, were tested in a series of MIKE 21C simulations to determine their sensitivities to changes. During these simulations, all other parameter values were kept constant at their default values.

The model setup is a simple rectangular channel with a length of 30m and a width of 1m. The discharge is 0.01m^3/s and the water depth is kept constant at a depth of 0.333m by damming at the downstream boundary. This depth is much larger than the normal flow depth. The flow is turbulent. The discharge is smaller, but the flow depth is the same as in the laboratory tests that will be discussed in chapter 6. These and other parameters are shown in Table 5-1.

Table 5-1: Sensitivity study model parameters

Hydraulic Parameters:

Q	0.010	m^3/s
Water depth	0.333	m
v	0.033	m/s
Starting Concentration	10 000	mg/ℓ
Simulated real time	1	hr
Actual run time per simulation	5	min

Sediment Characteristics:

Sediment particle size	0.0334	mm
Sediment density	2 650	kg/m3
Sediment porosity	0.5	-

Transport Parameters:

Bed roughness - Manning's M	90	$m^{0.33}/s$
- Manning's n	0.011	$s/m^{0.33}$
Settling velocity	0.001	m/s
Critical shear stress for deposition	0.05	N/m^2
Critical shear stress for erosion	1.04	N/m^2
Erosion constant	0.1	$g/m^2/s$
Exponent of erosion	2	-
Dispersion (Added molecular diffusion)	0	-

5.2 Sediment Particle Size

The sediment particle size distribution can be determined with a sieve analysis for coarse material and with the standard ASTM hydrometer method for fine material smaller than 0.075 mm in diameter. Here a sediment size of 0.0334mm (silt) was chosen. This relatively large value was chosen so that some deposition takes place and that the deposition patterns of the various simulations could also be compared. This size particle has a settling velocity of 0.001 m/s, according to Stokes' law for fine sediment (Chadwick and Morfett, 1998). In South African reservoirs though, clay (<0.004mm) is often the predominant suspended sediment component and it is likely that in reservoir applications, both the representative sediment size and settling velocity could be smaller.

5.3 Sediment Relative Density

The density of the sediment particles was taken as 2 650kg/m^3. The density of water was taken as 1 000kg/ m^3. The relative sediment density was therefore 2.650.

5.4 Sediment Porosity

The porosity is the ratio of the volume of voids to the total volume of the soil (Craig, 2001):

$$n = \frac{V_v}{V} \tag{5-1}$$

The porosity of the sediment was taken as 0.5 throughout this research.

5.5 Bed Roughness

In the MIKE 21C interface, the bed roughness is specified in terms of Manning's M value, which is the inverse of Manning's n value. In these sensitivity simulations using a glass channel, n was taken as 0.011, thus M = 90 $m^{0.33}/s$. For modelling of river and reservoir systems, n was taken as 0.020, which is equivalent to an M value of $50m^{0.33}/s$.

5.6 Settling Velocity w

Seven simulations were run using a different value of settling velocity in each case. The outputs of suspended sediment concentration and deposited layer thickness are shown in Figures 5-1 and 5-2 below. Note that the suspended sediment concentrations are depth averaged. The unit of the settling velocity values is m/s.

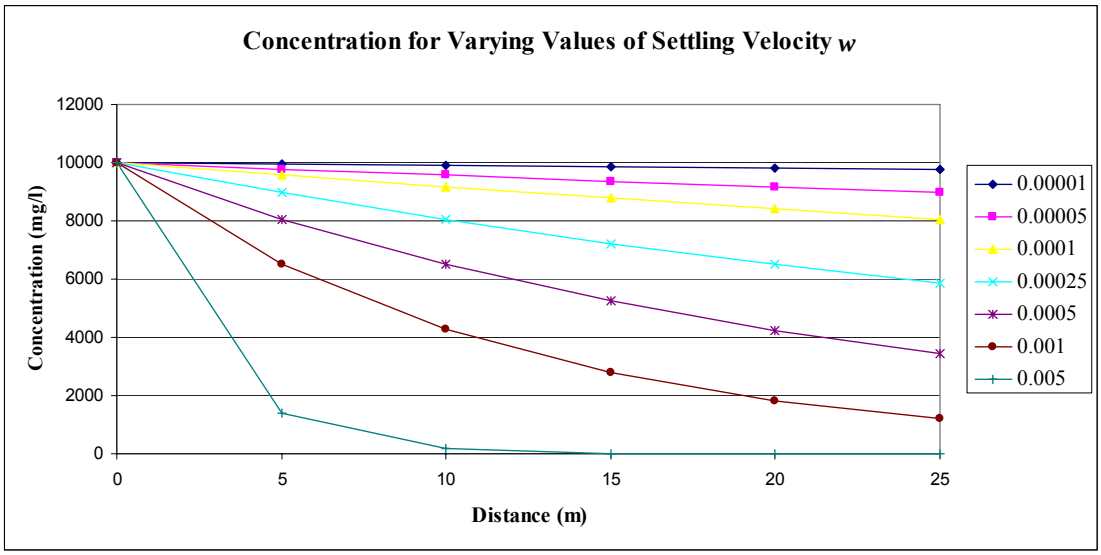

Figure 5-1: Sediment concentrations for different settling velocities

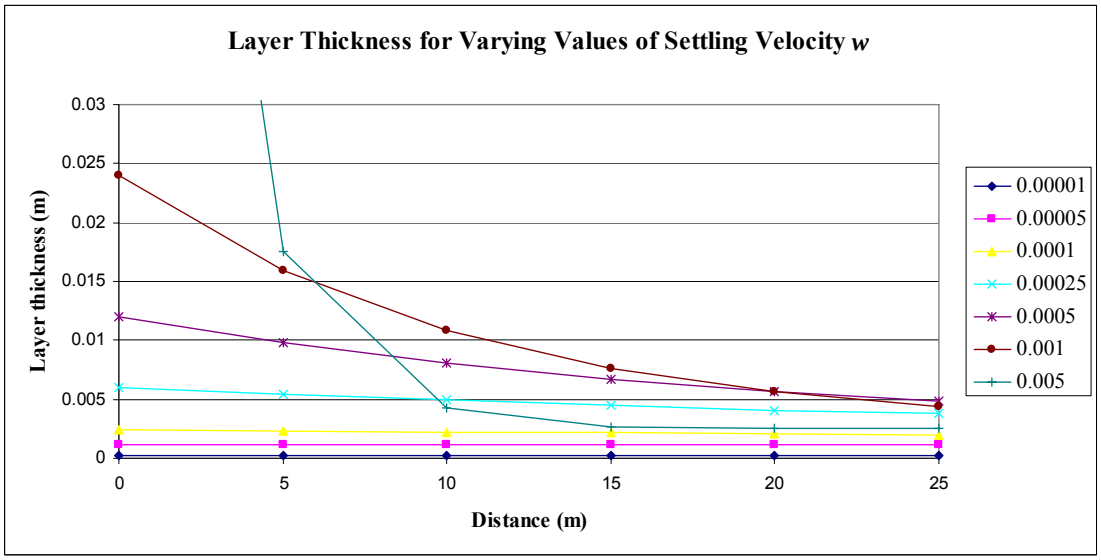

Figure 5-2: Deposited layer thickness for different settling velocities

As expected, sediments are deposited faster when particles with a higher settling velocity are used and therefore the concentration reduces more rapidly. When a lower value of settling velocity, such as 0.00001m/s is used, there is almost no deposition and the depth averaged concentration remains almost constant at 10 000mg/ℓ. For reservoir simulations where the fine sediments have to be carried far into the reservoir, smaller values such as 0.0001m/s will be more realistic. This value should however be related to sediment particle sizes as determined by field sampling.

5.7 The Stream Wise Advection Constant α_{01}

The stream wise constant α_{01} modifies the stream wise advection, and represents the fact that the sediment concentration increases towards the bed, while the velocity increases towards the surface. A value for α_{01} of 1.0 produces uniformly distributed sediment as in the case of very fine material while a value of 0.1 represents a distribution similar to that of an underflow density current. The results for various values of α_{01} are shown in Figures 5-3 and 5-4.

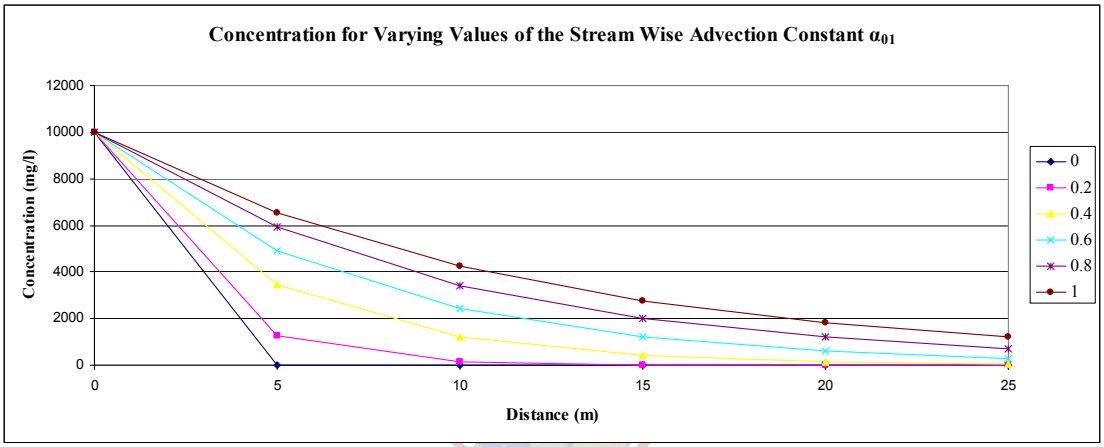

Figure 5-3: Sediment concentrations for different stream wise constants

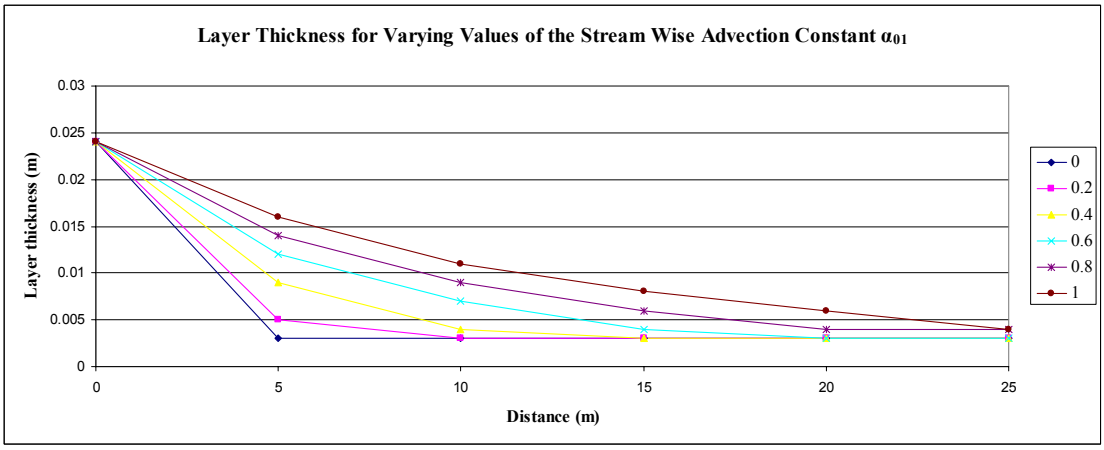

Figure 5-4: Deposited layer thickness for different stream wise constants

With α_{01} = 1, the concentrations gradually decrease. With a very low α_{01} value, such as 0.1 or 0.2, the concentrations are immediately reduced to almost 0, and a lot of

deposition is found at the upstream boundary (not so clear from the figure). It is evident that for reservoir applications, a value for α_{01} of 1.0 is appropriate to ensure that fine sediment is carried uniformly into the reservoir as far as possible.

5.8 Critical Shear Stress for Deposition τ_{cd}

Deposition takes place as soon as the bed shear stress reduces to this critical shear stress value or lower. The value of this parameter can determine whether deposition will take place in large quantities (smaller value) or not at all (too large a value) according to the deposition function (DHI, 2003):

$$D = w_s \cdot c\left(1 - \frac{\tau}{\tau_{cd}}\right) \tag{5-2}$$

The results for various values of τ_{cd} are shown in Figures 5-5 and 5-6.

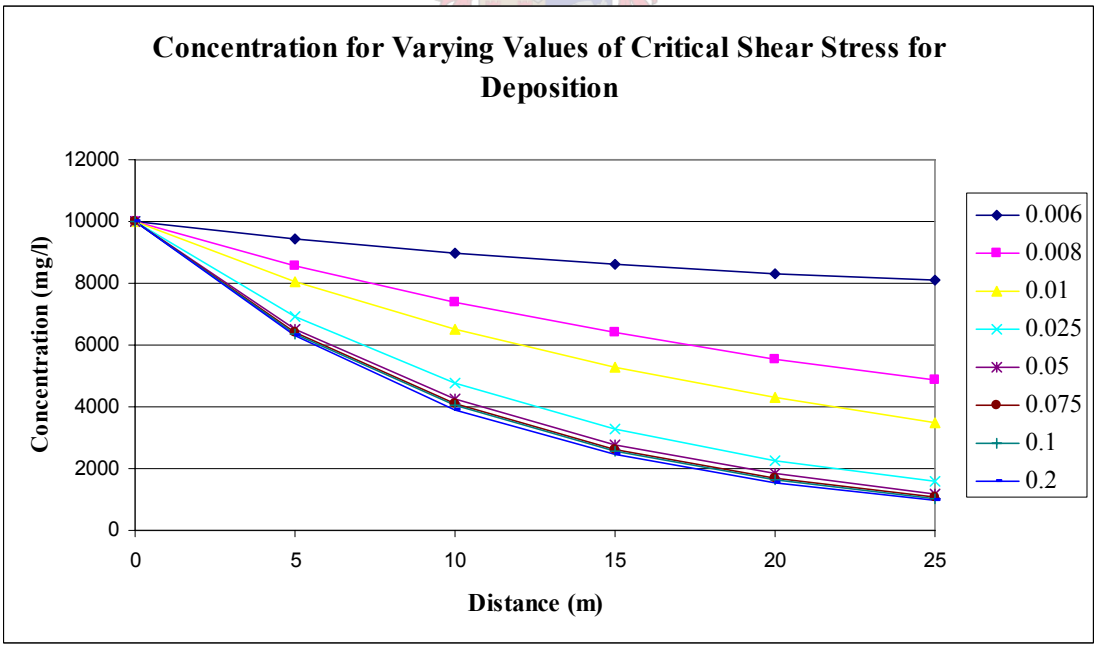

Figure 5-5: Sediment concentrations for different shear stresses for deposition

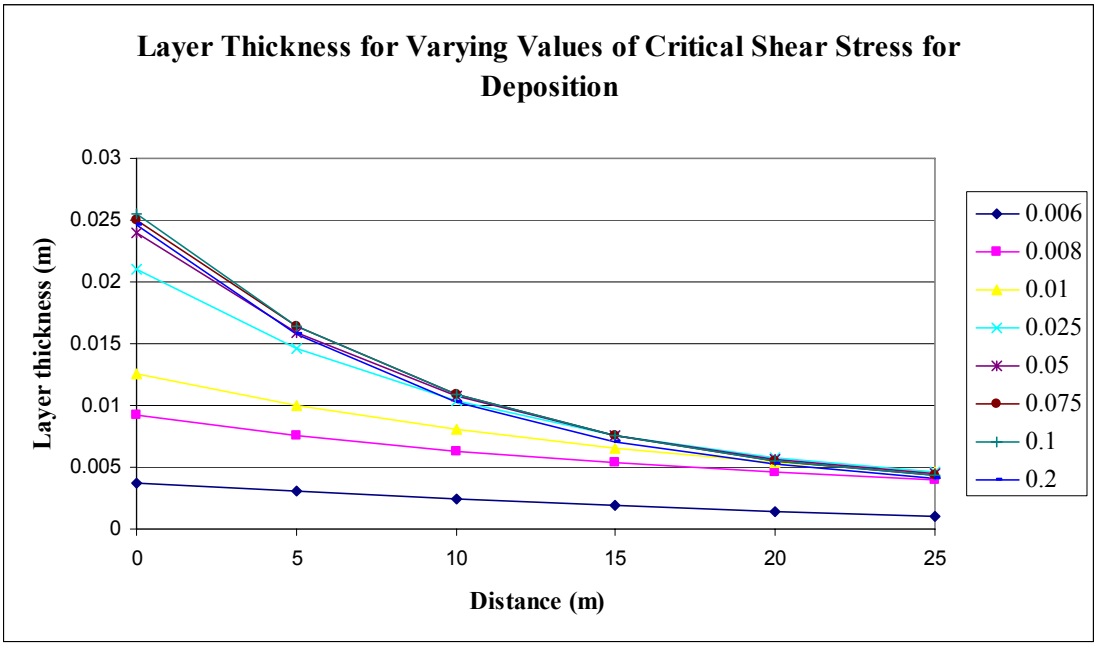

Figure 5-6: Deposited layer thickness for different shear stresses for deposition

These figures show that for the specific conditions of flow in this channel, deposition starts occurring at a limit value slightly lower than 0.006. All values below this limit showed no deposition and thus constant concentrations throughout the channel. The output from values between 0.05N/m^2 and 0.2N/m^2 are very similar, meaning that the critical shear stress reaches an upper limit at a value of 0.05N/m^2. This is because the bed stresses are mostly below the value of 0.05 N/m^2 and thus no more sediment can be deposited.

Bed shear stress is dependant on the flow velocity, the bed roughness and the water depth according to (DHI, 2003):

$$\tau = \frac{\rho g v^2}{C^2} \text{ or in terms of Manning's M: } \tau = \frac{\rho g v^2}{\left(Mh^{1/6}\right)^2} \qquad \text{(5-3), (5-4)}$$

For this channel setup the average bed shear stress, calculated with any of the equations above, equals 0.002N/m^2. It can be seen from the figures that this is the lower limit for τ_{cd}, since no deposition occurs for lower values.

5.9 Critical Shear Stress for Erosion τ_{ce}

This is the value of bed shear stress that has to be exceeded for the erosion process to commence. The results for various values of τ_{ce} are shown in Figures 5-7 and 5-8.

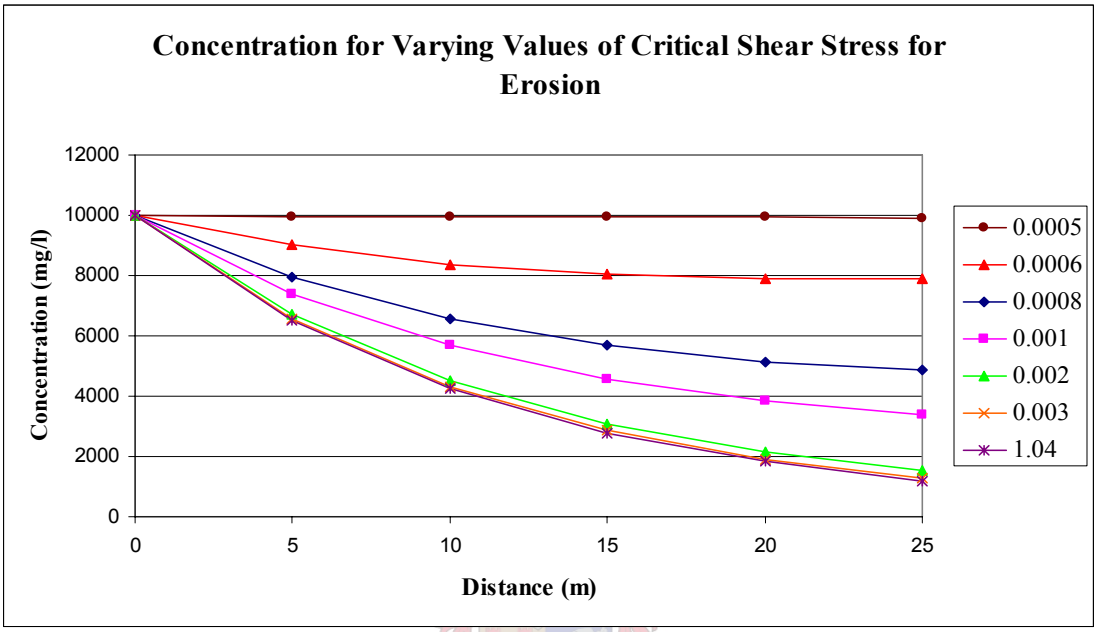

Figure 5-7: Sediment concentrations for different critical shear stresses for erosion

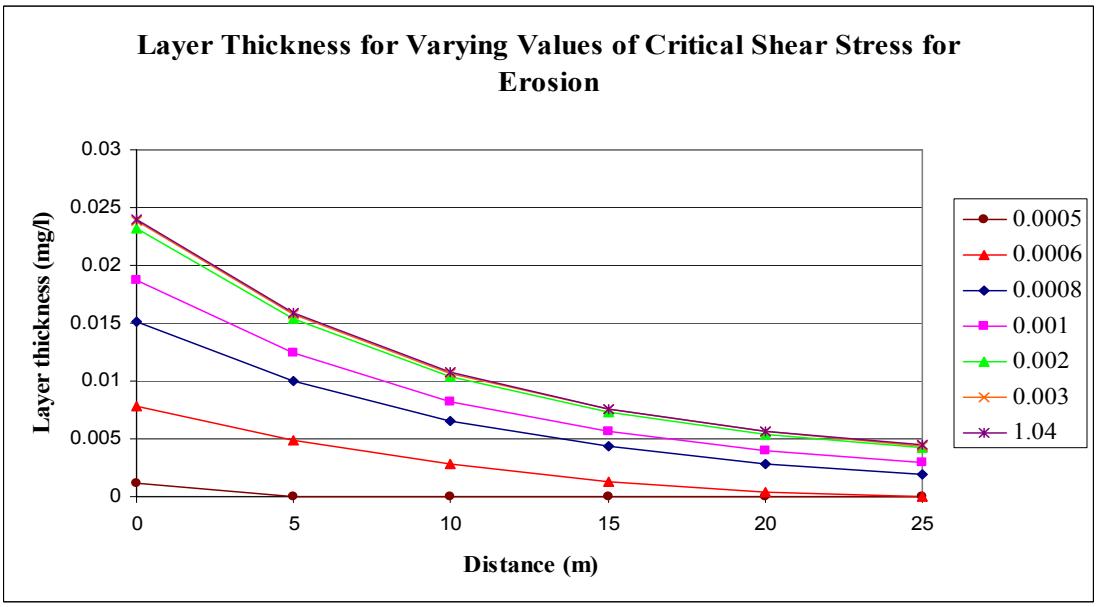

Figure 5-8: Deposited layer thickness for different critical shear stresses for erosion

The critical shear stress for erosion varies in a similar way as the critical shear stress for deposition. The simulation with a small value of 0.0005N/m^2 showed almost no difference in the longitudinal concentrations and no layer thickness either. This is because the critical stress for erosion was so small that the stresses were always larger than this value and erosion was thus constantly in progress. The simulations with values of 0.003N/m^2 and 1.04N/m^2 showed similar results. There were almost no erosion and a large layer thickness. The concentrations with these values also reduced at a constant rate. For these specific conditions of flow, the critical shear stress for erosion thus has a lower limit of 0.0005N/m^2 and an upper limit of 0.003N/m^2.

The shear stress for erosion is dependant on the cohesiveness of the bed sediment. The finer the bed sediment and the longer the allowed consolidation time, the larger the bed shear stresses required to erode it.

5.10 Erosion Constant E_0

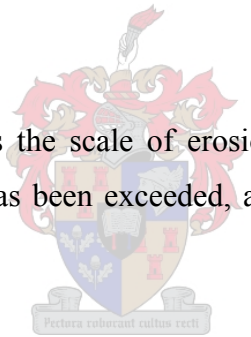

The erosion constant determines the scale of erosion that will take place once the critical shear stress of erosion has been exceeded, according to the erosion function (DHI, 2003):

$$E = E_0 \left(1 - \frac{\tau}{\tau_{ce}} \right)^m \qquad (5\text{-}5)$$

The results for various values of E_0 are shown in Figures 5-9 and 5-10.

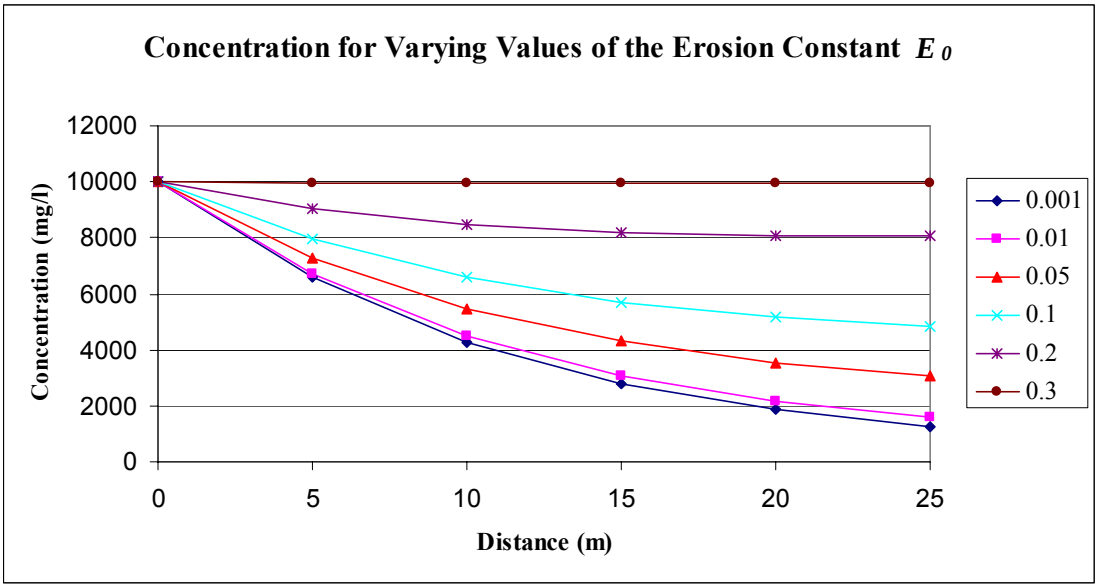

Figure 5-9: Sediment concentrations for different erosion constants

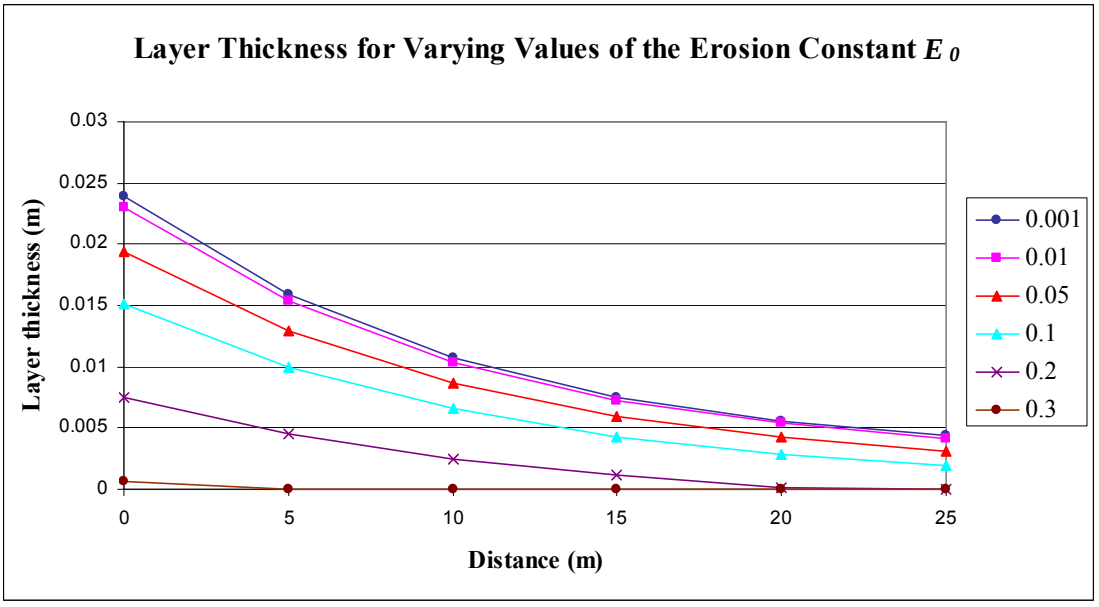

Figure 5-10: Deposited layer thickness for different erosion constants

As expected, the sensitivity study reveals that the erosion will be more severe given a larger erosion constant. This is applicable to all conditions of flow.

5.11 Exponent of Erosion *m*

Another parameter that determines the scale of the erosion process, is the exponent of erosion m. The erosion function is given by equation 5-5. The results for various values of *m* are shown in Figures 5-11 and 5-12.

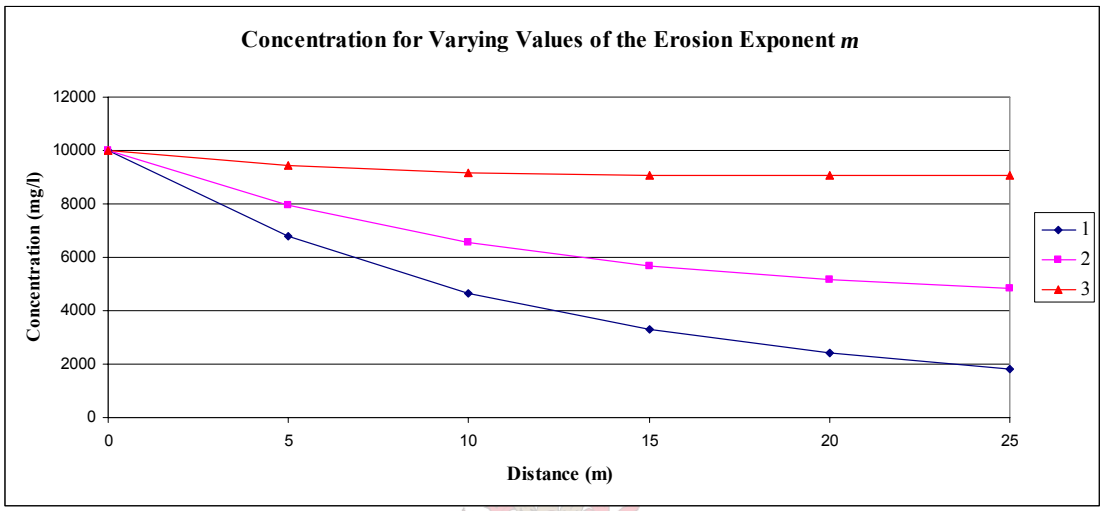

Figure 5-11: Sediment concentrations for different erosion exponents

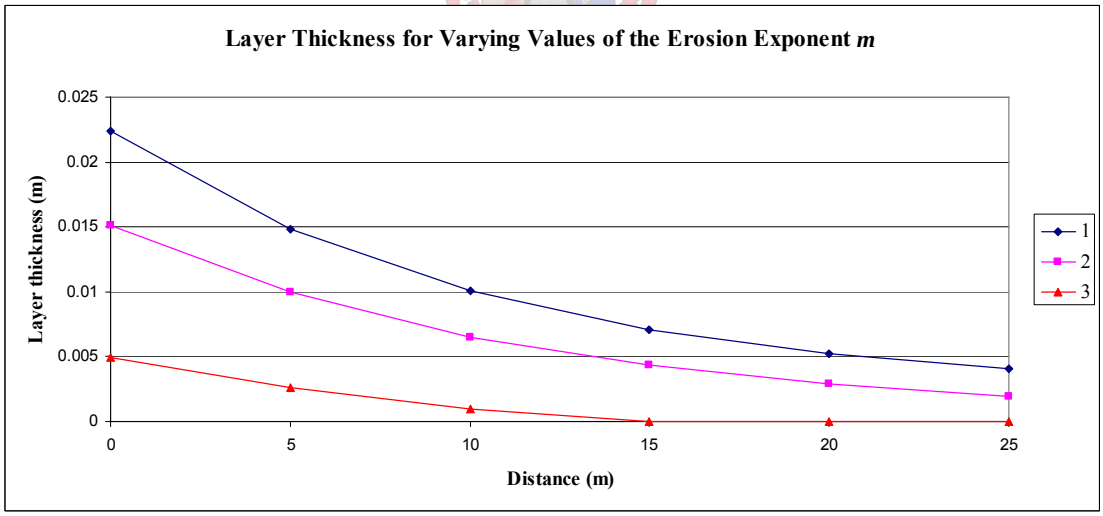

Figure 5-12: Deposited layer thickness for different erosion exponents

The results show that the layer thickness decreases and concentrations increase with a larger value of the erosion exponent. Also here, as expected, the sensitivity study reveals that the erosion will be more severe given a larger erosion exponent.

5.12 Dispersion

This parameter specifies the amount of added molecular diffusion required for the simulation. For all simulations in this research, this parameter is kept at a constant value of 0. The molecular diffusion has very little effect on the overall dispersion. The *x* and *y* horizontal dispersion coefficients are determined by the model itself (DHI, 2003).

6. LABORATORY TESTS

6.1 Objectives

In these tests steady uniform flow is created in a 35m long rectangular flume into which a concentrated mixture of fine sediments and water is added at a constant rate and concentration to the upstream end. The purpose of these tests was to measure the concentrations of the suspended sediment at regular intervals along the flume thereby obtaining the rates of decrease in suspended sediment concentration. The results of these tests would be compared to the results from numerical tests done with the MIKE 21C model, thereby gaining insight into the calibration of the sedimentation parameters.

6.2 Design and Methodology

Firstly a suitable channel had to be identified in which the desired flow conditions could be established. A rectangular horizontal glass flume with a length of 40m, width of 1m and depth of 1.2m was available. The flume is shown in Figure 6-1.

Figure 6-1: The dry laboratory channel

To minimize the effects of the shear stress due to friction on the flume's sides, the depth was limited to a third of the flume's width (0.333m). To simulate the subcritical

flow regime generally found in reservoirs, test velocities of 0.1m/s and 0.05m/s were chosen. Turbulent sediment transport was to be maintained in all the tests. These two flow velocities produce high enough Reynolds' numbers of 20 000 and 10 000 respectively. Flow calculations are shown in Appendix A.

To establish these velocities at a normal flow depth of 0.333m, discharges of $0.0333m^3/s$ and $0.0167m^3/s$ were required. To establish this depth and velocity in the horizontal channel, a sluice gate at the downstream end was used to control the flow. The water flowed over this sluice gate and fell into the laboratory's drainage system.

Four tests were performed, two with an upstream suspended sediment concentration of 5 000 mg/ℓ (0.5% by mass) and the other two with a concentration of 10 000 mg/ℓ (1% by mass), both very high flood concentrations compared to the suspended sediment concentration of 225 mg/ℓ (0.023% by mass) measured by RandWater during the February 1996 flood at Vaal Reservoir. These values are however of the same order as flood concentrations measured at Welbedacht Reservoir where extreme sediment concentrations up to 6.5% by mass have been recorded. A summary of the test parameters as discussed so far can be seen in Table 6-1 below:

Table 6-1: The laboratory test flow parameters

	Test 1	**Test 2**	**Test 3**	**Test 4**
Water depth (m)	0.333	0.333	0.333	0.333
Velocity (m/s)	0.10	0.10	0.05	0.05
Q_{total} (m^3/s)	0.0334	0.0334	0.0167	0.0167
Input Concentration (mg/ℓ)	5 000	10 000	5 000	10 000

6.3 Test Setup

To achieve these specified concentrations a large container with a volume of 1.692m^3 was used. For each test a concentrated sediment suspension was created in the container after which the suspension was released at a rate of 6.1 ℓ/s into the upstream end of the channel to create either the 5 000mg/ℓ or 10 000mg/ℓ concentrations in the channel. The calculations are shown in Appendix A. Figure 6-2 is a schematic drawing of the laboratory setup. The high sediment concentration in the mixing container was maintained in the container by turbulence created via a circular air pipe with orifices that released compressed air from the bottom of the container. It was assumed that the air released into the suspension did not have an effect on the solubility of the water. The release rate of 6.1 ℓ/s from the container was also not influenced by the released air. The sediment concentrate was released into the channel flow by a submerged horizontal pipe with holes drilled at regular intervals, specially designed to disperse the suspension uniformly downstream at three different heights and angles and over the whole width of the channel. The dispersing pipe is shown in Figure 6-3. Figure 6-4 shows the laboratory flume setup as seen from downstream.

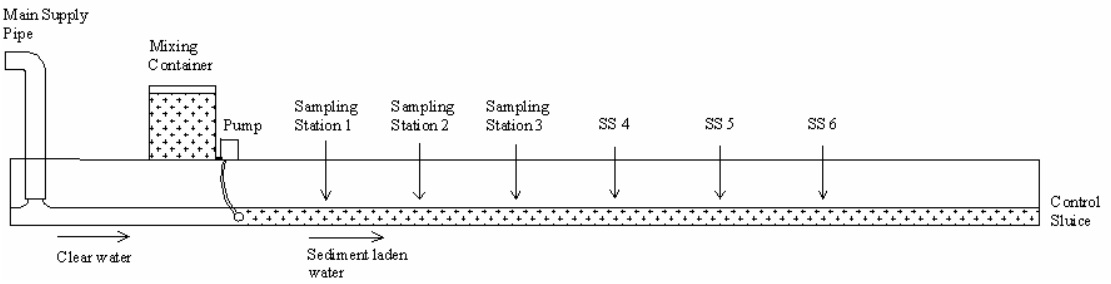

Figure 6-2: A schematic drawing of the laboratory setup

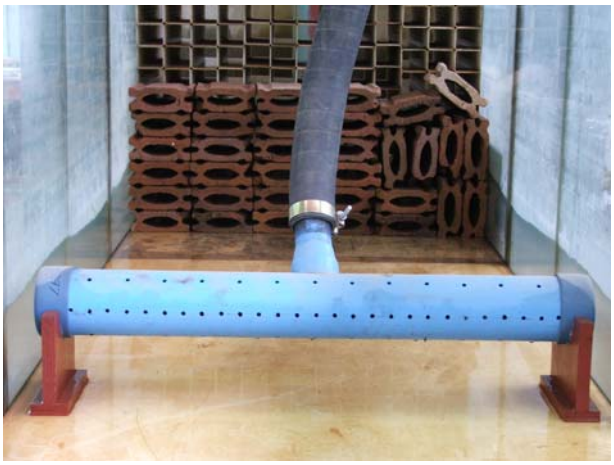

Figure 6-3: The sediment dispersing pipe

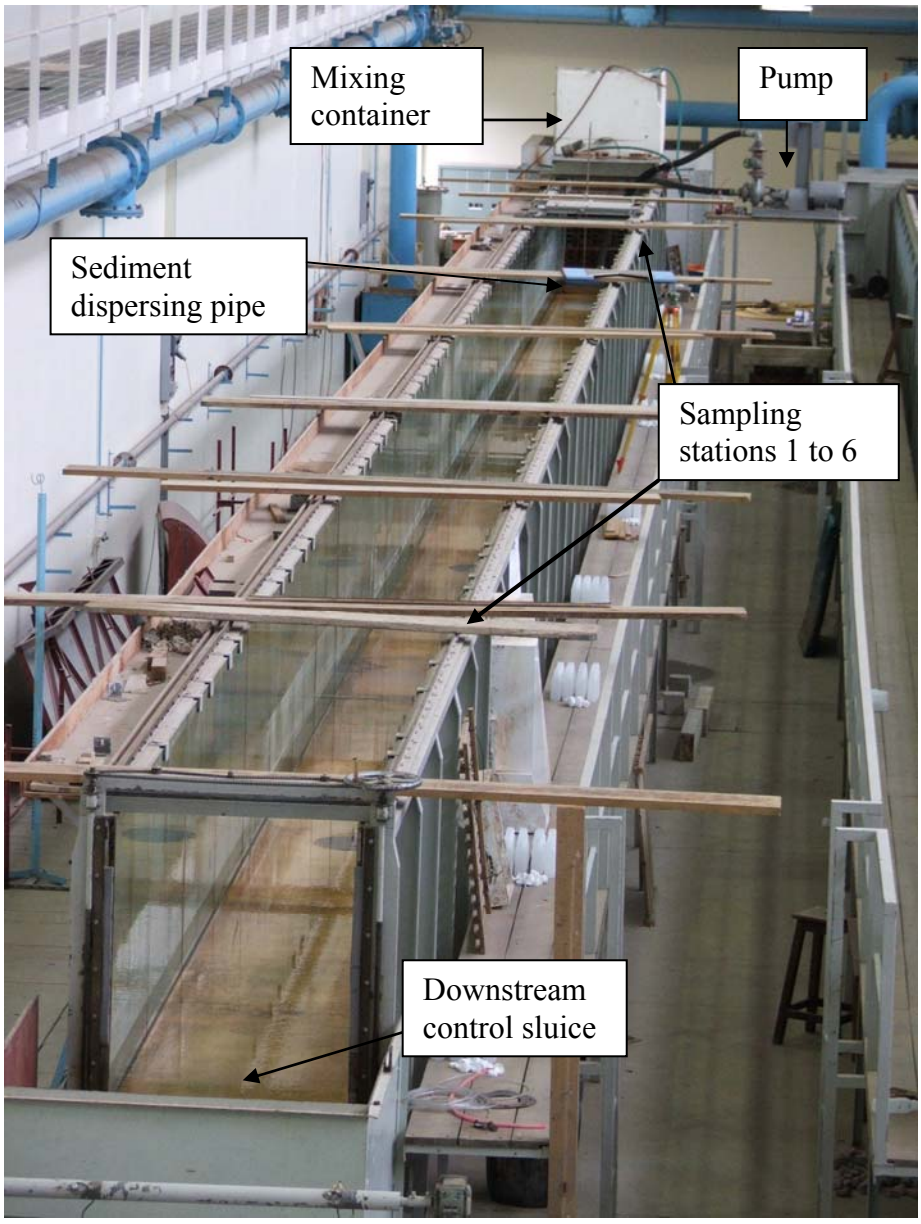

Figure 6-4: The laboratory test setup

6.4 Test Procedure

The test setup and sampling procedure for all the tests were similar, except that different discharges and concentrations were used. In the case of Test 1 the concentration in the channel was to be 5000 mg/ℓ. This was achieved by mixing 40kg of fine sediment in 1454.54ℓ of water in the container, thereby creating a concentration of 27 500 mg/ℓ in the container. This fills the container up to 86% of it's capacity, creating 164mm freeboard to prevent spillage. The mixture is released at a rate of 6.1ℓ/s into the stream, which is flowing at 27.3ℓ/s. The resultant flow in the channel is thus 33.3ℓ/s with a concentration of 5 000mg/ℓ. The container was able to supply this concentration to the channel for 240 seconds before running empty. At a flow velocity of 0.1m/s, this meant that there was a horizontal column containing suspended sediment of 24m moving through the channel. Samples were taken at the downstream sampling stations as the sediment laden water moved past each sampling station. Other test values were as shown in Table 6-2.

Table 6-2: Test flow and sediment parameters

	Test 1	Test 2	Test 3	Test 4
$Q_{channel}$ (m^3/s)	0.0273	0.0273	0.0106	0.0106
$Q_{container}$ (m^3/s)	0.0061	0.0061	0.0061	0.0061
Q_{total} (m^3/s)	0.0334	0.0334	0.0167	0.0167
Velocity (m/s)	0.10	0.10	0.05	0.05
Water depth (m)	0.333	0.333	0.333	0.333
Concentration (mg/ℓ)	5 000	10 000	5 000	10 000
Sediment mass mixed into container (kg)	40	80	20	40

In all the tests the same discharge of 6.1ℓ/s was released from the mixing container, but the concentration of that discharge and the discharge through the channel varied from one test to the other. In all the tests the container released sediment into the channel for a period of 240 seconds. The fact that there was a 240 second limit to the duration of the sediment release meant that less sediment loaded water entered the laboratory's drainage system. It also meant that the sampling programme had a definite time restriction.

6.5 Calibration

For each test three parameters had to kept constant to achieve the required flow conditions. They are the discharge through the main supply pipe into the channel, the sediment laden discharge from the container (constant at 0.0061m^3/s) and the downstream sluice height.

The discharge through the main pipe was measured using an upstream magnetic flow meter in the main pipe and a V-notch weir in the downstream channel. Discharges which were measured by means of the weir were calibrated against the voltage measured by the magnetic flow meter. Figure 6-5 shows the almost linear relationship between the two values.

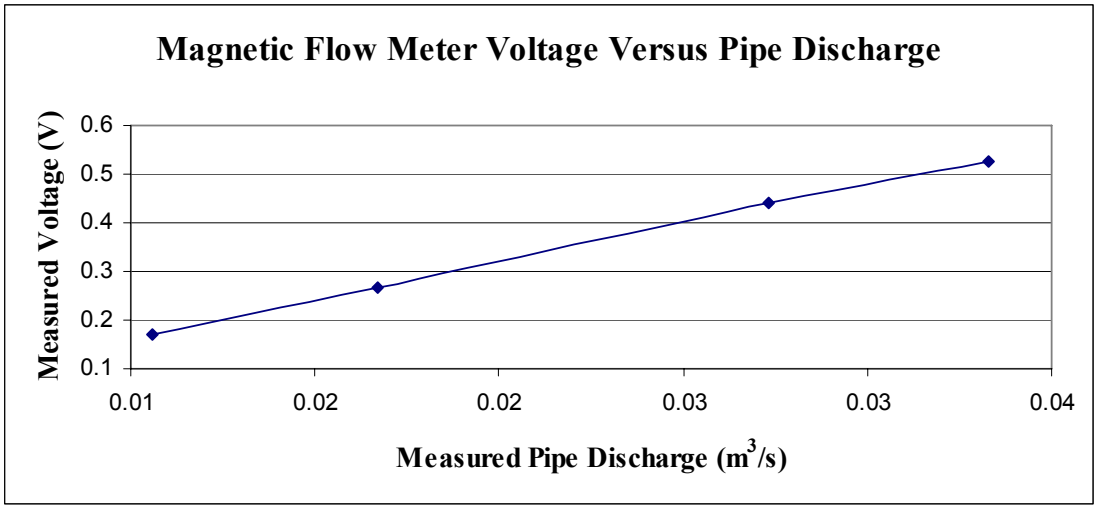

Figure 6-5: The magnetic flow meter voltage versus pipe discharge

Only two discharges from the supply pipe were required in the tests. They were 0.0273m^3/s for tests 1 and 2 and the 0.0106m^3/s for tests 3 and 4. These discharges corresponded with readings on the magnetic flow meter of 0.440V and 0.170V respectively.

Discharges of 0.0333m^3/s and 0.0167m^3/s were released from the pipe to simulate the total test discharges so that the downstream sluice could be set at either of the two heights to ensure an upstream depth of 0.333m in the channel for each discharge.

Regulation of the discharge from the mixing container presented a problem since the container had a bottom outlet and drawdown to the channel below by gravity alone would result in a varying discharge. The container was divided into ten horizontal sections from top to bottom, each exactly containing a tenth of the container's volume. By timing the drawdown as the container' s water level passed these marked intervals, the rate of discharge was established. For all the tests the required discharge was $0.006m^3/s$, which related to a drawdown time of 240 seconds for the container to empty and thus 24 seconds per tenth of the container volume. A pump was installed to eliminate the effect of gravity and to maintain a constant discharge towards the channel. This greatly succeeded, but the top and bottom sections still showed variations from the 24 second interval. The top section experienced uneven drawdown due to the difference between the pump's start up speed and it's average running speed, resulting in a drawdown time greater than 24 seconds. The bottom tenth section also took a longer time to empty, since the pump started to suck air through the inlet. The calibration runs produced the following times per interval drawdown as shown in Table 6-3.

Table 6-3: Time measurements of the drawdown intervals (seconds)

	Calibration run									
Interval	**1**	**2**	**3**	**4**	**5**	**6**	**7**	**8**	**9**	**10**
10	24	21	22	24	24	21	24	26	26	26
9	20	16	18	21	22	22	22	20	25	23
8	20	16	19	21	23	23	23	22	24	24
7	21	16	18	21	22	23	23	22	24	24
6	19	17	18	21	22	22	23	21	24	24
5	20	16	19	21	22	23	23	23	24	24
4	21	16	18	21	23	23	22	22	23	24
3	21	17	19	21	22	23	23	21	25	24
2	22	17	18	21	22	22	23	22	25	24
1	23	18	20	23	23	24	24	23	26	26
Total	**188**	**170**	**189**	**215**	**225**	**226**	**230**	**222**	**246**	**243**
Average	**20.9**	**17.0**	**18.9**	**21.5**	**22.5**	**22.6**	**23.0**	**22.2**	**24.6**	**24.3**

The tenth calibration run produced a fairly constant yield although some values still varied. It was decided that the tests would be carried out using the pump setting as in the tenth run.

6.6 Determining the Sediment Particle Size

Western Province Ball Clay was used as the laboratory sediment. It comes in the form of a very fine light brown powder. The particle size distribution was determined by the standard ASTM hydrometer method as shown in Appendix B. All the material passed through the 0.075mm sieve when wetted. It can be seen in Figure 6-6 below that 75% of the material is clay (smaller than 0.004mm). The material was found to be highly cohesive when wetted and difficult to work with in both wet and dry state. A density of 2 650kg/m^3 is used throughout further calculations.

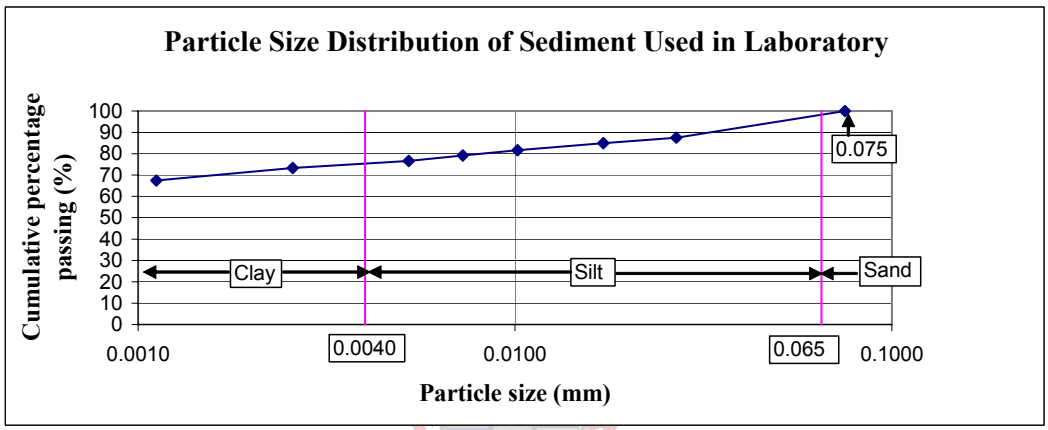

Figure 6-6: The particle size distribution of laboratory sediment

The curve shown above was extrapolated linearly down to a size of 0.0001mm. The extrapolated line indicated that the median (50%) size is 0.0001mm. It was decided to rather use a representative particle size based on a weighted average. This was done by assuming an average particle size of 0.00005mm for the smallest 50% and calculating median sizes for every 10% up to 100%. The result was a particle size of 0.00738mm. A particle of this size will have a settling velocity of 0.00005m/s. These calculations are shown in Appendix B.

6.7 Sampling Procedure

The concentrations were measured at three points at each of the 6 sampling stations. These three points were vertically aligned along the centre of the flow section. They were at depths of 80%, 40% and 20%, measured from the bed of the flume. These depths were labeled A, B and C respectively. The person at a sampling station would first take a sample at A, then B, then C and then repeat the sequence starting at A. A set of 6 sediment sampling instruments were designed specifically for this purpose (Figure 6-7). These were used to take two samples at each of the three points as the suspended sediment passes the measuring station.

Figure 6-7: The suspended sediment samplers at their three different measuring depths

For accuracy, the first and last tenths of the sediment containing section were disregarded because of varying sediment loads due to the uneven supply from the mixing container and pump. The 6 samples were taken 24 seconds after the first sediment passed through the sampling station. This left 192 seconds within which the 6 samples had to be taken. Figure 6-8 shows the sampling in progress.

Figure 6-8: Sampling in progress

This sampling procedure produced 36 samples per test, totalling 144 samples for all four tests. These samples were then analysed to determine the concentrations of suspended solids in each. A micro-pore filter attached to a vacuum flask was used to determine these concentrations. The vacuum sucks the sample through the filter and the sediment is left behind on filter paper. The filter papers were dried and weighed before and after sampling on an accurate scale which measures mass to four decimals of a gram. The concentrations were determined by simply dividing the difference between the original and end masses of the filter paper by the original volume of the sample.

The average concentrations in the two samples taken at each of the three depths were calculated and taken as the average concentration at that depth for the specific sampling station. The measured averages of the concentrations at each depth are shown in Appendix C.

6.8 Determining the Roughness of the Flume

The calculations in this section are included in Appendix D. To determine the roughness of the flume, a discharge was released from the main pipe into the flume and the hydraulic parameters recorded. Because the discharge of $0.0333m^3/s$ had already been calibrated with the magnetic flow meter, it was again used here.

With a discharge at 0.0333m^3/s, the upstream and downstream flow depths varied by 25mm over a length of 30m. The Reynold's number for these conditions was calculated as 28 800, which meant that the flow was turbulent.

The channel's Manning n value was found to be 0.0114 by using frictional energy loss equations. This value was substituted into Manning's equation and the discharge, which uniform flow at this average depth would produce, was calculated. To solve for the absolute roughness coefficient k_s, this discharge was set equal to the equation for discharge of turbulent flow, shown below. The value of k_s was found to be 0.00038m.

$$Q = A \cdot 5.75\sqrt{gRs}\log\left[\frac{12R}{k_s + \frac{3.3\upsilon}{\sqrt{gRs}}}\right] \tag{6-1}$$

$$\frac{\sqrt{gRs}\cdot k}{\upsilon} = 9.32 \ < \ 30 \tag{6-2}$$

The value of the parameter above was calculated to be smaller than 30. This meant that the flow was smooth turbulent, and that in fact it was necessary to calculate the values of n and k_s with the methods above, and not by direct methods such as Figure 3-8 (Rooseboom and van Zyl, 1978) of the SANRAL Road Drainage Manual.

6.9 The Vertical Velocity Profiles for the Test Conditions

The Reynolds' numbers for all the test conditions were found to be larger than 2 000, thus the flow conditions in all the laboratory tests were turbulent.

$$\text{Test 1\&2)} \ \text{Re} = \frac{\rho RV}{\mu} = \frac{1000*0.2*0.1}{1.003*10^{-3}} = 20008 \quad > 2000 \tag{6-3}$$

$$\text{Test 3\&4)} \ \text{Re} = \frac{\rho RV}{\mu} = \frac{1000*0.2*0.05}{1.003*10^{-3}} = 10004 \quad > 2000 \tag{6-4}$$

The vertical velocity profile for turbulent flow is given by:

$$v = \sqrt{2\pi gDs}.\ln\left(\frac{y}{y_0}\right) \tag{6-5}$$

For all the tests, y_0 was found to be 1.296 *10^{-5} by the equation:

$$y_0 = \frac{k_s}{29.6} = \frac{R_0}{14.8} \tag{6-6}$$

where: k_s = 0.000384 and thus R_0 = 0.000192.

Laboratory test conditions required significant damming of the flow. The differences in water levels between the upstream and downstream channel ends were too small to be measured. Energy principles could thus not be used to determine the energy slope accurately. Values of s, the energy slope, were determined through trial and error until the average velocity for the tests was reached. The average velocity for turbulent flow is given by:

$$\bar{v} = 5.75 \cdot \sqrt{gDs} \cdot \log\left(\frac{5.5D}{R_0}\right) \tag{6-7}$$

For Tests 1 and 2, a value of 0.00000584m/m was used for s in the equation for the velocity profile. For Tests 3 and 4, the value of s was 0.00000146m/m. These values corresponded with average velocities of 0.1 and 0.05 m/s respectively. The calculations are shown in Appendix E. The calculated velocity profiles are shown in Figures 6-9 and 6-10.

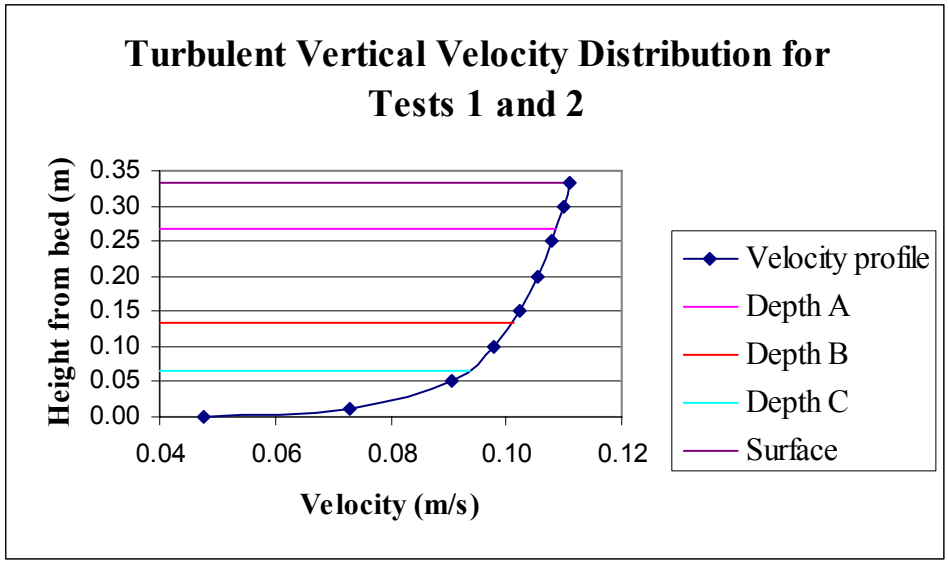

Figure 6-9: The calculated velocity profile for Tests 1 and 2, with an average velocity of 0.1 m/s

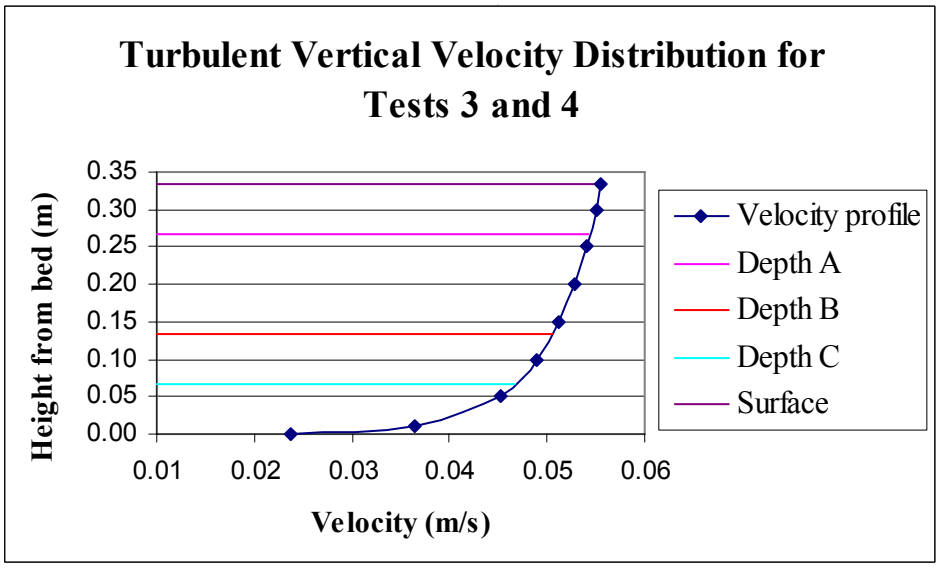

Figure 6-10: The calculated velocity profile for Tests 3 and 4, with an average velocity of 0.05 m/s

The velocities at each of the three depths were also calculated and these velocities were used to calculate a single value of concentration at each of the sampling stations on a weighted average basis. Each of the sampling stations was thus linked to only one depth integrated value of sediment concentration. This made the results of the

laboratory tests comparable to the two dimensional output (in plan) of the MIKE 21C model.

6.10 Results from the Laboratory Tests

The results of suspended sediment concentration from the laboratory tests are shown in Figure 6-11.

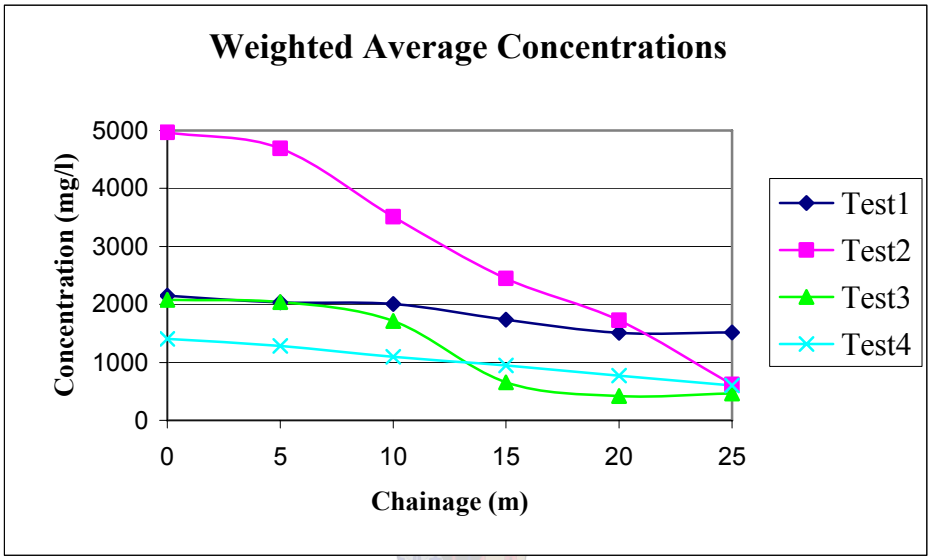

Figure 6-11: The results from the laboratory tests

It can be seen that the input concentrations are much lower than the 10 000 mg/ℓ and 5 000 mg/ℓ respectively that were originally expected from the test design. This is because a major proportion of the sediment was deposited in the container because of the extreme concentration of sediment that was in suspension in the container.

7. MIKE 21C SIMULATIONS OF LABORATORY TESTS

7.1 Numerical Model Setup

A numerical model of the straight rectangular flume was created with the exact dimensions and flow conditions as in the laboratory tests. The parameters used in these simulations were as shown in Tables 7-1 and 7-2.

Table 7-1: The simulation model constants

Hydraulic Constants

	Value	Unit
Water depth	0.333	m
Simulated real time	1	hr
Actual run time per simulation	5	min

Variable default values

Sediment relative density	2.65	kg/m3
Sediment porosity	0.5	-
Bed roughness - Manning's M	90	$m^{0.33}/s$
Settling velocity (laboratory sediment)	0.00005	m/s
Critical shear stress for erosion τ_{ce}	1.04	N/m^2
Erosion constant	0.1	$g/m^2/s$
Exponent of erosion	2	-
Dispersion	0	-

Table 7-2: The simulation model variables and input concentrations

Hydraulic variables	**Test 1**	**Test 2**	**Test 3**	**Test 4**
Q_{total} (m^3/s)	0.0334	0.0334	0.0167	0.0167
Velocity (m/s)	0.1	0.1	0.05	0.05
Design input concentrations (mg/ℓ)	5000	10 000	5000	10 000
Actual upsteam starting concentrations (mg/ℓ)	2150	4968	2080	1405

As noted before, the actual laboratory input concentrations were much lower than the 10 000 mg/ℓ and 5 000 mg/ℓ values that were originally assumed in the test design.

This was because a major proportion of the sediment was deposited in the mixing container because of the very high concentration of sediment that was in suspension in the container. The actual measured values as in Table 7-2 were thus used as input concentrations.

The value of the critical shear stress for erosion was assumed to be constant at 1.04 N/m^2. This is because the expected shear stresses were unlikely to exceed this value and no erosion was required. In most cases, lower concentrations were required from the numerical simulations. This could not be achieved by raising the critical shear stress for erosion in order to decrease the concentration. Even for an extreme value for τ_{ce} of 3.0N/m^2, no less erosion was found than with the default value of 1.04 N/m^2. With the value of τ_{ce} set, it greatly simplified the calibration process to only two parameters: τ_{cd} and α_{01}.

7.2 Laboratory Test Model Calibrations

All four tests were simulated with varying values of settling velocity w, critical shear stress for deposition τ_{cd}, and the stream wise constant α_{01}, to see which combination produces results that best resemble measured concentration values in the laboratory tests.

Since flow conditions in Tests 1 and 2 were similar, it was expected that the variables used to obtain the best results in both these tests would have the same values. The same was expected of Tests 3 and 4. The parameters and results from the calibration runs for Test 1 are shown in Table 7-3 and Figure7-1.

Table 7-3: Attempted calibration parameters for Test 1

Test 1	Lab.	1	2	3	4	5
Q (m^3/s)	0.0333	0.0333	0.0333	0.0333	0.0333	0.0333
V (m/s)	0.1	0.1	0.1	0.1	0.1	0.1
w (m/s)	*0.00005*	0.00005	0.00005	0.00005	0.00005	0.00005
α_{01}	-	1	1	0.1	0.05	0.075
τ_{cd} (N/m^2)	-	0.13	0.3	0.3	0.3	0.3

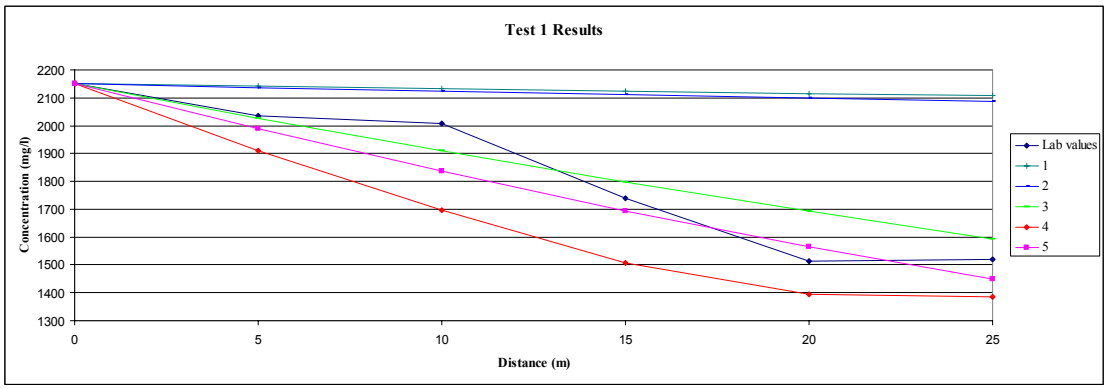

Figure 7-1: Concentration results of the calibration runs for Test 1

In the first attempt, α_{01} was kept at a conservative value of 1.0 since the slope of the laboratory concentrations decreased gradually. The value of τ_{cd} for this simulation was 0.13N/m^2, which is quite high. This is because previous simulations with α_{01} =1 and τ_{cd} = 0.05N/m^2, did not show any reduction in longitudinal concentration from the original 10 000 mg/ℓ input value. This is purely because the high velocity tends to sweep all sediment up into suspension. The results from the first run showed absolutely no decrease in concentration along the channel.

The second run also did not produce any significant decrease, even with the value of τ_{cd} increased to 0.3N/m^2. (A further increase of this value to 1.0N/m^2, in a simulation not shown here, produced the same result.) It was decided to keep the value of τ_{cd} at 0.3N/m^2 to ensure maximum deposition and to change the value of α_{01} in subsequent simulations. With a value for α_{01} of 0.1, concentrations were too high. With a value for α_{01} of 0.05, concentrations were too low. A value for α_{01} of 0.075 and a τ_{cd} of 0.3N/m^2 produced the best fit curve of the laboratory results. The parameters and results from the calibration runs for Test 2 are shown in Table 7-4 and Figure 7-2.

Table 7-4: Attempted calibration parameters for Test 2

Test 2	Lab.	1	2	3	4	5	6	7
Q (m^3/s)	0.0333	0.0333	0.0333	0.0333	0.0333	0.0333	0.0333	0.0333
V (m/s)	0.1	0.1	0.1	0.1	0.1	0.1	0.1	0.1
w (m/s)	*0.00005*	0.00005	0.00005	0.00005	0.00005	0.00005	0.00005	0.00005
α_{01}	-	0.5	0.1	0.075	0.05	0.05	0.01	0.03
τ_{cd} (N/m^2)	-	0.3	0.3	0.3	0.3	0.5	0.5	0.5

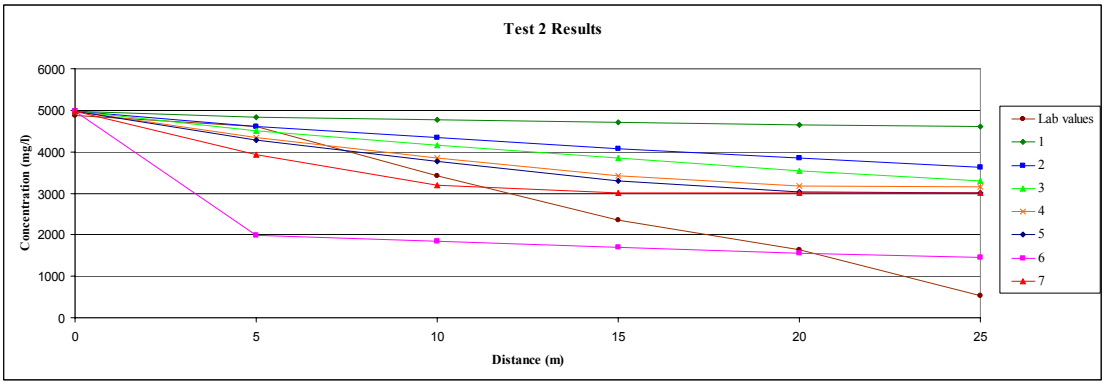

Figure 7-2: Concentration results of the calibration runs for Test 2

Test 2 was run under the same hydraulic conditions as Test 1, and therefore the first simulation attempt was with a τ_{cd} value of 0.3N/m^2. An average $\boldsymbol{\alpha_{01}}$ value of 0.5 was adopted to start of with. The simulation produced some reduction in concentration but was still nowhere near the laboratory result. In the subsequent three runs, the value of $\boldsymbol{\alpha_{01}}$ was decreased to 0.1, 0.075 and 0.05 respectively. Each of these did produce a further reduction in concentration, but still not enough. For the fifth run, $\boldsymbol{\alpha_{01}}$ was still kept at 0.05, but τ_{cd} was increased to 0.5N/m^2. This did not have much influence and it seemed from the results that, as in Test 1, a value of τ_{cd} above 0.3N/m^2 does not increase the deposition.

In the following two runs, τ_{cd} was kept high enough to ensure maximum deposition and the value of $\boldsymbol{\alpha_{01}}$ was lowered to 0.01 and 0.03. Both of these values produced sudden decreases in concentration in the first 5 to 10 meters and from then onwards gave an almost constant concentration. A further reduction in $\boldsymbol{\alpha_{01}}$ would only increase the initial sudden concentration reduction. It seems as if the simulation cannot produce a curve similar to the laboratory results curve. This is most likely because of the extreme range of laboratory concentrations from an initial value of 4 881mg/ℓ to the last value of 529mg/ℓ; an effective difference of 4 352mg/ℓ. This difference is much larger than in any of the other tests, where the begin and end values typically differ by 1 000 to 1 500mg/ℓ.

Test 2 was, however, the test that required the largest mass of sediment (80kg) of all the tests. The design concentration (10 000mg/ℓ) and velocity (0.1m/s) were the

highest values tested in the laboratory. It did present the greatest experimental challenge and the results are seemingly not accurate enough to be considered further in this research.

The parameters and results from the calibration runs for Test 3 are shown in Table 7-5 and Figure 7-3.

Table 7-5: Attempted calibration parameters for Test 3

Test 3	Lab.	1	2	3	4	5	6	7
Q (m^3/s)	0.0167	0.0167	0.0167	0.0167	0.0167	0.0167	0.0167	0.0167
V (m/s)	0.05	0.05	0.05	0.05	0.05	0.05	0.05	0.05
w (m/s)	*0.00005*	0.00005	0.00005	0.00005	0.00005	0.00005	0.00005	0.00005
α_{01}	-	1	1	0.5	0.1	0.075	0.05	0.1
τ_{cd} (N/m^2)	-	0.13	0.5	0.5	0.5	0.5	0.5	1

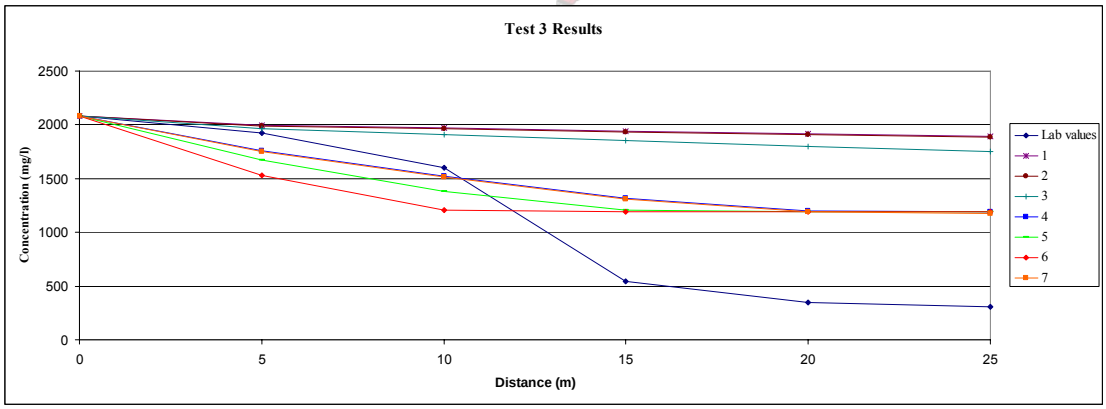

Figure 7-3: Concentration results of the calibration runs for Test 3

The results from the third test showed a large reduction in concentration along the 10m to 15m section. The shape of this curve can not be achieved with the typical parameters that are being used here. It was therefore attempted to produce a curve that at least gives values near to the test results. In the first 6 attempts the value of α_{01} was constantly lowered while the value of τ_{cd} was increased to once again ensure maximum deposition. The 6th run produced the best fitting curve although it's values are far from the test results. A further decrease in α_{01} would result in more deposition upstream and therefore an immediate drop in concentration. For the 7th run, α_{01} was therefore increased to 0.1 and τ_{cd} was increased to an absolute maximum of $1.0 N/m^2$.

The results from this run compared to the 5th simulation and the concentrations were thus still too high. The best fitting curve by default was thus produced by the 6th simulation with α_{01}=0.05 and τ_{cd} = 0.5N/m^2. It should be noted though that the results from this test are also considered to be suspect since there is such a significant drop in concentration for the 10m to 15m section, while the other sections experience gradually decreasing concentrations.

The parameters and results from the calibration runs for Test 4 are shown in Table 7-6 and Figure 7-4.

Table 7-6: Attempted calibration parameters for Test 4

Test 4	Lab.	1	2	3	4	5	6	7
Q (m^3/s)	0.0167	0.0167	0.0167	0.0167	0.0167	0.0167	0.0167	0.0167
V (m/s)	0.05	0.05	0.05	0.05	0.05	0.05	0.05	0.05
w (m/s)	*0.00005*	0.00005	0.00005	0.00005	0.00005	0.00005	0.00005	0.00005
α_{01}	-	0.5	1	1	1	1	1	1
τ_{cd} (N/m^2)	-	0.5	0.5	0.4	0.1	0.075	0.03	0.04

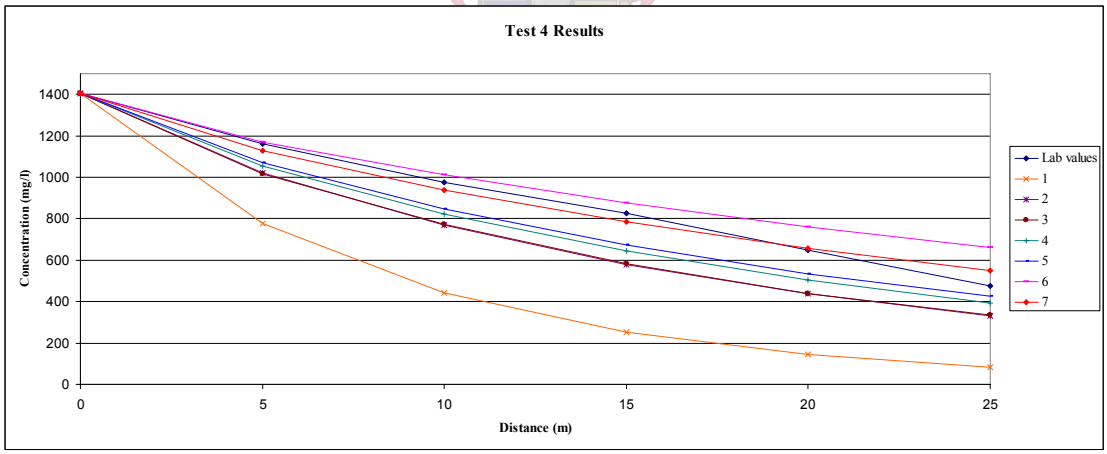

Figure 7-4: Concentration results of the calibration runs for Test 4

More success was achieved with the 4th test. The first attempt produced values that were too low because the value of α_{01} was underestimated at 0.5. In the following attempts, α_{01} was brought back to a value of 1.0 and kept constant. By the 6th attempt, the value of τ_{cd} had gradually reduced from 0.5 to 0.03N/m^2, which yielded concentrations that were only slightly too high. In the 7th simulation, the value of τ_{cd}

was slightly raised and it produced an almost perfectly fitting curve against the laboratory values.

7.3 Findings

It can be seen in the laboratory test result figures in Appendix C that very high concentrations were found at depths B and C, which were the deepest two measuring depths. For all four tests, the concentrations measured at B and C were much higher than those measured at the upper measuring depth A. Apart from Test 4, the other tests were calibrated in section 7.2 with very low values of the stream wise advection constant, which means there were high concentrations and velocities close to the bed. All of this indicates that the transport mechanism in the laboratory tests was rather a density current and not turbulent transport as intended. This phenomenon was not observed visually during the laboratory test procedure since the water in the flume carried a very heavy sediment load and the difference in concentrations over the depth of the flume was not visible.

This means that the initial assumption of turbulent transport was in error and that MIKE 21C's advection-dispersion model can therefore not be used to simulate the sediment transport in the flume. Turbulent velocity profiles were used to calculate the weighted average concentrations at the sections. This produced very low concentrations since the higher velocities were really near the bed and not near the surface as with a turbulent velocity profile. Vertical velocity profiles of turbulent flow and a density current is shown in the Figure 7-5. The three measuring depths are also indicated in Figure 7-5.

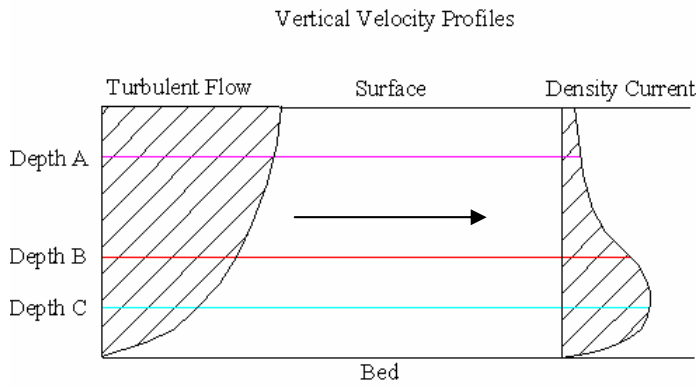

Figure 7-5: The vertical velocity profiles of turbulent flow and a density current

The laboratory tests therefore produced averaged concentrations that were far too low and these results were therefore deemed unreliable.

8. LONG TERM NUMERICAL STUDIES OF SEDIMENTATION

8.1 Background

In this chapter, MIKE 21C is used to model the transport of fine sediment for three case-studies; Welbedacht Reservoir, Vaal Reservoir and Winam Gulf in Lake Victoria. All of these three bodies of water experience silting of cohesive sediments from their main tributaries. The three are, however, very different in size, catchment area, annual runoff and sediment load. Welbedacht Reservoir is a narrow river channel that experiences extremely large sediment loads. Vaal Reservoir is considered to be a very large, wide and shallow reservoir with relatively low inflowing sediment loads. Vaal Reservoir has in the past experienced some heavy sediment loads during flood events.

These two reservoirs are thus extreme cases. Successful modelling of both with MIKE 21C will establish this software package as a powerful tool that can be used for all South African reservoir sedimentation studies.

The third case study is Winam Gulf, a massive body of water with a small channel that connects it to the main lake. The gulf is deep and wide and the water velocities are very low. The gulf experiences varying water levels and is modelled in the same way as the reservoirs. Application of the software to this case study is discussed in section 8.4.

8.2 Welbedacht Reservoir Model

Welbedacht Dam was completed in 1973 on the Caledon River, draining a high sediment yield region. During the first three years of operation the reservoir had lost 36 million m^3 of it's original 114 million m^3 storage capacity due to sedimentation. Figure 8.2-1 shows the losses in storage capacity over the years. Figure 8.2-2 shows the longitudinal profile of the reservoir bed determined by survey data. Also shown in Figure 8.2-2 is the future equilibrium sedimentation level of the reservoir as calculated by Rooseboom et al. (1986).

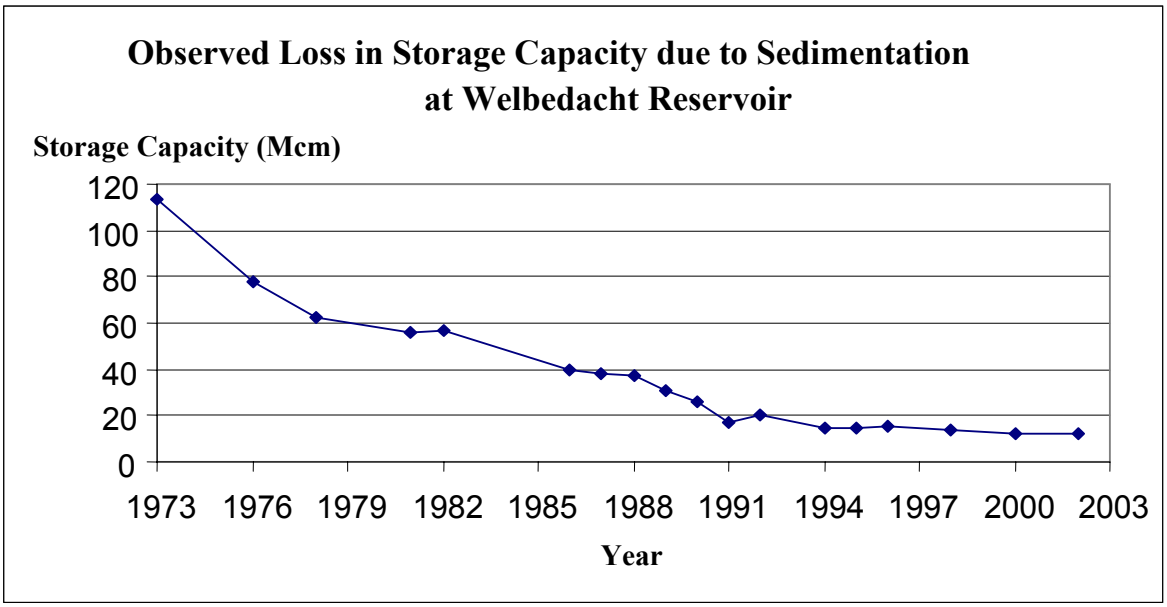

Figure 8.2-1: The observed loss in storage capacity of Welbedacht Reservoir

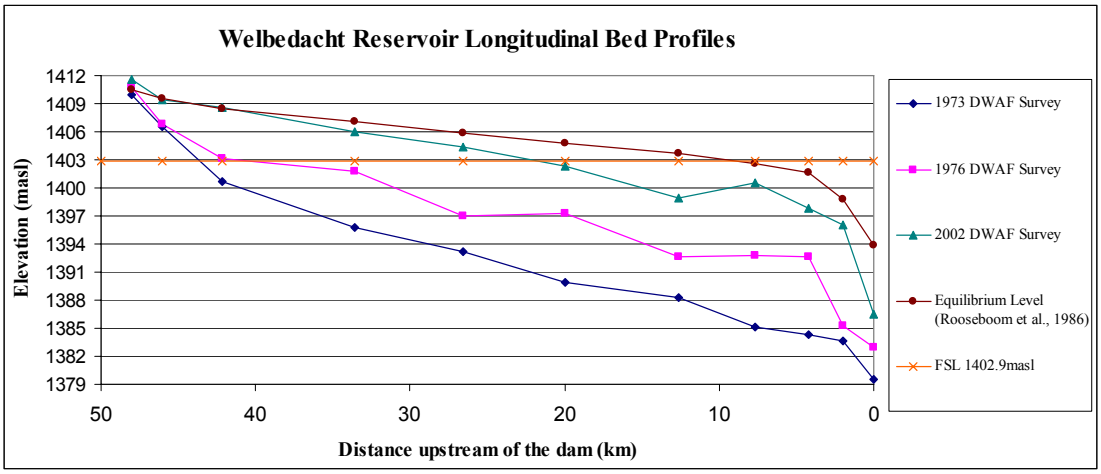

Figure 8.2-2: The longitudinal profiles of Welbedacht Reservoir

As a result of extreme sedimentation, the existing Jim Fouché Bridge, across the upper reaches of the reservoir, experiences regular flooding. This is because the height of the bridge openings has been reduced from 13m to only 1m since the dam was built. The bridge is located 42.5 km upstream of the dam.

All the historical data of inflows and reservoir levels that were used in the model were obtained from the Department of Water Affairs and Forestry (DWAF). The model was formulated with upstream inflow data from the flow measuring station at

Jammersdrift and downstream reservoir water level data from station D2R004 at Welbedacht Dam. An aerial photo of the reservoir can be seen in Figure 8.2-3.

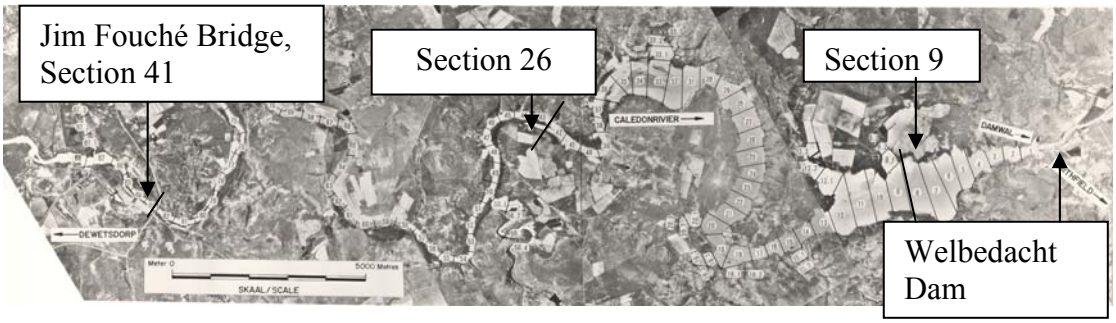

Figure 8.2-3: An aerial photo of Welbedacht Reservoir

8.2.1 Calibration: 1973 – 1976

As a calibration case the model simulated the three year period from 1973 to 1976. The Department of Water Affairs and Forestry carried out hydrographic surveys of the basin during both 1973 and 1976, thus the original and end bathymetries were known (DWAF 2006). The geometry of the reservoir was derived from the 1973 survey data, and mapped in a curvilinear grid, as shown below in Figures 8.2-4. The grid contains 360 cells in the longitudinal direction and 16 cells in the transverse direction, totalling 5 760 cells when the model is fully flooded. Figure 8.2-5 shows the original 1973 bathymetry of Welbedacht Reservoir, imposed on the grid.

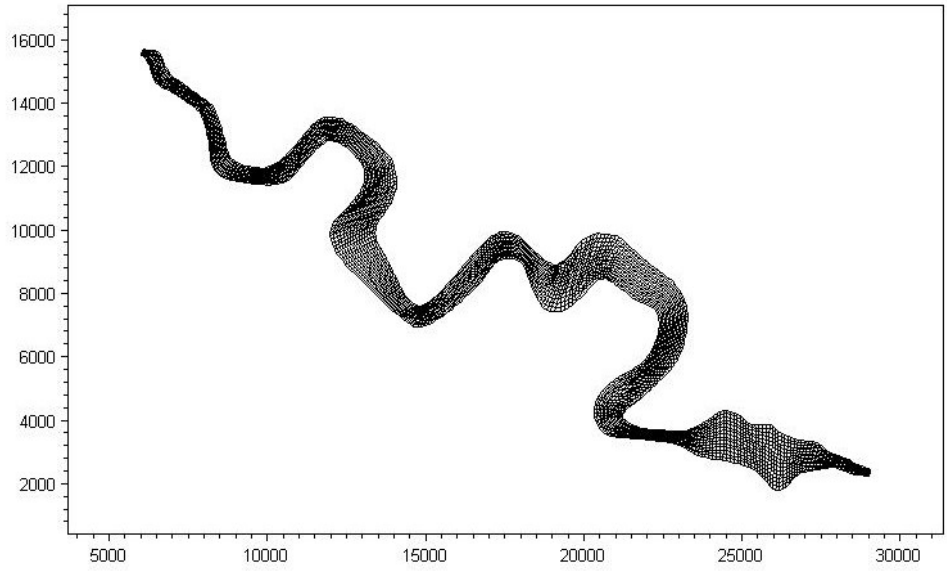

Figure 8.2-4: The curvilinear grid (in plan) used in the Welbedacht model

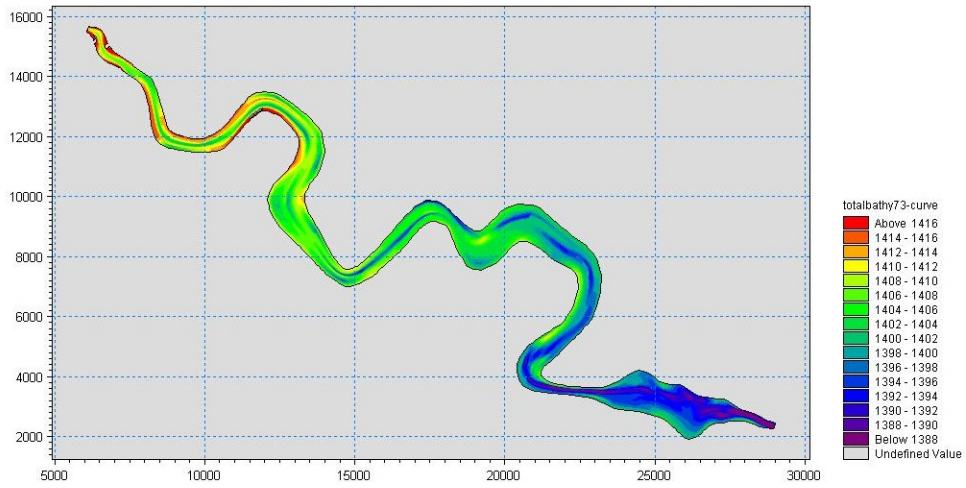

Figure 8.2-5: The 1973 bathymetry (in plan) used in the Welbedacht model

During this research, twenty-eight bed sediment samples were taken along the reservoir from 2km upstream of the Jim Fouche bridge down to the dam. Figure 8.2-6 shows the variation in the median particle sizes of the samples taken along the reservoir. Most of the median values lie around a size of 0.1mm. This means that the bed is sandy. However, all the samples had more than 7% of silt and clay (particles smaller than 0.065mm) and therefore the bed will have the characteristics of a cohesive bed, according to Beck and Basson (2003).

Since the model is required to transport the sediment deep into the reservoir, a median value for a sediment sample taken close to the dam will be a better estimation of the representative size, especially for the 1973 to 1976 period. The median sizes found close to the dam varies between 0.008mm and 0.011mm in diameter.

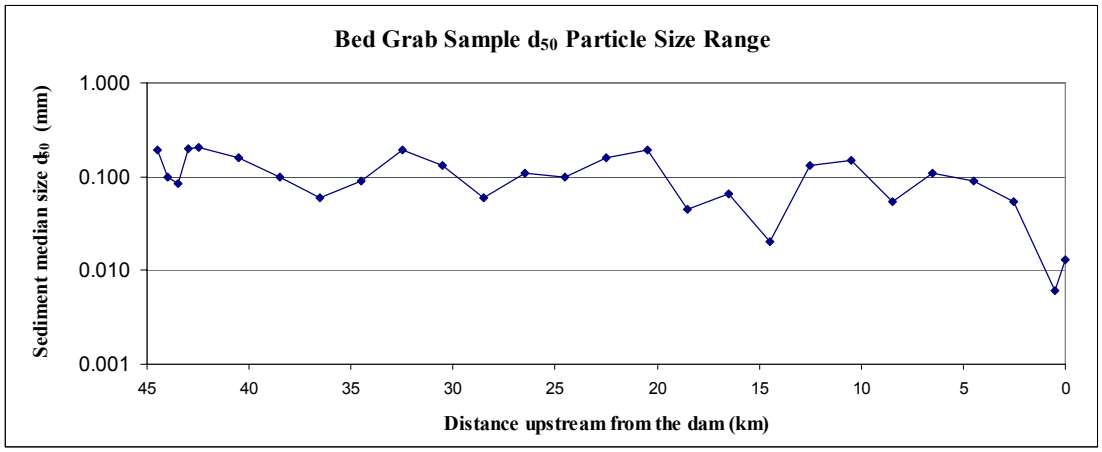

Figure 8.2-6: Median particle sizes of bed grab samples taken along Welbedacht Reservoir

Basson and Rooseboom (1997) used a suspended sediment size distribution from observed data for the Welbedacht Reservoir inflow as shown below:

- Fraction 1: $d_{50} < 0.05$mm, 76% (clay)
- Fraction 2: 0.05mm < $d_{50} < 0.106$mm, 19% (silt)
- Fraction 3: 0.106mm <d_{50} <0.25mm, 5% (fine sand)

Based on mass, these values produce a weighted average particle size of 0.0427mm, which will have a settling velocity of 0.00164m/s, as calculated by Stokes' law. The settling velocity is taken as 0.001m/s for the first calibration run. The following dependency rate of concentration to discharge was used in the study by Basson et al. (2003):

$$C = 793.32Q^{0.664} \qquad (8\text{-}1)$$

where C is in g/m^3 and Q in m^3/s. Basson et al. (2003) calibrated the Welbedacht model successfully with this dependency rate and therefore the same dependency rate will be used here. According to this rate, the catchment area yields sediment at 2 950 $t/km^2.a$ for the 1973 to 1976 period. In order to calibrate the model, the aim was that the simulated 1976 bathymetry would match the 1976 surveyed bathymetry. This was

first attempted using the historical time-series and variables as shown in Table 8.2-1 and Figures 8.2-7.

Table 8.2-1: Calibration model variables

Variable	Value
Bed roughness - Manning M ($m^{0.33}/s$)	50
Critical shear stress for deposition (N/m^2)	0.05
Critical shear stress for erosion (N/m^2)	1.04
Eddy viscosity (m^2/s)	0.01
Sediment porosity	0.5
Sediment relative density	2.65
Erosion constant E_0 ($g/m^2/s$)	0.1
Exponent of the erosion	2
Dispersion	0

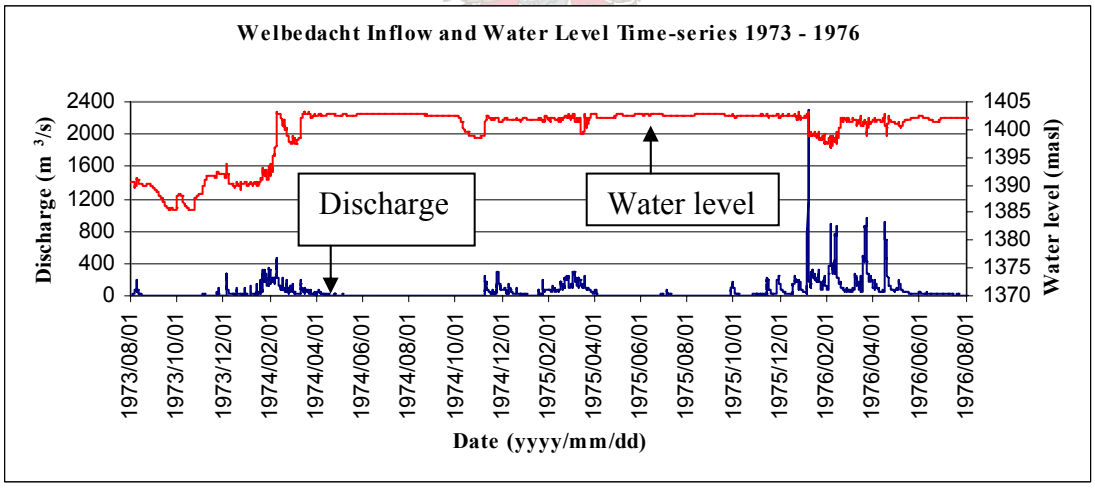

Figure 8.2-7: The 1973 to 1976 time-series for the model's inflow and downstream water level based on observed data (FSL = 1402.9 m)

The critical shear stress for erosion is kept at 1.04 N/m^2, the value used in the study by Basson et al. (2003), where some erosion did occur. The bed shear stress is unlikely to exceed this value. The value of α_{01} is at it's maximum value of 1.0 to ensure that the sediment concentration is evenly distributed throughout the depth of flow and that it carries as far as possible into the reservoir. The only remaining

parameters are those of critical stress for deposition and settling velocity. Both will have an influence on how even the sediment will deposit throughout the reservoir. Firstly the settling velocity will be calibrated and then the critical stress for deposition.

a) Settling Velocity Sensitivity Study

With all other parameters being kept constant as in Table 8.2-1, the sectional variations for different values of the settling velocity w are shown in Figures 8.2-8, 8.2-9 and 8.2-10. These are the DWAF survey sections 41, 26 and 9. Section 41 is 40km upstream of the dam, section 26 is 20 km upstream from the dam and section 9 is 3km from the dam. The locations of these sections are shown in Figure 8.2-3.

It is expected that the smaller the settling velocity, the further the sediment will be carried into the reservoir towards the dam. When the settling velocity is large, the sediment will be deposited close to the upstream boundary.

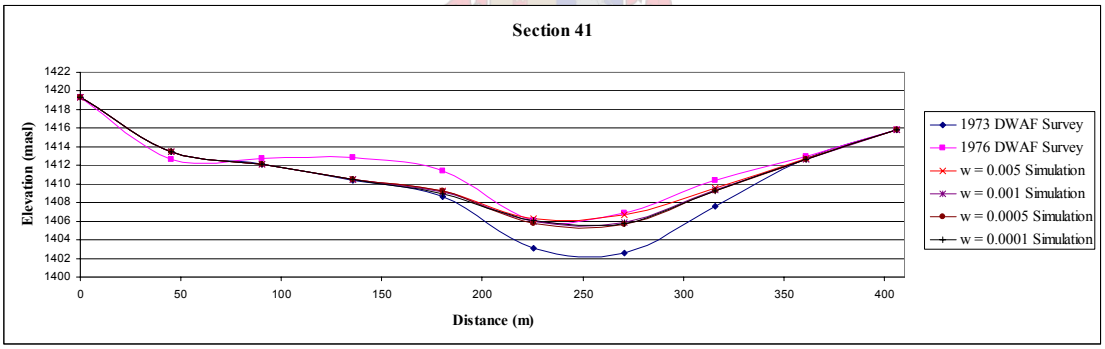

Figure 8.2-8: Deposited sediment layers at section 41 for different settling velocities

The upstream section 41 does not show large variation in deposited layer thickness for the various settling velocities. All the simulations did however, deposit a relatively accurate amount within the main channel of which simulation with the highest settling velocity, 0.005m/s, seemed to be most accurate.

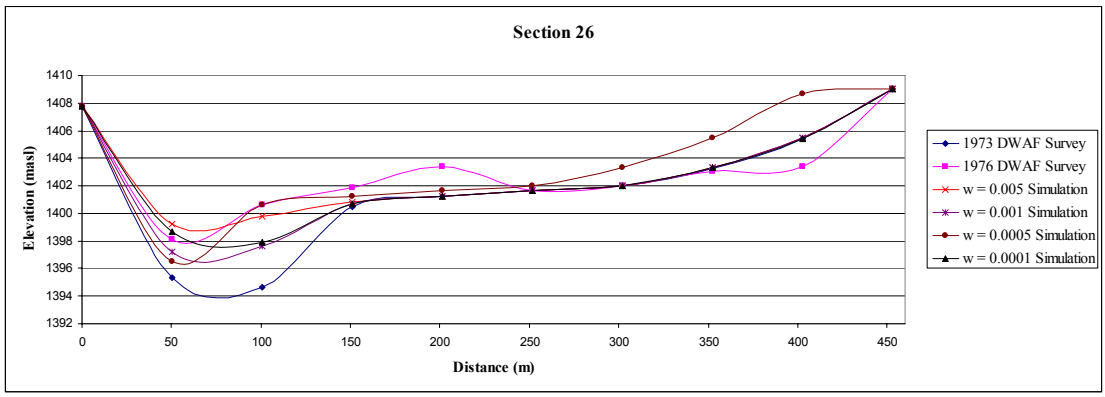

Figure 8.2-9: Deposited sediment layers at section 26 for different settling velocities

At section 26 the simulation with w = 0.005m/s delivered the sediment accurately within the main channel. The simulation with w = 0.0005m/s produces an evenly distributed layer over the whole section and also deposits the largest volume of all the simulations.

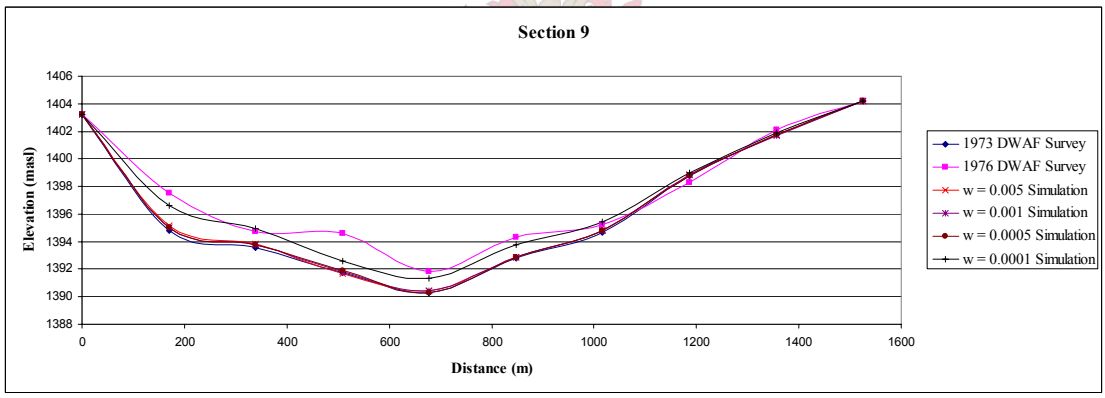

Figure 8.2-10: Deposited sediment layers at section 9 for different settling velocities

The downstream section 9 is the longest section throughout the reservoir and it lies only three kilometres from the dam wall in the area where the heaviest sediment deposits have occurred. This makes the section the most important section for evaluating the parameter of settling velocity. The simulation with w = 0.0001m/s produced the best results at this section.

The figures above each produced three different answers to the question of most appropriate settling velocity, and none of them is the estimated settling velocity of 0.00164m/s. It was however decided to use a settling velocity of 0.0001m/s since it performed well in all three sections and especially in section 9 where the largest deposits are expected. This settling velocity corresponds to a particle diameter of 0.011mm, which relates very well with the median particle sizes of the samples taken close to the dam.

b) Sensitivity Study for the Critical Shear Stress for Deposition, τ_{cd}

A new set of calibration simulations were run, with a fixed value for w of 0.0001m/s and varying values of critical shear stress. The results are again plotted and evaluated on the three sections as before in Figures 8.2-11, 8.2-12 and 8.2-13.

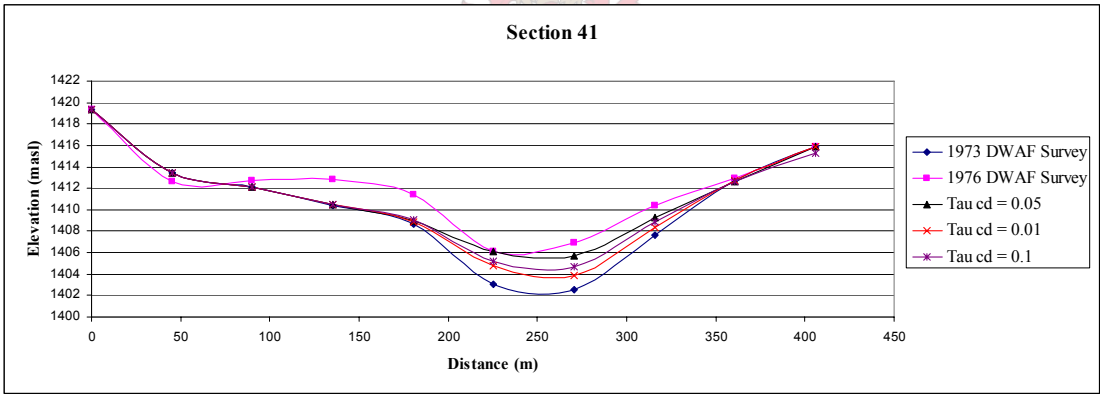

Figure 8.2-11: Deposited sediment layers at section 41 for different shear stresses for deposition

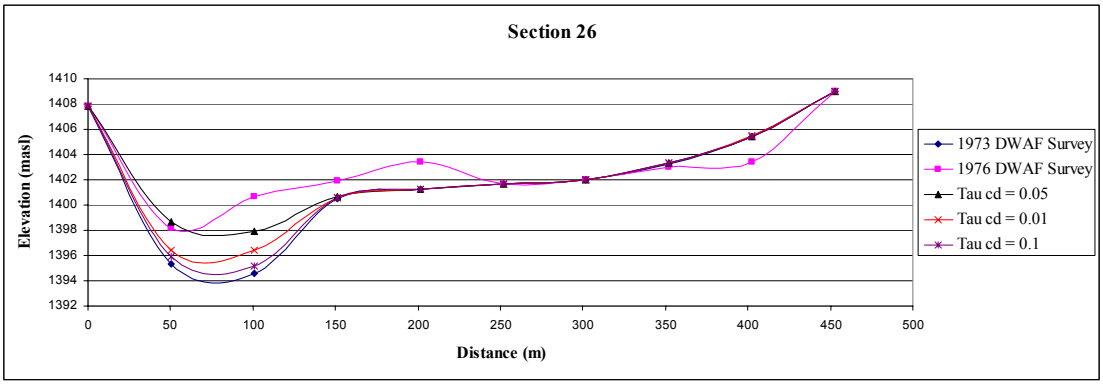

Figure 8.2-12: Deposited sediment layers at section 26 for different shear stresses for deposition

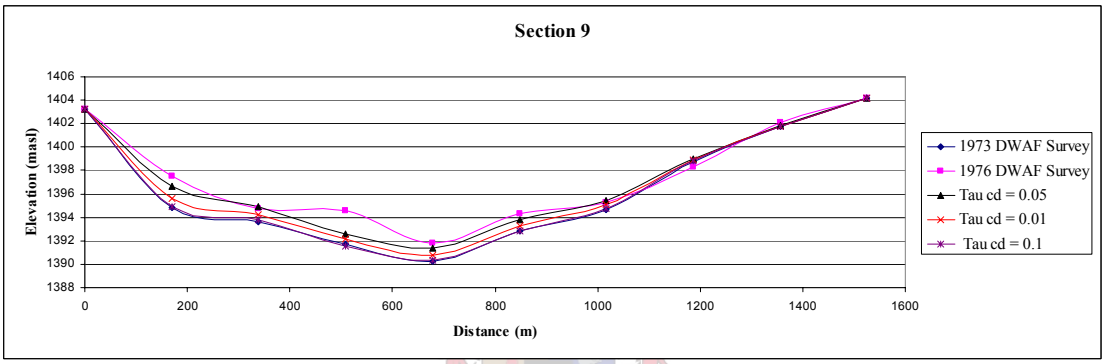

Figure 8.2-13: Deposited sediment layers at section 9 for different shear stresses for deposition

In all of the above sections, the deposited sediment layer produced by the simulation with τ_{cd} = 0.05N/m^2 is the closest to the surveyed bathymetry. Both the other simulations, with a larger τ_{cd} of 0.1N/m^2 and a smaller τ_{cd} of 0.01N/m^2, resulted in less deposition at these sections than with τ_{cd} = 0.05N/m^2. This is probably because a large value of τ_{cd} such as 0.1N/m^2 would deposit all the sediment already at the upstream boundary, while a smaller τ_{cd} such as 0.01N/m^2 would not cause large amounts of sediment to deposit and the sediment would remain in suspension and be flushed out at the downstream boundary. The best value adopted for τ_{cd} is thus 0.05N/m^2.

c) Sensitivity Study for the Stream Wise Advection Constant, α_{01}

The best values for τ_{cd} and w were determined as 0.05N/m^2 and 0.0001m/s respectively. It was decided to investigate more values of α_{01} since the deposition was still slightly less than what was expected, but this could be due to the assumed sediment concentration-discharge relationship. Simulations were run with τ_{cd} and w at the values mentioned above, and α_{01} values of 0.1, 0.5 and 1. The results are shown in Figures 8.2-14, 8.2-15 and 8.2-16.

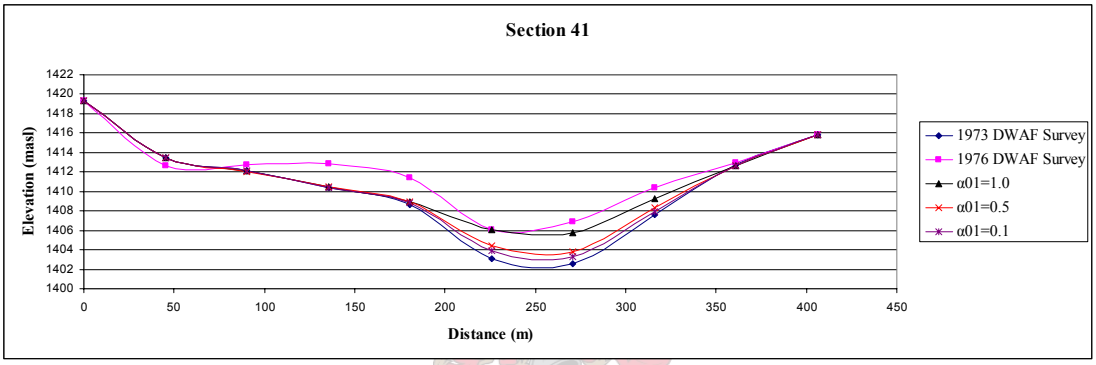

Figure 8.2-14: Deposited sediment layers at section 41 for different stream wise constants

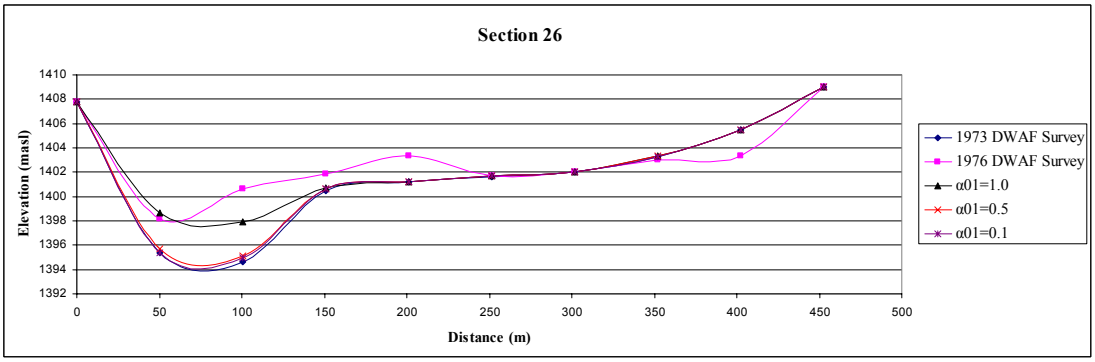

Figure 8.2-15: Deposited sediment layers at section 26 for different stream wise constants

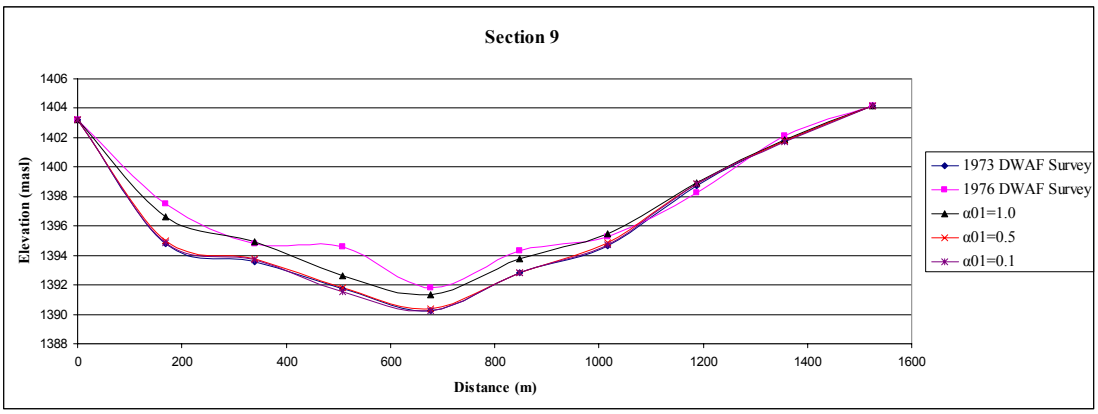

Figure 8.2-16: Deposited sediment layers at section 9 for different stream wise constants

It seems that a value for α_{01} of 1.0 still produced the most deposition as would be expected. The values for α_{01} of 0.5 and 0.1 produced less deposition because the velocity distribution was then at a maximum near the bed, which is not suitable for the process of deposition. It would have created high bed shear stresses which could even have exceeded the critical shear stress for erosion. A value for α_{01} of 1.0 was therefore used in the validation simulation.

8.2.2 Validation: 2000 – 2002

The values of τ_{cd}, w and α_{01} were calibrated at 0.05N/m^2, 0.0001m/s and 1.0 respectively. The result from the validation, using these values, would ultimately determine the validity and accuracy of the values.

This validation basically followed the same procedure as the 1973-76 calibration, but used observed data for the two year period from July 2000 to July 2002. Once again during both 2000 and 2002 basin surveys were carried out (DWAF, 2006). Thus the original and end bathymetries were known. The 2000 bathymetry can be seen in Figure 8.2-17. The same grid from the previous calibration was used for this simulation. Once again the observed dam water levels were used at the downstream boundary. For the upstream boundary, the observed releases from the dam were used

since the upstream Jammersdrift gauging station was no longer operational during this period.

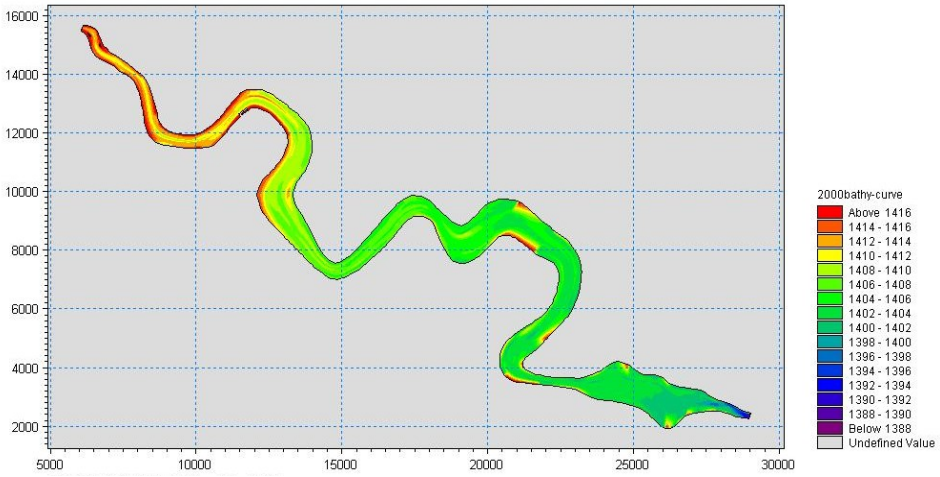

Figure 8.2-17: The 2000 survey bathymetry (in plan) used for the validation

Due to the high silt content the cohesive modelling approach adopted for the 1973-1976 simulation was again used for the 2000 to 2002 period. No upstream sediment concentrations have been monitored since 1976, and the original concentration-discharge relationship for 1973 to 1976 was again used for the sediment yield. The variables and historical time-series are shown in Table 8.2-2 and Figure 8.2-18:

Table 8.2-2: Validation model variables

Variable	Value
Bed roughness - Manning M ($m^{0.33}/s$)	50
Critical shear stress for deposition (N/m^2)	0.05
Critical shear stress for erosion (N/m^2)	1.04
Eddy viscosity (m^2/s)	0.01
Fall velocity (m/s)	0.0001
Stream wise constant α_{01}	1.0
Sediment porosity	0.5
Sediment relative density	2.65
Erosion constant E_0 ($g/m^2/s$)	0.1
Exponent of the erosion	2

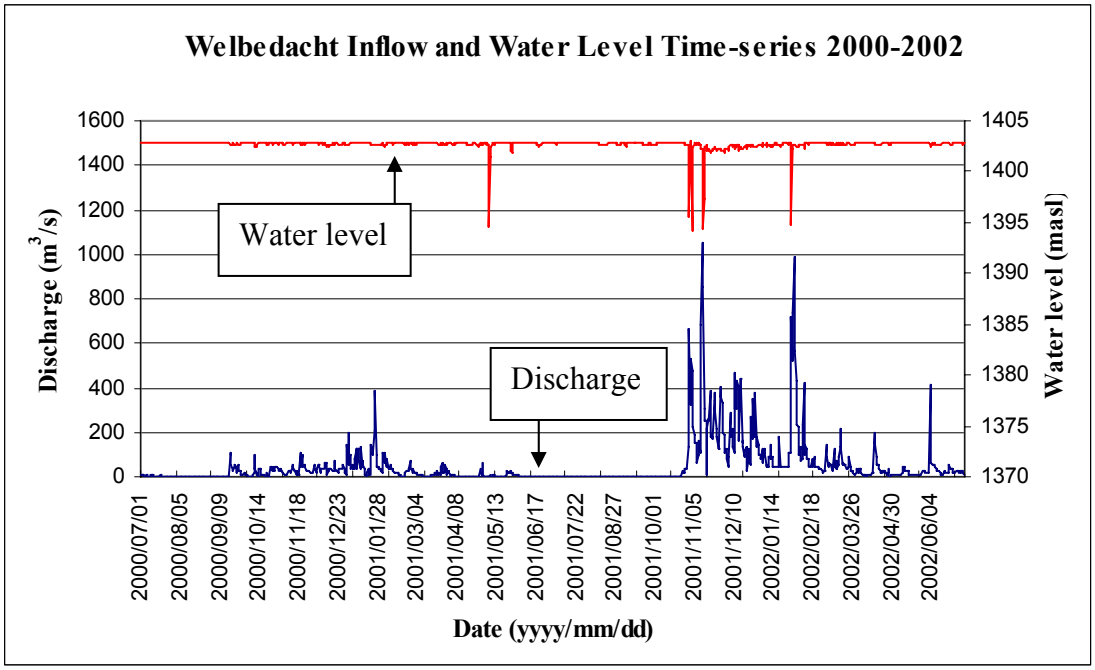

Figure 8.2-18: The 2000 to 2002 time-series for the model's inflow and downstream water level

The validation simulation produced the following results at the same three sections used previously, in Figures 8.2-19, 8.2-20 and 8.2-21.

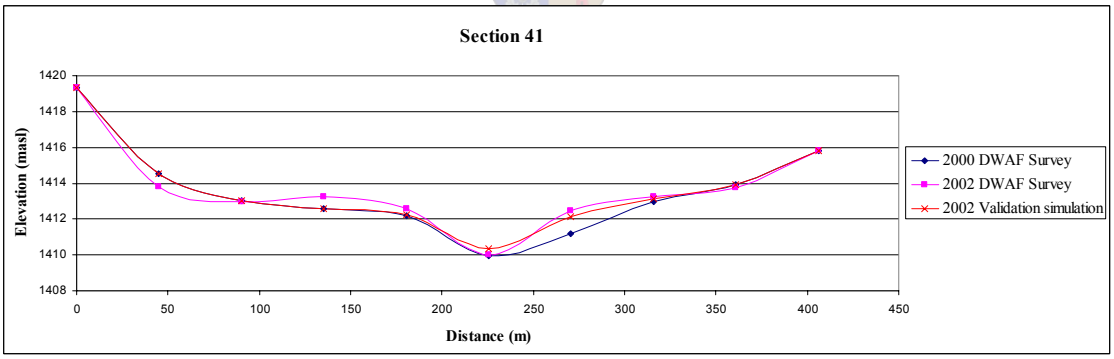

Figure 8.2-19: Deposited sediment layers at section 41 for the validation simulation

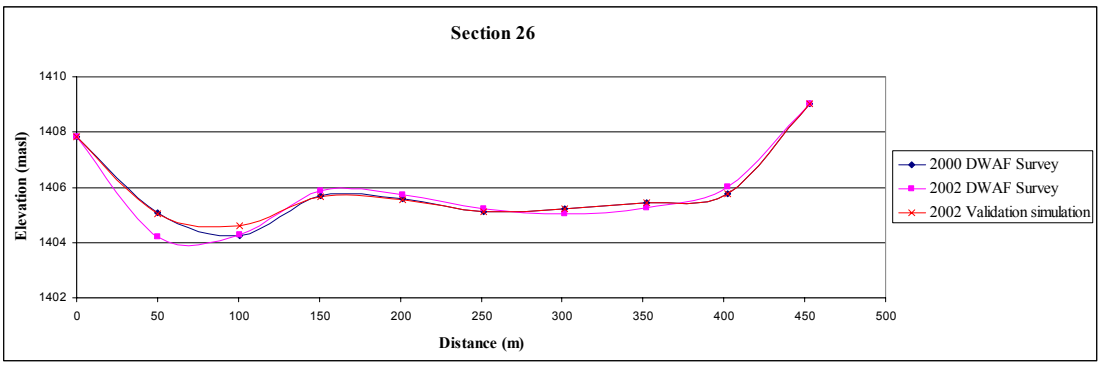

Figure 8.2-20: Deposited sediment layers at section 26 for the validation simulation

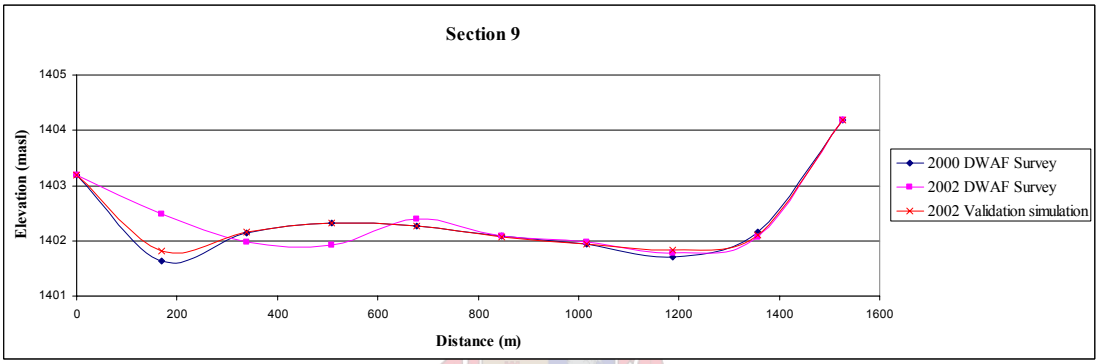

Figure 8.2-21: Deposited sediment layers at section 9 for the validation simulation

In general, there are no large differences between the 2000 and 2002 surveyed sections, although the main channel at section 9 has shifted to the right during this period. This is probably due to the flushing events during this period. The simulated 2002 bathymetry is not an exact match against the 2002 surveyed bathymetry. The simulation produced deposition at all three sections and section 41 seems especially well calibrated. At section 26 the simulation produced some deposition where there should have been slight erosion. Section 9 is difficult to evaluate because it seems to have shifted towards the right, probably due to the flushing operation. In general the validation can be considered successful since there was even deposition on all three sections as was the case with the successful calibration run. It should be noted that the original rate of dependency of the concentration to discharge is a slight underestimate of the real sediment yield. This can be seen in the results from the

calibrated and validation simulations. The resulting deposition at the sections is always slightly less than the surveyed profile.

The calibrated parameters related well with those in the Mike21C model study by Basson et al. (2003). The only difference was the change in settling velocity from 0.001m/s to 0.0001m/s. It should be noted that the model used in this research had a domain that was 50% longer than the model used by Basson et al. (2003). The change in settling velocity was necessary to carry the suspended sediment through the 48km length of the model.

8.2.3 Long Term Sedimentation Simulations

Further simulations were run with predicted future inflow and water levels from 2002 to 2011 and from 2002 to 2029. These inflows were basically the 1973 to 1976 time-series run continuously over the 9 and 27 year periods. The downstream water level was kept constant at the full supply of 1402.9masl. The results of longitudinal profile of these simulations are shown in Figure 8.2-22.

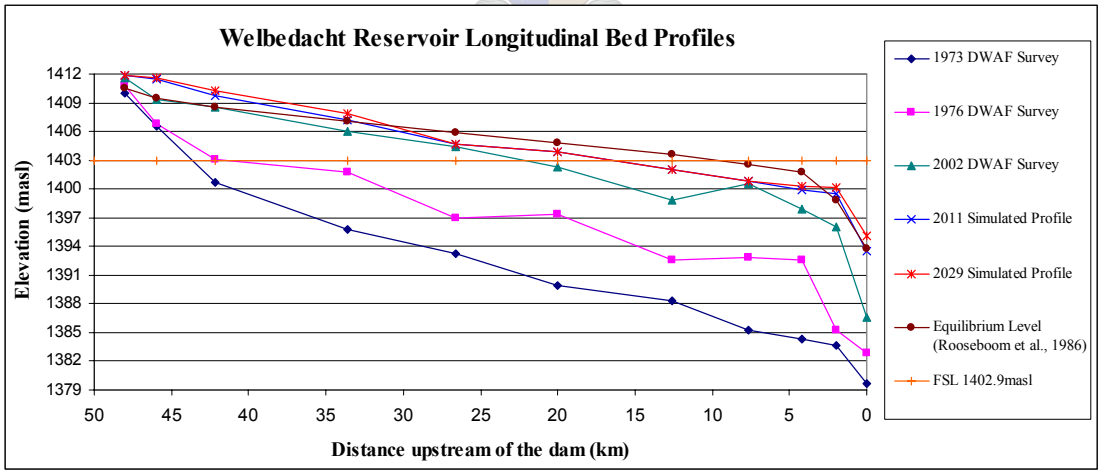

Figure 8.2-22: Historic longitudinal bed profiles with future sedimentation levels

It can be seen from Figure 8.2-22 that the simulations showed no large changes in the bathymetry after 2011. The 2011 and 2029 levels are very similar and it can be said that this represents the equilibrium sedimentation levels. The future equilibrium levels

predicted by Rooseboom et al. (1986) are still higher than even the 2029 levels simulated in this study close to the dam (30km), but in the upper reaches the simulated future bed levels are higher. The simulated 2029 bathymetry is shown in Figure 8.2-23. The Rooseboom et al. (1986) method assumed that Boegoeberg Reservoir, further downstream in the same river system, had reached equilibrium and its calculated shear stress was applied at Welbedacht Reservoir to adjust the bed profile. The method however adjusted the bed profile by assuming horizontal deposition in the deepest sections first.

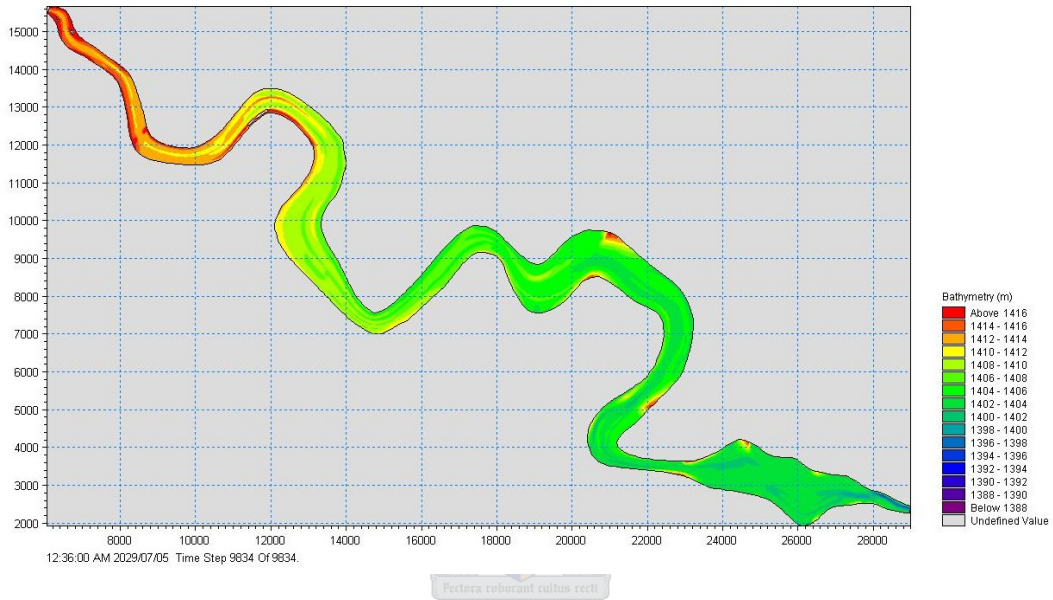

Figure 8.2-23: The simulated 2029 bathymetry in plan

With the calibrated model it was possible to predict future flood levels at any section of the reservoir. The 2011 bathymetry was set as a starting bathymetry for simulations of the 1:50 and 1:100 year floods, which are 3 500 m^3/s and 5 100 m^3/s respectively (Basson and De Villiers, 2005). Each flood simulation then produced a maximum water surface elevation throughout the reservoir. As an example Figure 8.2-24 shows the morphological change at section 41 and the simulated future flood levels for the year 2011.

This research showed that MIKE 21C, run in quasi-steady mode with an advection-dispersion module, is adequate for creating and calibrating a sedimentation model for extreme cases of reservoir sedimentation such as Welbedacht Reservoir. When simulations are performed into the future (2029) with the assumed sediment

concentration-discharge dependency, Welbedacht Reservoir reaches a dynamic equilibrium between the sediment transport processes of deposition and erosion.

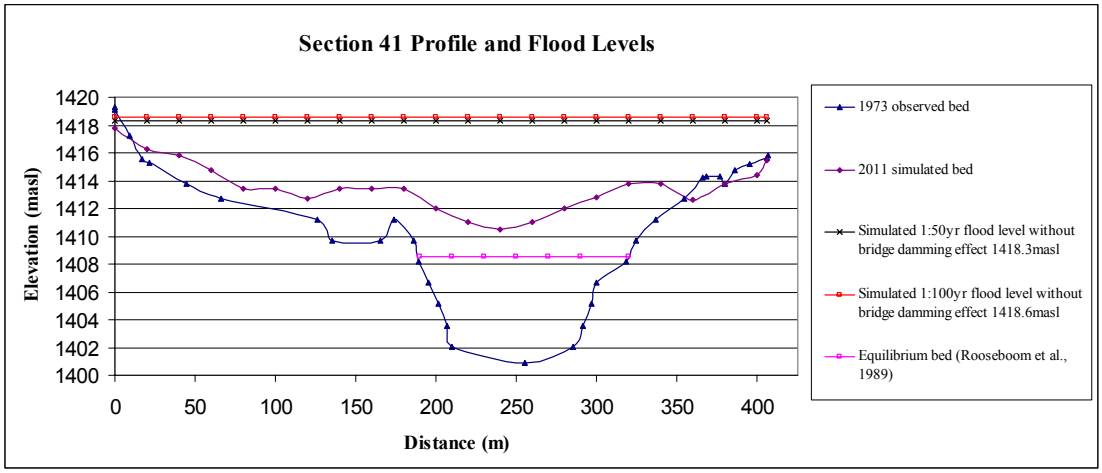

Figure 8.2-24: Section 41 profile and flood levels

8.3 Vaal Reservoir Model

The MIKE 21C software was used to simulate the morphology and hydrodynamics of Vaal Reservoir and upstream Vaal River leg, given historical time-series of inflow, suspended sediment concentration and reservoir water level.

At full supply level, Vaal Reservoir can store 2 577. 654 million m^3 water. Its surface area is approximately 320km^2, making it a relatively large and shallow reservoir.

The model was formulated with upstream inflow data from the flow measuring station C1H012 at Nooitgedacht on the Vaal River and downstream reservoir water level data from station C1R001 at Vaal Dam (Figure 8.3-1). All the historical data of inflows and reservoir levels that were used, were obtained from the Department Water Affairs and Forestry (DWAF). Time-series of suspended sediment concentrations in the river and reservoir, used for calibrating the model, were obtained from DWAF and RandWater respectively.

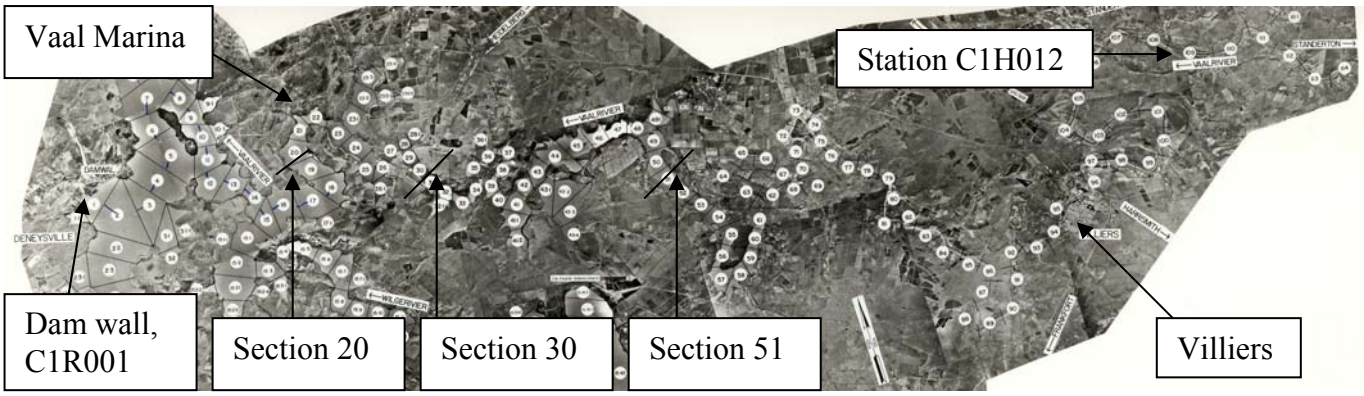

Figure 8.3-1: An aerial photo of Vaal Reservoir

8.3.1 Calibration: 1988 - 2003

The calibration was carried out by a simulation of the 15 year period from January 1988 to January 2003. During both 1988 and 2003 reservoir basin surveys were carried out. Thus the original and end bathymetries were known. The geometry of the reservoir and river was derived from the 1988 survey data and ortophotos, and mapped with a curvilinear grid, shown below in Figure 8.3-2. The 1988 survey data are added onto the grid to produce the original bathymetry shown in Figure 8.3-3. The grid contains 148 cells in the longitudinal direction and 16 cells across, totalling 2368 grid cells fully flooded.

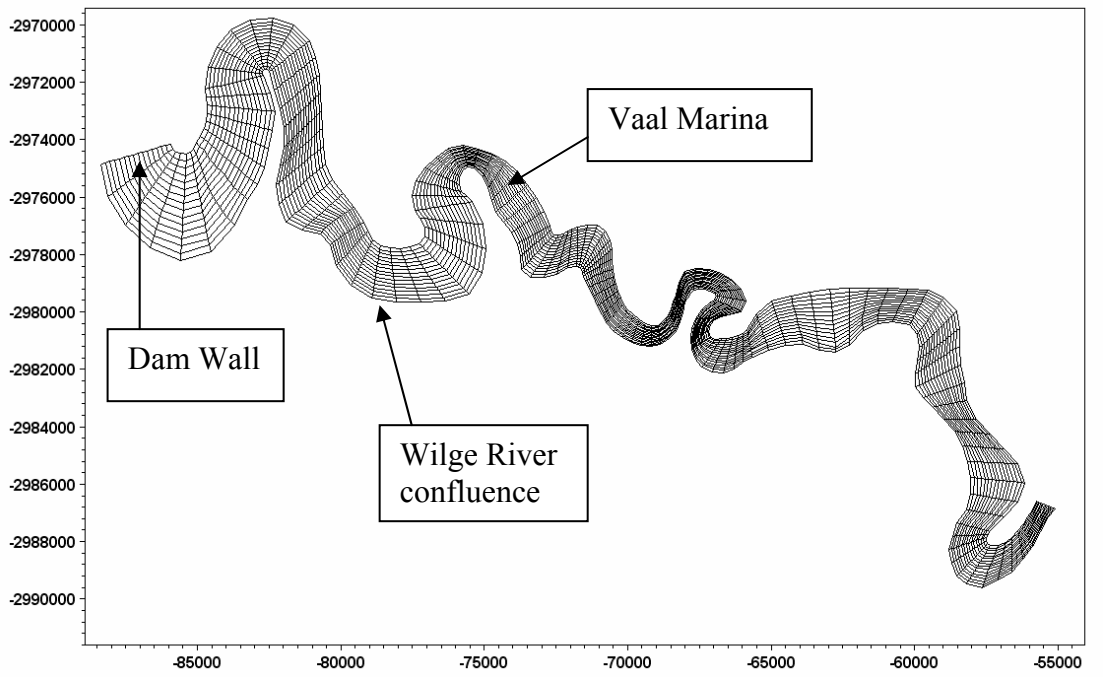

Figure 8.3-2: The curvilinear grid used for the Vaal Reservoir model

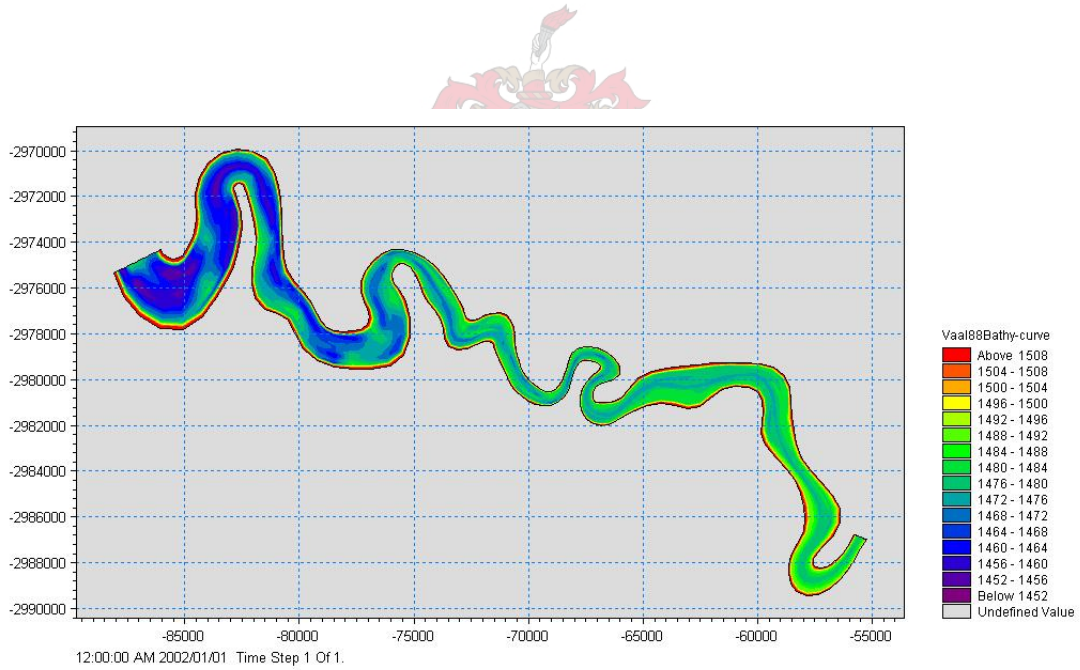

Figure 8.3-3: The original 1988 surveyed bathymetry

Forty-nine bed grab samples were taken along the Vaal River leg of the reservoir from the town of Villiers downstream to the dam during March 2005. Figure 8.3-4 shows a typical bed grab sample taken during the field work. A summary of the grading analysis of these samples is attached in Appendix H.

Figure 8.3-4: The grab sediment sampler with a typical load of cohesive sediment from Vaal Reservoir

No previous grading of the suspended sediment had been done and therefore the distribution was estimated using the grab sample size distributions. The following sediment characteristics were obtained from the data in Figure 8.3-5 and used for the Vaal River inflow sediment:

- Fraction 1: $d_{50} < 0.004$mm, 75% (clay)
- Fraction 2: $0.004\text{mm} < d_{50} < 0.065$mm, 25% (silt)

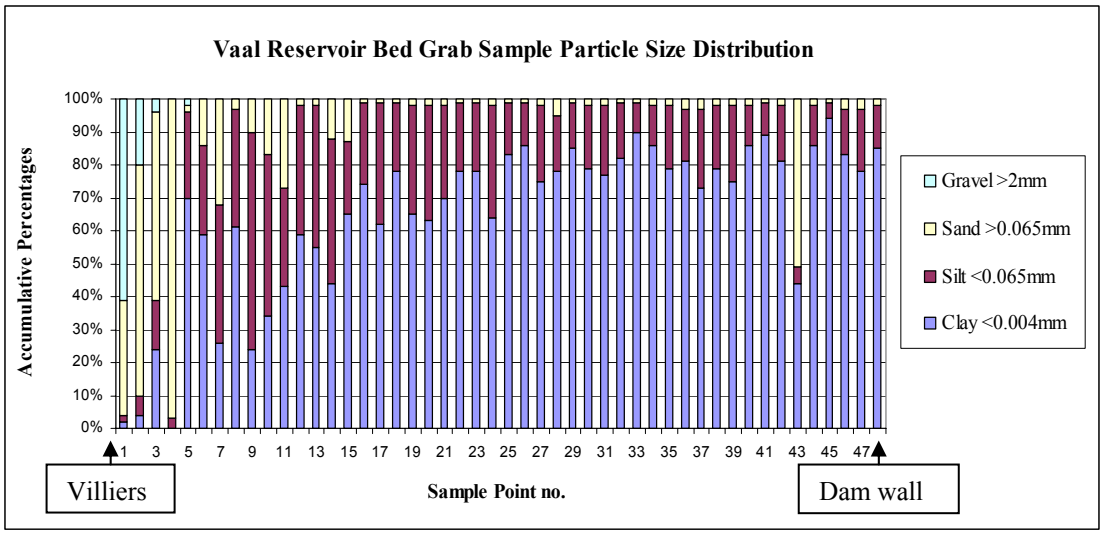

Figure 8.3-5: The bed sediment particle size distribution

This gives a weighted average suspended sediment particle size of 0.0281mm, which will have a settling velocity of 0.00071m/s (Appendix I). The settling velocity was taken as 0.001m/s for the first calibration run.

To calculate the sediment yield at the model's upstream inlet, suspended sediment yield data (Q_s = C*Q in t/s) from C1H012 were plotted against discharge (Q in m^3/s) on a logarithmic scale, shown in Figure 8.3-6. A line was fitted to these data points to quantify this dependency rate. These calculations are shown in Appendix I. Due to the limited data at high flows, a conservatively high sediment yield relationship was selected based on the measured data.

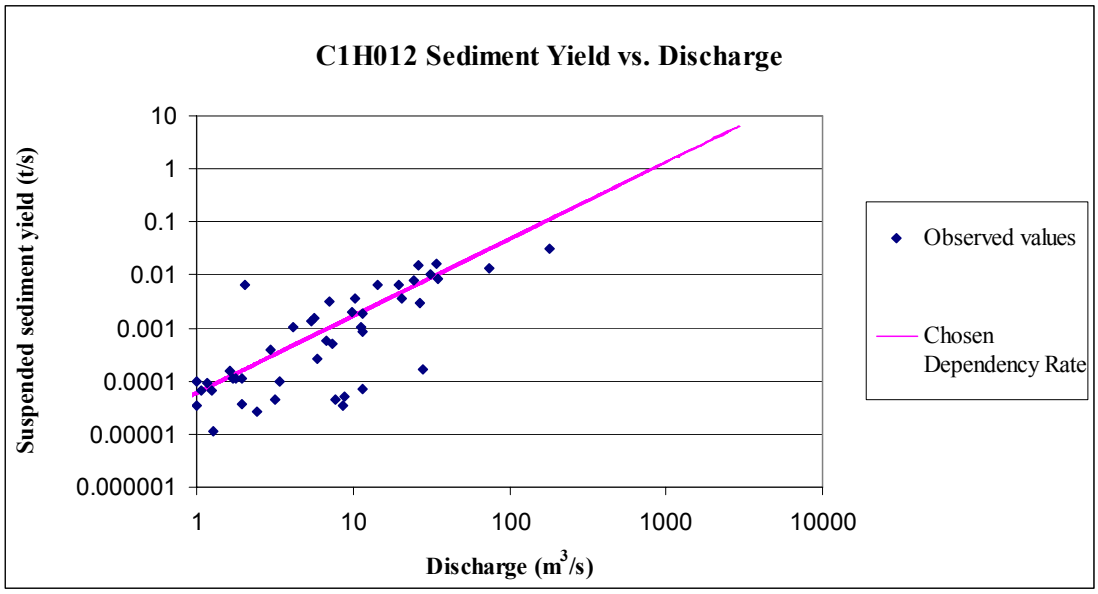

Figure 8.3-6: 1993-1995 Measured suspended sediment yield/discharge data (blue) and the trendline (purple)

The chosen trend line produced the following dependency equation, which was used to calculate the sediment yield for the 16-year calibration period.

$$C = 60.Q^{0.45} \qquad (8\text{-}2)$$

Where C is in mg/ℓ and Q in m^3/s. The total volume of sediment is calculated by integrating below the yield graph over the 16 year period. This amounts to 11.4 million tons of sediment. The catchment's annual sediment yield rate is thus 57.8

ton/km^2.a considering an effective catchment area downstream of Grootdraai Dam of 12 276 km^2. (Appendix I). This value is a lot less than the rate of 193 ton/km^2.a predicted by Rooseboom and Maas (1974) and the maximum observed regional yield of 150 t/km^2.a (Rooseboom et al., 1992).

To calibrate the model, the aim was that the simulated 2003 bathymetry matched the 2003 surveyed bathymetry. Also the output time series data of suspended sediment concentrations had to compare with the data from RandWater.

This was attempted using the following historical time series and variables as shown in Table 8.2-1 and Figures 8.2-7 and 8.2-8. All the measured values of discharge lower than 10m^3/s, were taken as 10m^3/s. This made it easier for the program to run the simulation, as lower flows can make the calculations unstable. This time series contained the 1:100 year flood of February 1996, for which the model's side boundaries had to be lifted by 10m so that the extreme flow would not overtop the model's sides and cause the simulation to become unstable. Very little or no erosion is expected to take place and therefore the critical shear stress for erosion is kept sufficiently high (1.04N/m^2) as was calibrated previously for Welbedacht Reservoir by DHI (2003). The bed shear stress is unlikely to exceed this value.

From the Welbedacht study it was clear that the value of α_{01} can not be any less than 1.0 for reservoir applications. A value for α_{01} of 1.0 was again used here. The other parameters were as shown in Table 8.3-1. The model's inflow and water level time-series are shown in Figure 8.3-7.

Table 8.3-1: Model calibration variables

Variable	Value
Bed roughness - Manning M ($m^{0.33}/s$)	50
Critical shear stress for deposition (N/m^2)	0.05
Critical shear stress for erosion (N/m^2)	1.04
Eddy viscosity (m^2/s)	0.01
Stream wise constant α_{01}	1.0
Sediment porosity	0.5
Sediment relative density	2.65
Erosion constant E_0 ($g/m^2/s$)	0.1
Exponent of the erosion	2

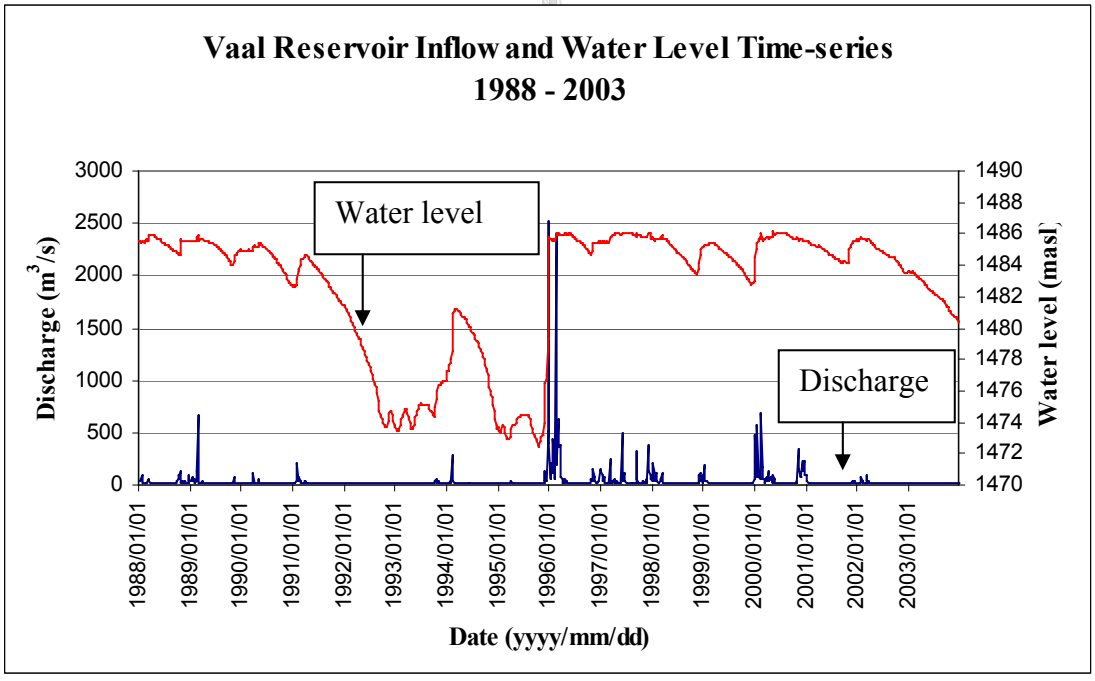

Figure 8.3-7: The 1988 to 2003 time-series for the Vaal Reservoir model's inflow and water level based on observed data

The discharge time-series was converted into a suspended sediment concentration time-series at the model's upstream boundary. The time-series of input sediment concentration is shown in Figure 8.3-8.

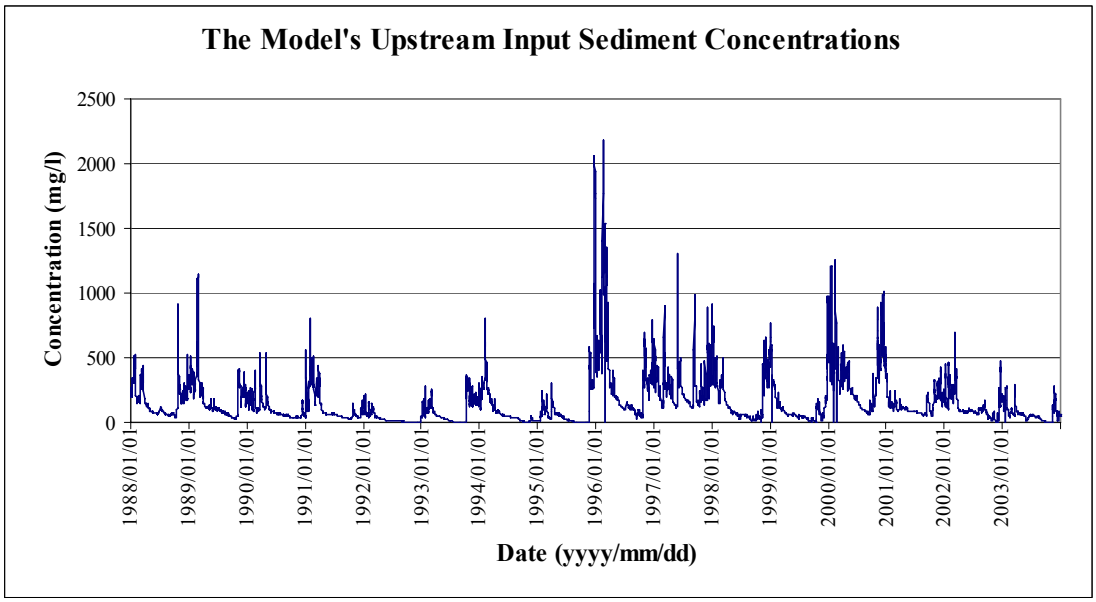

Figure 8.3-8: The upstream input sediment concentration time series

a) Settling Velocity Sensitivity Study

Two settling velocities were tested in a sensitivity study with the parameters as shown above. These settling velocities were the calculated value for the reservoir's sediment of 0.001m/s and the settling value of 0.0001m/s found for the Welbedacht Reservoir model.

The bathymetry from the 1988 and 2003 surveys are very similar. This can be seen when surveyed transverse sections from 1988 and 2003 are plotted together as below in Figures 8.3-9, 8.3-10 and 8.3-11. The layer of accumulated sediment is much thinner than would be expected for a 15 year period. This is because the average transverse section of the Vaal Reservoir is very wide (up to 2km) and also because the sediment concentration-discharge dependency is low. The results from the calibration runs are also shown on these figures. Section 51 (DWAF) is located just below the model's upstream boundary, 45km upstream of the dam. Section 30 is located 31km upstream of the dam and section 20 is located 22km upstream of the dam. The locations of these sections are shown on the aerial photo Figure 8.3-1.

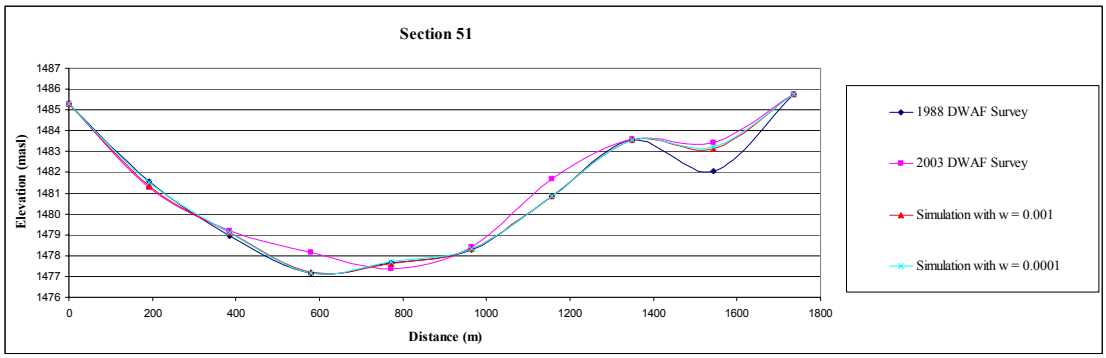

Figure 8.3-9: Deposited sediment layers at DWAF section 51 for different settling velocities

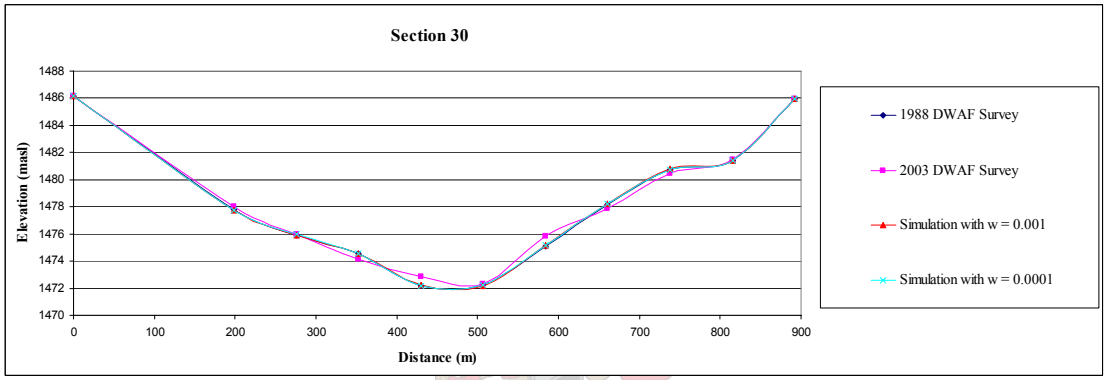

Figure 8.3-10: Deposited sediment layers at DWAF section 30 for different settling velocities

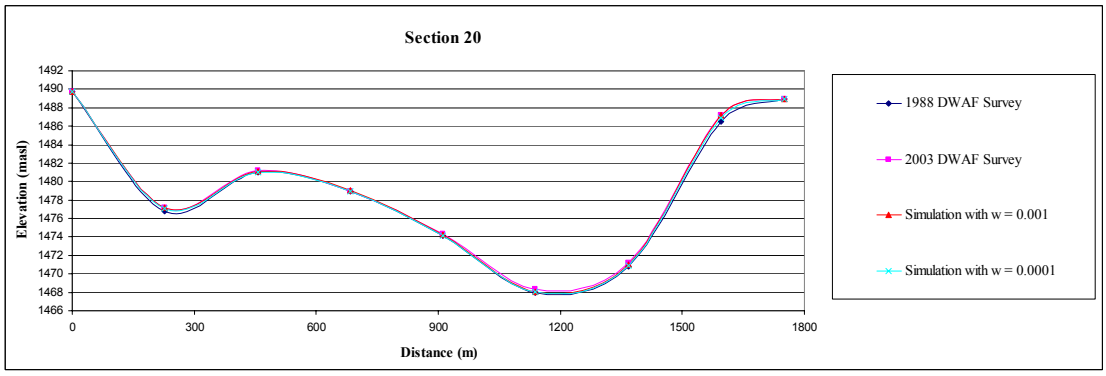

Figure 8.3-11: Deposited sediment layers at DWAF section 20 for different settling velocities

The surveyed sections and both simulated sections are very similar. On this scale it is difficult to see the minor changes in the layer thickness. Sediment deposition did take place, but on a very small scale. At section 51 the simulations produced far too little

deposition. This could be because of an initial underestimation of the concentration discharge dependency or simply because of non-calibrated parameters. Further sensitivity studies were conducted on the parameters of critical shear stress for deposition and the stream wise constant.

b) Sensitivity study for the critical shear stress for deposition, τ_{cd}

The logical step was to increase the critical shear stress for deposition since very little deposition was occurring. During the Welbedacht study this showed little promise. Vaal Reservoir and Welbedacht Reservoir are however different in many ways such as physical size, mean annual runoff and sediment yield rate and therefore it is necessary to investigate the parameters of Vaal Reservoir separately.

It was decided to increase τ_{cd} to a larger value of 0.15N/m^2 so that some deposition would be visible, especially upstream where more deposition was required. The results from the settling velocity sensitivity study did not show significant differences between the two values. It was decided to use the larger settling velocity of 0.001m/s in combination with the increased τ_{cd} to increase the deposition. Amongst others, these results are shown in Figures 8.3-12, 8.3-13 and 8.3-14.

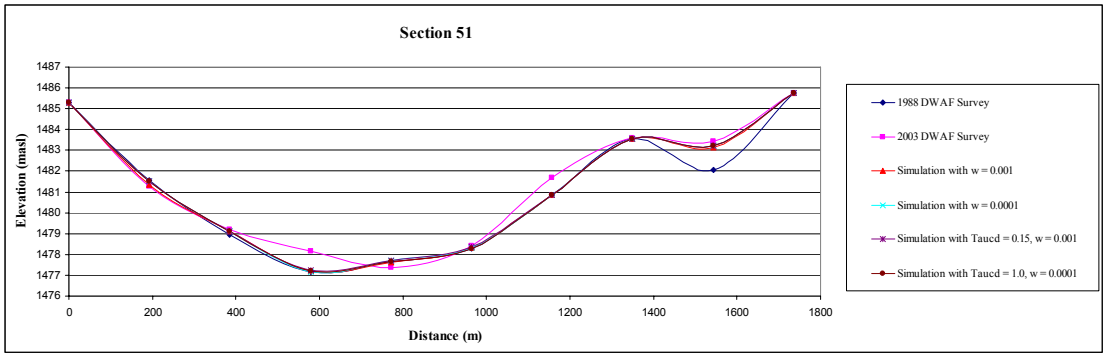

Figure 8.3-12: Deposited sediment layers at section 51 for different shear stresses for deposition

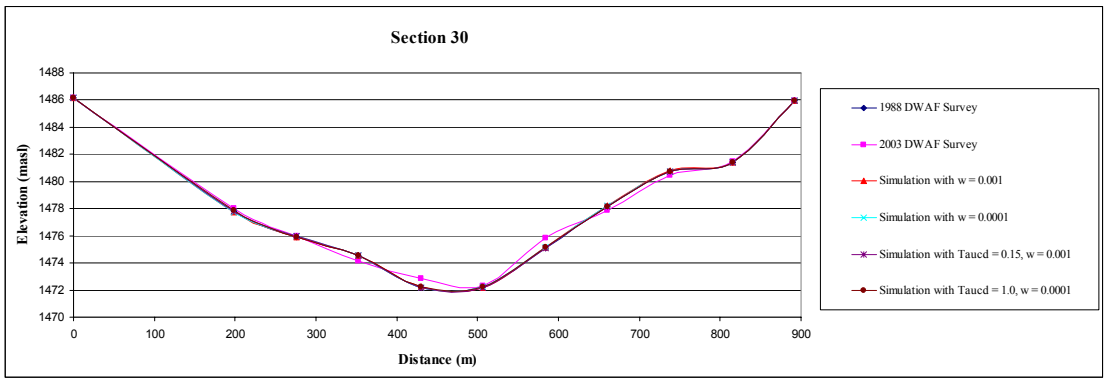

Figure 8.3-13: Deposited sediment layers at section 30 for different shear stresses for deposition

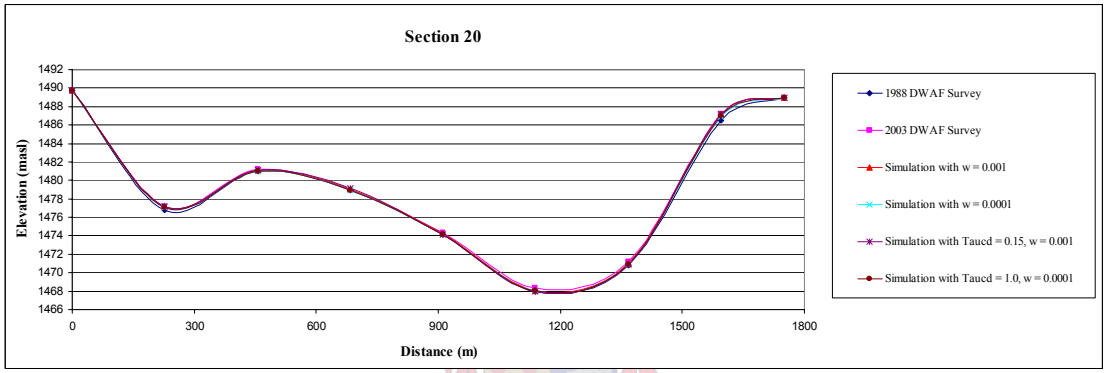

Figure 8.3-14: Deposited sediment layers at section 20 for different shear stresses for deposition

The upstream changes were still too small. There was however, extreme deposition of up to 13m just below the model's upstream boundary, but almost none at section 51. This was thought to be a result of the large settling velocity. The extreme upstream deposition is mostly because of the bathymetry; the river channel widens into the reservoir and the transport capacity therefore reduces, creating deposition. The fact that so much sediment is depositing at the upstream boundary means that reduced sediment concentrations are carried further into the reservoir which interferes negatively with the calibration procedure.

It was decided to reduce the settling velocity to 0.0001m/s for the next simulation. The τ_{cd} value was raised to 1.0N/m^2, a value that is much too large, but necessary to limit the amount of deposition. The extreme deposition below the boundary was then found to be only 7m, a value that is much more acceptable. The reason for this change

is the smaller settling velocity. The particles are less likely to deposit and remain suspended for a longer period.

The results from these simulations are also shown in Figures 8.3-12, 8.3-13 and 8.3-14. The problem was that this simulation produced even less regular deposition at the three sections. It seems thus that increasing τ_{cd} to a large and then a very large value has little effect on this reservoir's morphology and that the maximum deposition was already occurring at a value of 0.05N/m^2. This is possible because the reservoir is shallow and the velocities are low. Low bed shear stresses are thus expected, which is favourable for the deposition process.

c) Sensitivity Study for the Stream Wise Advection Constant, α_{01}

The last and only parameter left that could create some deposition was the stream wise constant α_{01}. With the value of the settling velocity kept at 0.0001m/s and a large τ_{cd} of 0.15N/m^2, two simulations were run. For the first, the value of α_{01} was 0.5 and for the second it was 0.1. The results once again did not show much deposition, as shown in Figures 8.3-15, 8.3-16 and 8.3-17.

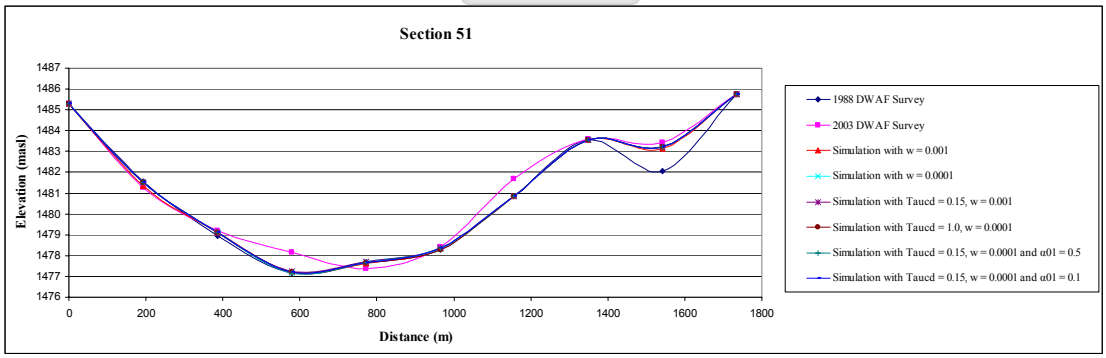

Figure 8.3-15: Deposited sediment layers at section 51 for different stream wise constants

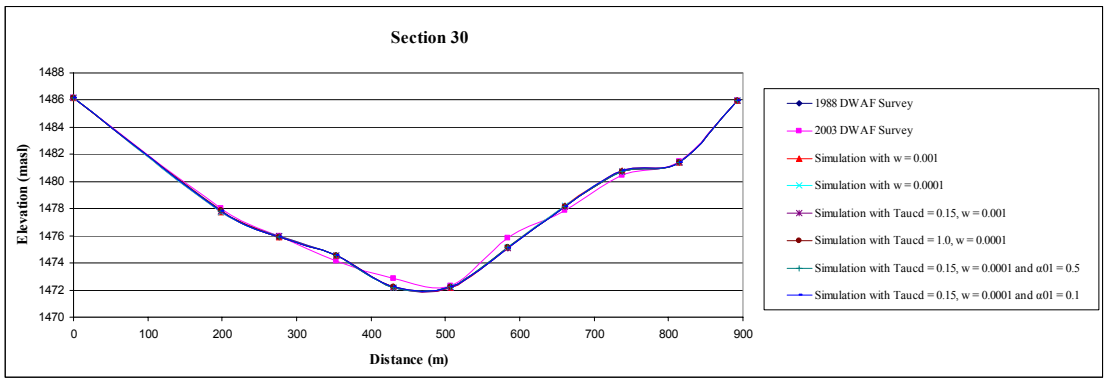

Figure 8.3-16: Deposited sediment layers at section 30 for different stream wise constants

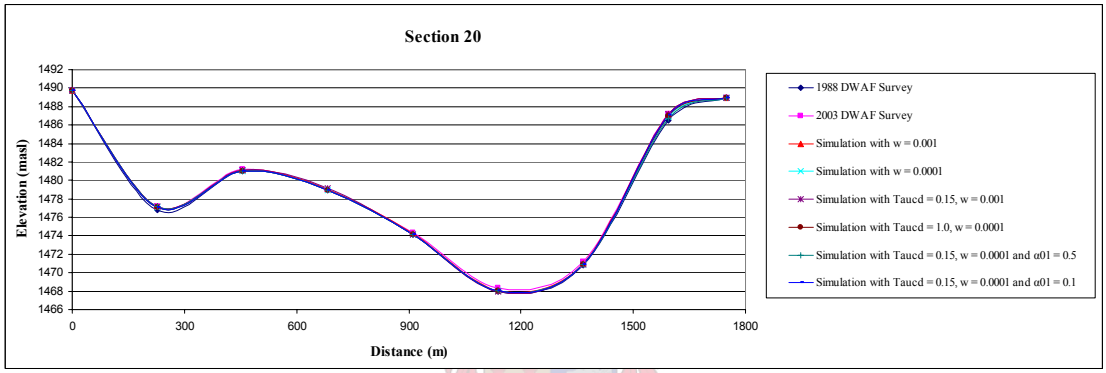

Figure 8.3-17: Deposited sediment layers at section 20 for different stream wise constants

From the figures above it is clear that a 15 year period of sedimentation in Vaal Reservoir will only slightly change it's bathymetry. It was thus decided to look at these changes on a smaller scale. For each of the data points on a section, a datum height was chosen against which the other survey and simulated data will be plotted. These new figures (Figures 8.3-18, 8.3-19 and 8.3-20) were found to be of great use in determining the most successful calibration run.

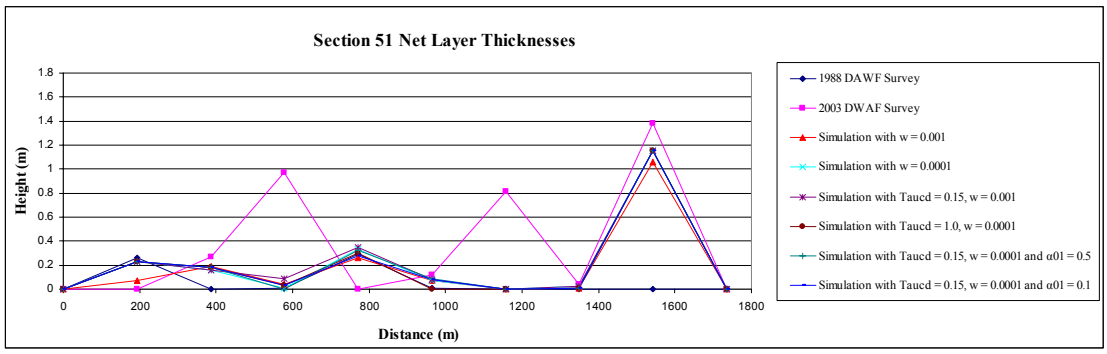

Figure 8.3-18: Deposited sediment layers at section 51 for the parameter variations

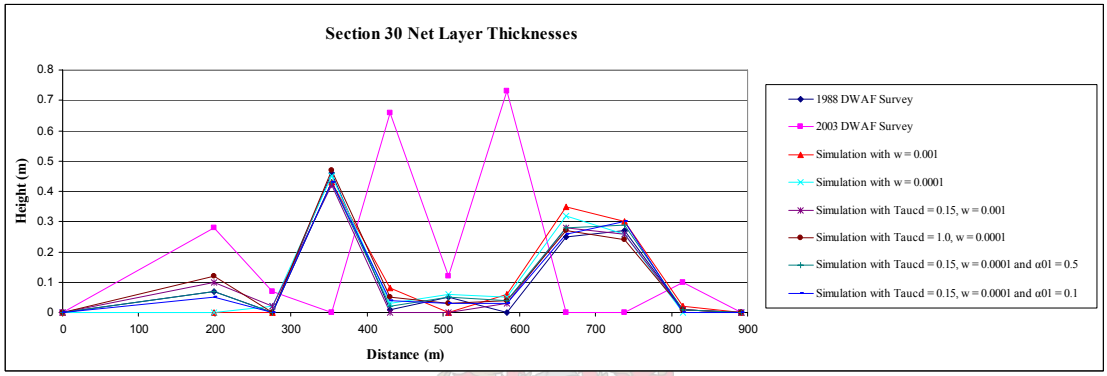

Figure 8.3-19: Deposited sediment layers at section 30 for the parameter variations

In Figure 8.3-19, the 1988 bathymetry and simulated data all lie within 100mm of each other. At section 30 the parameter changes really made little difference.

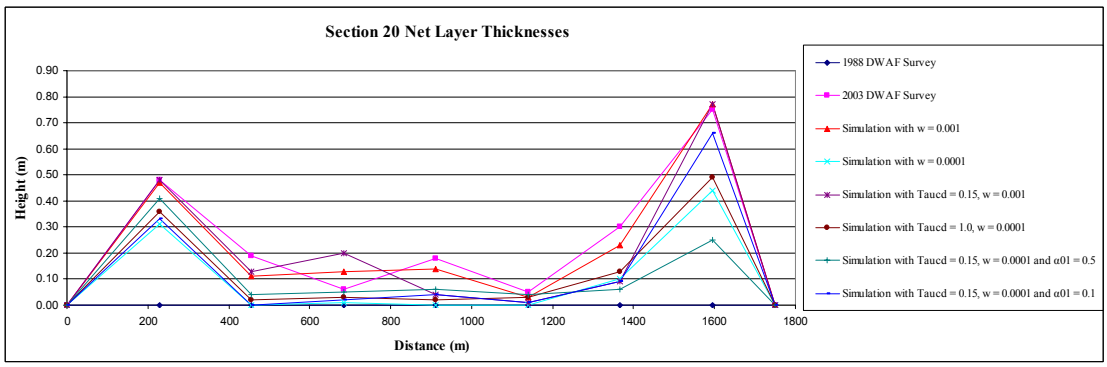

Figure 8.3-20: Deposited sediment layers at section 20 for the parameter variations

In Figure 8.3-20 the 1988 section lies right at the bottom of the figure. Larger changes in the simulated results are visible. From the results above it can be seen that it is still difficult to determine the best results. A set of results might be accurate at one place on the section but far from accurate at another.

However, when they are compared to each other one by one, it seems that the best result is from the simulation where the settling velocity is 0.001m/s, the critical stress for deposition is 0.15N/m^2 and the stream wise constant is 1.0. This is particularly evident in Figure 8.3-20. It should be noted that a critical shear stress for deposition of 0.05N/m^2 would also be sufficient in ensuring the same amount of deposition. The value of 0.15N/m^2 was chosen as a safe upper limit.

8.3.2 Validation

The model also produced a time series of suspended sediment concentration data which was compared to those from RandWater taken just upstream of Vaal Marina on a monthly basis during 1996. These simulated and measured values (Appendix I) were plotted versus their measured discharges in Figure 8.3-21. A trendline was fitted to the RandWater measured data. It can be seen that the concentrations produced by the simulations are generally higher than the values from RandWater during floods in excess of 100m^3/s. For flows smaller than 100m^3/s, the simulated values are smaller than the measured RandWater concentrations. In Figure 8.3-22 it can be seen that the flow only exceeds 100m^3/s for relatively short periods of time during the summers. During those flows, the model overestimates the concentrations. For all the smaller flows, the model underestimates the concentrations. All together it seems as though there was too little deposition on the chosen representative sections. This is because the model underestimates the concentrations and therefore deposition during the regular low flows.

Hydrographic surveys of Vaal Reservoir are only carried out every 15 years, so no other bathymetrical data was available to verify the calibrated parameters for another simulation period.

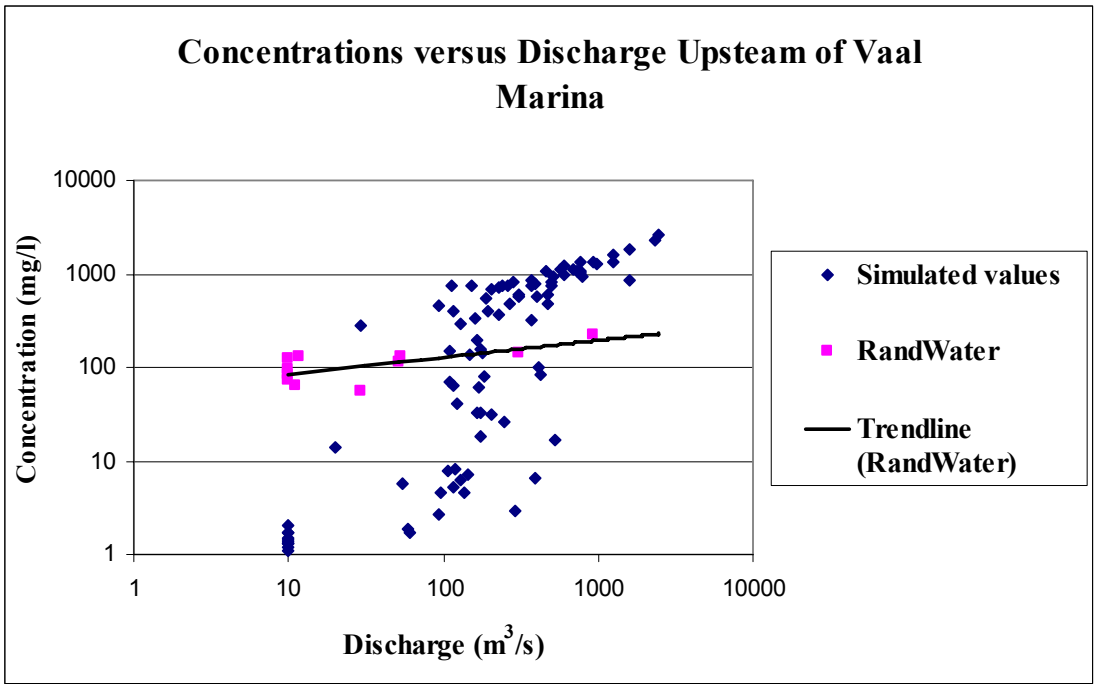

Figure 8.3-21: Simulated and measured concentrations versus discharge upstream of Vaal Marina

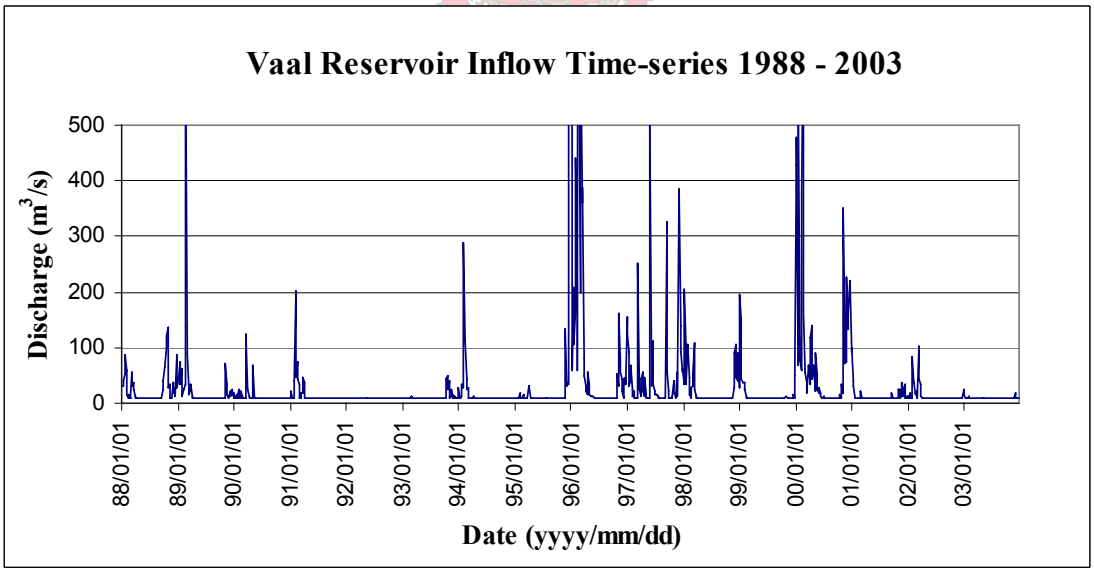

Figure 8.3-22: Vaal Reservoir Inflow Time-series

8.4 Winam Gulf Model, Lake Victoria, Kenya

A MIKE 21C numerical model was set up as part of an extensive environmental study on Winam Gulf, situated in the Nyanza province of Kenya. This model has been used here as a case study since it is very similar to a wide shallow reservoir (IWE, 2005). The Rusinga Channel connects Winam Gulf to the larger Lake. The largest river flowing into the gulf is the Nyando, which has a catchment area of 3 652 km^2 and an average discharge of 20.8m^3/s flowing into the gulf from the east (Figure 8.4-1). Kisumu, a city located on the Northern banks of the gulf, is experiencing degradation in water quality and turbidity along it's shores due to many factors. One of the main factors is the increased sediment loads from the Nyando River.

The study included a hydrometric survey of the gulf, sampling of bed and suspended sediment in both the river and the gulf. Sediment cores were also taken at various locations for the purpose of determining an average sediment deposition rate and also the particle size distribution of the bed sediment.

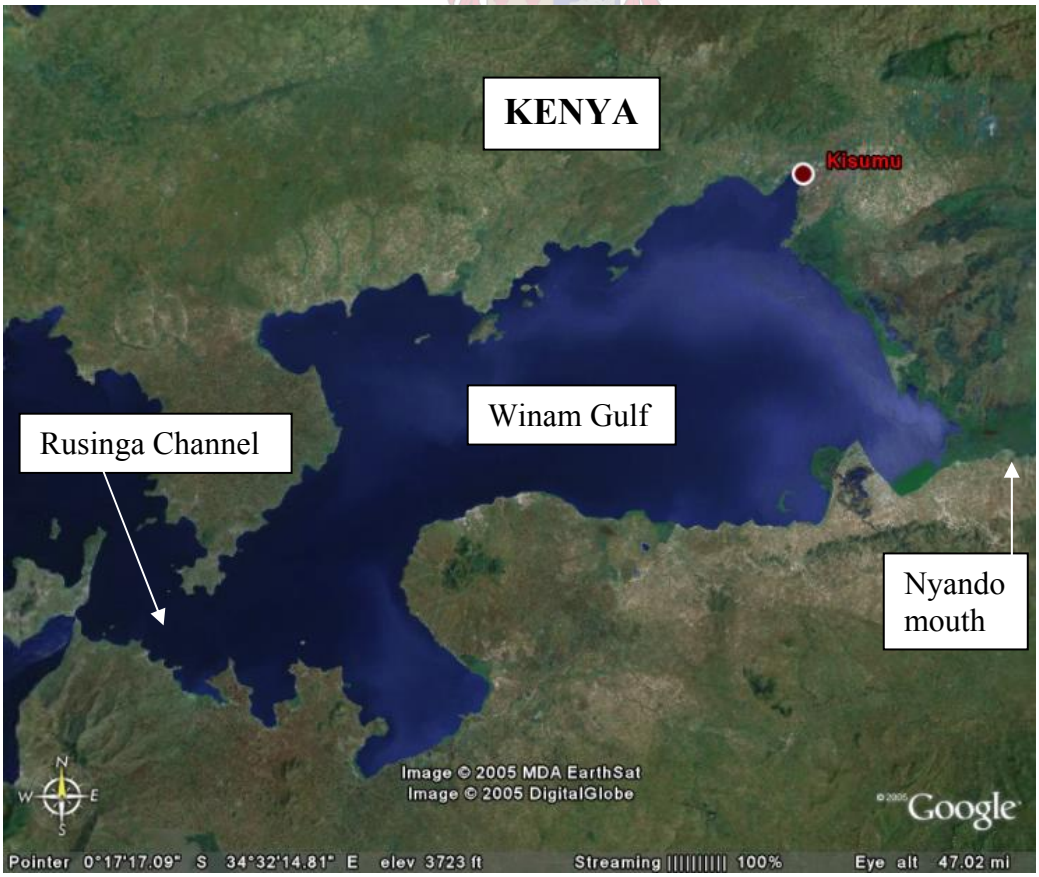

Figure 8.4-1: A satellite image of the Winam Gulf study area

Figure 8.4-2 shows the curvilinear grid used for the model. The grid contains 200 cells in the longitudinal direction and 100 cells in the transverse direction, totalling 20 000 cells when the model is fully flooded. The 2005 surveyed bathymetry is shown in Figure 8.4-3. The upstream boundary is the discharge from the Nyando River from the east, while the downstream boundary is the water level at the Rusinga Channel in the west.

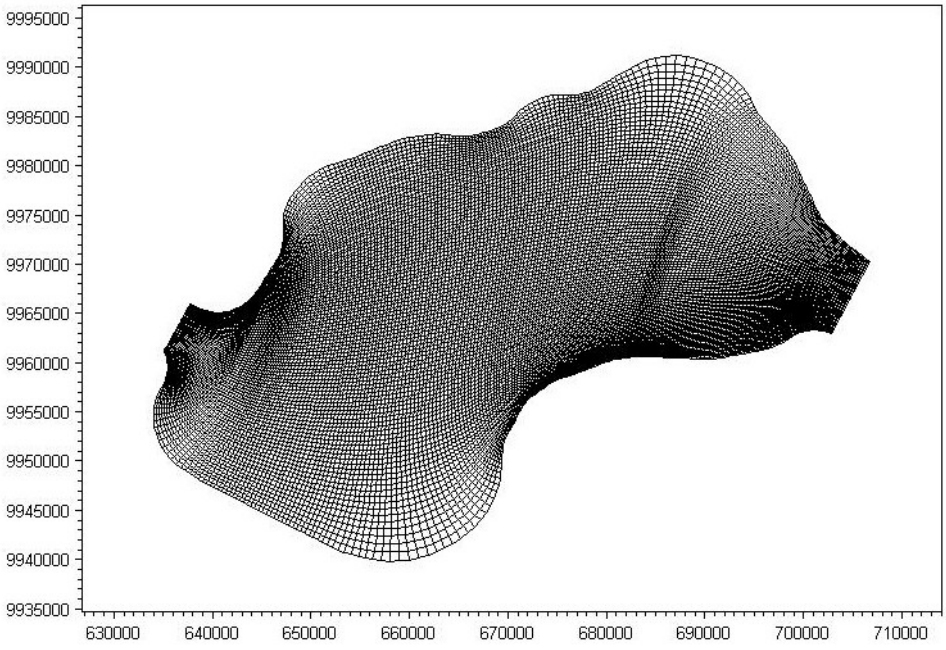

Figure 8.4-2: The curvilinear grid of the Winam Gulf study area

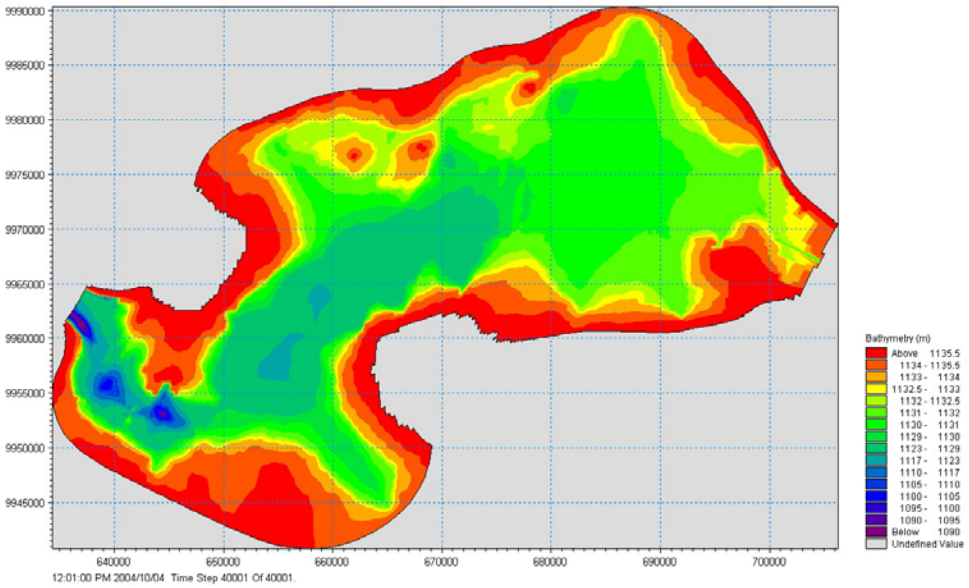

Figure 8.4-3: The 2005 surveyed bathymetry superimposed on the grid

8.4.1 Calibration: 1950 - 2004

The sediment was taken as 100% clay (<0.004mm) (IWE, 2005). The bed sediment sampled throughout the lake is a very fine dark brown mud. The representative median size is 0.00334mm. The settling velocity was therefore taken as 0.00001m/s for the first calibration run. All the sediment is taken as being of the same cohesive type.

All available data of sediment concentrations were plotted against the measured discharge as shown in Figure 8.4-4. A best fitting line was added to the data. This line was chosen to represent the dependency of the maximum measured concentrations on the discharge. According to this dependency line, the Nyando River produces a total sediment load of 1 million tons per year. These calculations are shown in Appendices J. LVEMP (2005) estimated the total sediment load to be only 350 000 tons per year. The dependency rate chosen was therefore a conservative one which would produce more deposition in the gulf than is expected.

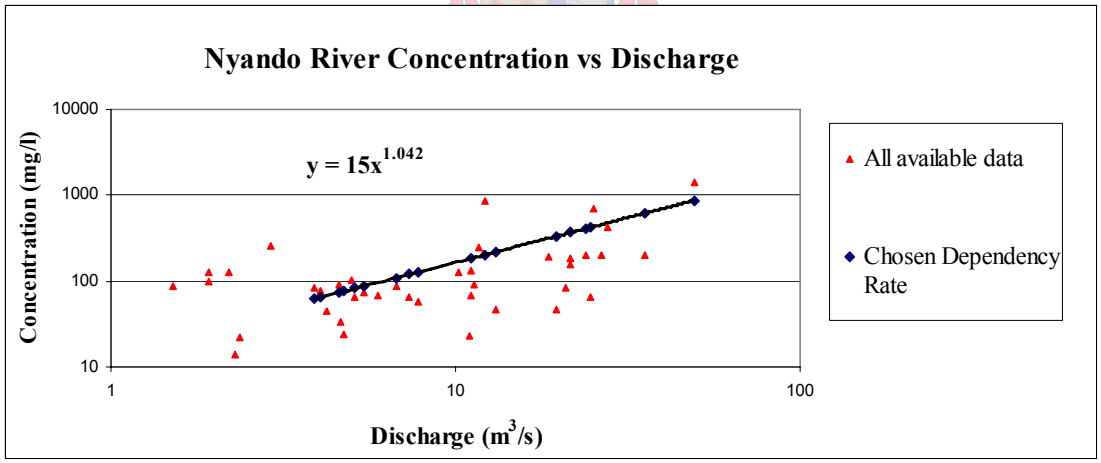

Figure 8.4-4: Nyando River measured concentrations versus discharge

The following dependency on the discharge was obtained:

$$C = 15Q^{1.042} \qquad (8\text{-}3)$$

Where C is in mg/ℓ and Q in m^3/s. The catchment area therefore yields sediment at a rate of 273.82 $t/km^2.a$ according to equation 8-3. (Appendix K).

Measured patched discharge data for the Nyando River was available for the last 54 years. Water level data at Rusinga Channel were also available for this same period. This data was obtained from the Kenyan LVEMP (Lake Victoria Environmental Management Project) authority. No previous bathymetrical information were available to calibrate results as in the Vaal and Welbedacht studies and it was therefore decided to run a 54 year simulation from 1950 to 2004 with the 2005 hydrographic survey data as the starting bathymetry. The parameters and time-series used for the first calibration simulation are shown in Table 8.4-1 and Figure 8.4-5 respectively.

Table 8.4-1: Calibration model variables

Variable	**Value**
Bed roughness – Manning M ($m^{0.33}/s$)	50
Critical shear stress for deposition (N/m^2)	0.05
Critical shear stress for erosion (N/m^2)	1.04
Eddy viscosity (m^2/s)	0.01
Sediment porosity	0.5
Sediment relative density	2.65
Erosion constant E_0 ($g/m^2/s$)	0.1
Exponent of erosion	2
Settling velocity (m/s)	0.00001
Stream wise constant	1.0

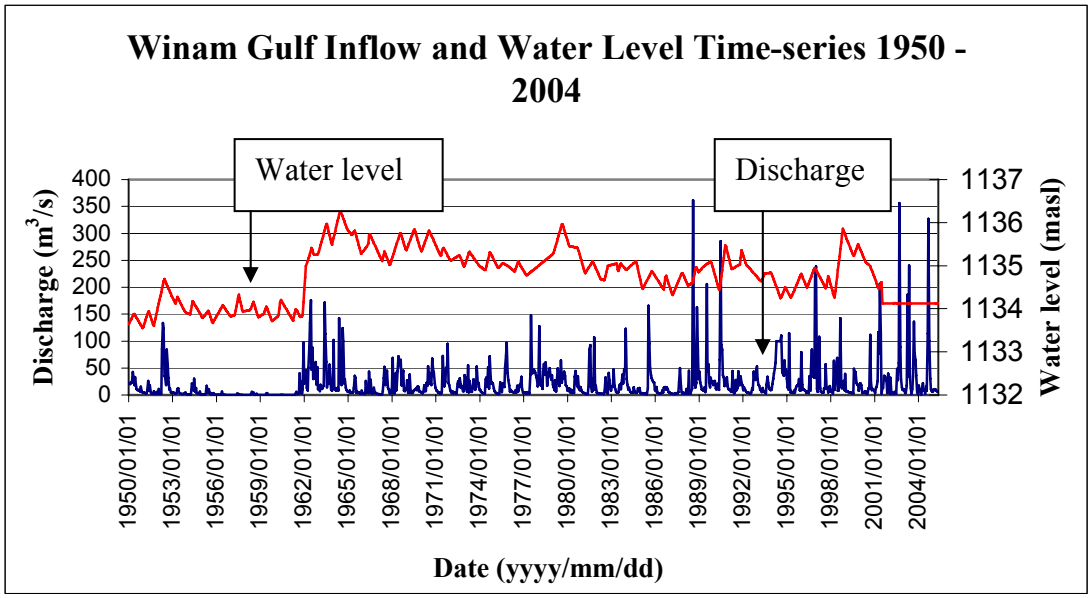

Figure 8.4-5: The 1950 to 2004 time-series for the Nyando River inflow and the Rusinga Channel water level based on observed data

The size of this grid, together with the 50 year long simulation period caused the computational time to exceed 120 hours. This limited the number of calibration runs to a trial and error basis. Fortunately, success was achieved with the first calibration run already.

At the end the simulation, estimations were made of the deposition rate and 54 year accumulated layer thickness. The simulation results were then compared to the results of deposited layer thickness from a study by the University of Exeter (IWE, 2005) in which sediment dating techniques were used.

8.4.2 Validation: the Sediment Core Dating Study

Four bed cores from different locations within Lake Victoria were sent to the University of Exeter, England. The original intention of the study was to use Caesium-137 (Cs-137) measurements to provide information on recent sedimentation rates within the past 50 years. The origins of the four cores are shown in Figure 8.4-6 below. The hydrographic survey lines are also shown on Figure 8.4-6.

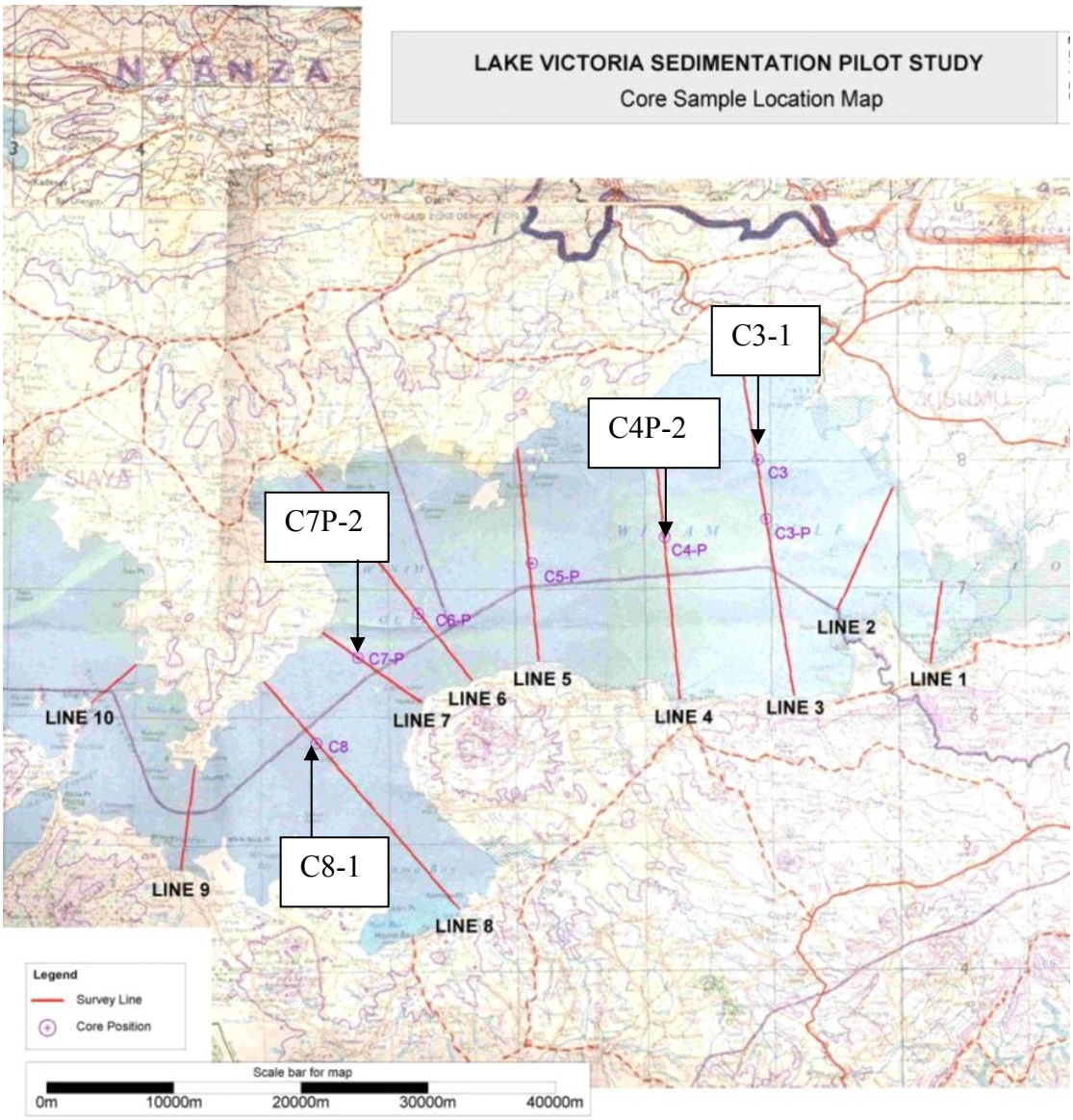

Figure 8.4-6: The original locations of the core samples (IWE, 2005)

Since Cs-137 fallout was a product of the testing of nuclear weapons in the latter part of the 1950s and the early years of the 1960s, this radionuclide is a means of estimating sedimentation rates over the past ca. 50 years (Figure 8.4-7). The basis of the approach is that significant amounts of Cs-137 would not be expected in sediment deposited prior to 1956 and that in many cases it is also possible to relate the depth distribution of Cs-137 to the pattern of fallout receipt and to identify a horizon containing maximum Cs-137 activities that can be equated with sediment deposited during the years 1963-1964. The Cs-137 content of the sediment would reflect both atmospheric fallout to the surface of the lake as well as Cs-137 carried to the lake with sediment eroded from the catchment.

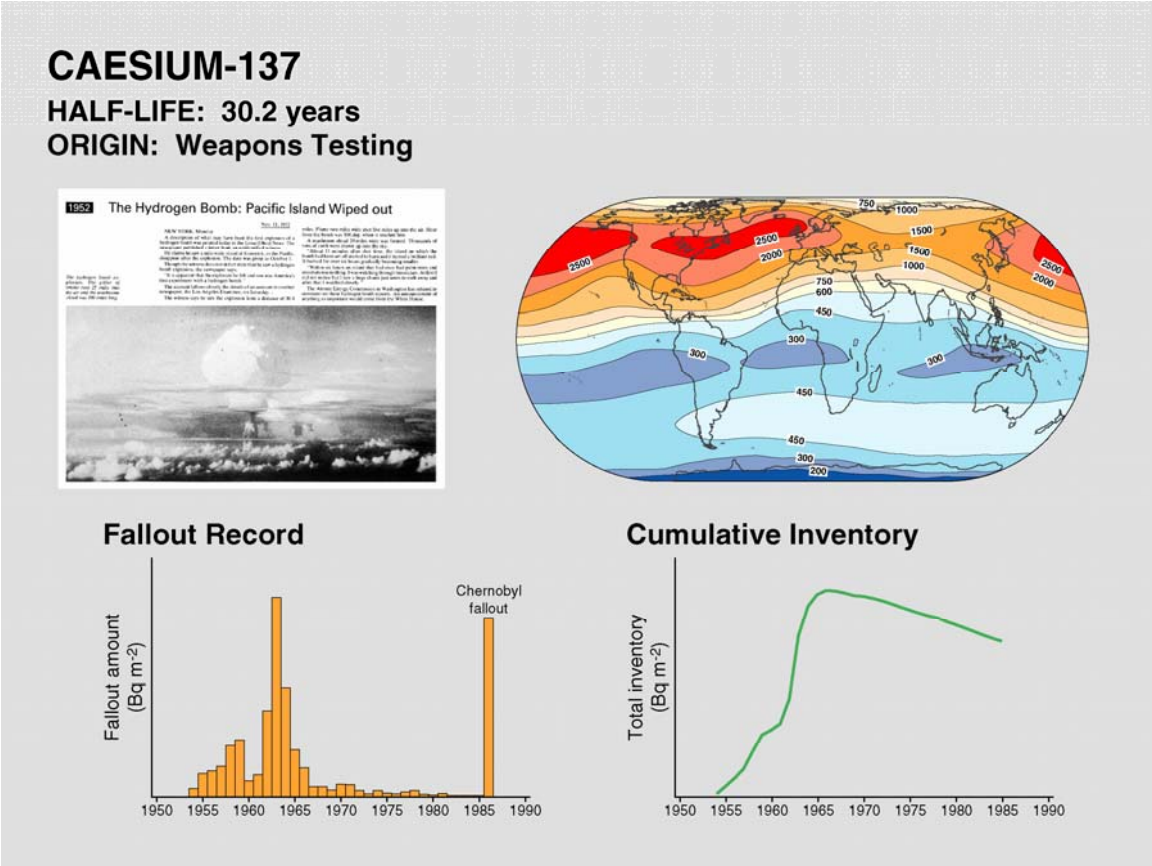

Figure 8.4-7: Historical Cs-137 fallout (IWE, 2005)

The four cores shipped to the University of Exeter for Cs-137 analysis were sectioned into 10mm depth incremental slices. Analysis of the sliced cores proceeded by starting with the upper slice of an individual core and proceeding downcore until the absence of Cs-137 from five successive slices suggested that the base of the sediment containing Cs-137 had been reached. Additional slices representing depths at 50mm intervals below this zone were analysed to confirm that the base of the sediment containing Cs-137 had been reached.

The results of this programme of analysis are presented in Table 8.4-2. As can be seen, no Cs-137 was detected in Core C8-1, but significant amounts of Cs-137 were detected in the other three cores. However, it is important to note that Cs-137 was only found in the surface and near surface horizons (i.e. 0-20mm or 0-30mm) of these three cores.

The data presented in Table 8.4-2 can be used to make a number of inferences regarding sedimentation rates at the sites from which the cores were collected. These are as follows:

a) Sedimentation rates are relatively low, with the rates estimated for the four cores containing Cs-137 lying in the range 20-30cm in 50 years.

b) The absence of measurable Cs-137 from core C8-1 suggests that little or no sediment accumulation has occurred at this site in the past 50 years.

Table 8.4-2: Measured Cs-137 in the cores analysed (IWE, 2005)

Core Number	Depth Below Bed Level (mm)	Sample Mass (g)	Total Mass (g)	Cs-137 Activity (mBq/g)	Inventory (Bq/m^2)	Cs-137 50 Year Sedimentation Depth (mm)	Mike21C Model 54 Year Deposition Depth (mm)
C8-1	10	2.91	2.91	0	0		
	20	2.38	2.38	0	0	**0**	**3**
					0		
C3-1	10	3.04	4.43	3.4	6.87		
	20	3.92	3.92	7.2	12.83	**20**	**7**
					19.7		
C4P-2	10	4.17	4.17	11.2	21.25		
	20	4.33	4.33	3.9	7.63	**20**	**54**
					28.87		
C7P-2	10	2.72	4.94	12.1	27.01		
	20	3.04	3.04	9.1	12.52	**30**	**4**
	30	3.32	3.32	11.4	17.19		
					56.71		

Table 8.4-2 also shows the simulated data from the calibration run which also indicate relatively low sedimentation rates. It can be seen that the layer thicknesses are in the same order of magnitude but slightly differently distributed. Nevertheless it does mean that the initial conservative overestimation of the concentration-discharge rate was justified.

The simulated results of the layer thicknesses are shown in Figure 8.4-8. The deposition pattern can be seen clearly. The deposition depth of sediment ranged from 1.5m at the river mouth to only a few millimeters at a distance of 40km from the mouth. Sediment dating carried out at the river mouth in a previous study indicated 0.5 to 1.0m deposition over 50 years (LVEMP, 2005).

Figure 8.4-9 shows a Landsat 5 image of Winam Gulf that was enhanced with field-measured soil reflectance spectra. The sediment plume from the Nyando River mouth has the same shape as the model's output deposition pattern. The model seems to be well calibrated.

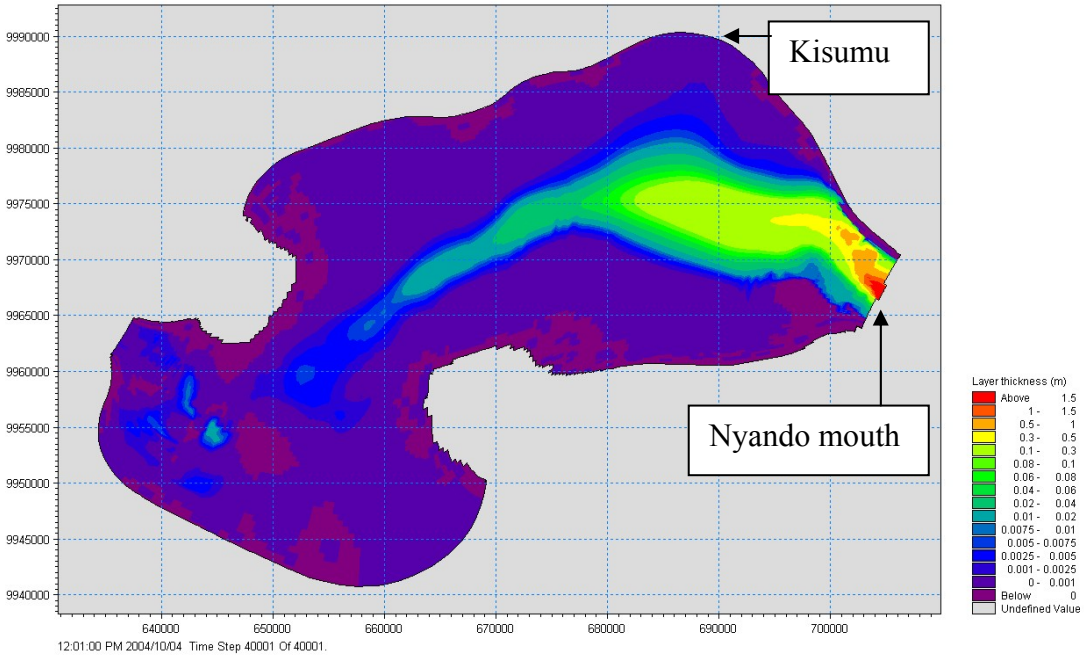

Figure 8.4-8: Plan view of the simulated 54 year accumulated sediment layer thickness

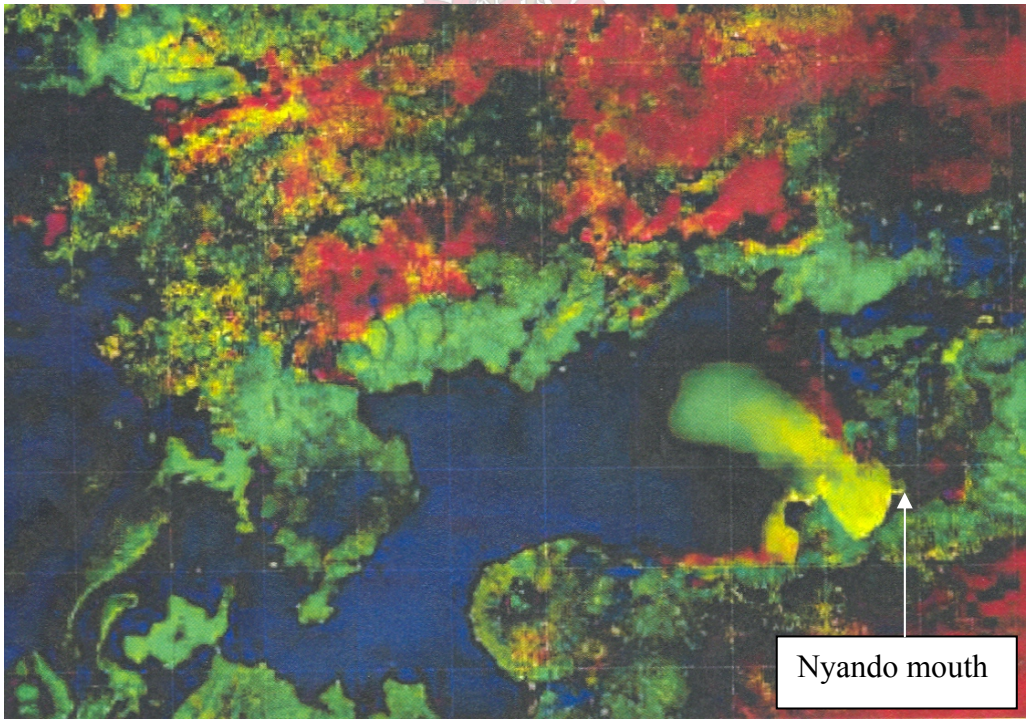

Figure 8.4-9: An enhanced satellite image showing the sediment plume from the mouth of the Nyando River

9. CONCLUSIONS AND RECOMMENDATIONS

9.1 Modelling with MIKE 21C

9.1.1 Small Scale Flume Modelling

The parameter sensitivity study in chapter 5 proved that parameter changes could have a significant influence on sediment transport when modelled on a small scale such as in a flume. Ranges can be established within which the values of a parameter have an effect on the sediment transport. These ranges will, however, differ for different flow conditions. These limits were quite easily established for the model with flow conditions as described in chapter 5. The simulation run time was only 5 minutes and a series of simulations could be run within the time limit. With large scale reservoir applications, the same calibration process is possible, but it will be a time consuming process.

Only some of the laboratory tests were successfully simulated using MIKE 21C. Although the same sediment was used in all the tests, no significant relation in the transport parameters could be identified. Table 9-1 shows the parameters of the simulations which produced the best fitting curves. Only the critical shear stress for deposition and the stream wise advection constant were calibrated.

Table 9-1: The laboratory test and simulation parameters

	Test 1	**Test 2**	**Test 3**	**Test 4**
Q_{total} (m^3/s)	0.0334	0.0334	0.0167	0.0167
Velocity (m/s)	0.1000	0.10	0.05	0.05
Water depth (m)	0.333	0.333	0.333	0.333
Design constant input concentration (mg/ℓ)	5 000	10 000	5 000	10 000
Actual constant input concentration (mg/ℓ)	2 150	4 881	2 020	1 371
Settling velocity (m/s)	0.00005	0.00005	0.00005	0.00005
Critical shear stress for erosion (N/m^2)	1.04	1.04	1.04	1.04
Critical shear stress for deposition (N/m^2)	0.30	0.50	1.00	0.04
Stream wise advection constant	0.075	0.03	0.10	1.00

It was decided to disregard the results from Test 3 because of the drastic fall in sediment concentration between the distances of 10m and 15m. The results are unrealistic and there probably was as error in the sampling or analysis procedures for this test. The critical shear stress for deposition for this test was also found to be much too high compared to the other tests.

It must be borne in mind that Tests 1 and 2 have the same flow depth, but double the discharge of Test 4. It is therefore unlikely that a single set of values for the two adjusted parameters will be identified that could create numerical results for all 4 tests that compares to the lab results.

The resultant curves from the simulations do compare to the curves from the laboratory tests, especially for Tests 1 and 4. The parameter values, however, do not compare.

It can be seen that the two parameters that were adjusted, τ_{cd} and α_{01}, vary significantly between Tests 1, 2 and 4. These values for Test 1 and 2 are comparable. The low values of α_{01} used in both Tests 1 and 2 indicate that the transport mechanism could well have been a density current and not turbulent suspension after all. This can also be seen in the drastic changes between the design constant input concentrations and the measured laboratory upstream concentrations. The sediment probably formed a density current which dived underneath the sampling instruments. The result was that lower weighted average concentrations were calculated at each sampling station for each test due to the assumed turbulent velocity distribution, producing unreliable results.

9.1.2 Large Scale Reservoir Modelling

When narrow reservoirs with relatively fast flowing water and high sediment loads are modelled, the effects of parameter changes are immediately visible when sections are plotted. This was the case with the Welbedacht Reservoir model.

Initially it seemed as though changes of the sediment transport parameters became almost insignificant for a large reservoir with a low average sediment load. This was really because the sediment layer is spread out over the width and length of the reservoir and the layer is thus much thinner and less visible. Changes of the transport parameters will cause differences in the sedimentation. These will however be less visible and they can sometimes only be observed and analysed on a smaller scale.

When large reservoirs, such as Vaal Reservoir, are modelled, large sediment deposits are found at the upstream boundary already. This is because the sediment enters into a flow with a low sediment transport capacity and thus is deposited. This low transport capacity is because of the low flow velocities caused by the damming and the sudden increase in width and depth of the flow area as the river enters the reservoir. This can be prevented by changing the bathymetry at the upstream boundary to a channel with an increasing sectional area so that the widening towards the reservoir is more gradual. The sediment will then deposit more gradually along the channel and into the reservoir. It must be kept in mind that the channel must still be able to handle the largest expected flood without the banks being overtopped. This will cause the simulation to become unstable. The parameters that were used in the reservoir models are shown in Table 9-2.

Table 9-2: The reservoir model parameters

Reservoir Model Summary	**Welbedacht Reservoir Model**	**Vaal Reservoir Model**	**Winam Gulf Model**
Source	Caledon River	Vaal River	Nyando River
Upstream boundary	Inflow time-series	Inflow time-series	Inflow time-series
Average discharge (m^3/s)	49	48	27
Downstream boundary	Water level time-series	Water level time-series	Water level time-series
Calibration simulation period (years)	3	15	54
Full supply level (masl)	1402.9	1484.5	1134
Catchment area (km^2)	15 245	12 276 (Vaal River leg, excluding Grootdraai Dam)	3 652
Catchment sediment yield ($t/km^2.a$)	2 950	58	274
Annual sedimentation rate (%)	4.53	-	-
Sediment type	Fine, cohesive	Fine, cohesive	Fine, cohesive
Field sediment size (mm)	0.0427	0.0281	0.00334
Sediment settling velocity (m/s)	0.00164	0.00071	0.00001
Calibrated Parameters			
Model sediment size (mm)	0.0105	0.0334	0.00334
Settling velocity w (m/s)	0.0001	0.001	0.00001
Crit. shear stress for erosion (N/m^2)	1.04	1.04	1.04
Crit. shear stress for deposition (N/m^2)	0.05	0.05 - 0.15	0.05
Stream wise advection constant α_{01}	1.0	1.0	1.0

From Table 9-2 above it can be seen that the calibrated shear stresses and the stream wise constant for all the models are more or less the same. The calibrated sediment sizes do vary between the models. The Vaal Reservoir and Winam Gulf models were calibrated with the representative sediment sizes and settling velocities as determined using the field data. The Welbedacht Reservoir model was calibrated using a falling velocity smaller than the value determined using the recent field data. This could be because of an initial overestimation of the average sediment particle size. The values initially found by Basson and Rooseboom (1996) had a weighted average size of 0.0427mm. Two samples taken close to the dam during 2005, had median values of 0.008mm and 0.011mm respectively, which compares well to 0.0105mm, the model calibrated value of sediment size.

9.2 Recommended Parameter Calibration Procedure

9.2.1 Sediment Size

The particle size grading of the sediment must be determined by sieve and hydrometer analyses of field samples. These samples should be taken close to the dam especially when the reservoir is silted up and operates like a run-of-river scheme, as proven in the case for the Welbedacht Reservoir model. A representative particle size (median or weighted average) is then used to calculate an expected average particle settling velocity.

9.2.2 Settling Velocity

In the case of reservoir models, the settling velocity calculated for a field sample's median or weighted average particle size can serve as a reliable parameter, as shown by the reservoir models.

9.2.3 Critical Shear Stress for Deposition

Calculating Expected Minimum Bed Shear Stress

It is recommended that firstly the reservoir model simulation is run for only hydrodynamics and no morphological changes. The results from this simulation will produce a minimum velocity at a certain time and place during the simulation. The depth as that point can also be determined from the hydrodynamic output.

With this information available, the bed shear stress at that point can then be calculated using the following equation:

$$\tau = \frac{\rho g v^2}{\left(Mh^{1/6}\right)^2} \qquad (9\text{-}1)$$

where M is the user specified bed roughness.

The used values of velocity and depth should actually be from the point of which the combination of velocity and depth produces the lowest bed stress, and not the point with the minimum velocity. To determine the point with the real minimum bed stress, however, could be problematic, since MIKE 21C does not give bed stress as output. This method will however still give a good approximation.

Knowing the expected minimum bed stress, the critical shear stress for deposition can be set around this value and evaluated in a sensitivity study format as done in this research. Any value larger than the expected minimum stress will produce some deposition.

The sensitivity studies in chapter 8 however, started out using a critical shear stress for deposition value that was recommended by Basson et al. (2003).

The minimum bed shear stress will, in effect, actually be $0N/m^2$. Some deposition will always occur where suspended sediment is available and the bed stresses are very low. The method to determine the minimum bed shear stress, as described above, should only be applied to points within the main channel of the reservoir.

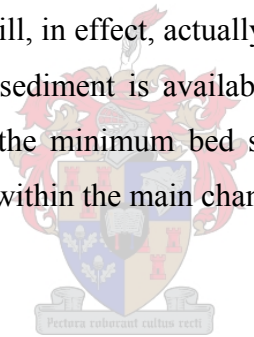

9.2.4 The Critical Shear Stress for Erosion

Calculating Expected Maximum Bed Stress

There is still uncertainty about the parameter of critical shear stress for erosion. What is recommended is that firstly the reservoir model simulation is run for only hydrodynamics and no morphological changes, as described in the method to determine the minimum bed shear stress. The results from this simulation will produce a maximum velocity at a certain time and place during the simulation. The depth as that point can also be determined from the hydrodynamic output.

With this information available, the bed shear stress at that point can then be calculated using equation 9-1.

The used values of velocity and depth should actually be from the point of which the combination of velocity and depth produces the largest bed stress, and not the point with the largest velocity. To determine the point with the real maximum bed stress, however, could be problematic, since MIKE 21C does not give bed stress as output. As stated before, this method will however still give a good approximation.

This stress can then be accepted as the maximum limit stress for erosion to occur. Any set value of the critical erosion stress below this value will produce erosion to a certain extent. Any value set above this, will limit erosion. For the models used in this research, little or no erosion was required and therefore the critical stress for erosion was kept at a value larger than the expected bed stresses. Further studies are needed so that the critical stress for erosion can be directly linked to cohesive bed sediment characteristics.

9.2.5 Stream Wise Advection Constant

The stream wise constant should be 1.0 for reservoir models. This ensures uniform distribution of the fine sediment over the depth and width of the section. It allows the sediment to be transported deep into the reservoir, as is expected from fine cohesive sediment. Reducing the value of α_{01} in reservoir models did not bring about more deposition since the maximum velocities are then brought closer to the bed, creating unfavourable conditions for deposition. In effect, erosion can occur because of the increased flow velocities close the bed.

9.2.6 Calibration Data

It is recommended that as much as possible field data are collected prior to the modelling of reservoir sedimentation. Any data related to the sedimentation can be of use in creating a reliable model. This includes data from various hydrographic surveys, measured data of discharge and water level, measured sediment concentration data, measured field data, laboratory flume data and even satellite images.

9.3 Research Recommendations

The recommended further research topics in this field that are:

- Calibration of the latest MIKE 21C software with the fully adjustable parameters of sediment transport and multi-fraction simulation capabilities.

- Calibration of MIKE 21C flume model with the use of reliable laboratory data. It is recommended to use lower sediment concentrations to prevent the formation of a density current. Higher flow velocities will help create turbulent transport.

- Research into the determination of critical shear stresses for erosion of cohesive sediments beds.

10. REFERENCES

Armanini, A. and Di Silvio, G. (1988). A One-dimensional Model for the Transport of a Sediment Mixture in Non-equilibrium Conditions. Journal of Hydraulic Research, 26 (3).

Arrifin, J. (2002). Evaluation of Equations on Total Bed Material Load. International Conference on Urban Hydrology for the 21st Century, October 2002, Kuala Lumpur.

Basson, G.R. and de Villiers, J.W.L. (2005). New Bridge Across Caledon River: Welbedacht Reservoir Sedimentation and Flood Level Study. ASP Technology (Pty) Ltd.

Basson, G.R.; Havno, K.; Tjerry, S. and Olesen, K.W. (2003). Modelling Sedimentation, Sluicing and Flushing in Shallow Reservoirs.

Basson, G.R., Melvill, J. and de Villiers, J.W.L. (2005). Vaal River Eastern Sub-System Augmentation Project (VRESAP): Abstraction Works Hydraulic Model Study. University of Stellenbosch Hydraulic Laboratory & ASP Technology (Pty) Ltd.

Basson, G.R. and Olesen, K.W. (2004). Control of Reservoir Sedimentation by Flood Flushing: Impacts, Operation and Mathematical Modelling.

Basson, G.R. and Rooseboom, A. (1997). Dealing with Reservoir Sedimentation. Water Research Commission Report No. TT 91/97.

Batuca, D.G. and Jordaan, J.M. (2000). Silting and Desilting of Reservoirs. Balkema Publishers, Rotterdam.

Beck, J.S. and Basson, G.R. (2003). The Hydraulics of the Impacts of Dam Development on the River Morphology. Water Research Commission Report No. 1102/1/03.

Beck, J.S. and Basson, G.R. (2002). Morphological Impacts and Mitigation Measures: Control of Reservoir Sedimentation and Environmental Flood Releases Short Course, Department of Civil Engineering, University of Stellenbosch, South Africa.

Chadwick, A. and Morfett, J. (1998). Hydraulics in Civil and Environmental Engineering - Third Edition. Spon Press, London.

Clark, J. (1990). Department of Water Affairs and Forestry - Vaal Dam Capacity Determination 1986 – 1990. Report No. C120-01.

Clark, J. (1990). Department of Water Affairs and Forestry – Welbedacht Dam Capacity Determination 1990. Report No. D200-01.

Craig, R.F. (2001). Soil Mechanics – Sixth Edition. Spon Press, London.

Cunge (1989). In Delft Hydraulics, 1992.

Cunge, J.A.; Holly, F.M. and Verwey, A. (1980). Practical Aspects of Computational River Hydraulics. Pitman Publishing Inc., Boston, USA.

Di Silvio, G. (1995). River Modelling. UNESCO IHP-IV Project H-1-2, Working Group on Erosion, Riverbed Deformation and Sediment Transport in River Basins as Related to National and Manmade Changes.

Delft Hydraulics (1992). The Control of Reservoir Sedimentation – A Literature Review. Ministry of Development Co-operation, Government of the Netherlands, Delft Hydraulics.

De Vriend, H.J. (1981). Steady Flow in Shallow Channel Bends. Communications on Hydraulics, 81-3. Delft University of Technology, The Netherlands.

Dou, G.R. (1963) Sediment Transport Theory. Nanjing Hydraulic Institute, China.

Dou, G.R. (1980). The Stochastic Theory and the General Law of all Flow Regions for Turbulent Open Channel Flows. Proceedings of the First International Symposium on River Sedimentation, China. Guanghua Press.

Dou, G.R.; Lu, Y.; Han, L.; Shao, X. and Yang, X. (2004). 3D Numerical Simulation for Water Flows and Sediment Deposition in Dam Area of the Three Gorges Project. Proceedings of the Ninth International Symposium on River Sedimentation, China.

DHI Water & Environment. (2001). MIKE 11, A Modelling System for Rivers and Channels – User Guide.

DHI Water & Environment. (2003). MIKE 21C River Hydrodynamics and Morphology – User Guide.

DHI Water & Environment. (2003). MIKE 21C River Morphology - A Short Description.

DWAF (2006). www.dwaf.gov.za. Home Page of the Department of Water Affairs and Forestry, South Africa.

Falconer, R.A. and Owens, P.H. (1990). Numerical Modelling of Suspended Sediment Fluxes in Estuarine Waters. Estuarine, Coastal and Shelf Science Vol. 31.

Han, Q. (1980). A Study on the Non-equilibrium Transport of Suspended Sediment. Proceedings of the First International Symposium on River Sedimentation, China.

Han, Q. and He, M. (1990). A Mathematical Model for Reservoir Sedimentation and Fluvial Processes. International Journal of Sediment Research., IRTCES.

H.R. Wallingford (1998). Reservoir Sedimentation Management, Tarbela Dam. Water and Power Development Authority.

Holly, F.M. and Cunge, J.A. (1975). Time Dependant Mass Dispersion in Natural Streams. Proceedings of the Symposium on Modelling Techniques. American Society of Civil Engineers, San Francisco.

IWE (2005). Pilot Study on Sedimentation and Sediment Characteristics on Nyando and Nzoia River Mouths and Winam Gulf of Lake Victoria. Institute for Water and Environmental Engineering, University of Stellenbosch.

Jia, Y. and Wang, S.S.Y. (1999). Numerical Model for Channel Flow and Morphological Change Studies. Journal of Hydraulic Engineering, ASCE, Vol. 125 No. 9.

Jordaan, J.M. (1989). The Sediment Problem in South African Reservoirs. Proceedings of the International Symposium on Sediment Transport Modelling, USA.

Karanshev (1963). In Delft Hydraulics, 1992.

Le Moigne, G. (1990). Dam Safety and the Environment. World Bank Technical Paper No. 115.

Lin, B.N.; Huang, J. and Li, X. (1983). Unsteady Transport of Suspended Load at Small Concentration. Journal of Hydraulic Engineering, ASCE, Vol. 109, No. 1.

Lin, B.N. and Shen, H. (1984). Two-dimensional Flow with Sediment by Characteristics Method. Journal of Hydraulic Engineering, ASCE, Vol. 110, No. 5.

Lopez, J.L. (1978). Mathematical Modelling of Sediment Deposition in Reservoirs. Ph.D. Dissertation . Colorado State University, USA.

LVEMP (2005). Lake Victoria Regional Water Quality Synthesis Report. October 2005.

Mehta, A.J. and Partheniades, E. (1973). Effects of Physico-chemical Properties of Fine Suspended Sediment on the Degree of Deposition. Paper A-41. Proceedings of the International Symposium on River Mechanics, Bangkok.

Olesen, K.W. and Basson, G.R. (2004). 1D and 2D Modelling of Sedimentation and Flushing in Shallow Reservoirs. Proceedings of the Ninth International Symposium on River Sedimentation, Yichang, China.

Palmieri, A. (2003). Social and Economic Aspects of Reservoir Conservation. World Water Forum, Kyoto, Japan.

Postel, S. (1989). Water for Agriculture, Facing the Limits. World Watch Paper 93.

Rahuel, J.L. and Holly, F.M. (1989). Modelling of Riverbed Evolution for Bedload Sediment Mixtures. Journal of Hydraulic Engineering, ASCE, 115 (11).

Rooseboom, A. (1975). Sediment Transport in Rivers and Reservoirs. D.Eng Dissertation, University of Pretoria, (In Afrikaans). (Later Published by Water Research Commission, South Africa, Report No. 297/1/92, English).

Rooseboom, A. (1992). Sediment Transport in Rivers and Reservoirs – A South African Perspective. Water Research Commission Report No. 297/1/92.

Rooseboom, A. and Maas, N.F. (1974). Sedimentafvoer in die Oranje-, Tugela- en Pongolariviere. Technical Report No. 59, Department of Water Affairs and Forestry.

Rooseboom, A. and Mulke, F.J. (1982). Recent Developments in the Explanation and Prediction of Erosion and Sediment Yield - Erosion Initiation. Proceedings of the Exeter Symposium, July 1982. IAHS Publishers.

Rooseboom, A.; Alexander, W.R.J. and Van Vuuren, S.J. (1986). Welbedacht Reservoir: The Effect of Different Operating Rules on the Sedimentation Rate and Reservoir Yield with Reference to Off-channel Storage in the Knellpoort Reservoir.

A Report to the Department of Water Affairs and Forestry by Sigma Beta Consulting Engineers, Pretoria.

Rouse, H. (1937). Modern Concept of the Mechanics of Turbulence. Transactions, ASCE 102.

Rozowskii, I.L. (1957). Flow of Water in Bends of Open Channels.

Sheng, Y.P. (1983). Mathematical Modelling of Three-dimensional Coastal Currents and Sediment Dispersion: Model Development and Application, Technical Report CERC-83-2, Aeronautical Research Associates of Princeton Inc., USA.

Shields, A. (1936). Anwendung der Aehnlichkeits-mechanic und der Turbulenz for schung auf die Geschliebe beweging. Mitteilungen der Preuss. Versuchsanstalt fur Wasserbau und Schiffsbau, Berlin.

Soares et al. (1982). In Delft Hydraulics, 1992.

Spasojevic, M. and Holly, F.M. (1993). Three-dimensional Numerical Simulation of Mobile-bed Hydrodynamics. Technical Report No. 367. Iowa Institute of Hydraulic Research, University of Iowa, USA.

Thomas, W.A. (1982). Mathematical Modelling of Sediment Movement, Gravel Bed Rivers. John Wiley and Sons, Ltd., USA.

Wang, S.S.Y. and Adeff, S.E. (1986). Three-dimensional Modelling of River Sedimentation Processes. Proceedings of the Third International Symposium on River Sedimentation. University of Mississippi, USA.

Wang, S.S.Y. and Wu, W. (2004). River Sedimentation and Morphology Modelling – The State of the Art and Future Development. Proceedings of the Ninth International Symposium on River Sedimentation, China.

Wu, W. and Vieira, D.A. (2002). One-dimensional Channel Network Model CCHE1D 3.0, Technical Manual. Technical Report No.NCCHE-TR-2002-1. National Centre for Computational Hydroscience and Engineering. University of Mississippi.

Wu, W.; Wang, S.S.Y. and Jia, Y. (2000). Non-uniform Sediment Transport in Alluvial Rivers. Journal of Hydraulic Research, IAHR, 38 (6).

Yang, C.T. (1972). Unit Stream Power and Sediment Transport. Proceedings of the American Society of Civil Engineers.

Yang, C.T. (1973). Incipient Motion and Sediment Transport, Journal of Hydraulics Division, ASCE, 99 (HY10), 1979-1704.

Yang, C.T. (1976). Minimum Unit Stream Power and Fluvial Hydraulics. Journal of Hydraulics Division, ASCE 102 (7).

Yang, C.T. (1984). Unit Stream Power Equation for Gravel. Journal of the Hidraulics Division, ASCE, Vol. 110. (HY12).

Yang, C.T. and Simoes, F.J.M. (2000). Users Manual for GSTARS2 Version 2.1. USBR Technical Service Centre, USA.

Yang, C.T. and Simoes, F.J.M. (2003). Application of GSTARS to River Sedimentation Studies. Proceedings of the Ninth International Symposium on River Sedimentation, China.

Yang, C.T. and Song, C. (1986). Theory of Minimum Energy and Energy Dissipation Rate. Encyclopedia of Fluid Mechanics Vol. 1, Chapter 11. Gulf Publishing Company.

Zhang, Q. (1980). Sediment Problems of Sanmexia Reservoir, Proceedings of the International Symposium on River Sedimentation, China.

Zhou, J. (1997). Research Report of Calculation of 2D Sediment Mathematical Model of the Dam Area of the Three Gorges Project. Collection of Sediment Research Reports for the Dam Area of Three Gorges Project on Yangtze River, Vol. 1. Patent Literature Press.

Zhou, J. and Lin, B. (1995). 2D Mathematical Model for Suspended Sediment, Part 1: Model Theory and Validations. Journal of Basic Science and Engineering, Vol. 3, No. 1.

Zhou, J. and Lin, B. (1998). One-dimensional Mathematical Model for Suspended Sediment by Lateral Integration. Journal of Hydraulic Engineering, ASCE, Vol. 124, No. 7.

Zhou, J.; Lin, B. and Lin, B. (2004). Rational Basis for Suspended Sediment Modelling. Proceedings of the Ninth International Symposium on River Sedimentation, China.

Zhou, J.; Spork, V.; Koengeter, J.; and Rouve, G. (1997). Bed Conditions of Non-equilibrium Transport of Suspended Sediment. International Journal of Sediment Research, Vol. 12, No. 3.

APPENDICES

Appendix A: Laboratory Test Calculations

Appendix B: ASTM Method for Determining Particle Size Distribution

Appendix C: Laboratory Results

Appendix D: Determining the Roughness of the Laboratory Channel

Appendix E: Laboratory Test Velocity Distribution Calculations

Appendix F: Welbedacht Reservoir Sediment Data

Appendix G: Welbedacht Sediment Load Calculations

Appendix H: Vaal Reservoir Sediment Data

Appendix I: Vaal Reservoir Suspended Sediment Data

Appendix J: Nyando River Suspended Sediment Data

Appendix K: Nyando Inflow Time-series and Sediment Concentrations

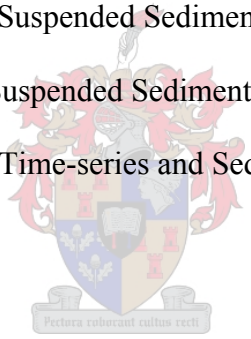

Appendix A : Laboratory Test Calculations

Input Sediment Concentrations

C_1	5 000	mg/ℓ
C_2	10 000	mg/ℓ

Mixture Container Volume =	1.692	m^3

Flow Calculations: Test 1 and 2

V	**0.1**	m/s

Channel Width	1	m	
Channel Length	37	m	
Channel Height	1.2	m	
Water depth = 1/3(Width)	0.333	m	
Fr	0.0553	-	
g	9.81	m/s^2	
R	0.20	-	
Re	20008.0	-	(turbulent flow)
V	0.100	m/s	
T	**370**	s	**240** s (Max flow period)
A	0.333	m^2	
Q	0.03333	m^3/s	
Q	33.333	ℓ /s	

Flow Calculations: Test 3 and 4

V	**0.05**	m/s

Channel Width	1	m	
Channel Length	37	m	
Channel Height	1.2	m	
Water depth = 1/3(Width)	0.333	m	
Fr	0.0277	-	
g	9.81	m/s^2	
R	0.20	-	
Re	10004.0	-	(turbulent flow)
V	0.050	m/s	
T	**740**	s	**240** s (Max. flow period)
A	0.333	m^2	
Q	0.01667	m^3/s	
Q	16.667	ℓ /s	

Sediment Calculations:

Test 1

Input Concentration	**5 000**	mg/ℓ	
Sediment flux Q_s	166666.67	mg/s	
	166.67	g/s	
Total mass over T	40000.0	g	
	40	kg	
Container sediment Mass	40000000	mg	
Container C	27 500	mg/ℓ	
Container Vol.	**1454.545**	ℓ	(86% - Maximum container level with freeboard)

1454.545	ℓ	in 240	s

Container inflow rate	0.0061	m^3/s
Channel inflow rate	0.0273	m^3/s

Test 2

Input Concentration	**10 000**	mg/ℓ
Sediment flux Q_s	333333.33	mg/s
	333.33	g/s
Total mass over T	80000.0	g
	80	kg
Container sediment Mass	80000000	mg
Container C	55 000	mg/ℓ
Container Vol.	**1454.545**	ℓ

(86% - Maximum container level with freeboard)

1454.545	ℓ	in	240

s

Container inflow rate	0.0061	m^3/s
Channel inflow rate	0.0273	m^3/s

Test 3

Input Concentration	**5 000**	mg/ℓ
Sediment flux Q_s	83333.33	mg/s
	83.33	g/s
Total mass over T	20000.0	g
	20	kg
Container sediment Mass	20000000	mg
Container C	13 750	mg/ℓ
Container Vol.	**1454.545**	ℓ

(86% - Maximum container level with freeboard)

1454.545	ℓ	in	240

s

Container inflow rate	0.0061	m^3/s
Channel inflow rate	0.0106	m^3/s

Test 4

Input Concentration	**10 000**	mg/ℓ
Sediment flux Q_s	166666.67	mg/s
	166.67	g/s
Total mass over T	40000.0	g
	40	kg
Container sediment Mass	40000000	mg
Container C	27 500	mg/ℓ
Container Vol.	**1454.545**	ℓ

(86% - Maximum container level with freeboard)

1454.545	ℓ	in 240	s

Container inflow rate	0.0061	m^3/s
Channel inflow rate	0.0106	m^3/s

V-weir Calculations

90° V-weir Q	0.0061	m^3/s
Cd	0.59	-
theta/2	45	deg.
(rad)	0.785	rad.
h1	**0.114**	m

Appendix B : ASTM Method for Determining Particle Size Distribution

Sediment used in laboratory experiments: Western Province Ball Clay
(a very fine light brown powder)

A sieve analysis showed that all the particles were smaller than 0.075mm (75μm), thus the ASTM hydrometer method was used to determine the size distribution of the particles In this method a 60g (w) sample of particles smaller than 2.36mm is mixed into 120ml of sodium hexametaphosphate solution (40g/ℓ) and left for 16 hours. Afterwards it is poured into a 1000ml sedimentation cylinder which is then filled up with distilled water and placed in a constant temperature bath until the suspension reaches 20°C. The cylinder is then taken out of the bath and turned upside down and back for 60 seconds, and placed back in the bath. Readings are taken with an ASTM 152H hydrometer at increasing time intervals. The temperature of the suspension is also measured after every reading.

Hydrometer Readings

Time (min)	Reading	*Corrected reading	Temp (°C)
2	57.5	52.5	20
5	56	51	20
15	54	49	19.7
30	52.5	47.5	19.7
60	51	46	19.5
250	49	44	21
1440	45.5	40.5	19.5

* The correction is made to bring the density of the sodium hexametaphosphate and distilled water solution into account. (subtracting it's hydrometer reading of 5)

Diameters of Particles

$$D = (Temperature\_const.) * \sqrt{\frac{Effective\_depth\_(cm)}{Time\_(\min)}}$$

Particle	Temp (°C)	Temp. const.	Eff. Depth (cm)	Time (min)	D (mm)
D_2	20	0.01365	7.7	2	0.0268
D_5	20	0.01365	7.9	5	0.0172
D_{15}	19.7	0.01365	8.3	15	0.0102
D_{30}	19.7	0.01365	8.5	30	0.0073
D_{60}	19.5	0.01365	8.8	60	0.0052
D_{250}	21	0.01348	9.1	250	0.0026
D_{1440}	19.5	0.01365	9.65	1440	0.0011

Concentration of Particles

$$P = \frac{Corrected\_reading}{w} \text{ x } 100$$

$$w = 60g$$

Particle	D (mm)	P (% of Conc.)
	0.0750	100
D_2	0.0268	87.50
D_5	0.0172	85.00
D_{15}	0.0102	81.67
D_{30}	0.0073	79.17
D_{60}	0.0052	76.67
D_{250}	0.0026	73.33
D_{1440}	0.0011	67.50

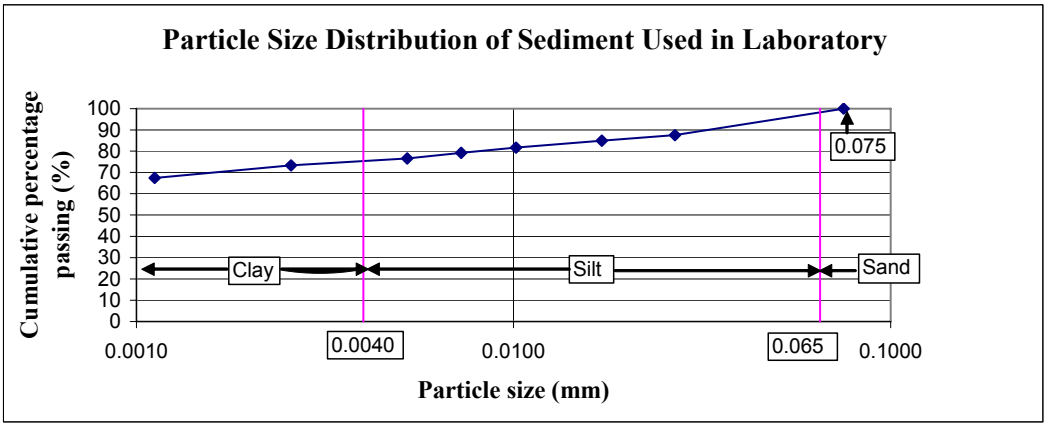

Laboratory Sediment Particle Size and Settling Velocity
(values determined from the size distribution)

Size (mm)	%	relative weight
0.00005	50	0.000025
0.0002	10	0.00002
0.00083	10	0.000083
0.0035	10	0.00035
0.019	10	0.0019
0.05	10	0.005

$$w = \frac{(\rho_s - \rho) g D^2}{18 \mu}$$

D 0.007378 mm

w_s 0.00005 m/s

Appendix C : Laboratory Results

Mixing Tank Concentrations Before Tests

	Design Concentration (mg/ℓ)	Measured Concentration (mg/ℓ)
Tank 1	27 500	**15992.06**
Tank 2	55 000	**34706.86**
Tank 3	13 750	**7507.14**
Tank 4	27 500	**17476.94**

Measured Concentrations (mg/ℓ)

Test1	Distance (m)	0	5	10	15	20	25
	Depth A	863.48	688.65	749.21	450.65	620.32	334.73
	Depth B	2955.26	2895.59	2840.28	2170.23	2122.17	2197.93
	Depth C	2776.11	2672.14	2572.28	2770.24	1891.35	2160.27

Test2	Distance (m)	0	5	10	15	20	25
	Depth A	465.70	865.00	750.00	257.13	208.30	147.90
	Depth B	6169.00	6824.35	6853.00	5283.92	3449.73	958.33
	Depth C	8903.00	6823.42	3105.00	1925.35	1631.49	790.47

Test3	Distance (m)	0	5	10	15	20	25
	Depth A	434.17	326.56	267.88	173.70	173.77	135.75
	Depth B	2926.00	2898.42	2532.65	1223.86	602.77	406.36
	Depth C	3078.74	3100.00	2511.82	604.78	512.80	898.14

Test4	Distance (m)	0	5	10	15	20	25
	Depth A	675.84	309.87	265.00	176.19	219.01	179.42
	Depth B	2485.88	2575.94	1982.00	1583.21	1259.49	907.67
	Depth C	1084.00	1026.75	1112.00	1164.59	891.03	758.97

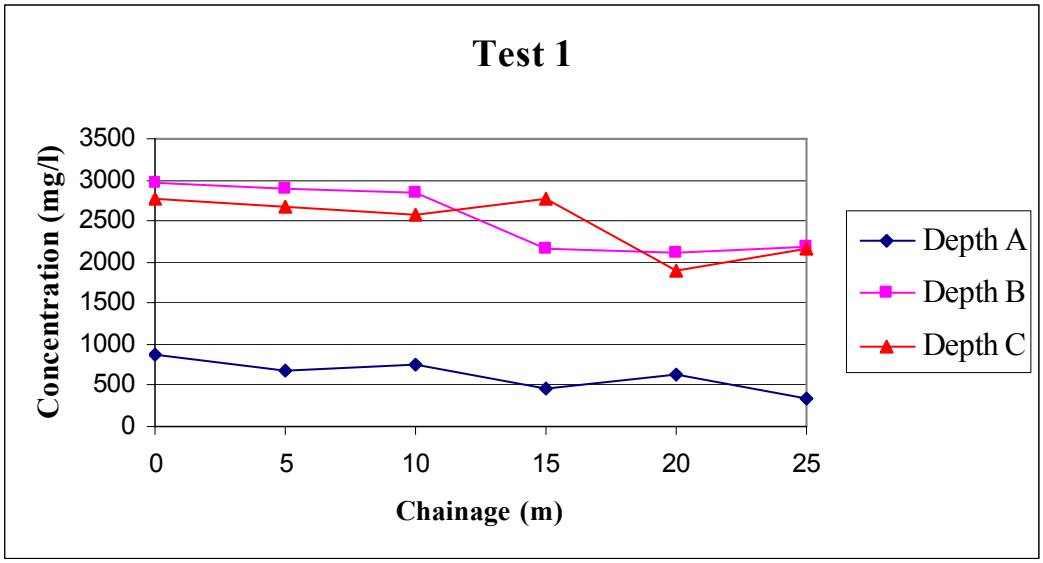
Test 1
Concentration (mg/l)
3500
3000
2500
2000
1500
1000
500
0
0
5
10
15
20
25
Chainage (m)
Depth A
Depth B
Depth C

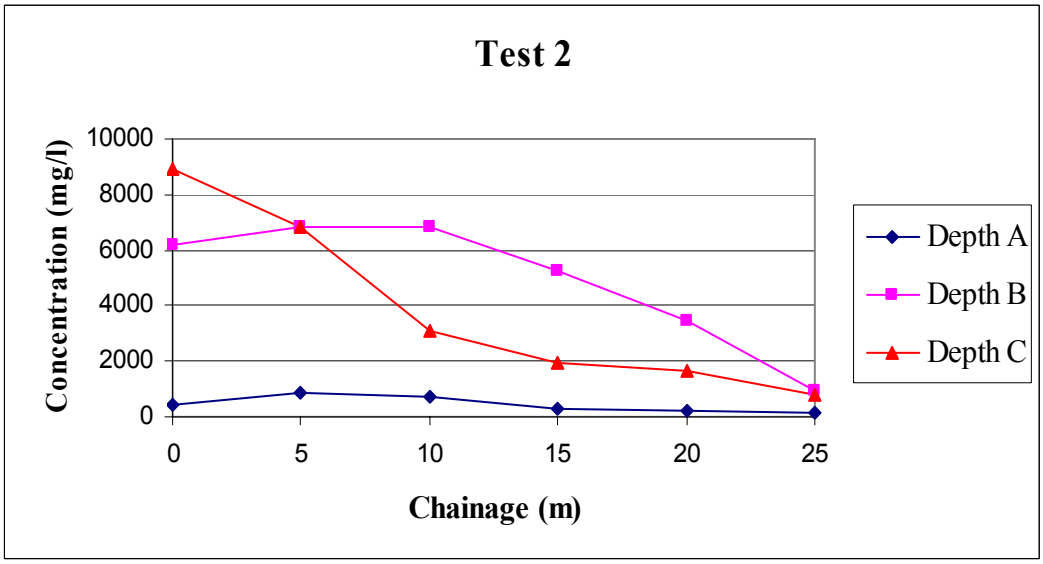
Test 2
Concentration (mg/l)
10000
8000
6000
4000
2000
0
0
5
10
15
20
25
Chainage (m)
Depth A
Depth B
Depth C

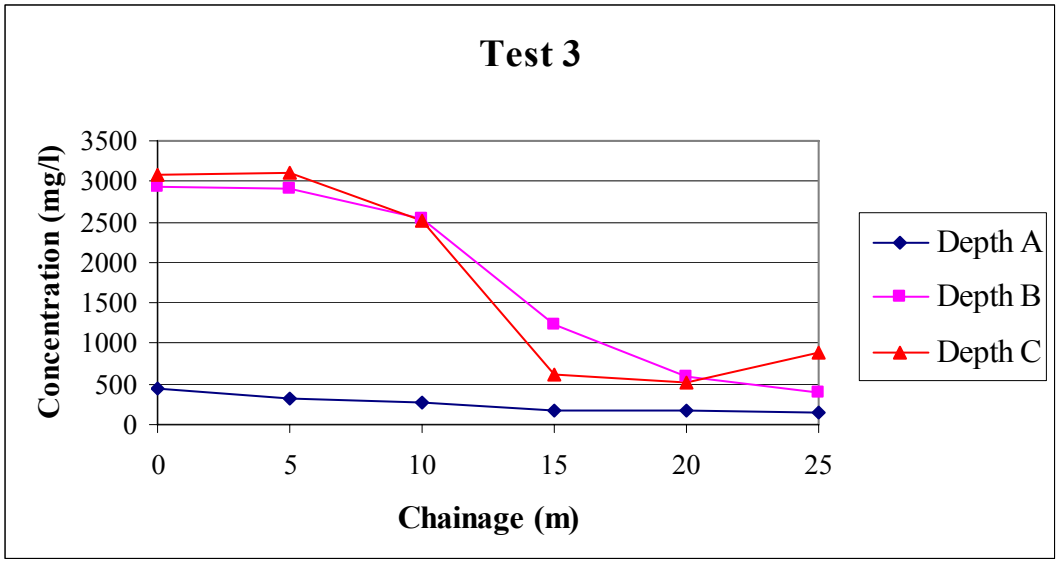
Test 3
Concentration (mg/l)
3500
3000
2500
2000
1500
1000
500
0
0
5
10
15
20
25
Chainage (m)
Depth A
Depth B
Depth C

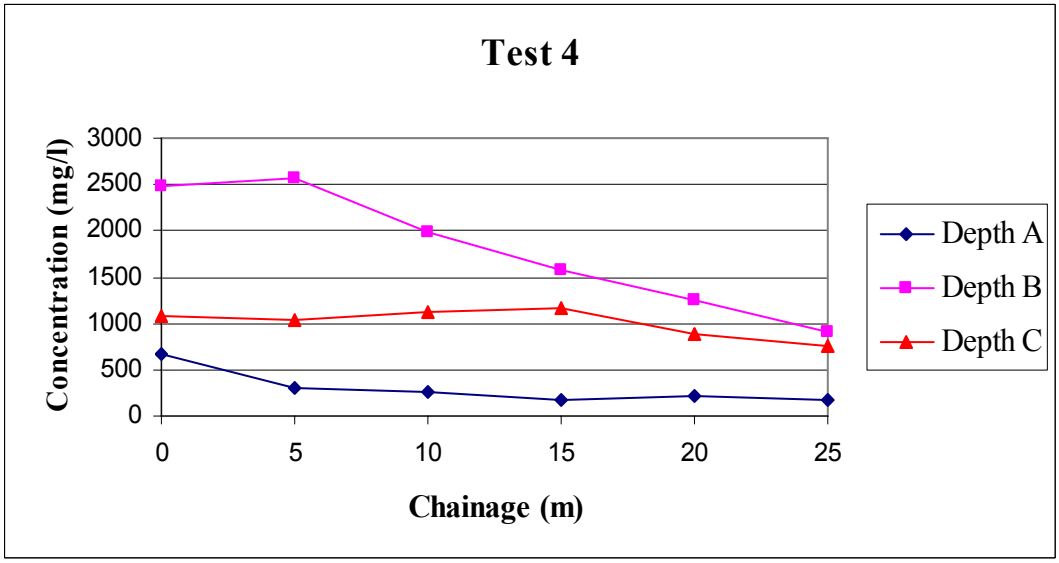
Test 4
Concentration (mg/l)
3000
2500
2000
1500
1000
500
0
0
5
10
15
20
25
Chainage (m)
Depth A
Depth B
Depth C

Appendix D : Determining the Roughness of the Laboratory Channel

The energy principle using a discharge of 0.0333m^3/s, non-uniform flow.

Q = 0.0333 m^3/s
L = 30m

Upstream Conditions:

Z_1	0.0090	m
Y_1	0.0890	m
A_1	0.0890	m^2
V_1	0.3742	m/s
P_1	1.1780	m
$V_1^2/2g$	0.007135	
R_1	0.0756	m

Average Conditions:

Y_{avg}	0.0765	m
A_{avg}	0.0765	m^2
V_{avg}	0.4353	m/s
P_{avg}	1.1530	m
R_{avg}	0.0663	m

Downstream Conditions:

Z_2	0.0000	m
Y_2	0.0640	m
A_2	0.0640	m^2
V_2	0.5203	m/s
P_2	1.1280	m
$V_2^2/2g$	0.013798	
R_2	0.0567	m

S_0	0.0003	m/m

$$R_e = \frac{\bar{v}\,R}{\upsilon}$$

*The kinematic viscosity, ע, is equal to $1x10^{-6}$ for a water temperature of 20°C

R_e	28881.2	(>2000, turbulent flow)

$$Bernouli: \; z_1 + y_1 + \frac{v_1^2}{2g} = z_2 + y_2 + \frac{v_2^2}{2g} + h_f$$

h_f	0.02734	m

$$h_f = \frac{v^2 n^2 L}{R^{4/3}}$$ (using average values of V and R)

n	0.0114

Assuming the same discharge and uniform flow:

Manning's equation:

$$Q = \frac{A^{5/3}\ S_o^{1/2}}{n\ P^{2/3}}$$ (using average values of A and P)

Q	0.0191	m^3/s

For turbulent flow:

$$Q = A \cdot 5.75\sqrt{gRs}\log\left[\frac{12R}{k + \frac{3.3\upsilon}{\sqrt{gRs}}}\right]$$

Solving for k:

k	0.00038	m

$$\frac{\sqrt{gRs}\cdot k}{\upsilon} = 9.32 \quad < 30$$

Thus figure 3.8 (SANRAL Road Drainage Manual) cannot be used to relate n and k, because the flow is smooth turbulent.

Appendix E : Laboratory Test Velocity Distribution Calculations

Tests 1 and 2

Vertical Velocity Distribution Calculations:

Sampling Height	y (m, from channel bed)	y_0 (m)	v (m/s)
Depth A	0.26640	0.00001296	0.1087
Depth B	0.13320	0.00001296	0.1011
Depth C	0.06660	0.00001296	0.0935
			0.3034 (Total)

$$v = \sqrt{2\pi g D s}.\ln\left(\frac{y}{y_0}\right)$$

k_s (m)	R=A/P	$y_0=k_s/29.62$ (m)	v_{avg} (m/s)
0.000384	0.2	1.29642E-05	**0.1000**

R_0	0.000192	m
s	0.00000584	m/m

$$\bar{v} = 5.75 \cdot \sqrt{gDs} \cdot \log\left(\frac{5.5D}{R_0}\right)$$

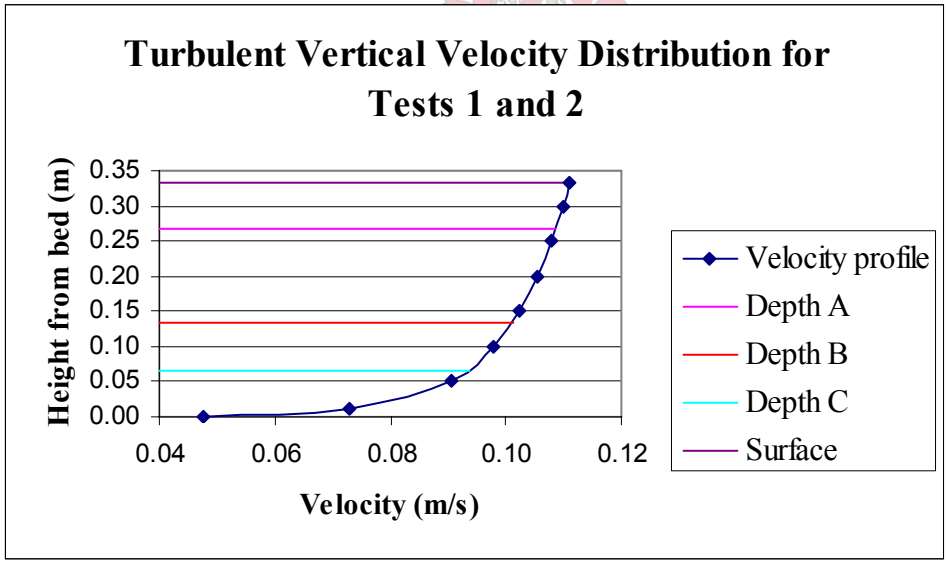

y	v
0.3330	0.1112
0.3000	0.1100
0.2500	0.1080
0.2000	0.1056
0.1500	0.1024
0.1000	0.0980
0.0500	0.0904
0.0100	0.0728
0.0010	0.0476

Weighted Average Concentrations (mg/ℓ)

Test 1

Chainage (m)	0	5	10	15	20	25
Depth A	863.48	688.65	749.21	450.65	620.32	334.73
Depth B	2955.26	2895.59	2840.28	2170.23	2122.17	2197.93
Depth C	2776.11	2672.14	2572.28	2770.24	1891.35	2160.27
	2150.44	**2035.85**	**2008.32**	**1739.02**	**1512.82**	**1518.65**

Test 2

Chainage (m)	0	5	10	15	20	25
Depth A	465.70	865.00	750.00	257.13	208.30	147.90
Depth B	6169.00	6824.35	6853.00	5283.92	3449.74	958.33
Depth C	8903.00	6823.43	3105.00	1925.35	1631.49	790.48
	4968.20	**4688.56**	**3510.43**	**2447.08**	**1727.58**	**616.16**

Tests 3 and 4

Vertical Velocity Distribution Calculations:

Sampling Height	y (m, from channel bed)	y_0 (m)	v (m/s)
Depth A	0.26640	0.00001296	0.0544
Depth B	0.13320	0.00001296	0.0506
Depth C	0.06660	0.00001296	0.0468
			0.1517 (Total)

$$v = \sqrt{2\pi g D s}.\ln\left(\frac{y}{y_0}\right)$$

k_s (m)	R=A/P	$y_0=k_s/29.62$ (m)	v_{avg} (m/s)
0.000384	0.2	1.29642E-05	**0.0500**

R_0	0.000192	m
s	0.00000146	m/m

$$\overline{v} = 5.75 \cdot \sqrt{gDs} \cdot \log\left(\frac{5.5D}{R_0}\right)$$

y	v
0.3330	0.0556
0.3000	0.0550
0.2500	0.0540
0.2000	0.0528
0.1500	0.0512
0.1000	0.0490
0.0500	0.0452
0.0100	0.0364
0.0010	0.0238

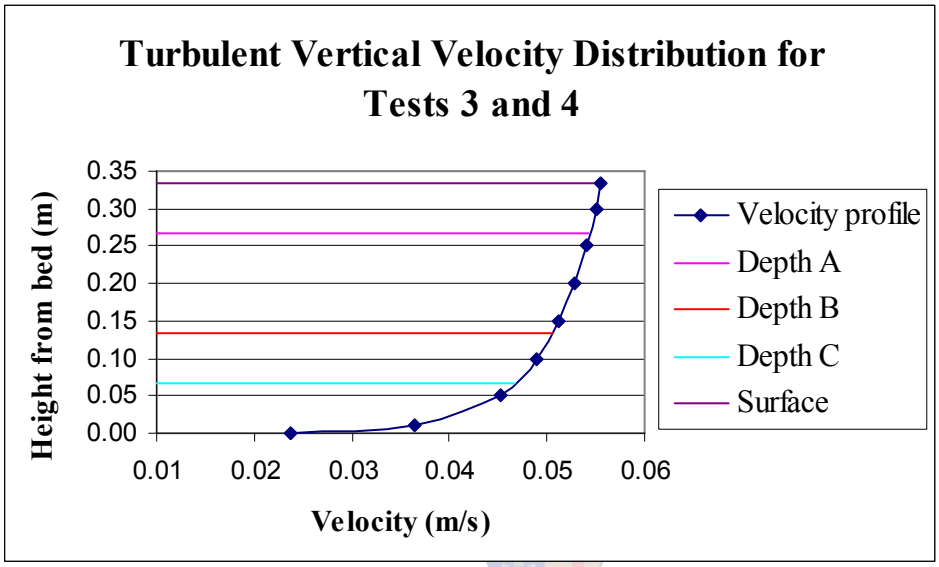

Weighted Average Concentrations (mg/ℓ)

Test 3

Chainage (m)	0	5	10	15	20	25
Depth A	434.17	326.56	267.88	173.70	173.77	135.75
Depth B	2926.00	2898.42	2532.65	1223.86	602.77	406.36
Depth C	3078.74	3100.00	2511.82	604.78	512.80	898.14
	2080.15	**2038.96**	**1714.66**	**656.66**	**421.30**	**461.02**

Test 4

Chainage (m)	0	5	10	15	20	25
Depth A	675.84	309.87	265.00	176.19	219.01	179.42
Depth B	2485.88	2575.94	1982.00	1583.21	1259.49	907.67
Depth C	1084.00	1026.75	1112.00	1164.59	891.03	758.97
	1405.03	**1286.26**	**1098.48**	**949.94**	**773.03**	**600.86**

Result Concentrations (mg/ℓ)

Chainage (m)	0	5	10	15	20	25
Test 1	2150.44	2035.85	2008.32	1739.02	1512.82	1518.65
Test 2	4968.20	4688.56	3510.43	2447.08	1727.58	616.16
Test 3	2080.15	2038.96	1714.66	656.66	421.30	461.02
Test 4	1405.03	1286.26	1098.48	949.94	773.03	600.86

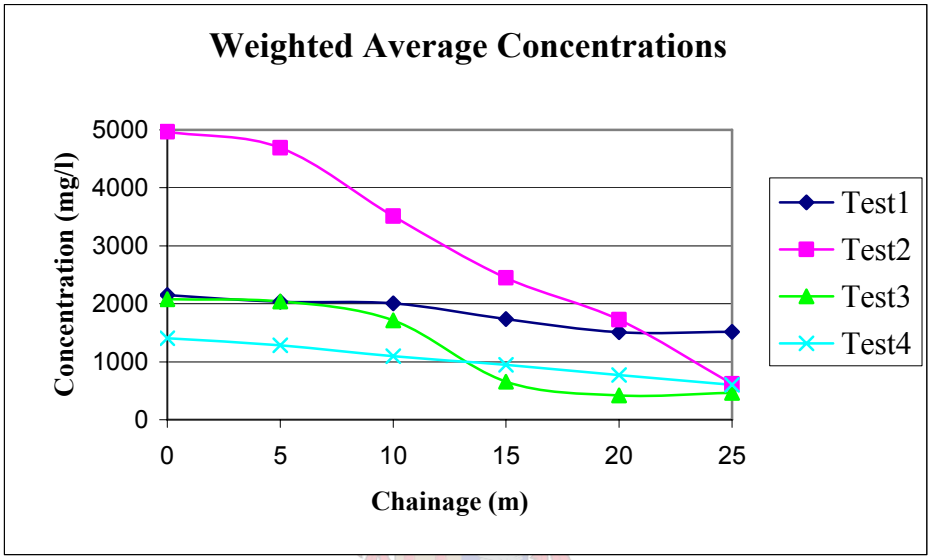

Appendix F : Welbedacht Reservoir Sediment Data

Bed Grab Sample Info

	S			E				0.065 - 0.004	< 0.004
Point nr.	degrees	minutes	seconds	degrees	minutes	seconds	D_{50} (mm)	Silt %	Clay %
Steel bridge	29	42	28.92	26	59	44.04	no sample	-	-
28	29	43	20.94	26	58	0.48	0.085	32	2
27	29	43	16.68	26	58	19.26	0.1	18	2
26	29	43	20.76	26	58	38.16	0.19	4	0
Jim Fouche	29	43	44.94	26	57	7.5	no sample	-	-
1	29	54	17.28	26	51	35.7	no sample	-	-
2	29	43	31.08	26	57	37.08	0.2	1	0
3	29	43	30.42	26	57	41.88	0.205	1.5	0
4	29	43	37.44	26	57	24.42	0.16	3.5	0
5	29	43	53.82	26	57	15.66	0.1	17.5	0
6	29	44	50.58	29	57	49.8	0.06	44.5	3
7	29	44	56.34	26	58	56.16	0.09	30	0
8	29	45	32.88	26	58	20.04	0.19	3.5	0
9	29	46	16.14	26	57	26.52	0.13	15	0
10	29	45	40.92	26	56	36.48	0.06	44	8
11	29	46	19.32	26	55	36.48	0.11	10	0
12	29	46	56.88	26	54	36.42	0.1	2	0
13	29	47	45.6	26	55	24.6	0.16	7	0
14	29	48	28.74	26	56	13.26	0.19	15	0
15	29	49	3.9	26	55	10.8	0.045	67	8
16	29	49	31.5	26	55	41.88	0.065	40	7
17	29	50	33.54	26	55	32.4	0.02	70	20
18	29	51	13.32	26	54	37.38	0.13	6.5	0
19	29	50	57.84	26	53	26.76	0.15	7	0
20	29	49	59.4	26	52	57.6	0.055	53	2
21	29	50	50.76	26	52	23.04	0.11	12	0
22	29	51	56.58	26	52	22.62	0.09	24.5	3
23	29	53	4.02	26	52	16.26	0.055	52	3
24	29	54	23.34	26	51	42.06	0.006	54.5	42.5
25	29	53	44.76	26	51	49.74	0.013	71	22

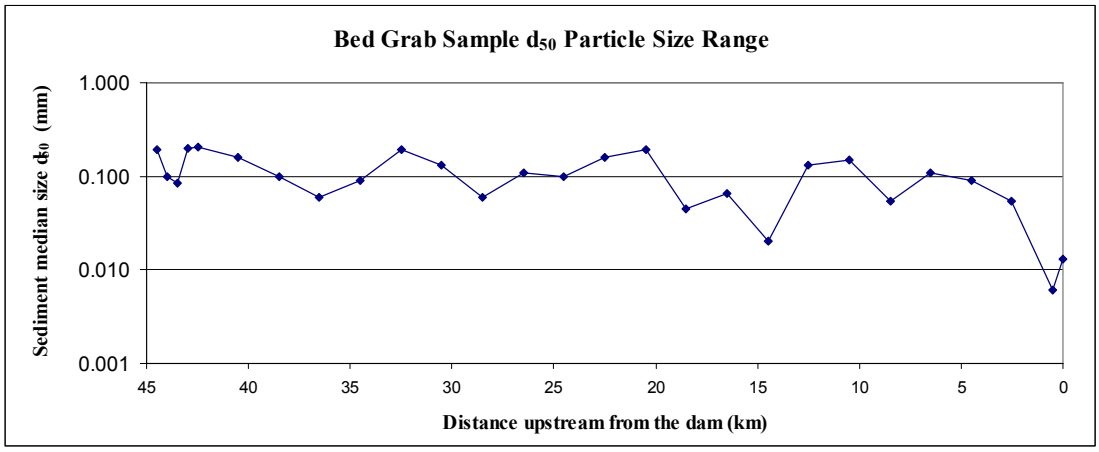

Welbedacht Suspended Sediment Size Range

(Basson and Rooseboom, 1997)

Fraction	Size (mm)	%	Median size	Rel. Weight
1	<0.05	76	0.025	**0.01900**
2	0.05-0.106	19	0.078	**0.01482**
3	0.106-0.25	5	0.178	**0.00890**
		100		**0.04272** mm

Settling velocity

0.00164 m/s

Appendix G : Welbedacht Sediment Load Calculations

constant	coefficient
793.32	0.664

$$C = \text{constant} * Q^{\text{coefficient}}$$

				Catchment Area =	15 245	km^2
	Q	C	Qs			
Time	m3/s	g/m3	t/s	interval (hr:min)	interval (sec)	ton/interval
1973/08/01 00:00:00	0.1069	179.78	1.922E-05	0	0	0.0000
1973/08/01 01:00:00	0.1067	179.5	1.915E-05	01:00	3600	0.0691
1973/08/01 02:00:00	0.1064	179.22	1.907E-05	01:00	3600	0.0688
1973/08/01 03:00:00	0.1062	178.94	1.9E-05	01:00	3600	0.0685
1973/08/01 04:00:00	0.1059	178.65	1.892E-05	01:00	3600	0.0683
1973/08/01 05:00:00	0.1057	178.37	1.885E-05	01:00	3600	0.0680
1973/08/01 06:00:00	0.1054	178.09	1.877E-05	01:00	3600	0.0677
1973/08/01 07:00:00	0.1052	177.81	1.87E-05	01:00	3600	0.0674
1973/08/01 08:00:00	0.1049	177.53	1.862E-05	01:00	3600	0.0672
1973/08/01 09:00:00	0.1047	177.24	1.855E-05	01:00	3600	0.0669
1973/08/01 10:00:00	0.1044	176.96	1.848E-05	01:00	3600	0.0666
1973/08/01 11:00:00	0.1042	176.68	1.84E-05	01:00	3600	0.0664
1973/08/01 12:00:00	0.1039	176.39	1.833E-05	01:00	3600	0.0661
1973/08/01 13:00:00	0.1037	176.11	1.825E-05	01:00	3600	0.0658
1973/08/01 14:00:00	0.1034	175.83	1.818E-05	01:00	3600	0.0656
1973/08/01 15:00:00	0.1031	175.54	1.811E-05	01:00	3600	0.0653
1973/08/01 16:00:00	0.1029	175.26	1.803E-05	01:00	3600	0.0651
1973/08/01 18:00:00	0.1024	174.69	1.789E-05	01:00	3600	0.0645

1973/08/01 19:00:00	0.1021	174.41	1.781E-05	01:00	3600	0.0643
1973/08/01 20:00:00	0.1019	174.12	1.774E-05	01:00	3600	0.0640
1973/08/01 21:00:00	0.1016	173.83	1.767E-05	01:00	3600	0.0637
1973/08/01 22:00:00	0.1014	173.55	1.76E-05	01:00	3600	0.0635
1973/08/01 23:00:00	0.1011	173.26	1.752E-05	01:00	3600	0.0632

***Continuous data from 1973/08/01 to 1976/09/29**

1976/09/29 11:00:00	125.16	19595	2.4524616	11:00	3600	9277.6308
1976/09/29 12:00:00	119.1	18961	2.2583111	01:00	3600	8479.3909
1976/09/29 13:00:00	114.73	18496	2.1220271	01:00	3600	7884.6088
1976/09/29 14:00:00	111.56	18155	2.0253615	01:00	3600	7465.2995
1976/09/29 15:00:00	109.04	17882	1.9498351	01:00	3600	7155.3538
1976/09/29 16:00:00	106.63	17618	1.8784769	01:00	3600	6890.9615
1976/09/29 17:00:00	103.76	17302	1.7952389	01:00	3600	6612.6885
1976/09/29 18:00:00	106.03	17552	1.8610664	01:00	3600	6581.3496
1976/09/29 19:00:00	104.68	17404	1.8218039	01:00	3600	6629.1665
1976/09/29 20:00:00	98.849	16754	1.6560837	01:00	3600	6260.1976
1976/09/29 21:00:00	99.187	16792	1.6655172	01:00	3600	5978.8815
1976/09/29 22:00:00	97.12	16559	1.6081629	01:00	3600	5892.6241
1976/09/29 23:00:00	95.71	16398	1.5694947	01:00	3600	5719.7838
1976/09/30 00:00:00	94.372	16246	1.533149	01:00	3600	5584.7587
avg.	**49.3**					**139994045.6** **t**
						2899.6 **t/km^2.a**
						Catchment area:
						15245 **km^2**

Appendix H : Vaal Reservoir Sediment Data

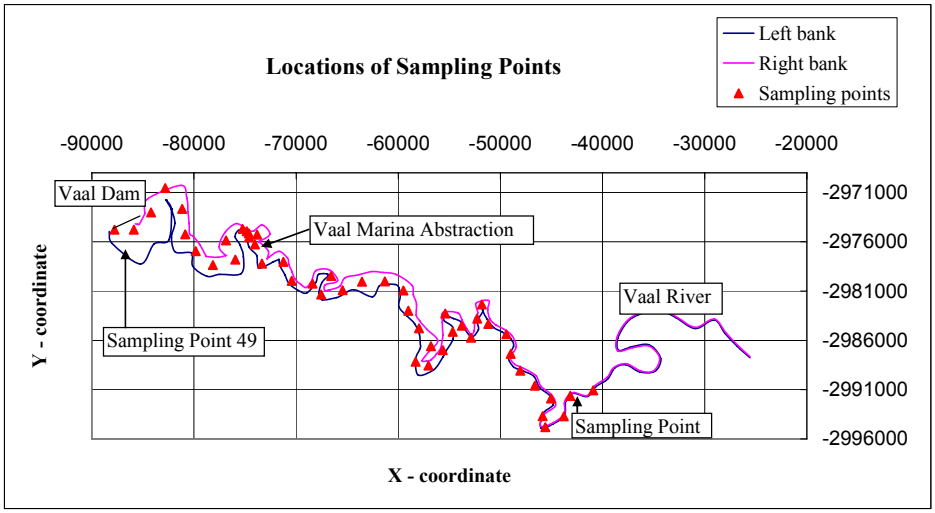

Sample Data:

	<0.004mm	<0.065mm	>0.065	>2mm	
Sample	%Clay	%Silt	%Sand	%Gravel	D_{50} (mm)
1	2	2	35	61	3.2
2	4	6	70	20	1
3	24	15	57	4	0.22
4	0	3	97	0	0.3
5	70	26	2	2	0.0005
6	59	27	14	0	0.0017
7	26	42	32	0	0.037
8	61	36	3	0	0.0014
9	24	66	10	0	0.029
10	34	49	17	0	0.021
11	43	30	27	0	0.011
12	59	39	2	0	0.0015
13	55	43	2	0	0.0026
14	44	44	12	0	0.0065
15	65	22	13	0	0.0011
16	74	25	1	0	0.0008
17	62	37	1	0	0.0011
18	78	21	1	0	0.0005
19	65	33	2	0	0.0014
20	63	35	2	0	0.0011
21	70	28	2	0	0.0004
22	78	21	1	0	0.0004
23	78	21	1	0	0.0005
24	64	34	2	0	0.0011
25	83	16	1	0	0.0004
26	86	13	1	0	0.00035

27	75	23	2	0	0.0006
29	78	17	5	0	0.00045
30	85	14	1	0	0.00011
31	79	19	2	0	0.0004
32	77	21	2	0	0.0006
33	82	17	1	0	0.0003
34	90	9	1	0	0.00025
35	86	12	2	0	0.00045
36	79	19	2	0	0.00026
37	81	16	3	0	0.00065
38	73	24	3	0	0.00024
39	79	19	2	0	0.0004
40	75	23	2	0	0.0005
41	86	12	2	0	0.0002
42	89	10	1	0	0.00027
43	81	17	2	0	0.0003
44	44	5	51	0	0.074
45	86	12	2	0	0.00014
46	94	5	1	0	0.000064
47	83	14	3	0	0.0001
48	78	19	3	0	0.00015
49	85	13	2	0	0.00024

(28 - no sample)

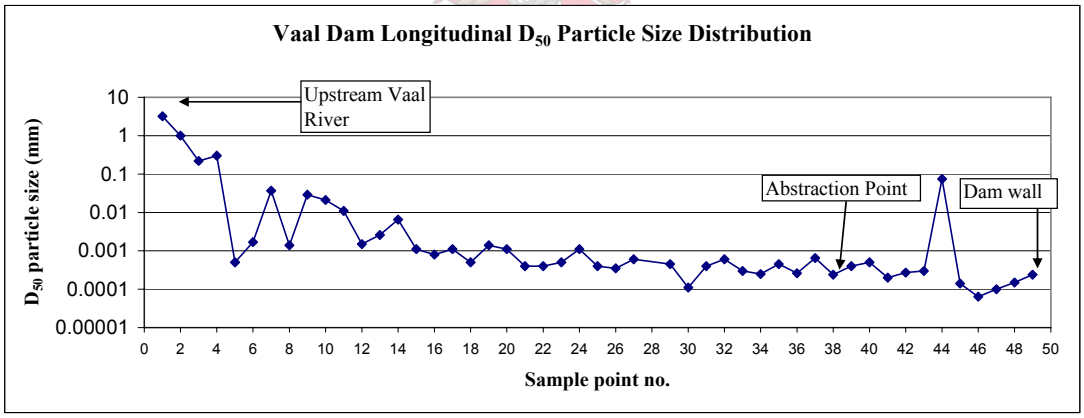

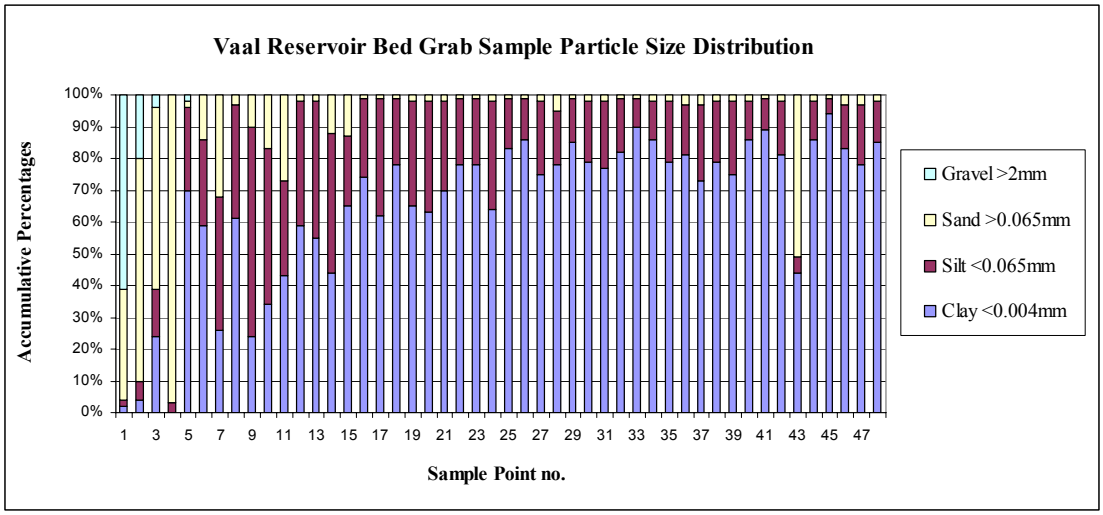

Vaal Reservoir Inflow and Sediment Concentration Time-series

	Q	C mg/ℓ	Qs (t/s)	Time interval (sec)	ton per interval
1988-01-01 05:30:00	29.251	274.10	0.00802	0	
1988-01-01 12:48:00	26.216	260.92	0.00684	26280	195.235
1988-01-01 15:12:00	26.608	262.67	0.00699	8640	59.743
1988-01-02 17:12:00	22.2	242.11	0.00537	93600	578.629
1988-01-02 17:54:00	23.193	246.92	0.00573	2520	13.988
1988-01-02 19:12:00	21.101	236.64	0.00499	4680	25.085
1988-01-02 21:42:00	21.645	239.37	0.00518	9000	45.785
1988-01-02 23:54:00	20.896	235.60	0.00492	7920	40.013
1988-01-03 07:24:00	19.924	230.61	0.00459	27000	128.490
1988-01-03 10:48:00	19.737	229.63	0.00453	12240	55.856
1988-01-03 12:54:00	19.196	226.78	0.00435	7560	33.587
1988-01-03 17:42:00	19.286	227.25	0.00438	17280	75.479
1988-01-03 18:12:00	21.507	238.68	0.00513	1800	8.564
1988-01-03 18:48:00	20.023	231.12	0.00463	2160	10.542
1988-01-03 19:06:00	20.896	235.60	0.00492	1080	5.157

1988-01-03 20:30:00	18.223	221.53	0.00404	5040	22.579
1988-01-03 21:42:00	19.601	228.92	0.00449	4320	18.412
1988-01-03 22:42:00	19.556	228.68	0.00447	3600	16.126
1988-01-04 00:48:00	18.181	221.30	0.00402	7560	32.113
1988-01-04 05:42:00	17.836	219.40	0.00391	17640	70.001
1988-01-04 08:54:00	17.496	217.51	0.00381	11520	44.460
1988-01-04 12:48:00	17.369	216.80	0.00377	14040	53.149

*Continuous data from 1988/01/04 to 2003/12/27

2003-12-27 10:17:48	0.79	53.96	0.00004	58500	2.451
2003-12-27 18:44:15	0.741	52.43	0.00004	30420	1.239
2003-12-27 19:49:48	0.792	54.02	0.00004	3900	0.159
2003-12-28 00:03:23	0.807	54.48	0.00004	15240	0.661
2003-12-28 04:39:01	0.793	54.05	0.00004	16560	0.719
2003-12-28 11:08:55	0.693	50.87	0.00004	23340	0.912
2003-12-28 17:46:08	0.682	50.51	0.00003	23880	0.832
2003-12-28 23:36:06	0.815	54.72	0.00004	21000	0.830
2003-12-29 08:15:17	0.925	57.93	0.00005	31140	1.529
2003-12-29 20:02:31	0.916	57.68	0.00005	42420	2.257
2003-12-29 22:46:37	0.949	58.60	0.00006	9840	0.534
2003-12-30 03:43:52	0.951	58.66	0.00006	17820	0.993
2003-12-30 07:56:02	0.876	56.53	0.00005	15180	0.799
2003-12-30 16:55:53	0.714	51.56	0.00004	32340	1.396
2003-12-31 00:15:02	0.714	51.56	0.00004	26400	0.972
2003-12-31 07:55:09	0.65	49.43	0.00003	27600	0.951

2003-12-31 12:21:34	0.53	45.09	0.00002	15960	0.447
2003-12-31 19:41:02	0.505	44.12	0.00002	26400	0.610
2003-12-31 22:09:41	0.563	46.33	0.00003	8880	0.215
avg.	48.3758				11353828.934 t

$C = \text{constant} * Q^{\text{coefficient}}$

constant	coefficient
60	0.45

Catchment Area =	12 276	km^2

57.81	$t/km^2.a$

Appendix I : Vaal Reservoir Suspended Sediment Data

Vaal Reservoir Suspended Sediment Size Range

Fraction	Size (mm)	%	Median size (mm)	Relative weight
1	<0.004	75	0.02	0.015
2	0.004-0.065	25	0.0525	0.013125
		100		**0.028125**

Weighted avg. size (mm)

0.00071 Settling velocity (m/s)

Suspended Sediment Data from C1H012 Upstream in the Vaal River

		(mg/L)	Discharge (m3/s)	Qs (mg/s)	Qs (t/s)
1993/02/22	3:38:00 PM	245	4.176	1023.12	0.001023
1993/03/01	4:59:00 PM	248	5.436	1348.128	0.001348
1993/04/19	3:19:00 PM	2876	0.692	1990.192	0.001990
1993/04/26	2:58:00 PM	2784	0.524	1458.816	0.001459
1993/05/17	3:37:00 PM	2665	0.322	858.13	0.000858
1993/05/24	3:05:00 PM	2641	0.238	628.558	0.000629
1993/05/31	2:45:00 PM	2612	0.163	425.756	0.000426
1993/06/07	4:38:00 PM	73	0.097	7.081	0.000007
1993/03/08	2:48:00 PM	339	10.337	3504.243	0.003504
1993/03/15	3:00:00 PM	3164	2.049	6483.036	0.006483
1993/03/29	3:09:00 PM	3126	0.933	2916.558	0.002917
1993/04/05	4:38:00 PM	35	1	35	0.000035
1993/04/12	3:18:00 PM	19	0.604	11.476	0.000011
1993/05/03	2:58:00 PM	2884	0.404	1165.136	0.001165
1993/05/10	3:28:00 PM	2781	0.37	1028.97	0.001029
1993/06/14	2:46:00 PM	241	0.088	21.208	0.000021
1993/06/21	3:41:00 PM	216	0.05	10.8	0.000011
1993/06/28	3:51:00 PM	170	0.035	5.95	0.000006
1993/07/05	3:38:00 PM	146	0.015	2.19	0.000002
1993/07/12	2:28:00 PM	161	0.01	1.61	0.000002
1993/10/11	2:51:00 PM	486	34.415	16725.69	0.016726
1993/10/18	3:13:00 PM	332	24.593	8164.876	0.008165
1993/10/25	2:56:00 PM	588	26.134	15366.792	0.015367
1993/11/01	2:46:00 PM	449	7.024	3153.776	0.003154
1993/11/08	3:19:00 PM	453	14.375	6511.875	0.006512
1993/12/06	7:50:00 PM	175	20.366	3564.05	0.003564
1993/12/13	11:42:00 AM	161	11.6	1867.6	0.001868
1993/12/20	3:01:00 PM	93	11.125	1034.625	0.001035
1993/12/27	3:16:00 PM	46	5.865	269.79	0.000270
1993/11/15	3:44:00 PM	330	19.784	6528.72	0.006529

	Time	(mg/L)	Discharge (m3/s)	Qs (mg/s)	Qs (t/s)
1993/11/22	4:48:00 PM	272	5.648	1536.256	0.001536
1993/11/29	4:16:00 PM	197	9.881	1946.557	0.001947
1994/01/03	3:01:00 PM	4	8.584	34.336	0.000034
1994/01/10	3:41:00 PM	28	3.402	95.256	0.000095
1994/01/24	4:23:00 PM	324	31.17	10099.08	0.010099
1994/01/31	5:51:00 PM	235	34.898	8201.03	0.008201
1994/02/07	4:38:00 PM	173	178.57	30892.61	0.030893
1994/02/14	2:59:00 PM	180	73.299	13193.82	0.013194
1994/02/21	3:15:00 PM	110	26.53	2918.3	0.002918
1994/02/28	3:02:00 PM	6	27.744	166.464	0.000166
1994/03/07	2:58:00 PM	6	8.723	52.338	0.000052
1994/03/14	2:45:00 PM	6	7.651	45.906	0.000046
1994/03/21	2:48:00 PM	68	7.396	502.928	0.000503
1994/03/28	3:38:00 PM	14	3.185	44.59	0.000045
1994/04/04	2:46:00 PM	6	11.616	69.696	0.000070
1994/04/11	2:07:00 PM	132	2.963	391.116	0.000391
1994/05/23	2:52:00 PM	27	0.926	25.002	0.000025
1994/05/30	2:16:00 PM	18	0.787	14.166	0.000014
1994/06/06	2:17:00 PM	21	0.787	16.527	0.000017
1994/06/13	2:10:00 PM	2	0.723	1.446	0.000001
1994/04/18	2:52:00 PM	67	1.718	115.106	0.000115
1994/05/02	2:35:00 PM	59	1.934	114.106	0.000114
1994/05/09	3:35:00 PM	62	1.792	111.104	0.000111
1994/05/16	2:47:00 PM	9	1.268	11.412	0.000011
1994/06/20	4:16:00 PM	29	0.616	17.864	0.000018
1994/06/27	2:20:00 PM	14	0.55	7.7	0.000008
1994/07/04	3:59:00 PM	11	0.534	5.874	0.000006
1994/07/11	4:00:00 PM	3	0.474	1.422	0.000001
1994/07/18	3:17:00 PM	10	0.441	4.41	0.000004
1994/07/25	3:07:00 PM	42	0.404	16.968	0.000017
1994/08/01	2:47:00 PM	11	0.346	3.806	0.000004
1994/08/08	2:35:00 PM	28	0.342	9.576	0.000010
1994/08/22	2:57:00 PM	24	0.285	6.84	0.000007
1994/08/29	3:12:00 PM	30	0.251	7.53	0.000008
1994/09/05	3:51:00 PM	15	0.19	2.85	0.000003
1994/09/12	3:04:00 PM	66	0.097	6.402	0.000006
1994/09/19	3:28:00 PM	16	0.043	0.688	0.000001
1994/09/26	3:10:00 PM	28	0.014	0.392	0.000000
1994/11/14	2:59:00 PM	134	0.015	2.01	0.000002
1994/11/21	3:15:00 PM	34	0.427	14.518	0.000015
1994/11/28	2:59:00 PM	25	0.101	2.525	0.000003
1994/12/05	3:03:00 PM	32	0.03	0.96	0.000001
1994/12/12	3:02:00 PM	34	0.03	1.02	0.000001
1994/12/19	3:31:00 PM	40	0.02	0.8	0.000001
1994/12/26	2:00:00 PM	27	0.035	0.945	0.000001
1995/01/02	3:45:00 PM	2	0.038	0.076	0.000000

		(mg/L)	Discharge (m3/s)	Qs (mg/s)	Qs (t/s)
1995/01/09	4:20:00 PM	51	0.024	1.224	0.000001
1995/01/16	4:15:00 PM	33	0.166	5.478	0.000005
1995/01/23	3:24:00 PM	19	1.934	36.746	0.000037
1995/01/30	5:02:00 PM	11	2.416	26.576	0.000027
1995/03/13	3:34:00 PM	13	0.464	6.032	0.000006
1995/03/20	3:46:00 PM	24	0.117	2.808	0.000003
1995/03/27	2:18:00 PM	14	0.89	12.46	0.000012
1995/04/03	3:03:00 PM	74	11.616	859.584	0.000860
1995/04/17	2:46:00 PM	99	1.615	159.885	0.000160
1995/04/10	2:48:00 PM	84	6.782	569.688	0.000570
1995/04/24	3:09:00 PM	97	1	97	0.000097
1995/05/01	2:56:00 PM	60	1.077	64.62	0.000065
1995/05/08	2:59:00 PM	81	1.158	93.798	0.000094
1995/05/15	3:44:00 PM	52	1.242	64.584	0.000065
1995/05/22	3:14:00 PM	52	0.848	44.096	0.000044
1995/05/29	3:25:00 PM	58	0.604	35.032	0.000035
1995/06/05	2:26:00 PM	48	0.474	22.752	0.000023
1995/06/12	2:01:00 PM	35	0.508	17.78	0.000018
1995/06/19	2:36:00 PM	37	0.267	9.879	0.000010
1995/06/26	2:21:00 PM	3	0.139	0.417	0.000000
1995/07/03	3:43:00 PM	10	0.099	0.99	0.000001
1995/07/10	4:08:00 PM	9	0.064	0.576	0.000001

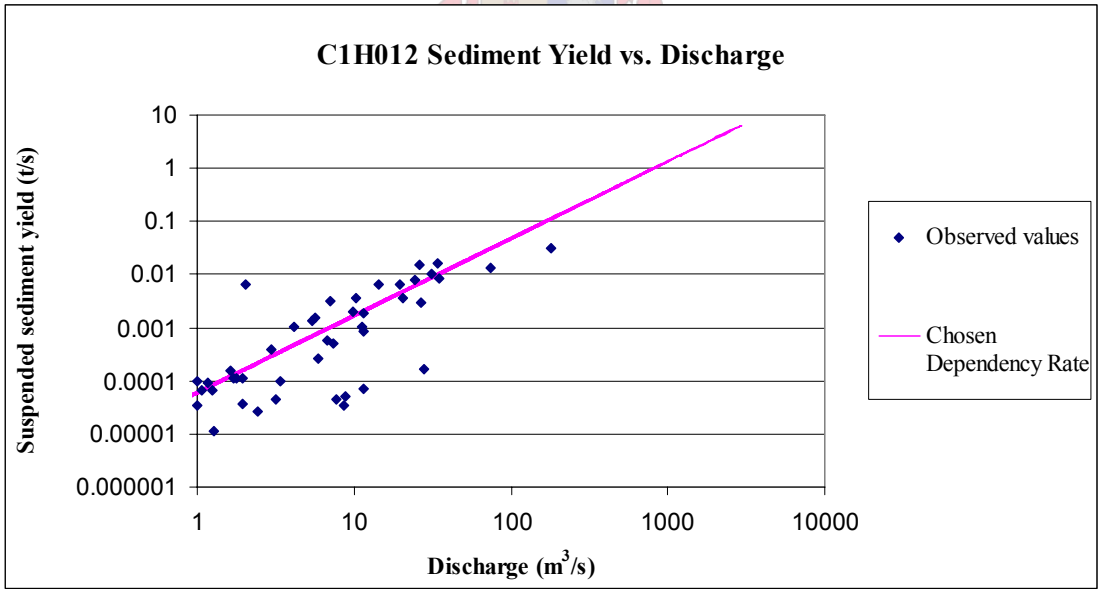

Trendline:

constant	coefficient
60	**0.45**

$C = \text{constant} * Q^{\text{coefficient}}$ $Q_s = C * Q$

Appendix J : Nyando River Suspended Sediment Data

Data from Station IGD003

Q	C (mg/L)
12.126	860.0
5.439	75.0
21.637	158.0
24.778	66.0
35.297	196.3
5.100	65.7
4.614	90.0
4.073	75.3
49.437	1383.6
13.036	47.3
23.883	201.7
19.691	46.3
7.824	58.0
6.730	86.7
3.888	82.3
4.761	24.3
11.062	67.7
7.307	66

Calculated Concentration Values

constant	coefficient
15	1.042

$$C = \text{constant} * Q^{\text{coefficient}}$$

Q	C (mg/L)
12.13	202.0
5.44	87.6
21.64	369.3
24.78	425.3
35.30	614.9
5.10	81.9
4.61	73.8
4.07	64.8
49.44	873.6
13.04	217.8
23.88	409.3
19.69	334.7
7.82	128.0
6.73	109.4
3.89	61.7
4.76	76.3
11.06	183.6
7.31	119.2

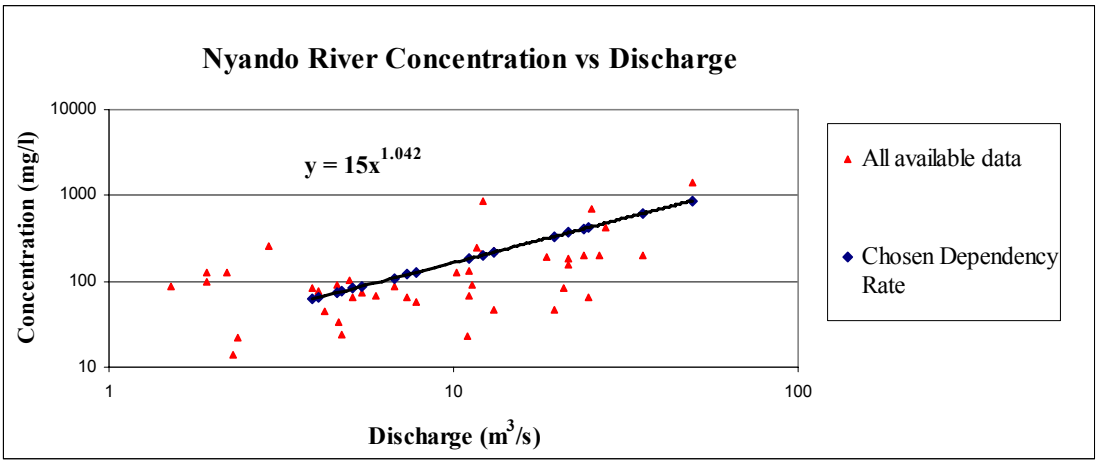

Appendix K : Nyando Inflow Time-series and Sediment Concentrations

constant	coefficient	$C = c\text{constant} * Q^{\text{coefficient}}$
15	**1.042**	

Time	Q (m3/s)	C (mg/L)	Qs (g/s)	Qs(t/day)
1950/01/01 00:00	23.3	398.911	9294.629	803.056
1950/01/02 00:00	23	393.561	9051.895	782.084
1950/01/03 00:00	22.9	391.778	8971.712	775.156
1950/01/04 00:00	22.8	389.995	8891.893	768.260
1950/01/05 00:00	22.7	388.213	8812.438	761.395
1950/01/06 00:00	22.6	386.431	8733.347	754.561
1950/01/07 00:00	22.5	384.650	8654.619	747.759
1950/01/08 00:00	22.4	382.869	8576.256	740.988
1950/01/09 00:00	22.3	381.088	8498.256	734.249
1950/01/10 00:00	22.2	379.307	8420.619	727.542
1950/01/11 00:00	22.1	377.527	8343.347	720.865
1950/01/12 00:00	22	375.747	8266.437	714.220
1950/01/13 00:00	21.9	373.968	8189.891	707.607
1950/01/14 00:00	21.8	372.188	8113.709	701.024
1950/01/15 00:00	21.7	370.410	8037.890	694.474
1950/01/16 00:00	21.6	368.631	7962.434	687.954
1950/01/17 00:00	21.4	365.075	7812.611	675.010
1950/01/18 00:00	21.3	363.298	7738.244	668.584
1950/01/19 00:00	21.2	361.521	7664.240	662.190
1950/01/20 00:00	21.1	359.744	7590.599	655.828
1950/01/21 00:00	21	357.968	7517.320	649.496
1950/01/22 00:00	20.9	356.192	7444.405	643.197
1950/01/23 00:00	21.7	370.410	8037.890	694.474

*Continuous data from 1950/01/23 to 2004/12/16

2004/12/16 00:00	17.4	294.268	5120.270	442.391
2004/12/17 00:00	27.8	479.497	13330.018	1151.714
2004/12/18 00:00	31.2	540.755	16871.548	1457.702
2004/12/19 00:00	30.4	526.315	15999.968	1382.397
2004/12/20 00:00	27.5	474.107	13037.929	1126.477
2004/12/21 00:00	25.6	440.025	11264.639	973.265
2004/12/22 00:00	23.7	406.050	9623.374	831.460
2004/12/23 00:00	21.8	372.188	8113.709	701.024
2004/12/24 00:00	20.3	345.543	7014.523	606.055
2004/12/25 00:00	18.1	306.614	5549.718	479.496
2004/12/26 00:00	15.4	259.112	3990.328	344.764
2004/12/27 00:00	12.8	213.700	2735.357	236.335
2004/12/28 00:00	10.7	177.300	1897.112	163.910
2004/12/29 00:00	8.9	146.338	1302.404	112.528

Time	Q (m3/s)	C (mg/L)	Qs (g/s)	Qs(t/day)
2004/12/30 00:00	7.6	124.136	943.436	81.513
2004/12/31 00:00	6.7	108.858	729.350	63.016
total	**417260.7**		**total t**	**54000309.75**
			t/year	**1000005.74**
			t/a.km2	**273.82**

Avg. Q	Avg. C
20.8	**366.15**

Catchment area =	3652	km^2